

Dissertation zur Erlangung des Doktorgrades
der Fakultät für Chemie und Pharmazie
der Ludwig-Maximilians-Universität München

**The eukaryotic small ribosomal subunit
in the context of translational recycling
and ribosome biogenesis**

André Heuer

Aus

Berlin, Deutschland

2018

Erklärung

Diese Dissertation wurde im Sinne von § 7 der Promotionsordnung vom 28. November 2011 von Herrn Prof. Dr. Roland Beckmann betreut.

Eidesstattliche Versicherung

Diese Dissertation wurde eigenständig und ohne unerlaubte Hilfe erarbeitet.

München, 25.05.2018

André Heuer

Dissertation eingereicht am: 25.05.2018

1. Gutachter: Prof. Dr. Roland Beckmann
2. Gutachter: Prof. Dr. Karl-Peter Hopfner

Mündliche Prüfung am: 19.07.2018

List of publications

Cryoelectron microscopic structures of eukaryotic translation termination complexes containing eRF1-eRF3 or eRF1-ABCE1.

Preis A, Heuer A, Barrio-Garcia C, Hauser A, Eyler DE, Berninghausen O, Green R, Becker T, Beckmann R.

Cell Rep. 2014 Jul 10;8(1):59-65. doi: 10.1016/j.celrep.2014.04.058.

Structure of the hypusinylated eukaryotic translation factor eIF-5A bound to the ribosome.

Schmidt C, Becker T, Heuer A, Braunger K, Shanmuganathan V, Pech M, Berninghausen O, Wilson DN, Beckmann R.

Nucleic Acids Res. 2016 Feb 29;44(4):1944-51. doi: 10.1093/nar/gkv1517.

Structure of the ribosome post-recycling complex probed by chemical cross-linking and mass spectrometry.

Kiosze-Becker K, Ori A, Gerovac M, Heuer A, Nürenberg-Goloub E, Rashid UJ, Becker T, Beckmann R, Beck M, Tampé R.

Nat Commun. 2016 Nov 8;7:13248. doi: 10.1038/ncomms13248.

The cryo-EM structure of a ribosome-Ski2-Ski3-Ski8 helicase complex.

Schmidt C, Kowalinski E, Shanmuganathan V, Defenouillère Q, Braunger K, Heuer A, Pech M, Namane A, Berninghausen O, Fromont-Racine M, Jacquier A, Conti E, Becker T, Beckmann R.

Science. 2016 Dec 16;354(6318):1431-1433.

Structure of the 40S-ABCE1 post-splitting complex in ribosome recycling and translation initiation.

Heuer A, Gerovac M, Schmidt C, Trowitzsch S, Preis A, Kötter P, Berninghausen O, Becker T, Beckmann R, Tampé R.

Nat Struct Mol Biol. 2017 May;24(5):453-460. doi: 10.1038/nsmb.3396.

Structural Basis for Polyproline-Mediated Ribosome Stalling and Rescue by the Translation Elongation Factor EF-P.

Huter P, Arenz S, Bock LV, Graf M, Frister JO, Heuer A, Peil L, Starosta AL, Wohlgemuth I, Peske F, Nováček J, Berninghausen O, Grubmüller H, Tenson T, Beckmann R, Rodnina MV, Vaiana AC, Wilson DN.

Mol Cell. 2017 Nov 2;68(3):515-527.e6. doi: 10.1016/j.molcel.2017.10.014.

Cryo-EM structure of a late pre-40S ribosomal subunit from *Saccharomyces cerevisiae*.

Heuer A, Thomson E, Schmidt C, Berninghausen O, Becker T, Hurt E, Beckmann R.

Elife. 2017 Nov 20;6. pii: e30189. doi: 10.7554/eLife.30189.

Contribution report

This dissertation contains the work which was conducted during my PhD research from January 2012 to April 2018 in the laboratory of Prof. Roland Beckmann at the Gene Center of the Ludwig-Maximilians University in Munich. Several project were done in the collaboration with scientist from the laboratories of Prof. Ed Hurt (Heidelberg, Germany), Dr. Rachel Green (Baltimore, USA) and Prof. Robert Tampé (Frankfurt, Germany).

Publication 1 (Preis et al., 2014)

This publication reports the structural basis for eukaryotic termination by eRF1 and eRF3 as well as recycling by ABCE1 and eRF1. I purified the recycling factor ABCE1 (Rli1 in yeast). I contributed to cryo-EM data evaluation, processing and sorting. I also contributed to the interpretation of the resulting cryo-EM structures of the pre-termination and pre-recycling complexes.

Publication 2 (Kiosze-Becker et al., 2016)

This publication reports the first structural characterization of an archeal post-recycling complex by X-link/MS and low resolution cryo-EM. I designed and optimized the sample for cryo-EM. I performed the cryo-EM data evaluation, processing, sorting and refinement. I contributed to the interpretation of the resulting cryo-EM structure and built the model. I contributed in the preparation of figures involving the cryo-EM structure. I helped writing the manuscript.

Publication 3 (Heuer, Gerovac et al., 2017)

This publication reports the first high resolution cryo-EM structure of the post-recycling complex in eukaryotes as well as an initiation factor bound intermediate. These structures result in a model for ribosomal splitting in general and further strengthen the link between ribosome recycling and translation initiation. I supported the purification of the post-recycling complex and optimized the sample for high resolution

cryo-EM. I designed and optimized the purification of the native post-recycling complex. I conducted the cryo-EM data evaluation, processing, sorting and refinement. I interpreted the resulting cryo-EM structures and contributed to the building of the model. I contributed in the preparation of the figures and in writing of the manuscript.

Publication 4 (Heuer A, Thomson E et al., 2017)

This publication reports the first high resolution cryo-EM structure of a pre-40S ribosome intermediate of small subunit biogenesis. In addition to novel structural insights, this work resulted in a new model for the function of late stage ribosome biogenesis factors. I contributed in the design of the complex and optimized it for cryo-EM. I contributed in data collection and conducted all cryo-EM data evaluation, processing, sorting and refinement. I interpreted the resulting cryo-EM structures and built and refined the models. I prepared the figures and wrote the manuscript.

Summary

The translation of mRNA into proteins by the ribosome is a central element in all domains of life and is divided into four phases: initiation, elongation, termination and recycling. After the translation of a mRNA has been terminated, the subunits of the ribosomes are separated into the small and large subunit during the recycling phase. While the initiation and elongation phases have been extensively studied, it gets more and more important to investigate the splitting process and the fate of the small subunit with its associated factors after termination. In the last years, evidence accumulated that termination coupled to recycling coordinates the initial steps of initiation, on the next or re-initiation on the same mRNA. A central player in these events is the highly conserved and essential ATPase ABCE1. This work provides important structural insights into the function of this eukaryotic recycling factor, which splits the ribosome after termination. We investigated the post-termination, pre-recycling and post-recycling phases of translation and clarify the role of ABCE1 and the importance of its functionally crucial iron-sulfur cluster domain. The splitting mechanism in eukaryotes can be explained by conformational changes of ABCE1. In concert with the release factor eRF1, present in the ribosomal A-site, ABCE1 destabilizes the inter-subunit bridges between the subunits. After the splitting reaction, ABCE1 stays bound to the small subunit and prevents a timely rejoining of the large subunit. We further provide the first native recycling structure containing 40S and ABCE1 and additionally find initiation factors bound. This suggests a physical link of termination and recycling to initiation via ABCE1, closing the gap in the cycle of translation.

The second part of this thesis investigates ribosome biogenesis of the small ribosomal subunit. The first stable intermediate of ribosome biogenesis, the 90S pre-ribosome, as well as many maturation steps of the large ribosomal subunit have been intensively studied by cryo-EM in the recent years. In contrast, structural insights into the maturation of process of the small subunit, after it emerges from the 90S pre-ribosome, are lacking and the state of the rRNA as well as the interaction with the associated ribosome biogenesis factors remained unclear. We were able to solve a 3.6 Angström structure of the 40S

pre-ribosome revealing in molecular detail how assembly factors regulate the timely folding of pre-rRNA. In contrast to previous models, we could show that the associated biogenesis factors Tsr1, Enp1, Rio2 and Pno1 prevent folding of essential active sites of the pre-rRNA, thus making them in-accessible. In addition we could explain how the last cleavage step of the small subunit rRNA and maturation of the 3'end is coordinated by the factor Pno1. We illustrate that the small subunit is in a translationally incompetent state, which prevents untimely m/tRNA binding during ribosome biogenesis and prevents error-prone and potentially harmful translation events in the cell.

List of Abbreviations

aa-tRNA	Aminoacyl-tRNA
A-site	Aminoacyl-site
A	Adenine
ATP	Adenosine triphosphate
ADP	Adenosine diphosphate
AMP-PNP	Adenylyl-imidodiphosphate
cryo-EM	Cryo-electron microscopy
DC	Decoding center
DNA	Deoxyribonucleic acid
<i>E. coli</i>	Escherichia coli
EF	Elongation factor
E-site	Exit-site
ETS	External transcribed spacers
FeS	Iron-sulphur cluster
GTP	Guanosine triphosphate
GDP	Guanosine diphosphate
GDPNP	Guanylyl imidodiphosphate
<i>H. sapiens</i>	Homo sapiens
IF	Initiation factor
ITS	Internal transcribed spacers
ISS	Inter-subunit space
kDa	Kilodalton
LSU	Large ribosomal subunit
pLSU	Premature large ribosomal subunit
SSU	Small ribosomal subunit
pSSU	Premature small ribosomal subunit
MDa	Megadalton
mRNA	Messenger RNA

NC	Nascent chain
NES	Nuclear export signal
NBD	Nucleotide binding domain
NBS	Nucleotide binding site
NPC	Nuclear pore complex
NGD	No-go mRNA decay
NSD	Non-stop mRNA decay
PTC	Peptidyl transferase centre
PABP	Poly(A)-binding protein
pt-RNA	Peptidyl tRNA
PRC	Post recycling complex
RNA	Ribonucleic acid
mRNA	Messenger RNA
rRNA	Ribosomal RNA
tRNA	Transfer RNA
snoRNA	Small nucleolar RNA
RBF	Ribosome biogenesis factor
RP	Ribosomal protein
RF	Release factor
UTR	Intranslated region

Contents

List of publications	ii
Contribution report	iii
Summary	v
List of Abbreviations	vii
Contents	viii
1 Introduction	1
1.1 The ribosome	1
1.2 Translation cycle	2
1.2.1 Initiation	3
1.2.2 Elongation	4
1.2.3 Termination	6
1.2.4 Recycling	8
1.3 The role of ABCE1 in termination and recycling	9
1.4 Ribosome biogenesis	11
1.4.1 The 90S Preribosome	12
1.4.2 Separation of pre-40S and pre-60S maturation	14
1.5 Small subunit maturation	16
1.5.1 Cytoplasmic biogenesis and involved factors	17
1.5.2 Preventing premature translation	20
1.5.3 Proposed final maturation steps	21
2 Aims of thesis	23
3 Cumulative Thesis: Summary of Publications	25
3.1 Publication 1	25
3.2 Publication 2	28

3.3	Publication 3	30
3.4	Publication 4	32
4	Discussion	35
4.1	ABCE1: Recycling and (re)initiation	35
4.2	Maturation of the eukaryotic small subunit	38
	Acknowledgements	41
	Appendix	45
	References	46
	Publications	54

List of Figures

1.1	Model of translation initiation in eukaryotes	5
1.2	Model of termination and recycling in eukaryotes	7
1.3	Domain organization and motifs of ABCE1	10
1.4	RNA processing steps during subunit maturation in <i>Saccharomyces cerevisiae</i>	13
1.5	Biogenesis pathway of eukaryotic ribosomes	15
1.6	Cryo-EM structures of human and yeast pre-40S complexes	18

1 Introduction

The DNA stores the genetic information of an organism and the transformation of this information into functional proteins is summarized in the central dogma of molecular biology (Crick, 1970). It describes the flow of genetic information from DNA via RNA to proteins. In detail, DNA dependent RNA polymerases create a transcript of the genetic information, called RNA. Different types of RNAs exist - ribosomal (rRNA), messenger (mRNA), transfer (tRNA) - and each of them have a specific role in the cell. The mRNAs specifically encode information in the form of nucleotide triplets called codons and tRNAs carry a corresponding amino acid to a specific codon. The ribosome, a huge macromolecular machinery, is built out of proteins and rRNAs and can translate the mRNA codons into an amino-acid chain with the help of tRNAs. Any resulting translated polypeptide chain emerging from the ribosome is folded into a three-dimensional functional protein, often with the help of chaperones guiding the process, until it is able to fulfill its role in the cell, either on its own or with the help of other DNAs, RNAs or proteins.

1.1 The ribosome

In all cells, protein biosynthesis is executed by the ribosome. While the overall architecture - large ribosomal subunit (LSU) and small ribosomal subunit (SSU) - as well as important functional sites are conserved across all domains of life, ribosomes still show significant differences between prokaryotes, archaea and eukaryotes. Ribosomal subunits are termed by their sedimentation coefficients (Svedberg): Prokaryotic and archaeal ribosomes sediment as a 70S particle (30S for the SSU and 50S for the LSU), while eukaryotic ribosomes sediment at

80S (40S and 60S for the SSU and LSU respectively). These differences, from prokaryotes over archaea to eukaryotes, result from the increased amount of ribosomal proteins (RP), rRNA as well as RNA expansion segments (Melnikov et al., 2012; Anger et al., 2013).

Despite their slight difference in composition, the important functional sites of the two ribosomal subunits are conserved across all domains of life: The small subunit harbors the mRNA binding tunnel and the decoding-centre (DC) at which the mRNA codons are read by their decoding tRNAs (Crick et al., 1961). The large subunit accommodates the peptidyl transferase centre (PTC), where peptide bond formation is catalyzed. From there, the polypeptide chain grows - with every new amino acid added C-terminally - into the peptide tunnel towards the tunnel exit (Frank et al., 1995). After emerging from the LSU tunnel exit, the growing peptide chain folds co-translationally (Evans et al., 2008). The functionally important and conserved A-, P- and E-sites, through which the tRNAs and mRNA move during the translation cycle, are located in the inter-subunit space (ISS) between the LSU and SSU. An amino-acyl tRNA (aa-tRNA), carrying the next amino acid to be translated, can enter the ISS of the ribosome through the A-site. The subsequent P-site contains the peptidyl tRNA (pt-RNA), on which the nascent polypeptide chain is growing into the LSU tunnel. The E-site contains the already de-acylated tRNA, which is ready to dissociate from the ribosome.

1.2 Translation cycle

The translation of mRNA into amino acids can be divided into four phases: (1) initiation, (2) elongation, (3) termination and (4) Recycling. These processes are executed in a similar manner in all domains of life. Eukaryotes however, require a much larger amount of factors during initiation and show significant differences in the termination and recycling phases. Specific codons on the mRNA control these phases: The AUG-codon or start codon, can only be decoded by the initiation tRNA and thus marks the start of all protein sequences. In contrast the stop codons (UAA, UAG, UGA) which serve as a translation termination signal, do not encode for any amino acid but are

decoded by termination factors. mRNAs in eukaryotes undergo additional processing and only encode for one protein. During the 5' cap addition, an eukaryotic mRNA is modified with guanine nucleotide that is co-transcriptionally added to the 5' end (Shatkin, 1976; Mizumoto and Kaziro, 1987). This modification prevents mRNA degradation and enables initiation factors and ribosomes to identify the mRNA (Sonenberg, 1993). In addition, the 3' end of eukaryotic mRNA is modified with a poly-adenyl moiety, which is bound by poly(A)-binding proteins (PABP) (Wahle and Rügsegger, 1999; Mangus et al., 2003). Presence of a poly(A)-tail as well as the PABPs prevent degradation by exonucleases and promote export of the mRNA from the nucleus (Guhaniyogi and Brewer, 2001). PABPs can also interact with the 5' cap initiation factor eIF4-E, leading to mRNA circularization and efficient translation (Wells et al., 1998).

1.2.1 Initiation

In eukaryotes, initiation involves at least 12 initiation factors (eIFs) which guide the 40S subunit and the initiator tRNA (Met-tRNA_i) to the first start codon on the mRNA - a process called "scanning" (reviewed in detail: Jackson et al., 2010; Hinnebusch and Lorsch, 2012; Hinnebusch, 2017) (Figure 1.1). First, in order to form a scanning competent 40S subunit the pre-initiation complex (PIC) is assembled. This step involves several eIFs binding to the small ribosomal subunit - eIF1, eIF1A, eIF3 and eIF5. Together they promote binding of the ternary complex (TC): the start codon competent Met-tRNA_i bound to eIF2-GTP. The multi-subunit complex eIF3 promotes PIC assembly, but further coordinates several events throughout the whole initiation pathway: 43S attachment to mRNA, scanning, and accurate start codon selection (Asano et al., 2000). The yeast eIF3 (yeIF3) complex contains six subunits: eIF3a (Tif32), eIF3b (Prt1), eIF3c (Nip1), eIF3g (Tif35), eIF3i (Tif34) and the non-essential, substoichiometric subunit eIF3j (Hcr1). The factors eIF1A and eIF1 are necessary for start codon recognition and induce the unlocked conformation of the mRNA binding channel, which is essential for scanning from the 5' mRNA cap. The whole assembled 43S PIC is recruited to the eIF4F cap complex, which consist of eIF4-A, eIF4-B, eIF4-E, and the scaffold protein eIF4-G (Gingras et al., 1999). It can bind to the 43S PIC directly, forming the

48S complex, thus linking it to the m7G cap binding protein eIF4-E. eIF4-G can also interact with PABPs bound to the 3' poly-A tail of the mRNA leading to mRNA circularization, which creates a closed localized translation environment for initiation and post termination complexes and ribosomal subunits (Wells et al., 1998).

To bind the first AUG start codon, the 48S complex starts 'scanning' for base complementarity of the Met-tRNA_i already bound to it, along the 5' untranslated region (UTR) of the mRNA in a 5'-to-3' direction. During this process RNA helicases (eIF4A, Ddx3 and Dhx29) can unwind mRNA secondary structure elements which would hinder the scanning process. Usually the first AUG codon detected by the scanning 43S is used for initiation, but 'leaky scanning' depending on the surrounding sequence of the AUG can result in downstream AUG initiation (Dong et al., 2008). Upon start codon recognition the factor eIF5 together with eIF5-B stimulates GTP hydrolysis of eIF2. This leads to the dissociation of the eIF2-GDP-eIF5 complex and allows recruitment of the large ribosomal subunit. After subunit joining and accommodation of the Met-tRNA_i into the P-site, an empty A-site for the next tRNA is displayed, marking the transition from the initiation to the elongation phase.

1.2.2 Elongation

Every new aa-tRNA, which can decode the next mRNA triplet displayed at the ribosomal A-Site, is delivered to the ribosome as a ternary complex together with GTP bound eEF1- α (EF-Tu in prokaryotes). If a cognate aa-tRNA is bound to the A-Site codon, GTP-hydrolysis by eEF1- α is triggered and the factor dissociates. After accommodation of the correct A-Site tRNA a peptide bond is formed with the P-site peptide or peptide chain. The result is a deacylated tRNA in the P-Site and an elongated nascent-chain tRNA in the A-site, termed the pre-translocation (PRE) state. While the tRNAs remain fixed in respect to the SSU, they can move in translocation direction on the LSU resulting in hybrid A/P and P/E states (Dorner et al., 2006). This translocation of tRNAs into hybrid states is coupled to the rotation of the SSU and LSU relative to each other and is a highly dynamic process (Blanchard et al., 2004; Frank and Agrawal, 2000). The translational GTPase

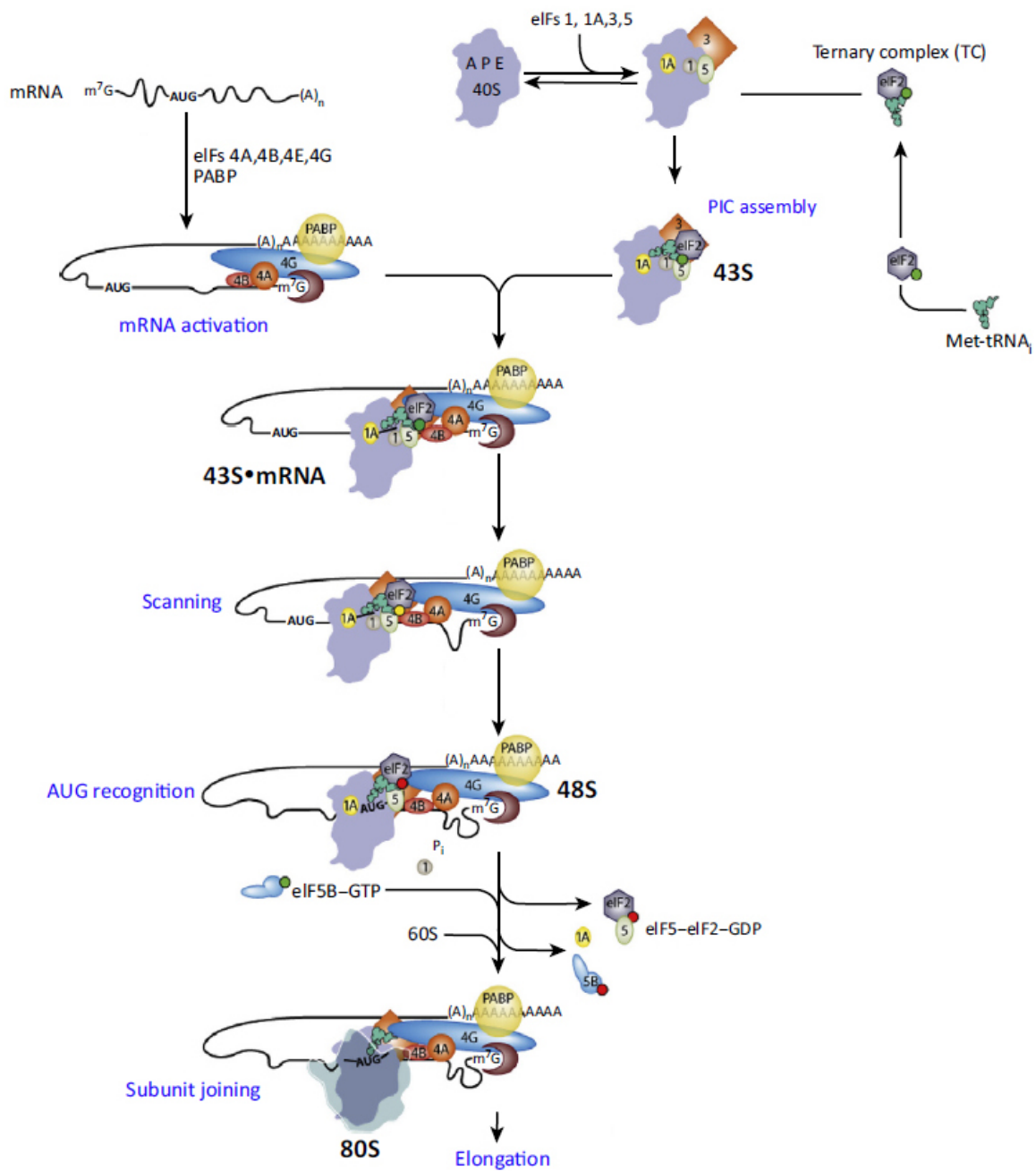


FIGURE 1.1: **Model of translation initiation in eukaryotes.** The 43S PIC is separately assembled: eIF1, eIF1A and eIF3 bind to the 40S subunit and promote binding of the TC and eIF5. Formation of the eIF4F cap complex enables recruitment of the 43S PIC, which enables scanning the mRNA for the start codon. Upon recognition of the AUG codon eIF1 dissociates and eIF5B-GTP promotes binding of the 60S subunit. During the subunit joining phase eIF5-eIF2-GDP as well as eIF1A and eIF5B-GDP dissociate from the complex. The assembled 80S subunit continues to the elongation phase and thus protein synthesis. Adapted from Hinnebusch, 2017.

eEF2 (EF-G in prokaryotes) prefers binding to ribosomes in such hybrid states (Dever and Green, 2012). GTP hydrolysis of eEF2 induces a conformational change which translocates the mRNA and tRNA by one codon in respect to the ribosome. The former P-Site tRNA (now deacylated) moves to the ribosomal E-Site, the former A-Site tRNA (now connected to the nascent chain) moves to the ribosomal P-Site, resulting in the post-translocation (POST) state. Thus, the classical tRNA positioning is re-established and the next codon is displayed in an empty A-site, restarting the elongation cycle anew, until a stop codon is displayed.

1.2.3 Termination

When the translating ribosome displays a stop codon in the A-Site, it can only be decoded by a release factor (RF), not a tRNA. Prokaryotes need two class-I release factors to read all 3 stop codons: UAG is recognized by RF1, UGA by RF2 and UAA by both RF1 and RF2. Mutagenesis studies of prokaryotic class I release factors as well as crystal structures of 70S ribosomes with RF1/2 bound, showed that RF1 and RF2 are similarly composed out of four domains: Domain 1 is interaction site for the class-II RF3 (Pallesen et al., 2013), domain 2 contains the stop codon decoding region (PxT motif for RF1 and SPF motif for RF2) and domain 3 contains the essential GGQ motif. This motif, which mediates hydrolysis of the peptidyl-tRNA and subsequent peptide release (Caskey et al., 1968; Jin et al., 2010), is the only conserved motif between prokaryotes and eukaryotes. After peptide hydrolysis, the class-II release factor RF3 binds the 70S ribosome and removes any bound RF in a GTPase like manner.

Eukaryotes, in contrast to the prokaryotes, only have one class-I release factor (eRF1), which is delivered to the ribosome by the class-II release factor eRF3. It can decode all three stop codons combinations (Frolova et al., 1994). eRF1 can be segmented into 3 functional domains (Frolova et al., 2000; Song et al., 2000): (1) the N-terminal domain which interacts and recognizes the stop codons by the NIKS motif (Bertram et al., 2000) (2) the M-domain, which contains the conserved GGQ motive, essential for peptide hydrolysis and subsequent release and (3) the C-terminal domain, which interacts with the GTPase eRF3 that delivers eRF1 (Frolova et al., 1999). Binding of the ternary complex

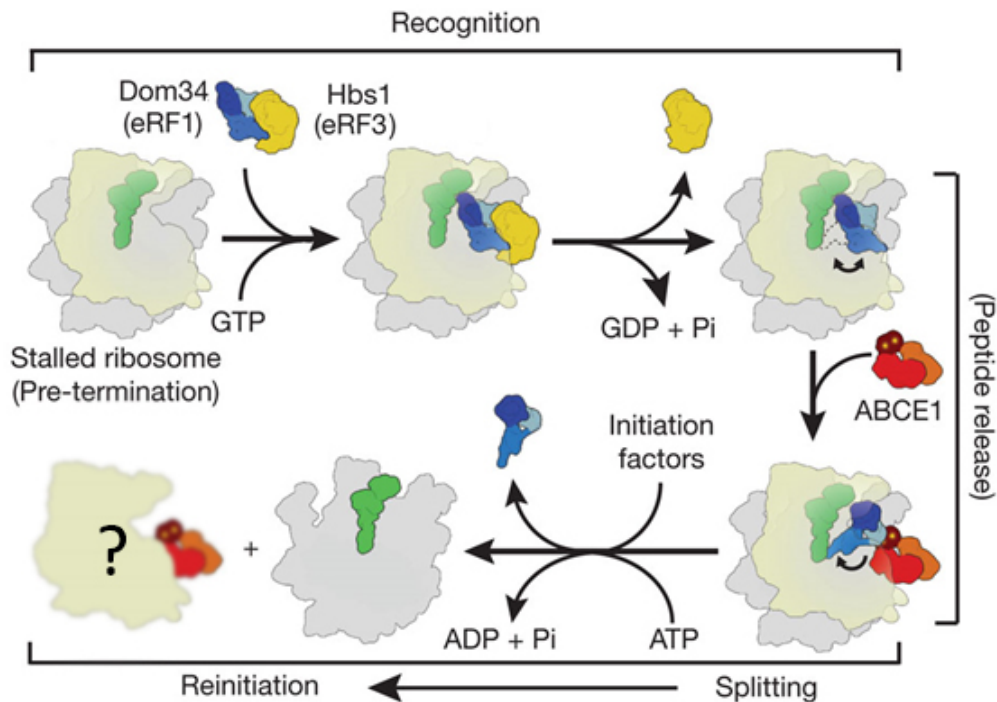


FIGURE 1.2: **Model of termination and recycling in eukaryotes.** Ribosomes (small subunit in light-brown, large subunit in grey) which are stalled or in a pre-termination state can be recognized by Dom34 or eRF1 respectively. A translational GTPase (Hbs1/eRF3) delivers its partner to the translation factor binding site on the ribosome and dissociate after GTP hydrolysis. Binding of ABCE1 stabilizes or induces a conformational change in the A-site factor (Dom34/eRF1) and promotes peptide release in the case eRF1. Subsequent ATP hydrolysis by ABCE1 splits the ribosome and recycles the subunits. While Dom34/eRF1 dissociate during this process, ABCE1 most likely stays bound to the small subunit. Adapted from Becker et al., 2012.

- eRF1 together with eRF3-GTP - to the ribosome, forms the so called pre-termination complex (Taylor et al., 2012). Subsequent hydrolysis of GTP by eRF3 results in a conformational change, which causes eRF1 to accommodate fully into the ribosomal A-Site. In addition, eRF3 dissociates from the ternary complex and the ribosome (Salas-Marco and Bedwell, 2004), which is then termed the post-termination complex.

Detailed structural insights into eukaryotic ribosome termination was

lacking and only low resolution cryo-EM of *in vitro* reconstituted complexes (Des Georges et al., 2014; Taylor et al., 2012) and crystal structures of the involved factors were available (Kong et al., 2004; Cheng et al., 2009; Saito et al., 2010). However, a model for eukaryotic termination could be proposed based on the structural and functional similarity between the canonical termination factors (eRF1, eRF3) and their ribosome rescue counterparts (Dom34, Hbs1) (Becker et al., 2011). Furthermore, the ribosome recycling factor ABCE1 (see chapter below) does not only recognize and recycle stalled ribosomal complexes containing Dom34/Hbs1 (Becker et al., 2011), but is also able to split ribosomes after canonical termination containing eRF1 and eRF3. In the model proposed by Becker et al., 2012 (Figure 1.2), which is based on the recycling of stalled ribosomal complexes, the ternary complex (eRF1 and eRF3) recognizes and binds the pre-termination complex. After disassociation of eRF3, ABCE1 would bind to the ribosomal A-site and interact with the C-terminal domain of eRF1. This could promote or stabilize the extended conformation of eRF1's central domain and position the conserved GGQ motif in a close proximity to the CCA end of the tRNA, enabling peptide release. Publication 1 of this cumulative thesis explores the role of eRF1 and eRF3 as well as ABCE1 in the context of this model and illustrates the structural background for termination and recycling. In addition, it gives insight into the mechanism of peptide-release stimulation by eRF1, explaining canonical termination in eukaryotes.

1.2.4 Recycling

After the termination of translation the remaining ribosomal complex has to be disassociated into its components: mRNA, deacylated tRNA, SSU, LSU and RF. In prokaryotes the ribosome recycling factor (RRF) mediates this process, together with the elongation factor EF-G (Barat et al., 2007; Hirashima and Kaji, 1973; Peske et al., 2005). RRF consists out of 2 domains connected by two flexible linkers: Domain I is important for ribosome binding, while domain II is flexible and thought to destabilize the inter-subunit bridge B2a after EF-G binding (Fu et al., 2016). The RRF was shown to bind in the ribosomal P-site, stabilizing a ratcheted ribosome conformation with the deacylated tRNA in the P/E hybrid state (Dunkle 2011, Weixlbaumer 2007). Binding

of EF-G-GTP was shown to split the ribosome together with the RRF into subunits after GTP hydrolysis. Interestingly, the initiation factor IF3 can already bind post-termination intermediates, supports dissociation of m/tRNA and further prevents re-association of the subunits, thus linking termination and re-initiation in prokaryotes. (Julián et al., 2011; McCutcheon et al., 1999; Dallas and Noller, 2001; Fabbretti et al., 2007; Pioletti et al., 2001).

In eukaryotes the highly conserved and essential recycling factor ABCE1 prepares ribosomal complexes for recycling by binding to eRF1 bound ribosomes after canonical termination (Pisarev et al., 2007; Jackson et al., 2012, Shoemaker and Green, 2011). Additionally, ABCE1 can further recycle vacant and stalled ribosomal complexes and could be implicated in late ribosome biogenesis quality control steps (Strunk et al., 2012). Despite its importance, the exact mode of action of ABCE1 as well as recycling in eukaryotes is poorly understood.

1.3 The role of ABCE1 in termination and recycling

The eukaryotic recycling factor ABCE1 is a member of the ATP binding cassette (ABC) enzyme family. Generally, ABC-ATPases are involved in a multitude of functions which involve trans-membrane transport, DNA repair or eukaryotic translation (Holland and A. Blight, 1999) and can be classified in several subfamilies (A-E). The twin ATPase protein ABCE1 is the only member of the subfamily E and essential in all archaea and eukaryotes (Winzeler et al., 1999; Coelho, 2005; Estévez et al., 2004).

The 68-kDa protein has three domains (Figure 1.3): A unique cysteine-rich N-terminal domain that is followed by two nucleotide binding domains (NBDs). Both of the NBDs are known to possess ATP binding pockets characteristic for ABC-ATPases: a Walker A and Walker B box, Q-loop, and signature motif. Since the NBDs are arranged in a head-to-tail manner, the Walker A/B and Q-loop of one nucleotide binding site (NBS), coordinate the binding and splitting of ATP with the signature motif of the other NBS. Because of this arrangement it has been suggested that ATP binding to ABC-ATPases (Lu et al., 2005; Smith et al., 2002) can result in a tweezer-like motion of both NBDs (Chen et al., 2003a), which in turn might be transmitted to other conformational

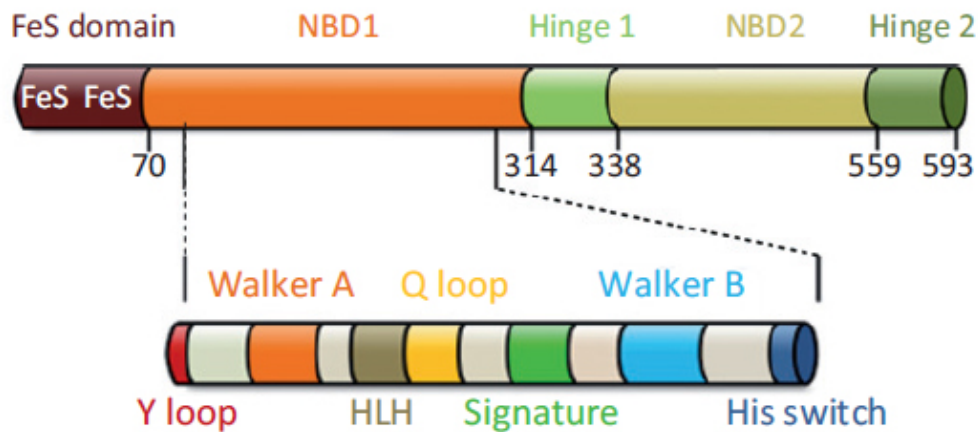


FIGURE 1.3: **Domain organization and motifs of ABCE1.** ABCE1 displays five motifs in three domains: The N-terminal iron-sulphur cluster (FeS) domain, which contains two FeS clusters, is coupled by a flexible linker to NBD1. The two NBDs display the same motifs typical for ABC transporters: Walker A/B, Q-loop and the signature motif. In addition they contain the three conserved His-switch, D-loop and Y-loop motif. NBD1 contains a specific HLH structural motif, which not present in NBD2 and other ABC classes. Two hinge regions frame NBD2, which result in a unique orientation of the NBDs towards each other. Adapted from Nürenberg and Tampé, 2013.

changes in associated domains (Does and Tampé, 2004). In this context, the unique N terminal part of ABCE1 is supposed to play an important role. It contains a iron-sulphur cluster (FeS) domain with two [4Fe-4S] clusters (Barthelme et al., 2007), followed by an anti-parallel beta-sheet (termed "cantilever arm") and flexible linker (termed "cantilever hinge"), which connects the N-terminal FeS domain to the first NBD. Since the FeS clusters are sensitive to oxidation, it has been suggested that reduced cell growth during oxidative stress can be linked to inhibition of ABCE1 (Barthelme et al., 2007). So far, typical functions like electron transfer could not be demonstrated for the FeS of ABCE1, suggesting an alternate role for this domain. ABCE1 also contains a conserved helix-loop-helix (HLH) motif inside NBD1, which is not present in other ABC enzymes, and two hinges domains (H1 and H2), which are conserved sequence regions arranged behind each NBD. The first hinge connects NBD1 and NBD2 while the second hinge is c-terminal, but both of them interact with hydrophobic areas in the NBD1:NBD2 interface. In addition the hinges mark the pivot point for the tweezers-like motion of the two NBDs. Taken together, they might

provide the structural framework to coordinate the NBDs positioning towards each other, allowing clamp-like motions of the NBDs (Karcher et al., 2005; Karcher et al., 2008). ATP binding by ABCE1 leads to the movement of both NBDs towards each other and subsequent ATP hydrolysis reverses that state (Barthelme et al., 2011). In the model proposed by Becker et al., 2012, these mechanochemical properties of ABCE1, in addition to the interaction of its iron–sulphur cluster domain with an A-site factor (Dom34/eRF1), promote the dissociation of the ribosome. It is however unclear, how this motion of ABCE1 is triggered and how it manages to split the ribosome exactly. Also its state and role after ribosome recycling is not fully understood.

In eukaryotes, termination and initiation was thought to not be connected directly (Jackson et al., 2010; Hinnebusch and Lorsch, 2012). Surprisingly, ABCE1 was found to be associated to 40S subunits bound with initiation factors eIF2, eIF5, and eIF3, implicating a possible role for ABCE1 in (re-)initiation (Skabkin et al., 2013; Andersen and Leevers, 2007; Dong et al., 2004). ABCE1 even associates with with elements of the MFC (eIF3 and eIF5) and the subunit eIF3j is suggested to directly bind to ABCE1 (Kispal et al., 2005). While canonical initiation of translation does not rely on ABCE1, it is probable that it stays transiently associated to the 40S after recycling. Thus, ABCE1 promises to closes the loop between termination, recycling and initiation (Shoemaker and Green, 2011; Nürenberg and Tampé, 2013), but experimental data proving these hypotheses were lacking. Publications 1, 2 and 3 of this cumulative thesis illustrate ABCE1 in post-termination and recycling complexes. We further explain how the eukaryotic recycling factor splits the ribosome. In addition, Publication 3 reveals the native ABCE1 complex, associated with initiation factors on small ribosomal subunits *in vivo*, which substantiates a role for ABCE1 during translation re-initiation.

1.4 Ribosome biogenesis

The cell has a constant demand for proteins and is therefore in need of a stable pool of ribosomes and ribosomal subunits. To maintain that amount and increase it during cell growth and after cell division, new functional subunits have to be biosynthesized. This complex, energy

intensive and highly regulated process is called ribosome biogenesis. In eukaryotes it requires the concerted activity of 200 assembly and ribosome biogenesis factors (RBF) and more than 75 small nucleolar RNAs (snoRNAs). Together they bind and modify the polycistronic precursor (35S pre-rRNA), which is generated by RNA polymerase POL-I. The pre-rRNA contains the 16S rRNA for the small, as well as the 5.8S and 25S rRNA for the large ribosomal subunit. The remaining 5S rRNA of the LSU is transcribed separately by POL-III. On the 35S p-rRNA, the rRNA elements of the subunits are separated by internal transcribed spacers (ITS) and flanked by external transcribed spacers (ETS), all of which are removed during the biogenesis process by endo- and exonucleolytic cleavage events (reviewed in Henras et al., 2015) (Figure 1.4).

In eukaryotes the majority of RBFs are essential (Fromont-Racine et al., 2003) and about 20% them are GTPases, ATPases, and kinases, which guide the modeling of the ribosomal subunits (Strunk and Karbstein, 2009) and the removal of snoRNAs which extensively modify the precursor rRNA (Martin et al., 2013). All RBFs and RPs which are needed for ribosome biogenesis steps in the nucleus have to be imported by importins. They can form a heterodimer out of two subunits: 1) Importin α acts as a transport adapters and recognizes the nuclear localization signals (NLS) of potential target proteins or protein complexes. 2) Importin β mediates the import by interacting with the hydrophobic environment of the nuclear pore complex (NPC). Coordinated import of whole macromolecular complexes needed for the maturation of the subunits, is used to ensure correct temporal and spatial regulation of biogenesis. (Kressler et al., 2012).

1.4.1 The 90S Preribosome

Parallel to the transcription of the rDNA by POL-I, the nascent pre-35S rRNA starts to fold with the help of snoRNAs. Four huge RBF-complexes bind the 5'ETS as well as parts of the emerging 18S rRNA element and coordinate the initial folding of rRNA. The resulting 5'-ETS-complex (U3 snoRNP, UTP-A, UTP-B and UTP-C modules) form a cradle that enables integration of SSU RPs and subsequently give rise to the 90S pre-ribosome, also termed small subunit processosome

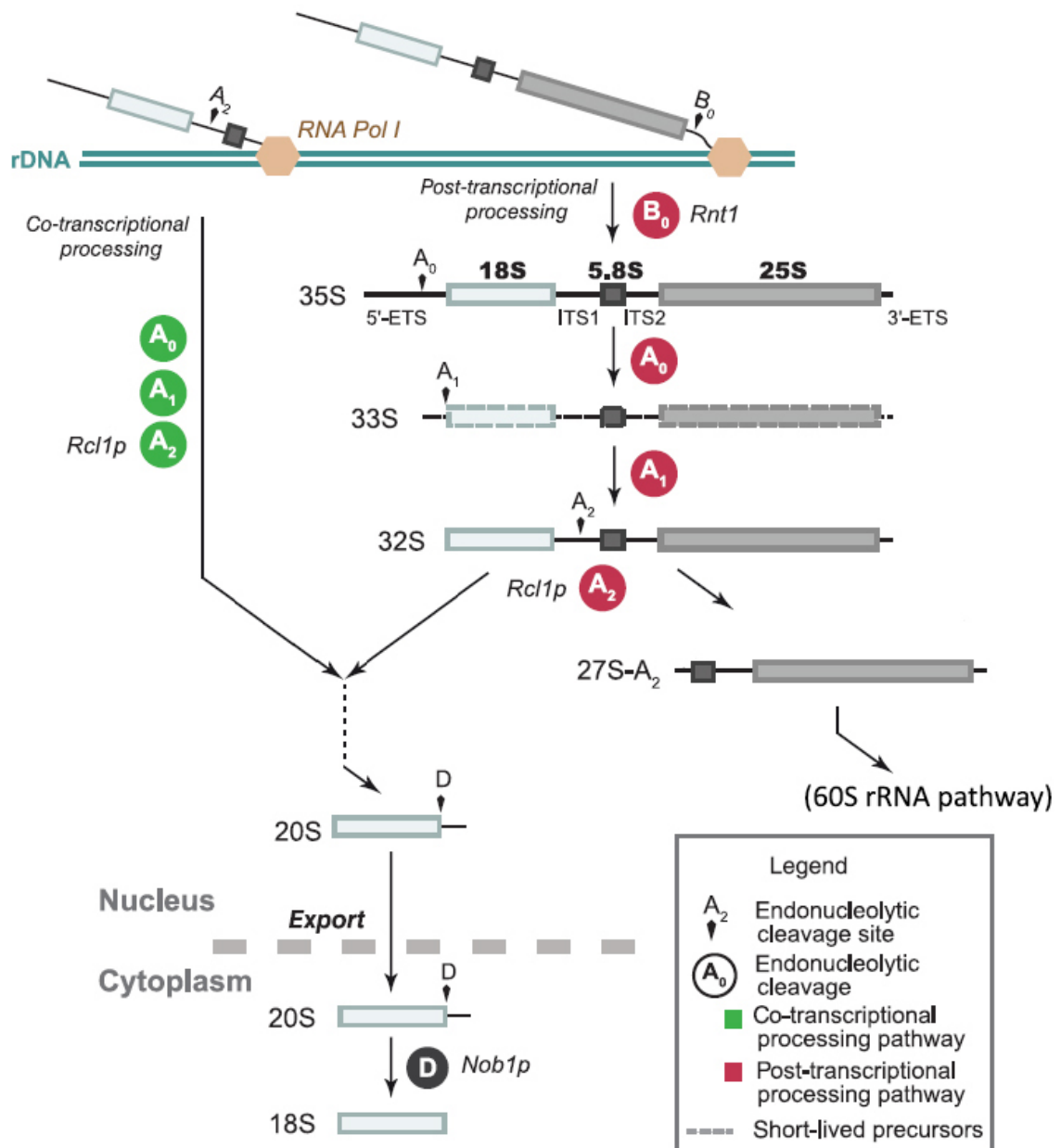


FIGURE 1.4: RNA processing steps during subunit maturation in *Saccharomyces cerevisiae*. Parallel to the transcription of the rDNA by Pol I, the resulting precursor rRNA is cleaved at the sites A₀, A₁, and A₂ (green). Alternatively, any full-length 35S pre-rRNA is processed in a similar manner (red) post-transcriptionally. Formation of 18S rRNA requires processing of the 5'-ETS at A₀ and A₁, as well as separation from the large subunit rRNA by processing of ITS1 at A₂. Afterwards, the 20S pre-rRNA of the small subunit and the 27S pre-rRNA of the large subunit are further processed during several maturation steps in the nucleus and after export. As a final maturation step, the 20S pre-rRNA is processed by Nob1p in the cytoplasm (D-site cleavage) resulting in mature 18S rRNA. Adapted from cite Henras et al., 2015.

(reviewed in Kressler et al., 2017). This huge 5 MDa complex represents the first stable intermediate of ribosome biogenesis to date and is therefore well studied and structurally investigated (Sun et al., 2017; Chaker-Margot et al., 2017; Kornprobst et al., 2016). In the 90S, elements which will later constitute to the body of the SSU (5' domain and central domain) are already folded correctly on an rRNA level and many RPs of these regions are correctly associated. The 3' major domain however, which will later form the head of the SSU, still has to undergo significant structural rearrangements and also the 3' minor domain, which mainly contains helix h44/45, has to be reorganized to be able to be accommodated at its mature position. Elements crucial for the translational activity of the subunit are also not yet formed in these 90S particles.

1.4.2 Separation of pre-40S and pre-60S maturation

As transcription of the rDNA continues, the 5'-ETS-complex is thought to disassociate, with the help of the RNA helicase Dhr1 (Sardana et al., 2015). Afterwards, endonucleolytic cleavage within ITS1 (A2 site) separates the early premature-SSU (pSSU) particle from the following LSU rRNA transcription and folding. The exact timing and multitude of factors involved in this transition have yet to be determined and the state in which the pSSU moiety is in, after it emerges from the 90S pre-ribosome is unclear. However, a huge exchange of RBFs and integration of RPs is most likely happening during this stage, as the pSSUs which are exported to the cytoplasm, were shown to only contain a handful of biogenesis factors and display many features of the mature 40S (see chapter below).

Biogenesis and required rRNA folding steps are more complex for the LSU as compared to the SSU (reviewed in detail Kressler et al., 2017) and have been intensively investigated by cryo-EM (Barrio-Garcia et al., 2016; Wu et al., 2016; Greber et al., 2016; Kater et al., 2017; Ma et al., 2017). It has been shown that correct assembly of the PTC, as well as A-, P-, and E-tRNA-binding sites on the premature-LSU (pLSU) must be completed before export from the nucleus. Activation of the RBFs Rea1 and Nog2 reshape the pre-60S subunit into an export competent structure and once inside the cytoplasm, integration of remaining RPs is coupled to detachment of the remaining associated RBFs leading to

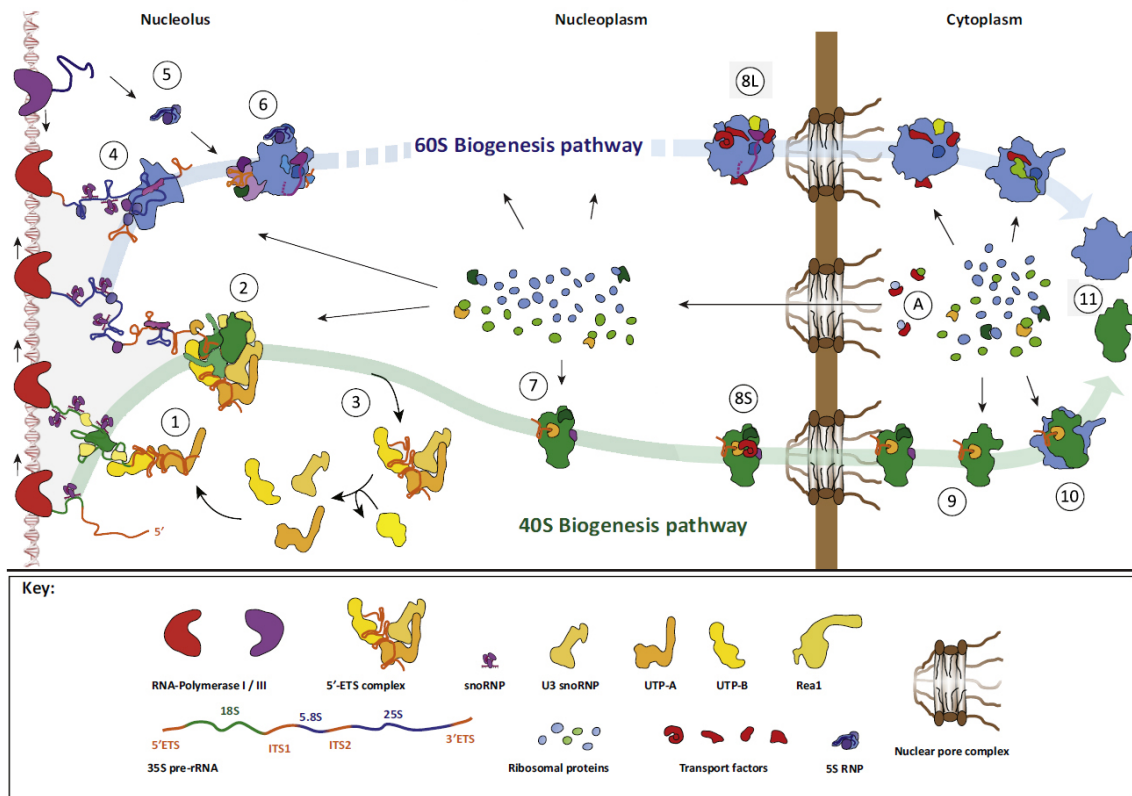


FIGURE 1.5: Biogenesis pathway of eukaryotic ribosomes. The maturation of large subunits (top, blue) and small subunits (bottom, green) is a complex process relying on more than 200 RBFs. (A) Newly biosynthesized or recycled RBFs are constantly transported (back) into the nucleus, where they are needed for proper maturation of ribosomal subunits. (1/2) While the rDNA is transcribed by RNA polymerase I, the 5'ETS complex assembles on the emerging pre-rRNA forming the 90S pre-ribosome. During the maturation of this early ribosomal particle, the components of the 5'ETS are recycled (3) and the pre-40s emerges (7). The pre-60S particle (4) form after separation from the 90S entity and completed transcription of the rDNA. (5) The separately transcribed 5S RNP binds to the early pre-60S complex (6). (8L/S) The pre-mature subunits are exported separately through the nuclear pore complex into the cytoplasm. After the last rRNA processing steps (9) the final maturation could include a joining of subunits (10). After all RBFs have disassociated from the mature subunits, they are ready to engage in translation (11). Adapted from Kressler et al., 2017.

a mature large ribosomal subunit.

1.5 Small subunit maturation

Detailed structural insight into the pre-40S maturation directly after the 90S processosome is limited. The only available complexes, which could be solved by cryo-EM (Strunk et al., 2011; Ghalei et al., 2015; Larburu et al., 2016) were able to position the overall location of late stage RBFs (Figure 1.6). These complexes depicting pSSUs from yeast and human are most likely already exported and matured in the cytoplasm (see chapter below), as they display most of the features of a mature 40S. Thus, a huge exchange of RBFs and integration of RPs did already take place, suggesting that the transition of from the much larger 90S particle to pre-40S intermediates is a rapid and possibly transient process, resulting in a fast export of pSSUs to the cytoplasm. The nuclear export factor Crm1 can export substrates containing a loosely conserved leucine-rich nuclear export signal (NES) pattern out of the nucleus into the cytoplasm (Wen et al. 1995; Fornerod and Ohno 2002; la Cour et al. 2004) and both ribosomal subunits are exported from the nucleus by Crm1 with the help of the Ran GTPase Gsp1 (Hurt et al., 1999; Moy and Silver, 1999 ; Stage-Zimmermann et al., 2000; Moy and Silver, 2002). While for the LSU, the export adaptor protein could be unambiguously identified (Nmd3) (Gadal et al., 2001) the analogous adapter could not yet be determined for the pSSU. Instead, several RPs and at least 3 NES containing RBFs (Ltv1, Pno1 and Rio2) are implicated in Crm1 mediated export (Zemp et al., 2009; Seiser et al., 2006; Vanrobays et al., 2008). Since Ltv1 is not essential, efficient pSSU export most likely does not rely on that RBF, but might require several export adapters. Another possibility is that it serves as a redundancy between different pSSU export adapters (Fas-sio et al., 2010). The RBF Rrp12, which is already present in early 90S complexes, is also suggested to be involved in subunit export (Vanrobays et al., 2008; Oeffinger et al., 2004). It could additionally be able to interact with the FG-repeats of nucleoporins of the NPC and thereby protect any hydrophilic surfaces of the pSSUs during export. In addition to several RBFs, the RP uS19 is implicated in the formation

of export competent pre-40S particles, despite not showing any functional nuclear export signal (Léger-Silvestre et al., 2004). Depletion of uS19 results in accumulation of 20S pre-rRNA containing pSSUs in the nucleus, which display late pre-40S RPs bound. This suggests that the role of uS19 integration is export related rather than maturation related.

In conclusion, the intermediates of the small subunit which emerge from the 90S particles could not be investigated yet and the adaptor protein(s) for pSSU export are also not yet clearly identified. In addition, the export process for the pre-40S subunit is poorly understood. In this context, it is also up to debate whether the currently available structures of pSSU complexes have already been exported to the cytoplasm. Understanding the detailed interactions between RBFs and pre-rRNA after the pSSU emerges from the 90s, will most likely be the first step to map the early maturation phases of small subunits in greater detail.

1.5.1 Cytoplasmic biogenesis and involved factors

The cytoplasmic maturation of pre-40S subunits can be segmented into two events: (a) maturation and endonucleolytic cleavage of the 20S pre-rRNA to the mature 18S rRNA and (b) finalizing the formation of the 'beak' structure and thereby complete maturation of the SSU 'head'. The RBFs which are thought to be still present after export and most likely play a role in these cytoplasmic maturation steps are: Dim1, Enp1, Ltv1, Nob1, Pno1, Rio2 and Tsr1 as well as Hrr25 and possibly Prp43.

The essential 18S rRNA dimethylase (Dim1) is responsible for the conserved dimethylation of two adjacent adenosines near the decoding site in 3'-terminal loop of 18S rRNA (Lafontaine et al., 1994). In addition, it is implicated in nucleolar pre-rRNA cleavage at sites A1 and A2 in the early 90S particle Lafontaine et al., 1995; Lafontaine et al., 1998, however its role in this context is not fully understood.

Enp1 is already present in the 90S (Sun et al., 2017; Chaker-Margot et al., 2017; Kornprobst et al., 2016) and implicated in 35S pre-rRNA processing at sites A0, A1 and A2 (Chen et al., 2003b), together with the U3 and U14 snoRNAs. It remains bound to the maturing SSU and after export to the cytoplasm and facilitates uS3 integration together

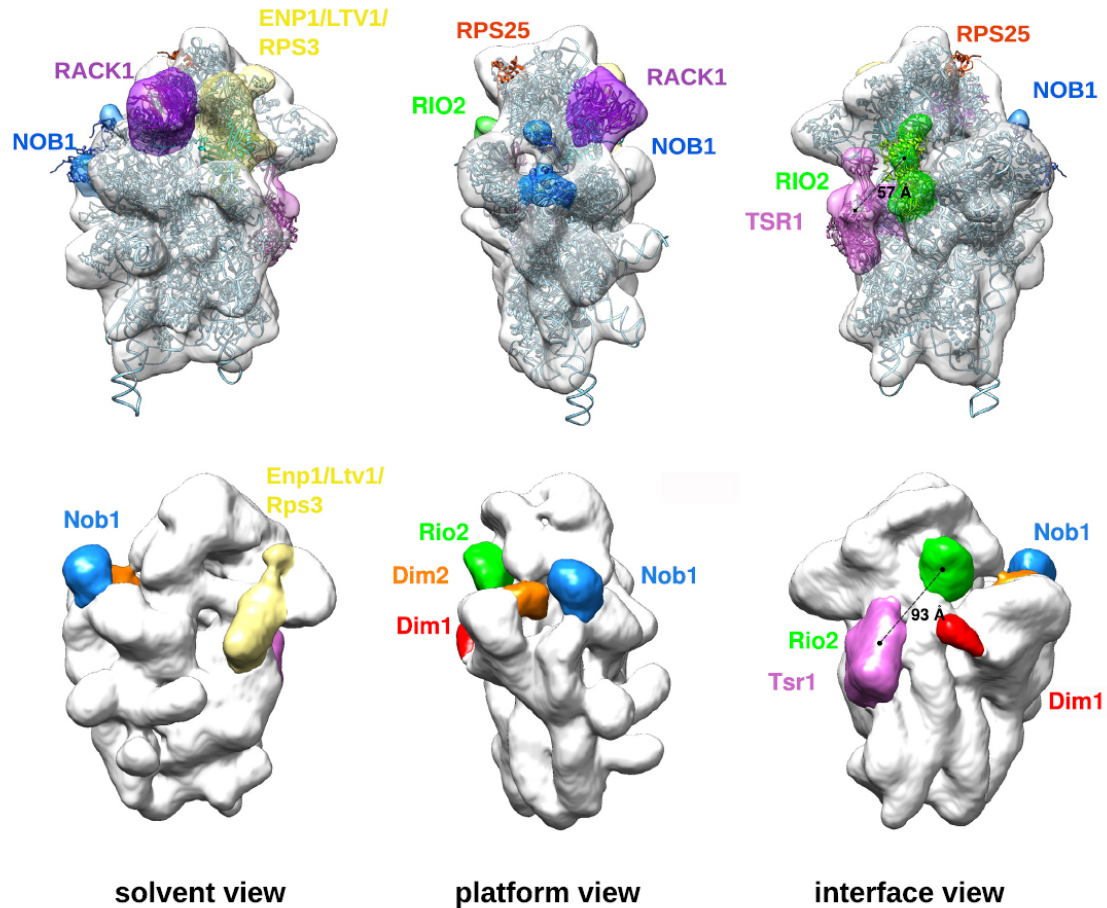


FIGURE 1.6: Cryo-EM structures of human and yeast pre-40S complexes. Electron density maps of HAST-LTV1 purified human pre-40S particles (top) compared to Rio2-TAP purified pre-40S particle from *Saccharomyces cerevisiae*. The quality of the maps allows to compare the overall position of known RBFs / RBF-complexes. The solvent view illustrates the absence of RACK1 (dark-pink) in the yeast particle and a similar position for the Enp1/Ltv1/Rps3 complex (yellow) near the beak of the small subunit. In the platform view, Nob1 (blue), which processes the 3' end of the 20S pre-rRNA, is located in a similar position in both structures. Dim2 (orange) could not be allocated in the human map. Interestingly, the position of Rio2 (green) differs significantly between the two particles while Tsr1 (light-pink) is at a similar position (interface view). The RBF Dim1 (red) could not be allocated in the human map. Adapted from Larburu et al., 2016.

with Ltv1 and Hrr25. (Ghalei et al., 2015; Schäfer et al., 2006).

The non-essential low temperature viability protein 1 (Ltv1) is a largely unstructured protein implicated in nuclear export (Schäfer et al., 2003; Seiser et al., 2006). It also plays a role in uS3 integration together with the RPFs Yar1 and Hrr25 (Loar et al., 2004; Ghalei et al., 2015). Ltv1 can form a very stable complex together with Enp1 and uS3, which is supposed to play a role during the 'beak' formation of the pSSU (Schäfer et al., 2006).

The Nin one binding protein (Nop1) cleaves 20S pre-rRNA at the conserved D-Site with its N-terminal PIN domain, to generate the mature 3' end and 18S rRNA (Fatica et al., 2003; FATICA, 2004). While already associated with pre-40S complexes in the nucleus, this essential cleavage takes place in the cytoplasm after export. Together with the regulator Pno1, Nob1 is located at the platform region of the pSSU. It has been suggested that the DEAH box RNA helicase Prp43, which is also involved pre-60S and 90S processing (Lebaron et al., 2005), can act together with Ltv1 to further enhance the cleavage of 20S by Nob1 (Combs et al., 2006; Pertschy et al., 2009). The ATPase Fap7 is also required for cleavage at site D, while most likely not directly involved in the cleaving of site D (Granneman et al., 2005).

The RBF partner of Nob1 (Pno1) belongs to the family of single-stranded RNA binding proteins and is thought to interact with the 3' end of the 18S rRNA with its KH-domains (Vanrobays et al., 2004). It regulates the maturation of 20S to 18S rRNA by cleavage at site D together with the endonuclease Nob1 (Lamanna and Karbstein, 2009; Lamanna and Karbstein, 2011; Woolls et al., 2011) and is bound already to early 90S pre-ribosomes in the area which will later mature to the platform of the SSU (Kornprobst et al., 2016; Senapin et al., 2003).

The essential serine kinase Rio2 plays a central role in processing of the 20S pre-rRNA into mature 18S rRNA (Schäfer et al., 2003; Geerlings et al., 2003; Vanrobays et al., 2003), is conserved in all archaea and eukaryotes and binds to the pSSU at the subunit interface (Strunk et al., 2011). hRio2 is implicated in the recycling of cytoplasmic maturation factors to the nucleus (Zemp et al., 2009) but not essential for nuclear export of pSSUs. However, it can still bind to the export factor Crm1 via its C-terminal NES.

The essential RBF twenty-S rRNA accumulation 1 (Tsr1) connects the head and the body of the pre-40S particle (Strunk et al., 2011; Larburu

et al., 2016), binding to the region which later forms the universal translation factor binding site. The four domains of the protein display a similar domain architecture compared to translational GTPases (Wegierski et al., 2001), however due to a lacking active site, Tsr1 is unable to bind or hydrolyse GTP (McCaughan et al., 2016). Its positioning on the pSSU would prevent binding of several initiation factors (eIF1A, DHX29 and eIF5b) (Larburu et al., 2016), suggesting its removal is an essential step in late biogenesis stages.

In conclusion, the universally conserved generation of the mature 18S rRNA from 20S rRNA in eukaryotes (Rouquette et al., 2005) involves at least three RBFs: Pno1, Nob1, Rio2 as well as other trans-acting factors. While the role of these RBFs has been investigated on their own, how they coordinate maturation events together is not fully understood. The final conformational changes of the SSU 'beak' maturation are regulated by a (de-)phosphorylation cycle(s) of uS3, Ltv1 and Enp1 by Hrr25, but the exact sequence of events and targets is also not yet known. The only available structures from yeast and human (Strunk et al., 2011; Ghalei et al., 2015; Larburu et al., 2016) gave the first insight into the overall shape of the pSSU and location of the RBFs involved. To extend these models, publication 4 of this cumulative thesis presents the first high resolution structure of a late stage pSSU complex. Detailed molecular insight into the state of the rRNA and its interaction with the RBFs are presented.

1.5.2 Preventing premature translation

Previous cryo-EM reconstructions combined with RNA–protein cross-linking experiment let to the conclusion that pre-40S particles exported to the cytoplasm contain seven to ten RBFs (Strunk et al., 2011; Larburu et al., 2016; Granneman et al., 2010). In the current model resulting from these preliminary studies, the majority of RBFs are thought to be specifically positioned to protect the pSSU from premature interaction with the mRNA, translation initiation factors or the LSU. In detail, the RBFs located in the subunit interface of the pSSU (Tsr1, Rio2, and Dim1) prevent initiation factors eIF1, eIF1A, and eIF2-tRNAⁱ Met from binding the not yet matured SSU. Furthermore the RBFs Nob1 and Pno1, which are thought to bind at the platform region of the pSSU and later cleave the 20S pre-rRNA, would also overlap with

binding sites of eIF3, which has a central role in the process of translation initiation. Finally, recruitment of mRNA is most likely omitted by Enp1 and Ltv1 which would interfere with the opening of the mRNA channel. The binding sites of several RBFs overlaps with the positions of RPs not integrated in the pSSU, suggesting that their cytoplasmic release is essential for integration of uS3, uS10a and uS26 and making the small subunit initiation competent. However, it must be stated that the positioning of the RBFs is not just solely a steric hindrance for potential tRNAs and eIFs, but their location might rather be related to the maturation process itself. Publication 4 of this cumulative thesis provides an alternative interpretation for the positioning and role of late stage maturation RBFs.

1.5.3 Proposed final maturation steps

To ensure that only properly matured SSUs, which have all active sites correctly folded, can enter the pool of translating ribosomes, a quality control step has been suggested. This model of a "translation-like" cycle coupled to the final maturation steps, originates from 80S like particles containing a fully matured LSU, but a premature SSU. These complexes could be purified from cells lacking any late stage RBFs (Fab7, Rio1 and Nob1) which are involved in 20S pre-rRNA processing (Granneman et al., 2005; Soudet et al., 2010; Ferreira-Cerca et al., 2014). These 80S-like particles, lack mRNA as well as translation and initiation factors, which suggests that these complexes did not originate from a canonical translation event (Strunk et al., 2012). However, it could be shown that the GTPase eIF5b (Fun12 in yeast) together with the 60S subunit, promote processing of the 20S rRNA (Lebaron et al., 2012). It could further be shown that depletion of ABCE1 or Dom34 leads to the accumulation of late stage RBFs (Nob1, Pno1, Enp1 and Dim1) (Soudet et al., 2010). The model suggests that ABCE1 together with Hbs1/Dom34 could disassociate the ribosomal subunits after their final maturation stage in a similar manner as in dissociating inactive ribosomes originating from starvation stress (Van Den Elzen et al., 2014).

Still, it is unclear how these 80S-like complexes form. Especially with several RBFs still attached in the inter-subunit space, proper binding of the LSU is questionable. Also, whether the "translation-like" cycle

is the final maturation step for the LSU and SSU or a functional way of recycling immature subunits from the ribosomal pool of translation is unclear. Taken together, the functional relevance of the proposed process needs to be tested in future studies.

2 Aims of thesis

Eukaryotic ribosome recycling (Publication 1,2 and 3)

In contrast to prokaryotes, detailed insight into the eukaryotic termination and recycling process was lacking. Previously, only low resolution cryo-EM structures of in vitro reconstituted complexes (Des Georges et al., 2014; Taylor et al., 2012) as well as crystal structures of the release factors were known (Song et al., 2000; Kong et al., 2004). Also the mechanism of the recycling factor ABCE1 during canonical translation remained largely enigmatic (Pisarev et al., 2007; Jackson et al., 2012). However, no-go mRNA decay (NGD) and non-stop mRNA decay (NSD) pathways which are also dependent on the splitting of ribosomes by ABCE1 gave first insights into the structural basis of ribosome recycling by ABCE1 (Becker et al., 2011; Becker et al., 2012). The aim of this project was to investigate ABCE1's role and function during the canonical termination and recycling phases in eukaryotes and archaea and to gain insight into these final moments of translation. Further analysis focused on unraveling the mechanism of ribosomal splitting, the fate of the eukaryotic recycling factor thereafter and its potential role in re-initiation.

Biogenesis of the small subunit in eukaryotes (Publication 4)

Ribosome biogenesis involves numerous assembly intermediates, generated along a complex pathway (Kressler et al., 2017). In contrast to the large ribosomal subunit, the maturation path of the small subunit after it emerges from the 90S processosome, is largely unexplored. So far only two structures were able to investigate the overall location of ribosome biogenesis factors in *S. cerevisiae* and *H. sapiens* (Strunk et al., 2011; Larburu et al., 2016). However, the detailed mode of operation of these RBFs and the maturation state of the pre-RNA could not be determined. We intended to present detailed answers to these

open questions by resolving a high resolution cryo-EM structure of an eukaryotic pre-mature small ribosomal subunit. In addition, we addressed the role of the RBFs in concert with each other and how they guide pre-rRNA folding and the maturation of the small subunit.

3 Cumulative Thesis: Summary of Publications

3.1 Publication 1

Cryo-EM structures of eukaryotic translation termination complexes containing eRF1-eRF3 or eRF1-ABCE1

Preis A, *Heuer A* , Barrio-Garcia C, Hauser A, Eyler DE, Berninghausen O, Green R, Becker T, Beckmann R.

Cell Reports - 2014 Jul 10

The structural and mechanistic insight for ribosomal termination was limited to low resolution cryo-EM of *in vitro* reconstituted complexes (Taylor et al., 2012) and was lacking for eukaryotic recycling complexes. Therefore, many key questions are left unanswered: (1) How is peptide release induced in eukaryotes ? (2) How does eRF1 recognize the stop-codon (3) What is the role of the eukaryotic recycling factor ABCE1 during termination ? (4) How are the ribosomes technically split ?

With the goal to provide answers to these key questions we investigated termination and recycling complexes with high resolution cryo-EM obtain molecular insights into the underlying mechanisms. In order to enrich these transient complexes, the ternary complex (eRF1 + eRF3) was bound to ribosomal complexes stalled by a cytomegalovirus mRNA to display a UAA-stop-codon in the A-site. A hybrid interspecies mix of ribosomes from wheat and yeast release or recycling factors in

the presence of non-hydrolyzable GTP analog guanylyl imidodiphosphate (GDPNP) had to be used to further stabilize the transient complexes for cryo-EM. Consequently, the termination complex containing eRF1 and eRF3 as well as the pre-recycling complex containing eRF1 and ABCE1 could both successfully be assembled and resolved to a resolution of 9 Angström by cryo-EM. While this result would no longer be considered high resolution for current standards, it was a significant improvement in the era before direct electron detectors became available for cryo-EM.

The structure of the pre-termination complex displayed the ternary complex (eRF1/eRF3) as well as the P-site tRNA in similar positions observed in previous low resolution termination and mRNA surveillance complexes (Taylor et al., 2012; Becker et al., 2012; Des Georges et al., 2014). Due to the higher resolution we could show that the N-terminal domain (NTD) of the release factor eRF1 reaches from the A-site into the decoding center of the SSU. The NIKS-loop of eRF1, which is critical in stop-codon recognition in eukaryotes could be positioned in the similar decoding position as compared to the equivalent PVT/SPF-loop in bacterial release factors (Laurberg et al., 2008; Weixlbaumer et al., 2008). This indicated that the mechanism of stop codon decoding is conserved in prokaryotes and eukaryotes, despite their significant differences. Later, high resolution structures by the Beckmann lab and other labs disproved this conclusion (see discussion).

At the interface of eRF1 and eRF3 we could visualize the essential GGQ-loop of eRF1, which mediates peptide release. In its current state, dramatic conformational changes would be needed to position the central domain and the GGQ-motif of eRF1 proximal to the PTC. These changes are essential to allow peptide release and termination of translation.

Exactly this transition is observed in the in the post-termination/pre-recycling complex containing eRF1 and ABCE1. While the overall conformation of the ribosome and position of eRF1 remained essentially unchanged, indeed the central domain compromising the GGQ-motif is stretched out towards the PTC of LSU, contacting the CCA-end of the P-site tRNA. Despite being otherwise unrelated to prokaryotes the positioning of the GGQ-loop as well as the elongated conformation of the central domain is equivalent to the conformational changes observed with bacterial RFs (Laurberg et al., 2008; Weixlbaumer et al., 2008),

further highlighting a mechanistic conserved mode of action. The C-terminal domain of eRF1 contacts the FeS-domain of ABCE1, which is located in the same position as seen previously in stalled ribosome recycling complex (Becker et al., 2012). Due to the limited resolution of ABCE1, no further insights than already observed in NDG and NSD recycling complex could be gained. The triggers for ribosome splitting remained enigmatic.

In conclusion we could show that stop codon decoding and peptide release is uncoupled during termination and that the catalytically important GGQ loop is either packed against eRF3 or positioned toward the PTC when bound to ABCE1, explaining the termination of translation in eukaryotes.

3.2 Publication 2

Structure of the ribosome post-recycling complex probed by chemical cross-linking and mass spectrometry

Kiosze-Becker K, Ori A, Gerovac M, Heuer A, Nürenberg-Goloub E, Rashid UJ, Becker T, Beckmann R, Beck M, Tampé R.

Nat Communications - 2016 Nov 8

Structural insights into the eukaryotic recycling factor ABCE1 are available from stand alone X-ray structures (Karcher et al., 2008; Karcher et al., 2005) as well cryo-EM of pre-recycling complexes from canonical termination and mRNA surveillance (Becker et al., 2012; Preis et al., 2014). While, it has been suggested that ABCE1 remains bound to the 30S/40S subunit after ribosomal splitting, the structure of this post recycling complex (PRC) and the function of ABCE1 remained unknown (Barthelme et al., 2011; Nürenberg and Tampé, 2013).

To investigate the fate of ABCE1 after ribosomal splitting we combined chemical cross-linking with mass spectrometry and cryo-EM to address the architecture of the post-recycling complexes in the archaea *S. solfataricus*. We used non-hydrolysable adenylyl-imidodiphosphate (AMP-PNP) to stably arrest ABCE1 in the presence of 30S subunits, which is crucial to prevent release of ABCE1 from the complex. Lysine-specific cross-linking was conducted on the 30S-ABCE1-AMP-PNP complexes, which were assembled *in vitro*. We can show that ABCE1 is bound at the translation factor binding site on the small subunit by XL-MS. This finding is supported by the 17 Angström low resolution cryo-EM structure. The overall positioning of ABCE1 on the SSU is similar to those observed in the canonical recycling and mRNA surveillance complexes (Becker et al., 2012). The Fe-S cluster domain however, could be observed in a novel position. A significant rotation of the whole domain towards a cleft between h44 and e12 could be visualized in the cryo-EM map. The cross-links of ABCE1 and its position in the cryo-EM map reveal that solely NBD1 and the FeS cluster contact the small ribosomal subunit. NBD1 is contacting e24 in a similar manner as observed in

the canonical recycling and mRNA surveillance complexes. We speculate that the binding of AMP-PNP and lack of an A-site factor allows the conformational change observed. We further suggest that the observed rotation of the Fe-S cluster domain most likely plays a role in the splitting mechanism of ribosomes.

3.3 Publication 3

Structure of the 40S-ABCE1 post-splitting complex in ribosome recycling and translation initiation

Heuer A, Gerovac M, Schmidt C, Trowitzsch S, Preis A, Kötter P, Berninghausen O, Becker T, Beckmann R, Tampé R.

Nature Structural and Molecular Biology (NSMB) - 2017 May 7

Already several structures could visualize the eukaryotic recycling factor ABCE1 in a pre-splitting state and previous studies showed that eRF1 is required for ABCE1-dependent ribosomal subunit splitting (Pisarev et al., 2010; Shoemaker and Green, 2011). A direct interaction of the Fe-S domain of ABCE1 with the C-terminal part of eRF1 could further be revealed by cryo-EM (Preis et al., 2014; Brown et al., 2015). Still, no post-splitting complex could be structurally investigated and splitting mechanism itself remained speculative (Becker et al., 2012). Targeting post-splitting or splitting intermediate complexes proved very challenging, as any attempts to target the transient (post-)splitting complexes by arresting ABCE1 with non-hydrolysible AMP-PNP resulted in pre-splitting complexes. In addition, mutations which would limit the activity of ABCE1 were shown to be either lethal to the cell or abolished splitting (Karcher et al., 2005). In order enable ribosomal splitting but preserve the resulting complex, ribosomes were chemically split in low magnesia and high salt conditions in the presence of ABCE1 and AMP-PNP. This enabled us to purify an ABCE1 containing post splitting complex. Novel emerging GPU accelerated in silico data processing techniques enabled us to refine the data beyond 4 Angström despite the orientation bias of the particles. The resulting high resolution cryo-EM structure depicted ABCE1 with both NBDs completely compacted, making it the first visualize closed E-type ATPase. Furthermore, it showed the drastic 150 degree rotation of the whole FeS cluster domain into the inter-subunit space, right next to h44, in much greater detail then observed in arachea (Kiosze-Becker et al., 2016). Detailed analysis of the *S. cerevisiae* post-recycling complex confirmed the compaction of the NBDs of ABCE1 and revealed the first closed

state of an E type ABC ATPase system. While, we could show that both NBS are occupied, the densities inside the NBS could not unambiguously identified as AMP-PNP, due to the orientation bias of the cryo-EM sample, which prevented refinement to even higher resolution. We show however, that the movement of the NBDs towards each other forces the FeS cluster to change its position. The drastic rearrangement of the FeS cluster from the pre-splitting to the post splitting state exhibits a force onto any A-site factor. We propose that in the case of canonical termination the release factor eRF1 is pushed like a wedge into the inter-subunit space by the FeS cluster of ABCE1 in a concerted mode of action. This decreases the stability of inter-subunit bridges and results in the splitting of the ribosome. We claim that this splitting process is conserved in archaea and eukaryota and identical for all ribosomal splitting process. After ribosomal splitting, ABCE1 exhibits an additional property as an anti-associative factor. We show that the FeS cluster would clash with the large subunit protein uL14, thus preventing timely re-association of the two subunits with each other. This finding further agrees with the anti-associative property of ABCE1 observed during the purification process.

To complement our observations and underline that the observed state and its conclusions for the eukaryotic splitting process are applicable *in vivo* we used affinity-tagged ABCE1 to purify native ABCE1-containing 40S complexes. The native complex displayed the same conformation of ABCE1 as observed in the *in vitro* splitting experiments. Also the location of the FeS cluster domain is identical in the native complex, further substantiating our mechanistic model of ribosomal splitting. The native complex did also contain the initiation factors eIF1A and eIF2 and subunits of eIF3. We could, for the first time, resolve eIF1A together with a tRNA/eIF2 density and ABCE1 in a post-splitting complex. Future investigation will likely unravel the role of ABCE1 in re-initiation, which was outlined by the native complex.

In conclusion we could observe the repositioning of ABCE1 after the splitting of the ribosome and explaining the splitting mechanism in eukaryotes. In addition the novel position of the FeS cluster of ABCE1 explains a newly observed anti-association activity. The structure of the native post-splitting complex suggest a coordination of termination, recycling, and initiation by ABCE1.

3.4 Publication 4

Cryo-EM structure of a late pre-40S ribosomal subunit from *Saccharomyces cerevisiae*

Heuer A, Thomson E, Schmidt C, Berninghausen O, Becker T, Hurt E, Beckmann R.

Elife - 2017 Nov 20

Structural insights into the maturation states of the small subunit, after the intermediates emerge from the 90S processosome, is very limited. To date, only the general shape and overall position of the RBFs was made available by cryo-EM in *S. cerevisiae* and *H. sapiens* (Strunk et al., 2011; Ghalei et al., 2015; Larburu et al., 2016). With the goal to gain a better mechanistic understanding of the SSU maturation process on a molecular level, we investigated pre-40S maturation with the help of high resolution cryo-EM. Using the well-defined biogenesis factor Ltv1 with a Flag-TEV-ProteinA (FTpA) tag as bait we were able to obtain homogeneous pre-40S particles, resulting in a map with an average resolution of 3.6 Angström. This enabled us to determine the state of the pre-rRNA as well as build and refine the models of all RBFs bound to the pSSU.

We observed the stably bound RBFs Enp1, Tsr1, Rio2 and Pno1 and identified the absence of several not yet incorporated RPs (RACK1, uS10, uS14, eS10, eS26 and uS3). Atomic models could be build for Tsr1 and Pno1, while in the flexible regions Enp1 and Rio2 were modeled on a secondary structure level. The overall architecture of the pSSU did mainly show mature 40S features, but several regions of the pre-18S rRNA displayed distinct conformational differences. We show, that major rRNA condensation events have to be coordinated by the bound RBFs to allow complete maturation of the pSSU on a rRNA level. The functionally important elements of the small subunit: the A-,P- and E-site as well as the mRNA entry and exit path, were not correctly folded yet. We further observe that h34 is dislocated in our structure and does not form a three-way junction with h35 and h38. This prevents proper integration of many RPs which contact h34: uS3, uS10, eS10 and uS14. We show that the biogenesis factor Enp1 locks h34 in its premature state, by connecting it to h16 and forming a link

between beak and body of the pSSU. Thereby, Enp1 retains the beak and also the head of the SSU in position. This effect is supported by Tsr1 from the opposite side of the head (see below) and results in a tilt of the whole head by a bend at h28.

On the platform of the pSSU, Pno1 together with the endonuclease Nob1, control the final cleavage events of the pre-18S rRNA by producing the mature 3' end (Lamanna and Karbstein, 2009). While we lack Nob1 in our purification, we do observe Pno1 in detail and in a unique positioning. It protects the 3' end against cleavage upstream of the D-site by Nob1 and in parallel is able sense conformational changes of the head by interacting with the tilted h28. Pno1 coordinates the pre-rRNA of the 3'end with a multitude of interactions up to the pre-terminal base (U1799) of D-Site cleavage by Nob1. Pno1 further forms interactions with last base of the h44-h45 linker (U1769), which later will form a part of the active P- and mRNA binding sites.

Critical rRNA sites of the small subunit are also located at the tip of h44. It contains two universally conserved adenosine bases (A1754 / A1755, A1492 / A1493 in *E. coli*) which are essential for mRNA decoding (Ogle et al., 2003). We observe that h44 is bend outwards and the rRNA at the tip as well as the nucleotides connecting h44 to h28 (1630-1644) as well as h44 to h45 (1754 - 1769), to be flexible and unstructured. Consequently the pSSU does not contain a functional A or P site and is thereby inapt to initiate translation.

We further observe that the accommodation of h44 and maturation of these essential rRNA elements is obstructed by the GTPase-like RBF Tsr1. We were able to build the N-terminal part of Tsr1, which forms a 35 Angström α -helix, which pierces into the ribosome between h5 and h44. Thereby, Tsr1 supports the bend conformation of h44 and the unfolded tip of h44, serving as a distance enforcing wedge. The C-terminal part of Tsr1 contacts h30 to h32 at the immature head of the pSSU, providing an additional stabilization of the complex together with Enp1 and Ltv1 which connect from the opposite side. This makes Tsr1 a unique RBF, which is involved in the maturation of several domains of the SSU as structural support.

Taken together, we resolved the late stage RBFs and their interactions with the pre-rRNA to great detail. This enabled us visualize that essential rRNA elements of the A-,P- and E-site as well as the mRNA entry and exit path are still not matured. We propose that the final rRNA

folding steps of these functionally important sites is coordinated by a concerted disassociation of the bound RBFs.

4 Discussion

4.1 ABCE1: Recycling and (re)initiation

Our studies show that eukaryotic termination and recycling involve the three factors eRF1, eRF3 and ABCE1 and that they exhibit similar conformational transitions as previously predicted in the context of stalled ribosome rescue by Pelota, Hbs1, and ABCE1 (Becker et al., 2012). We indicate that the binding of ABCE1 is dependent on the departure of eRF3 and show that the interaction of eRF1 and ABCE1 stabilizes the fully extended conformation of the GGQ motive of eRF1. Follow-up investigations of *H. sapiens* termination complexes by Mathiesl et al., 2015 and Brown et al., 2015 further confirmed our initial findings and revealed the mechanisms of stop codon decoding by eRF1 in greater detail. However, in the context of ribosome recycling, these pre-splitting complexes (pre-SC) did not provide additional insight.

Our facilitated splitting approach however, from the archaea *S. solfataricus* and *S. cerevisiae* did yield the 40S–ABCE1 post-splitting complex (post-SC). These structures provided the first example of an asymmetric twin-ABC-type ATPase system in a fully closed state. We describe the FeS cluster domain of ABCE1 as the central element responsible for the splitting of ribosomal subunits. The whole FeS cluster domain of ABCE1 rotates by 150 degrees when transitioning from pre-SC to post-SC. Meanwhile, the structure of the FeS cluster proved itself to be a very rigid entity and therefore remained essentially unchanged when comparing the 80S and 40S bound state. Based on these findings we projected the movement of the FeS cluster from the pre-SC to the post-SC, which enabled us to propose the model for ribosome splitting in eukaryota in two phases:

- (1) In the first phase, the FeS cluster domain is in direct contact with an A-site factor (eg. eRF1 or Pelota). Upon closure of the two NBDs, and ATP binding, the rigid FeS domain has to move and therefore

pushes the A-site factor, which acts as a ‘molecular wedge’, into the inter-subunit space. The wedge, powered by ABCE1, destabilizes the inter-subunit bridges and subsequently splits the ribosome in eukaryota. This model of the first phase is in agreement with studies showing that the presence of an A-site factor is essential for the splitting activity of ABCE1 (Pisarev et al., 2010; Shoemaker and Green, 2011; Van Den Elzen et al., 2014). Similar to other disassembly machines (Sauer et al., 2004; Monroe and Hill, 2016) phase one of this splitting process may be dependent on multiple rounds of ATP binding, occlusion, and hydrolysis.

(2) In the second phase, the FeS cluster domain will complete its transition by fully rotating 150 degrees into a cleft near h44. This position and new contacts made with eS12 and h5/44 stabilize ABCE1 on the 40S subunit. In addition, 60S re-association is prevented through steric hindrance by the FeS cluster with uL14. It is yet not clear however, at what point ABCE1 disassociates from the small subunit after splitting. Splitting assays conducted with ATP display no ABCE1 bound to the SSU, suggesting that the disassociation is promoted by ATP hydrolysis and can be inhibited via AMP-PNP. Interestingly, the two ATP binding sites located in NBS-I and NBS-II are structurally and functionally not equivalent (Barthelme et al., 2011). It can therefore be reasoned that, if the NBSs can differentiate between an 80S and SSU bound state and that the two NBS of ABCE1 could hydrolyze ATP at different phases in a diverse manner. The fact that the A-loop of NBS-I is directly connected to the cantilever hinge of the FeS cluster domain supports this model, since this intermolecular crosstalk could enable an NBS-I to sense the state of rotation of the FeS domain. Any interaction with the small subunit after splitting could further be communicated to Q-loop of NBS-I by the HLH motif. Taken together, these findings would allow a model in which the rearrangements of the FeS cluster and HLH domain from pre- to post-splitting state could be transmitted into the nucleotide-binding pocket of NBSI. ABCE1 could be able to have two different modes of ATP hydrolysis and differentiate a pre-splitting from a small subunit bound environment.

However, the question remains, if ABCE1 has a functional role when bound to the 30S/40S beyond being a transient anti-association factor. Notably, in agreement with previous biochemical data (Skabkin et al., 2013; Andersen and Leever, 2007; Dong et al., 2004), we obtained

a native ABCE1-containing 40S-complex associated with several initiation factors from *S. cerevisiae* (eIF1A and eIF2 and sub-units of eIF3). In our cryo-EM map we could resolve eIF1A together with a tRNA/eIF2 density as well as ABCE1. This supports the existing models, which envision a role for ABCE1 in the formation of initiation complexes (Skabkin et al., 2013; Andersen and Leever, 2007; Dong et al., 2004). Interestingly a study conducted in parallel by (Simonetti et al., 2016) depicted the mammalian 48S scanning initiation complex, claiming a relocation of the eIF3 subunits i and g. Reevaluation of the data revealed a misinterpretation of the eIF3i density, which could be shown to be ABCE1. Interestingly, it did depict the same conformation in the mammalian 48S scanning complex as observed in our facilitated splitting and native complexes. This result further shows, that also in higher eukaryotes ABCE1 is present in ribosomal initiation complexes. Taken together, we could further establish that ABCE1 is persisting on the small subunit after recycling and during the initiation phases and confirm previous experiments highlighting the connection of ABCE1 and eIF3 (Kispal et al., 2005). The exact role of ABCE1 during initiation and scanning yet remained enigmatic.

Recently, ribosome profiling revealed that mRNAs indeed have several functional start codons in the 5' untranslated region (UTR), which can be either translated or bypassed by leaky scanning (Andreev et al., 2017; Archer et al., 2016). Once a uORF is translated, the initiation factors as well as the bound initiator Met-tRNA_i are consumed. In order to be able to translate the main downstream protein coding ORF, translation has to be terminated and the ribosome has to be split (Skabkin et al., 2013). It is self evident that ABCE1 splits these ribosomes and it could be shown that the bound tRNA/mRNA can be released by eIF1/eIF1A, eIF2D or MCT1/DENR after splitting. Experimental data further suggests that re-initiation competent 40S subunits might remain on the mRNA to later translate the downstream ORF (Skabkin et al., 2010). Hence, complexes that contain ABCE1 and initiation factors might result from the splitting of such uORF post-termination complexes rather than the splitting of canonical termination complexes. Furthermore, the involved re-initiation factors MCT1/DENR and eIF2D can bind the SSU in the presence of ABCE1 without any clashes. Therefore they could promote re-initiation by stabilizing eIF2 independent P-site tRNA binding, if an AUG codon is positioned directly in the P site

of the 40S subunit (Lomakin et al., 2017).

Still, why ABCE1 is still present in such complexes and how the recycling factor is removed from the small subunit and during what stage of (re-)initiation is not understood. However, it should be highlighted that the post splitting state and also the positioning of the FeS cluster of ABCE1 is conserved in archaea, yeast and human and independent of the initiation factors observed in these complexes. Taken together, post uORF re-initiation complexes could explain the presence of ABCE1 together with initiation factors and canonical 5'cap-dependent initiation complexes might not rely on ABCE1 bound subunits. It needs to be investigated whether ABCE1 operates in different modes during recycling and initiation phases. In addition, the disassociation of ABCE1 from the small subunit might be dependent on its mode of action in uORFs and ORFs.

4.2 Maturation of the eukaryotic small subunit

Our structure of a late pre-40S particle at 3.6 Angstrom resolution, revealed the state of the pre-rRNA in great detail and its interactions with the bound RBFs (Enp1, Tsr1, Rio2 and Pno1) up to a molecular level. Furthermore we could provide a definite and complete inventory of not yet incorporated RPs: RACK1, uS10, uS14, eS10, eS26 and uS3. We propose, that major rRNA condensation events controlled by the bound RBFs will subsequently result in a matured small subunit. The correct formation of the h34/h35/h36 junction will allow integration of many of the RPs which are missing from the beak region: uS3, uS10, eS10 and uS14. Thus the maturation of the beak is likely to relate on the disassociation of Enp1 and integration of uS3. The establishment of this three-way junction is likely connected to the activity of Hrr25 and Yar1 during uS3 integration ((Loar et al., 2004; Schäfer et al., 2006; Ghalei et al., 2015). Recent structural investigations of human pre-40s ribosome complexes investigated later stages of pSSU biogenesis (Ameismeier, Cheng et al, 2018 (in press)). They could show that after the release of Enp1 and Ltv1, h34 is able to accommodate in mature position in the presence of uS3, uS10, eS10 and uS14, further confirming our model.

The final maturation of the beak is likely recognized by domain IV of

Tsr1 which coordinates the head and body and is further involved in h44 maturation. Furthermore, the maturation of the beak and disassociation of Enp1 will increase the flexibility of the head of the pSSU, which is likely coupled to a relaxation of h28. Pno1, located at the platform of the pSSU, forms an interaction with h28 and will therefore be able to sense the maturation of the beak. Whether both, Enp1 and Tsr1, will have to release the beak to create a strong enough flexibility to be recognized by Pno1 will be an interesting research target. It must be noted that D-site cleavage by Nob1 which is dependent on Pno1 could thereby be synchronized to other maturation events on the pSSU. *In vitro* reconstituted mature subunits with Pno1 and Nob1 adopted a similar conformation as depicted in our complex, which suggests that the disassociation of Pno1/Nob1 and 3' cleavage is a later step of pSSU maturation (Ameismeier, Cheng et al, 2018 (in press)). Since eS26 has to be accommodated in the platform, its binding is most likely coupled to the disassociation of Pno1, which occupies its binding region. It is unclear however, how the cleavage by Nob1 is coordinated after Pno1 has disassociated. The protection of the rRNA up to the pre-terminal base (U1799) by Pno1 seems needless if it disassociates before processing by the unspecific PIN domain from Nob1 is concluded. Further, research focused on the processing of D-Site by Pno1/Nob1 should be able to answer the open questions of this final maturation step.

An additional final maturation step of the pSSU is suggested by the model of a translation-like quality control cycle involving the small and large ribosomal subunits (Strunk et al., 2012; Ferreira-Cerca et al., 2014; Turowski et al., 2014; Hector et al., 2014). However, our structure indicates that several RBFs and immature rRNA elements would likely prevent the joining of 60S subunits due to a multitude of clashes. Especially h44 would have to be fully accommodated and thereby Tsr1 disassociated to prevent major clashes with the LSU. In addition h28 should no longer be obstructed by Pno1 to allow head rotation. It is likely that the disassociation of RBFs located in the inter-subunit space rather results in a less stable and less structurally defined pSSU and that this has an adverse effect on LSU binding.

In conclusion, we discovered that the necessary final rRNA folding steps are coordinated by a few late stage RBFs: Enp1, Tsr1 and Pno1. We show that the 40S subunit is maintained in a translationally incompetent state and that functionally important sites are not correctly

folded. This prevents immature subunits from engaging in translation, which could be harmful to the cell. The presented structure marks the first step of deciphering the involved pSSU complexes during the maturation of the small subunit. What factors orchestrate the exact order of events during these final moments as well as the involvement of quality control in the form of joined subunits remains to be revealed by future studies.

Acknowledgements

The Beckmann-lab is a special place and home to very unique, great and amazing people. But little did I know any of that, when I started as an intern (feels like decades ago - and is ?). I started by picking a nearly insurmountable quantity of particles (getting payed by the hour) for the mighty Shashi Bhushan. But it was Thomas Becker who originally recruited me into the Beckmann-family and it was not long, until I met the boss....

Dear Roland, thank you for accepting me as a PhD student in your lab and allowing me to conduct all that amazing research. The amount of freedom and trust I received from you was immense and the right words are difficult to find to express my gratefulness. I will remember all the great - also funny - but always open and direct discussions, independent of their scientific or personal nature. You enabled me to shift the focus of my Ph.D from wet-lab to processing and were always supportive when needed. You are a true role model, just maybe not for answering those emails ;). Thank you also for involving me in many different areas that go beyond science. I felt like part of the family. May the power-waves you surf on never ebb away.

I would also like to thank the GRK-1721 and in this context Karl-Peter Hopfner for all the support and also the trust placed in me as a student speaker. Bringing all the structural labs and Ph.D. students from the Munich area closer together, forged a great hybrid-methods team, where everyone was interested in structural biology. It also promoted a much better understanding for different approaches to science and everyday life. Thank you for all the open discussions and willingness to adapt the program from a bottom-up approach. You enabled me to learn quite a lot in the GRK1721 and it was great throwing a few dice with you as well. Thank you also for being part of my thesis committee.

I also thank PD Dietmar Martin for being part of my thesis committee and for your great lectures during my time as a master student. I remember when you started giving talks after you joined the GeneCenter here in Munich - it was a refreshing experience. I can only hope to be able to reach running speed later in my life. See you on the track.

I further want to thank Prof. Klaus Förstemann for enabling me to take part in teaching and education. You gave me the opportunity to

join as a part time BC1 exercise course lecturer during my masters and also supported the opportunity to lecture parts of Methoden-I series later on. Of course thank you also for being part of my thesis committee. I will always remember your pure professionalism and quality as lecturer and that picture of you sitting on top a car ;)

Thank you also Franz Herzog as being my 5th advisor and Julian Stingle for agreeing to be the 6th advisor on such short notice.

I further thank Prof. Ed Hurt and Prof. Robert Tampe for the great collaborations. Working with you and bringing the science of different laboratories from different parts of the world together, taught me a lot. I really enjoyed working with the members of your lab: Emma Thompson (Hurt-lab) and also Milan Gerovac, Elina Nuerenberg and Holger Pfitzner (Tampe-lab).

I would like to thank the FOR1805 for all their funding and for bringing all the ribosome science of Germany together. It was great to learn and interact with so many people in such a professional network.

Everything is in some way a team effort. A huge thank you to my "other" family ... my Beckmann-family:

I never had an older brother. But once I joined the Beckmann lab and Thomas took me under his wing (probably made out of heavy-metal-steel), surely felt like I had one. The willingness to support and help others, combined with your (almost) eternal patience makes you the great person you are and makes you the best supervisor there is. You taught me so much, promoted me and pushed me to new frontiers. Thank you for the great time at work and not-at-work. I tried to find a nice fitting metal-music-quote, i hope that hits the spot: "It's when life's so precious that every moment hurts - White Omega, Moonspell"

While the EM-Facility is not directly located in the institute, it still always felt like home in the "dungeon" of Otto Berninghausen. Thank for all the free coffee, your teaching, answering all the technical questions and for the great work together with the TitanPipeLine. I know the door was always open and I hope you enjoyed the music ;). It was always truly great working with you and even more fun working for you #pokemonmaster. Celebrating birthdays in Bonn was really wild as well! Thank you for all your support.

A big thank you goes to Susi Rieder and Charlotte Ungewickell for all their work and efforts in the EM-facility: Blotting all the grids and

setting up all the data collections. It would not work so smoothly without out.

I want to thank the strong backbone of the lab as well:

Andrea Gilmozzi and Joanna Musial (master of cats). You welcomed me with open arms at the very beginning and until the end. I also want to highlight Heidi Sieber. Not only did you let me get away with breaking some of the pipettes - it was also a great to purifying proteins with you and just working with you in general (before I escaped the wet-lab). Thank you for giving me all the help, guidance and support when i needed it.

Ladies and gentleman. I hope you seated in a stable position. ... *breathing in* ... BEHOLD ! ... His code is as soft as the winter-fall snow. His modules are bursting with intense one line AWK coding ... and if that is not already enough, all of the things he creates are aerodynamically designed to fit the Four-Sided-Quantum-Klein manifold, so that you may process your data AT THE SPEED OF MAXIMUM ENJOYMENT. It is LUKAS KATER ! Well.....Starting as just the "the-guy-from-the-practical" and later "student-of-clara" you managed to boulder/climb and code and science it at a level that is just amazing. Please just promise me I can collect some data at your lab one day ;). Coding was great...coding with you was the best. And hey, sometimes I have a cool geek joke .. and I turn around hoping you are there. #HerbesDeProvence

Michi is one of a kind. Truly one of the only normal guys out there. What i mean is: One of these, which works with the only thing that really matters in life: the small subunit. Jokes aside: Thank you for all the professional and relaxed discussions and for being the "voice of reason" in the thing we call "the raptor cage". You are a #Marathon-Vorbild and an essential part of the ALuMi. Thank your for sharing the scientific expertise and also your flat for #afterparty.

I guess some of you know JCVD = Jean-Claude van Damme. He is from Belgium and a top movie actor, super fit and did a full split between two trucks, while they were driving. Maybe you also know JDC - JingDong Cheng. He is from China and is also all of the things i just mentioned above, but he models at least 5 proteins during that process in addition. He is really humble and a master of noodle making. Thank you for supporting me and the lab with your post-doc knowledge and calm wisdom. You are a model of "work-hard and deliver harder".

Golden phone and a laptop .. well lets just say we did not start off right, but we managed more than well in the end. Dear Birgitta / Gitty / Royal-Gittness: you are a stable entity of professionalism and safety etiquette in the lab. You are also extremely essential for keeping the "jokes" in check so thank you for that as well. It was great to "steal your fridge" (still working and doing well) and spending time at work and after-work with you. If we ever meet randomly in some place, I am pretty sure it will be in the US - LA.

I am sitting in the subway. An old lady sits next to me, while I browse some pictures I took on my phone. She looks over - at a picture of Katharina and Hanna and then talks to me: "Dear sir. Are these your daughters? They are really pretty. You are truly blessed!" - Me: "*nodding in silent agreement and slight embarrassment - but proud* Yes.". Thank you two for the great times, running through the forest, cookings and everything we managed to pull off. Katharina will soon become the most famous science cat-dancer the world has ever seen. You were one of my greatest students...before you evolved to a colleague :D. I hope you will have **PHinished** soon #kaddajokes. Because of her cakes, Hanna has already more fans on Instagram and the internet than me .. grrrrr. #downstreamconsequences ? None. Also the only person which understands owls. #NoMango!

Chris - no longer in the lab - but truly a friend and partner in cri...science. While your first days in the lab with us were rather crazy...you managed to stay ahead of things. Always in a calm way...the Schmidt way. You were my bro-cessing bro from the start and will stay a friend despite we are no longer working together. The adventures we had - digital and real - are too many to count. I have to confess: Ulm has found a place in my heart, despite I visited it only once. I will never forget the commitment from you to push me into the 3D-modeling process and that you were there for me - always. You are an amazing scientist and a friend for life.

All members of the entire Beckmann- and Wilson lab (yes you aga .. Agnieszka :)). Thank you for providing the great atmosphere and making work an amazing place to be: Robert Buschauer (#BestRave #ColdBrewBro), Ting (#DragonPrincess), Kathi (besti) (#Rat-Sayer&CakeCrafter), Petr (#GwentMaster), Jen (#trapmusic, #eleven) as well as Tsai (#saposin;) and Viviek (#DontBreakMoreBones).

I thank Pascaline for the strong support and being the person she is.

Thank you for being there for me - even if I am not there ;). You are the stability, the constant, the lifeline.

I thank my parents and my family for the support before and during my Ph.D. Going this far was only possible with your help and support. Thank you Mum, thank you Dad and thank you brother. My thoughts are also with my grandfather - Uwe Heuer - I know he would have loved to see me in some of his footsteps.

References

- Andersen, D. S. and S. J. Leever (2007). “The essential drosophila ATP-binding cassette domain protein, pixie, binds the 40 S ribosome in an ATP-dependent manner and is required for translation initiation”. In: *Journal of Biological Chemistry* 282.20, pp. 14752–14760.
- Andreev, D. E. et al. (2017). *Insights into the mechanisms of eukaryotic translation gained with ribosome profiling*. arXiv: 1611.06654.
- Anger, A. M. et al. (2013). “Structures of the human and Drosophila 80S ribosome”. In: *Nature* 497.7447, pp. 80–85.
- Archer, S. K. et al. (2016). “Dynamics of ribosome scanning and recycling revealed by translation complex profiling”. In: *Nature* 535.7613, pp. 570–574.
- Asano, K. et al. (2000). “A multifactor complex of eukaryotic initiation factors, eIF1, eIF2, eIF3, eIF5, and initiator tRNA(Met) is an important translation initiation intermediate in vivo”. In: *Genes and Development* 14.19, pp. 2534–2546.
- Barrio-Garcia, C. et al. (2016). “Architecture of the Rix1-Rea1 checkpoint machinery during pre-60S-ribosome remodeling”. In: *Nature Structural and Molecular Biology* 23.1, pp. 37–44.
- Barthelme, D. et al. (2007). “Structural organization of essential iron-sulfur clusters in the evolutionarily highly conserved ATP-binding cassette protein ABCE1”. In: *Journal of Biological Chemistry* 282.19, pp. 14598–14607.
- Barthelme, D. et al. (2011). “Ribosome recycling depends on a mechanistic link between the FeS cluster domain and a conformational switch of the twin-ATPase ABCE1.” In: *Proceedings of the National Academy of Sciences of the United States of America* 108.8, pp. 3228–33.
- Becker, T. et al. (2011). “Structure of the no-go mRNA decay complex Dom34-Hbs1 bound to a stalled 80S ribosome”. In: *Nature Structural and Molecular Biology* 18.6, pp. 715–720.
- Becker, T. et al. (2012). “Structural basis of highly conserved ribosome recycling in eukaryotes and archaea”. In: *Nature* 482.7386, pp. 501–506.
- Bertram, G. et al. (2000). “Terminating eukaryote translation: Domain 1 of release factor eRF1 functions in stop codon recognition”. In: *RNA* 6.9, pp. 1236–1247.
- Blanchard, S. C. et al. (2004). “tRNA dynamics on the ribosome during translation”. In: *Proceedings of the National Academy of Sciences* 101.35, pp. 12893–12898.
- Brown, A. et al. (2015). “Structural basis for stop codon recognition in eukaryotes”. In: *Nature* 524.7566, pp. 493–496. arXiv: arXiv:1011.1669v3.
- Chaker-Margot, M. et al. (2017). “Architecture of the yeast small subunit processome”. In: *Science (New York, N.Y.)* 355.6321, pp. 1–9.
- Chen, J. et al. (2003a). “A tweezers-like motion of the ATP-binding cassette dimer in an ABC transport cycle”. In: *Molecular Cell* 12.3, pp. 651–661.

- Chen, W. et al. (2003b). *Enp1, a yeast protein associated with U3 and U14 snoRNAs, is required for pre-rRNA processing and 40S subunit synthesis.*
- Cheng, Z. et al. (2009). “Structural insights into eRF3 and stop codon recognition by eRF1”. In: *Genes and Development* 23.9, pp. 1106–1118.
- Coelho, C. M. A. (2005). “Growth and cell survival are unevenly impaired in pixie mutant wing discs”. In: *Development* 132.24, pp. 5411–5424.
- Combs, D. J. et al. (2006). “Prp43p is a DEAH-box spliceosome disassembly factor essential for ribosome biogenesis.” In: *Molecular and cellular biology* 26.2, pp. 523–34.
- Crick, F (1970). “Central dogma of molecular biology.” In: *Nature* 227.5258, pp. 561–3. arXiv: arXiv:1011.1669v3.
- Crick, F. H. C. et al. (1961). “General nature of the genetic code for proteins”. In: *Nature* 192.4809, pp. 1227–1232.
- Des Georges, A. et al. (2014). “Structure of the mammalian ribosomal pre-termination complex associated with eRF1•eRF3•GDPNP”. In: *Nucleic Acids Research* 42.5, pp. 3409–3418.
- Dever, T. E. and R. Green (2012). “The elongation, termination, and recycling phases of translation in eukaryotes”. In: *Cold Spring Harbor Perspectives in Biology* 4.7, pp. 1–16.
- Does, C. van der and R. Tampé (2004). *How do ABC transporters drive transport?*
- Dong, J. et al. (2004). “The essential ATP-binding cassette protein RLI1 functions in translation by promoting preinitiation complex assembly”. In: *Journal of Biological Chemistry* 279.40, pp. 42157–42168.
- Dong, J. et al. (2008). “Genetic identification of yeast 18S rRNA residues required for efficient recruitment of initiator tRNA^{Met} and AUG selection”. In: *Genes and Development* 22.16, pp. 2242–2255.
- Dorner, S. et al. (2006). “The hybrid state of tRNA binding is an authentic translation elongation intermediate”. In: *Nature Structural and Molecular Biology* 13.3, pp. 234–241.
- Estévez, A. M. et al. (2004). “Effects of depletion and overexpression of the Trypanosoma brucei ribonuclease L inhibitor homologue”. In: *Molecular and Biochemical Parasitology* 133.1, pp. 137–141.
- Evans, M. S. et al. (2008). “Cotranslational Folding Promotes β -Helix Formation and Avoids Aggregation In Vivo”. In: *Journal of Molecular Biology* 383.3, pp. 683–692.
- Fassio, C. A. et al. (2010). “Dominant mutations in the late 40S biogenesis factor Ltv1 affect cytoplasmic maturation of the small ribosomal subunit in Saccharomyces cerevisiae”. In: *Genetics* 185.1, pp. 199–209.
- FATICA, A. (2004). “PIN domain of Nob1p is required for D-site cleavage in 20S pre-rRNA”. In: *RNA* 10.11, pp. 1698–1701.
- Fatica, A. et al. (2003). “Nob1p Is Required for Cleavage of the 3' End of 18S rRNA”. In: *Molecular and Cellular Biology* 23.5, pp. 1798–1807.
- Ferreira-Cerca, S. et al. (2014). “Dominant Rio1 kinase/ATPase catalytic mutant induces trapping of late pre-40S biogenesis factors in 80S-like ribosomes”. In: *Nucleic Acids Research* 42.13, pp. 8635–8647.
- Frank, J. and R. K. Agrawal (2000). “A ratchet-like inter-subunit reorganization of the ribosome during translocation”. In: *Nature* 406.6793, pp. 318–322.

- Frank, J. et al. (1995). “A model of protein synthesis based on cryo-electron microscopy of the E. coli ribosome”. In: *Nature* 376.6539, pp. 441–444.
- Frolova, L. Y. et al. (1999). “Mutations in the highly conserved GGQ motif of class I polypeptide release factors abolish ability of human eRF1 to trigger peptidyl-tRNA hydrolysis”. In: *RNA* 5.8, pp. 1014–1020.
- Frolova, L. Y. et al. (2000). “Translation termination in eukaryotes: Polypeptide release factor eRF1 is composed of functionally and structurally distinct domains”. In: *RNA* 6.3, pp. 381–390.
- Frolova, L. et al. (1994). “A highly conserved eukaryotic protein family possessing properties of polypeptide chain release factor”. In: *Nature* 372.6507, pp. 701–703.
- Fromont-Racine, M. et al. (2003). *Ribosome assembly in eukaryotes*.
- Fu, Z. et al. (2016). “Key Intermediates in Ribosome Recycling Visualized by Time-Resolved Cryoelectron Microscopy”. In: *Structure* 24.12, pp. 2092–2101.
- Gadal, O. et al. (2001). “Nuclear Export of 60S Ribosomal Subunits Depends on Xpo1p and Requires a Nuclear Export Sequence-Containing Factor, Nmd3p, That Associates with the Large Subunit Protein Rpl10p”. In: *Molecular and Cellular Biology* 21.10, pp. 3405–3415.
- Geerlings, T. H. et al. (2003). “Rio2p, an evolutionarily conserved, low abundant protein kinase essential for processing of 20 S pre-rRNA in *Saccharomyces cerevisiae*”. In: *Journal of Biological Chemistry* 278.25, pp. 22537–22545.
- Ghalei, H. et al. (2015). “Hrr25/CK1 δ -directed release of Ltv1 from pre-40S ribosomes is necessary for ribosome assembly and cell growth”. In: *Journal of Cell Biology* 208.6, pp. 745–759.
- Gingras, A.-C. et al. (1999). “eIF4 Initiation Factors: Effectors of mRNA Recruitment to Ribosomes and Regulators of Translation”. In: *Annual Review of Biochemistry* 68.1, pp. 913–963.
- Granneman, S. et al. (2005). “The putative NTPase Fap7 mediates cytoplasmic 20S pre-rRNA processing through a direct interaction with Rps14.” In: *Molecular and cellular biology* 25.23, pp. 10352–64.
- Granneman, S. et al. (2010). “Cracking pre-40S ribosomal subunit structure by systematic analyses of RNA–protein cross-linking”. In: *The EMBO Journal* 29.12, pp. 2026–2036.
- Greber, B. J. et al. (2016). “Insertion of the Biogenesis Factor Rei1 Probes the Ribosomal Tunnel during 60S Maturation”. In: *Cell* 164.1-2, pp. 91–102.
- Guhaniyogi, J. and G. Brewer (2001). *Regulation of mRNA stability in mammalian cells*.
- Hector, R. D. et al. (2014). “Snapshots of pre-rRNA structural flexibility reveal eukaryotic 40S assembly dynamics at nucleotide resolution”. In: *Nucleic Acids Research* 42.19, pp. 12138–12154.
- Henras, A. K. et al. (2015). *An overview of pre-ribosomal RNA processing in eukaryotes*.
- Hinnebusch, A. G. (2017). *Structural Insights into the Mechanism of Scanning and Start Codon Recognition in Eukaryotic Translation Initiation*.
- Hinnebusch, A. G. and J. R. Lorsch (2012). “The mechanism of eukaryotic translation initiation: New insights and challenges”. In: *Cold Spring Harbor Perspectives in Biology* 4.10.

- Holland, I. B. and M. A. Blight (1999). *ABC-ATPases, adaptable energy generators fuelling transmembrane movement of a variety of molecules in organisms from bacteria to humans*.
- Hurt, E. et al. (1999). “A novel in vivo assay reveals inhibition of ribosomal nuclear export in Ran-cycle and nucleoporin mutants”. In: *Journal of Cell Biology* 144.3, pp. 389–401.
- Jackson, R. J. et al. (2010). *The mechanism of eukaryotic translation initiation and principles of its regulation*. arXiv: NIHMS150003.
- (2012). *Termination and post-termination events in eukaryotic translation*.
- Karcher, A. et al. (2005). “X-ray structure of RLI, an essential twin cassette ABC ATPase involved in ribosome biogenesis and HIV capsid assembly”. In: *Structure* 13.4, pp. 649–659.
- Karcher, A. et al. (2008). “X-ray structure of the complete ABC enzyme ABCE1 from *Pyrococcus abyssi*”. In: *Journal of Biological Chemistry* 283.12, pp. 7962–7971.
- Kater, L. et al. (2017). “Visualizing the Assembly Pathway of Nucleolar Pre-60S Ribosomes”. In: *Cell* 171.7, 1599–1610.e13.
- Kiosze-Becker, K. et al. (2016). “Structure of the ribosome post-recycling complex probed by chemical cross-linking and mass spectrometry”. In: *Nature Communications* 7.
- Kispal, G. et al. (2005). “Biogenesis of cytosolic ribosomes requires the essential iron-sulphur protein Rli1p and mitochondria”. In: *EMBO Journal* 24.3, pp. 589–598.
- Kong, C et al. (2004). “Crystal structure and functional analysis of the eukaryotic class II release factor eRF3 from *S. pombe*”. In: *Mol Cell* 14.2, pp. 233–245.
- Kornprobst, M. et al. (2016). “Architecture of the 90S Pre-ribosome: A Structural View on the Birth of the Eukaryotic Ribosome”. In: *Cell* 166.2, pp. 380–393.
- Kressler, D. et al. (2012). “Synchronizing nuclear import of ribosomal proteins with ribosome assembly”. In: *Science* 338.6107, pp. 666–671.
- Kressler, D. et al. (2017). *A Puzzle of Life: Crafting Ribosomal Subunits*.
- Lafontaine, D. L. et al. (1998). “Yeast 18S rRNA dimethylase Dim1p: a quality control mechanism in ribosome synthesis?” In: *Molecular and cellular biology* 18.4, pp. 2360–70.
- Lafontaine, D. et al. (1994). “The DIM1 Gene Responsible for the Conserved m62Am62A Dimethylation in the 3-Terminal Loop of 18 S rRNA is Essential in Yeast”. In: *Journal of Molecular Biology* 241.3, pp. 492–497.
- Lafontaine, D. et al. (1995). “The 18S rRNA dimethylase Dim1p is required for pre-ribosomal RNA processing in yeast”. In: *Genes and Development* 9.20, pp. 2470–2481.
- Lamanna, A. C. and K. Karbstein (2009). “Nob1 binds the single-stranded cleavage site D at the 3'-end of 18S rRNA with its PIN domain.” In: *Proceedings of the National Academy of Sciences of the United States of America* 106.34, pp. 14259–14264.
- Lamanna, A. C. and K. Karbstein (2011). “An RNA conformational switch regulates pre-18s rRNA cleavage”. In: *Journal of Molecular Biology* 405.1, pp. 3–17.
- Larburu, N. et al. (2016). “Structure of a human pre-40S particle points to a role for RACK1 in the final steps of 18S rRNA processing”. In: *Nucleic Acids Research* 44.17, pp. 8465–8478.

- Laurberg, M. et al. (2008). “Structural basis for translation termination on the 70S ribosome”. In: *Nature* 454.7206, pp. 852–857.
- Lebaron, S. et al. (2005). “The Splicing ATPase Prp43p Is a Component of Multiple Preribosomal Particles”. In: *Molecular and Cellular Biology* 25.21, pp. 9269–9282.
- Lebaron, S. et al. (2012). “Proofreading of pre-40S ribosome maturation by a translation initiation factor and 60S subunits”. In: *Nature Structural and Molecular Biology* 19.8, pp. 744–753.
- Léger-Silvestre, I. et al. (2004). “The ribosomal protein Rps15p is required for nuclear exit of the 40S subunit precursors in yeast”. In: *EMBO Journal* 23.12, pp. 2336–2347.
- Loar, J. W. et al. (2004). “Genetic and biochemical interactions among Yar1, Ltv1 and RpS3 define novel links between environmental stress and ribosome biogenesis in *Saccharomyces cerevisiae*”. In: *Genetics* 168.4, pp. 1877–1889.
- Lomakin, I. B. et al. (2017). “Crystal Structure of the Human Ribosome in Complex with DENR-MCT-1”. In: *Cell Reports* 20.3, pp. 521–528.
- Lu, G. et al. (2005). “ATP hydrolysis is required to reset the ATP-binding cassette dimer into the resting-state conformation”. In: *Proceedings of the National Academy of Sciences* 102.50, pp. 17969–17974.
- Ma, C. et al. (2017). “Structural snapshot of cytoplasmic pre-60S ribosomal particles bound by Nmd3, Lsg1, Tif6 and Reh1”. In: *Nature Structural and Molecular Biology* 24.3, pp. 214–220. arXiv: 15334406.
- Mangus, D. A. et al. (2003). *Poly(A)-binding proteins: Multifunctional scaffolds for the post-transcriptional control of gene expression*.
- Martin, R. et al. (2013). *DExD/H-box RNA helicases in ribosome biogenesis*.
- Matheisl, S. et al. (2015). “Structure of a human translation termination complex”. In: *Nucleic Acids Research* 43.18, pp. 8615–8626. arXiv: arXiv:1011.1669v3.
- McCaughan, U. M. et al. (2016). “Pre-40S ribosome biogenesis factor Tsr1 is an inactive structural mimic of translational GTPases”. In: *Nature Communications* 7.
- Melnikov, S. et al. (2012). *One core, two shells: Bacterial and eukaryotic ribosomes*.
- Mizumoto, K. and Y. Kaziro (1987). “Messenger RNA Capping Enzymes from Eukaryotic Cells”. In: *Progress in Nucleic Acid Research and Molecular Biology* 34.C, pp. 1–28.
- Monroe, N. and C. P. Hill (2016). *Meiotic Clade AAA ATPases: Protein Polymer Disassembly Machines*.
- Moy, T. I. and P. A. Silver (1999). “Nuclear export of the small ribosomal subunit requires the Ran-GTPase cycle and certain nucleoporins”. In: *Genes and Development* 13.16, pp. 2118–2133.
- Moy, T. I. and P. A. Silver (2002). “Requirements for the nuclear export of the small ribosomal subunit”. In: *J Cell Sci* 115.14, pp. 2985–2995.
- Nürenberg, E. and R. Tampé (2013). *Tying up loose ends: Ribosome recycling in eukaryotes and archaea*.
- Oeffinger, M. et al. (2004). “A pre-ribosome-associated HEAT-repeat protein is required for export of both ribosomal subunits”. In: *Genes and Development* 18.2, pp. 196–209.
- Pertschy, B. et al. (2009). “RNA helicase Prp43 and its co-factor Pfa1 promote 20 to 18 S rRNA processing catalyzed by the endonuclease Nob1”. In: *Journal of Biological Chemistry* 284.50, pp. 35079–35091.

- Pisarev, A. V. et al. (2007). “Recycling of Eukaryotic Posttermination Ribosomal Complexes”. In: *Cell* 131.2, pp. 286–299. arXiv: NIHMS150003.
- Pisarev, A. V. et al. (2010). “The Role of ABCE1 in Eukaryotic Posttermination Ribosomal Recycling”. In: *Molecular Cell* 37.2, pp. 196–210.
- Preis, A. et al. (2014). “Cryoelectron microscopic structures of eukaryotic translation termination complexes containing eRF1-eRF3 or eRF1-ABCE1”. In: *Cell Reports* 8.1, pp. 59–65.
- Rouquette, J. et al. (2005). “Nuclear export and cytoplasmic processing of precursors to the 40S ribosomal subunits in mammalian cells”. In: *EMBO Journal* 24.16, pp. 2862–2872.
- Saito, K. et al. (2010). “Omnipotent role of archaeal elongation factor 1 alpha (EF1 α) in translational elongation and termination, and quality control of protein synthesis.” In: *Proceedings of the National Academy of Sciences of the United States of America* 107.45, pp. 19242–7.
- Salas-Marco, J. and D. M. Bedwell (2004). “GTP hydrolysis by eRF3 facilitates stop codon decoding during eukaryotic translation termination.” In: *Molecular and cellular biology* 24.17, pp. 7769–78.
- Sardana, R. et al. (2015). “The DEAH-box Helicase Dhr1 Dissociates U3 from the Pre-rRNA to Promote Formation of the Central Pseudoknot”. In: *PLoS Biology* 13.2.
- Sauer, R. T. et al. (2004). *Sculpting the proteome with AAA+ proteases and disassembly machines*.
- Schäfer, T. et al. (2003). “The path from nucleolar 90S to cytoplasmic 40S pre-ribosomes”. In: *EMBO Journal* 22.6, pp. 1370–1380.
- Schäfer, T. et al. (2006). “Hrr25-dependent phosphorylation state regulates organization of the pre-40S subunit”. In: *Nature* 441.7093, pp. 651–655.
- Seiser, R. M. et al. (2006). “Ltv1 is required for efficient nuclear export of the ribosomal small subunit in *Saccharomyces cerevisiae*”. In: *Genetics* 174.2, pp. 679–691.
- Senapin, S. et al. (2003). “RRP20, a component of the 90S preribosome, is required for pre-18S rRNA processing in *Saccharomyces cerevisiae*”. In: *Nucleic Acids Research* 31.10, pp. 2524–2533.
- Shatkin, A. J. (1976). *Capping of eucaryotic mRNAs*.
- Shoemaker, C. J. and R. Green (2011). “Kinetic analysis reveals the ordered coupling of translation termination and ribosome recycling in yeast”. In: *Proceedings of the National Academy of Sciences* 108.51, E1392–E1398.
- Simonetti, A. et al. (2016). “eIF3 Peripheral Subunits Rearrangement after mRNA Binding and Start-Codon Recognition”. In: *Molecular Cell* 63.2, pp. 206–217.
- Skabkin, M. A. et al. (2010). “Activities of Ligatin and MCT-1/DENR in eukaryotic translation initiation and ribosomal recycling”. In: *Genes and Development* 24.16, pp. 1787–1801.
- Skabkin, M. A. et al. (2013). “Reinitiation and other unconventional posttermination events during eukaryotic translation”. In: *Molecular Cell* 51.2, pp. 249–264.
- Smith, P. C. et al. (2002). “ATP binding to the motor domain from an ABC transporter drives formation of a nucleotide sandwich dimer”. In: *Molecular Cell* 10.1, pp. 139–149. arXiv: NIHMS150003.
- Sonenberg, N. (1993). *Remarks on the mechanism of ribosome binding to eukaryotic mRNAs*.

- Song, H. et al. (2000). “The Crystal Structure of Human Eukaryotic Release Factor eRF1—Mechanism of Stop Codon Recognition and Peptidyl-tRNA Hydrolysis”. In: *Cell* 100.3, pp. 311–321.
- Soudet, J. et al. (2010). “Immature small ribosomal subunits can engage in translation initiation in *Saccharomyces cerevisiae*”. In: *EMBO Journal* 29.1, pp. 80–92.
- Stage-Zimmermann, T et al. (2000). “Factors affecting nuclear export of the 60S ribosomal subunit in vivo.” In: *Molecular biology of the cell* 11.11, pp. 3777–89.
- Strunk, B. S. and K. Karbstein (2009). “Powering through ribosome assembly”. In: *RNA* 15.12, pp. 2083–2104.
- Strunk, B. S. et al. (2011). “Ribosome assembly factors prevent premature translation initiation by 40S assembly intermediates”. In: *Science* 333.6048, pp. 1449–1453. arXiv: arXiv:1106.5958.
- Strunk, B. S. et al. (2012). “A translation-like cycle is a quality control checkpoint for maturing 40S ribosome subunits”. In: *Cell* 150.1, pp. 111–121. arXiv: NIHMS150003.
- Sun, Q. et al. (2017). “Molecular architecture of the 90S small subunit pre-ribosome”. In: *eLife* 6.
- Taylor, D. et al. (2012). “Cryo-EM structure of the mammalian eukaryotic release factor eRF1-eRF3-associated termination complex”. In: *Proceedings of the National Academy of Sciences* 109.45, pp. 18413–18418.
- Turowski, T. W. et al. (2014). “Rio1 mediates ATP-dependent final maturation of 40S ribosomal subunits”. In: *Nucleic Acids Research* 42.19, pp. 12189–12199.
- Van Den Elzen, A. M. G. et al. (2014). “Dom34-Hbs1 mediated dissociation of inactive 80S ribosomes promotes restart of translation after stress”. In: *EMBO Journal* 33.3, pp. 265–276.
- Vanrobays, E. et al. (2008). “TOR regulates the subcellular distribution of DIM2, a KH domain protein required for cotranscriptional ribosome assembly and pre-40S ribosome export”. In: *RNA* 14.10, pp. 2061–2073.
- Vanrobays, E. et al. (2003). “Late cytoplasmic maturation of the small ribosomal subunit requires RIO proteins in *Saccharomyces cerevisiae*.” In: *Molecular and cellular biology* 23.6, pp. 2083–95.
- Vanrobays, E. et al. (2004). “Dim2p, a KH-domain protein required for small ribosomal subunit synthesis.” In: *RNA (New York, N.Y.)* 10.4, pp. 645–56.
- Wahle, E. and U. Rügsegger (1999). *3'-End processing of pre-mRNA in eukaryotes*.
- Wegierski, T. et al. (2001). “Bms1p, a G-domain-containing protein, associates with Rcl1p and is required for 18S rRNA biogenesis in yeast”. In: *RNA* 7.9, pp. 1254–1267.
- Weixlbaumer, A. et al. (2008). “Insights into translational termination from the structure of RF2 bound to the ribosome”. In: *Science* 322.5903, pp. 953–956.
- Wells, S. E. et al. (1998). “Circularization of mRNA by eukaryotic translation initiation factors”. In: *Molecular Cell* 2.1, pp. 135–140.
- Winzeler, E. A. et al. (1999). “Functional characterization of the *S. cerevisiae* genome by gene deletion and parallel analysis”. In: *Science* 285.5429, pp. 901–906. arXiv: arXiv:1011.1669v3.
- Woolls, H. A. et al. (2011). “Roles of Dim2 in ribosome assembly”. In: *Journal of Biological Chemistry* 286.4, pp. 2578–2586.
- Wu, S. et al. (2016). “Diverse roles of assembly factors revealed by structures of late nuclear pre-60S ribosomes”. In: *Nature* 534.7605, pp. 133–137.

Zemp, I. et al. (2009). "Distinct cytoplasmic maturation steps of 40S ribosomal subunit precursors require hRio2". In: *Journal of Cell Biology* 185.7, pp. 1167–1180.

Publications

Cryoelectron Microscopic Structures of Eukaryotic Translation Termination Complexes Containing eRF1-eRF3 or eRF1-ABCE1

Anne Preis,^{1,2} Andre Heuer,^{1,2} Clara Barrio-Garcia,^{1,2} Andreas Hauser,^{1,2} Daniel E. Eyler,^{3,4} Otto Berninghausen,^{1,2} Rachel Green,^{3,4} Thomas Becker,^{1,2,*} and Roland Beckmann^{1,2,*}

¹Gene Center Munich, Department of Biochemistry, Feodor-Lynen-Strasse 25, University of Munich, 81377 Munich, Germany

²Center for Integrated Protein Science Munich, Department of Biochemistry, Feodor-Lynen-Strasse 25, University of Munich, 81377 Munich, Germany

³Howard Hughes Medical Institute, Chevy Chase, MD 20815-6789, USA

⁴Department of Molecular Biology and Genetics, Johns Hopkins University School of Medicine, Baltimore, MD 21205, USA

*Correspondence: becker@lmb.uni-muenchen.de (T.B.), beckmann@lmb.uni-muenchen.de (R.B.)

<http://dx.doi.org/10.1016/j.celrep.2014.04.058>

This is an open access article under the CC BY-NC-ND license (<http://creativecommons.org/licenses/by-nc-nd/3.0/>).

SUMMARY

Termination and ribosome recycling are essential processes in translation. In eukaryotes, a stop codon in the ribosomal A site is decoded by a ternary complex consisting of release factors eRF1 and guanosine triphosphate (GTP)-bound eRF3. After GTP hydrolysis, eRF3 dissociates, and ABCE1 can bind to eRF1-loaded ribosomes to stimulate peptide release and ribosomal subunit dissociation. Here, we present cryoelectron microscopic (cryo-EM) structures of a pretermination complex containing eRF1-eRF3 and a termination/prerecycling complex containing eRF1-ABCE1. eRF1 undergoes drastic conformational changes: its central domain harboring the catalytically important GGQ loop is either packed against eRF3 or swung toward the peptidyl transferase center when bound to ABCE1. Additionally, in complex with eRF3, the N-terminal domain of eRF1 positions the conserved NIKS motif proximal to the stop codon, supporting its suggested role in decoding, yet it appears to be delocalized in the presence of ABCE1. These results suggest that stop codon decoding and peptide release can be uncoupled during termination.

INTRODUCTION

Translation termination and ribosome recycling are essential processes in ribosome-driven protein synthesis triggered by the appearance of a stop codon in the A site of the ribosome during elongation. In the first stage of this cycle, the release factor (RF) eRF1 is delivered to the ribosome by the guanosine triphosphatase (GTPase) eRF3, which departs following guanosine triphosphate (GTP) hydrolysis. Next, ABCE1 binds to the factor-binding site of ribosomes loaded with eRF1 and facilitates

peptide release and then subunit dissociation. These events are tightly coordinated through their common utilization of eRF1 (Pisarev et al., 2010; Shoemaker et al., 2010; Shoemaker and Green, 2011).

To date, several X-ray and cryoelectron microscopic (cryo-EM) structures exist for individual eRFs as well as unbound and ribosome-bound eRF1-eRF3 complexes (Cheng et al., 2009; des Georges et al., 2014; Kong et al., 2004; Song et al., 2000; Taylor et al., 2012). Recent cryo-EM structures of a rabbit pretermination complex show eRF1 trapped in the process of delivery to the ribosome by eRF3 bound to the nonhydrolyzable GTP analog guanylyl imidodiphosphate (GDPNP). As a result, the catalytically essential GGQ motif of eRF1 is positioned approximately 90 Å apart from the peptidyl transferase center (PTC) where peptide release is ultimately catalyzed. Therefore, it remains an open question what the active conformation of eRF1 on the terminating ribosome might be. Moreover, whereas it has previously been shown that ABCE1 can stimulate eRF1-dependent peptide release before dissociating ribosomes into subunits, thereby coupling translation termination with ribosome recycling (Shoemaker and Green, 2011), we have little structural understanding of these processes.

Important clues regarding the possible behavior of eRF1 and eRF3 come from the closely related mRNA surveillance (or ribosome rescue) factors Pelota (Dom34p in yeast) and Hbs1. These factors are paralogs of eRF1 and eRF3, recognize stalled ribosomes, and initiate subsequent ribosome rescue/recycling together with ABCE1 that ends in degradation of aberrant mRNA and proteins (Barthelme et al., 2011; Doma and Parker, 2006; Pisareva et al., 2011; Shoemaker and Green, 2011). Cryo-EM structures of stalled ribosomes in complex with Pelota and either Hbs1 or ABCE1 showed that the central domain of Pelota undergoes a dramatic conformational change in these different complexes. In the prerecycling state (in the presence of Hbs1:GDPNP), Pelota is packed against Hbs1 and not fully engaged in the A site, whereas in the recycling complex bound to ABCE1:adenylyl imidodiphosphate (ADPNP), Pelota stretches out within the A site reaching toward the P site-tRNA (Becker et al., 2011, 2012; Franckenberg et al., 2012). Based on the

homology between these rescue factors and eukaryotic-RFs, similar behavior of eRF1 may explain how ABCE1 exerts its influence on peptide release. However, direct structural evidence for this model is not available so far.

RESULTS AND DISCUSSION

Generation and Cryo-EM of Pretermination and Termination/Prerecycling Complexes

Stable ribosomal complexes bound to eRF1 and eRF3 or ABCE1 were generated by employing a stalling polypeptide sequence from the human cytomegalovirus (CMV) *gp48* uORF. This peptide sequence stalls translation by inhibiting eRF1-mediated peptide release with a UAA stop codon-programmed ribosomal A site (Bhushan et al., 2010; Janzen et al., 2002). The detailed molecular changes responsible for prohibiting peptide release by eRF1 and also puromycin activity in this seemingly normal ribosomal termination complex are not known (Figure S1A).

We used a wheat germ in vitro translation system to generate CMV-stalled ribosome-nascent chain complexes (RNCs) (Bhushan et al., 2010) and then added either purified recombinant *Saccharomyces cerevisiae* eRF1-eRF3:GDPNP (Sup45p-Sup35p) ternary complex or eRF1 and ABCE1:ADPNP. eRF3 lacks the prion-forming domain (N-terminal 97 amino acids) that has been shown to be nonessential for termination activity in yeast (Alkalaeva et al., 2006; Frolova et al., 1996). To test the functional activity of these heterologous complexes, we performed release assays where we followed peptide release by immunodetection of the HA-tagged peptidyl tRNA and free peptide. In this case, the CMV-stalled RNCs were directly compared with RNCs prepared on a truncated mRNA. Although peptide was quantitatively released from the peptidyl tRNA by puromycin on the truncated mRNA RNCs, the CMV-stalled RNC peptides were substantially less reactive with puromycin (Figure S1A). These data confirmed the known downregulation of the PTC by the CMV-stalling peptide. Similarly, as expected, neither eRF1 alone nor in conjunction with eRF3 displayed detectable release activity with the CMV RNCs. Interestingly, eRF1 and ABCE1 together resulted in a detectable increase in the relative amounts of free peptide, consistent with earlier studies showing a stimulation of peptide release by ABCE1 (Shoemaker and Green, 2011). This limited peptide-release activity provides support for the functional relevance of the heterologous ribosome complexes analyzed in this manuscript.

We performed cryo-EM and single-particle analysis including in silico sorting procedures to obtain structures of CMV RNC-eRF1-eRF3:GDPNP and CMV RNC-eRF1-ABCE1:ADPNP at a resolution of 9.15 and 8.75 Å at a Fourier shell correlation (FSC) cutoff of 0.5, respectively (8.9 and 8.6 Å at a FSC cutoff at 0.143 after processing according to the so-called gold standard approach) (Figures 1A, S1B, and S1C). For molecular interpretation, we used an updated model of the *Triticum aestivum* ribosome (Gogala et al., 2014) and placed homology models of eRF1, eRF3, and ABCE1 in the assigned densities, where most secondary structure was resolved. This was validated by calculating the cross-resolution between the models and the maps (Figures 1B and S2).

The pretermination complex showed extra densities for eRF1-eRF3 and P site-tRNA in positions consistent with previous observations in the rabbit eRF1:eRF3 pretermination complex (des Georges et al., 2014; Taylor et al., 2012) and in the yeast RNC-Pelota-Hbs1-complex (Becker et al., 2011). eRF1 is located in the A site, and its N-terminal domain (NTD) reaches into the decoding center of the small ribosomal subunit (SSU). The C-terminal domain (CTD) and central domain of eRF1 are packed against eRF3, which binds the ribosome like a classical EF-Tu-like translational GTPase. No density could be identified for the NTD of eRF3 (residues 97–255), suggesting a relatively flexible nature for this domain in our complex.

The termination/prerecycling complex showed dramatic conformational changes wherein eRF1 stretches between the P site-tRNA and ABCE1 that is located in the same position as seen previously in the Pelota ribosome complex (Becker et al., 2012). The CTD of eRF1 contacts the iron-sulfur (FeS) domain of ABCE1, whereas the central domain bearing the GGQ motif is stretched out toward the PTC of the large ribosomal subunit (LSU) where it contacts the P site-tRNA at the CCA end. Surprisingly, density for the NTD of eRF1 appeared to be fragmented and can only be visualized when the map is low-pass filtered at around 20 Å. This behavior is indicative of increased flexibility or disorder in this region that we confirmed in analysis of difference maps (Figure S3).

The Pretermination Complex

As mentioned briefly above, in the CMV RNC-eRF1-eRF3 pretermination complex, the ribosome adopts a similar overall conformation as observed for a stalled ribosome with Pelota-Hbs1 harboring a P site-tRNA (Becker et al., 2011) and the mammalian pretermination complex containing eRF1 and eRF3 (des Georges et al., 2014).

Consistent with the rabbit pretermination complex, the main contacts between eRF1 and the ribosome are found between the SSU and the NTD of eRF1 (Figure 2; Table S1). The conserved (TAS)NIKS loop is proximal to the stop codon poised in the A site, consistent with its critical role in stop codon recognition (Figure 2C). The NIKS loop is located in a similar position relative to the stop codon as for the equivalent loop (PVT/SPF) in bacterial RF1/RF2 that is involved in decoding (Korostelev et al., 2008; Laurberg et al., 2008; Weixlbaumer et al., 2008).

Density for the NTD of eRF1 was not defined clearly enough as to allow for unambiguous positioning of the mRNA and individual residues of the (TAS)NIKS motif. Conformational changes of the NTD upon ribosome binding and during the event of decoding have indeed been postulated on the basis of toeprinting and chemical-crosslinking assays (Alkalaeva et al., 2006; Kryuchkova et al., 2013). In a previously proposed two-step model, recognition of the first two nucleotides in the codon is followed by a conformational change of the NTD of eRF1 that allows for decoding of the second and third nucleotides (Kryuchkova et al., 2013). The existence of distinct somewhat different conformations of eRF1 in this region might explain the limited resolution of the NTD during decoding in our structure.

The contacts between the CTD of eRF1 and domain III of eRF3 are formed by similar structural elements as previously reported in the crystal structure of human eRF1-eRF3 complex (Cheng

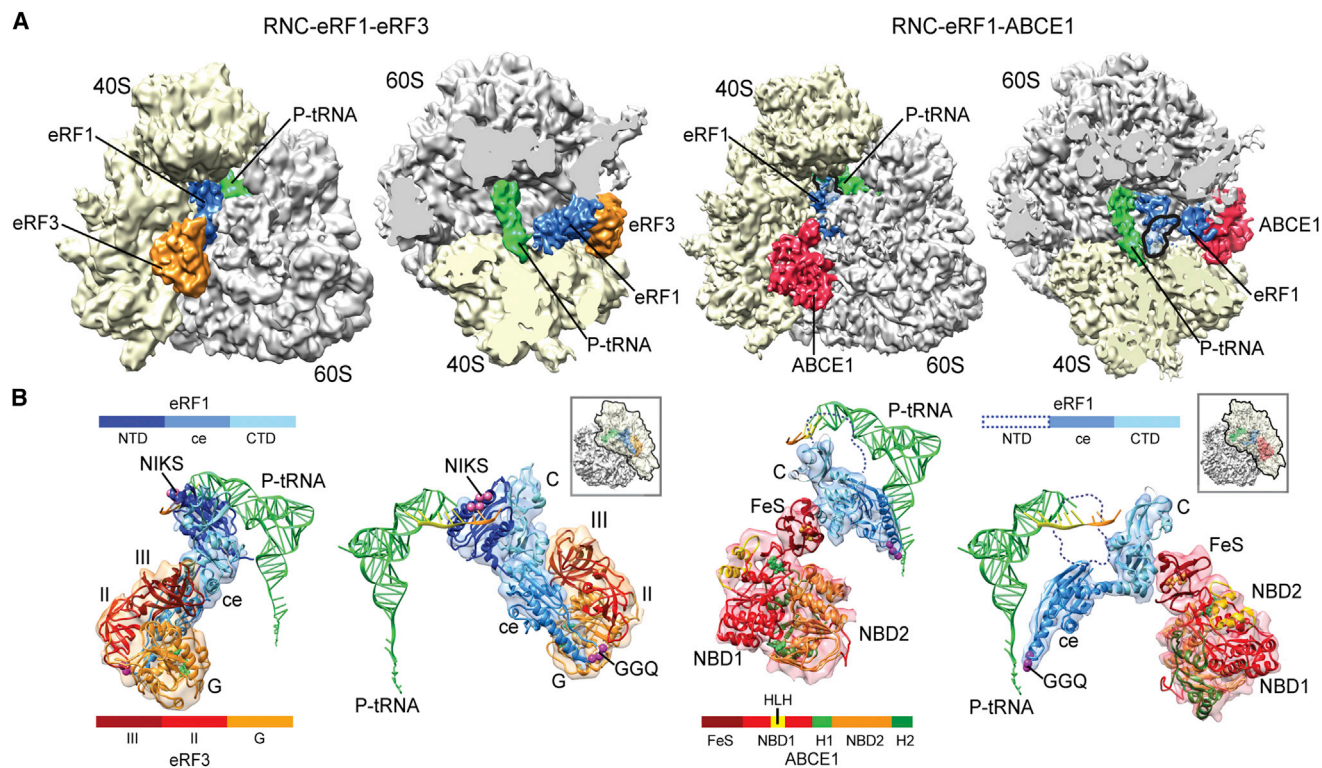


Figure 1. Cryo-EM Structures of Pretermination and Termination/Prerecycling Complexes

(A) Side and top views of the 80S ribosome pretermination complex with eRF1 and eRF3 (left) and termination/prerecycling complex with eRF1-ABCE1 (right). Density attributed to eRF1 occupies the A site. In the termination/prerecycling complex, the position of the flexible NTD of eRF1 is outlined with a black line. (B) Molecular models for peptidyl tRNA, eRF1, eRF3, and ABCE1 on the ribosome. The NIKS motif (pink spheres) of eRF1 is positioned in close proximity to the stop codon (orange). The central domain of eRF1 containing the GGQ loop (magenta spheres) is packed against eRF3. In complex with ABCE1, the central domain of eRF1 is swung toward the PTC.

et al., 2009). Here, however, helices $\alpha 8$ and $\alpha 11$ even more closely contact domain III of eRF3 (Figure S4). The minidomain in the CTD of eRF1 (that is only present in the nuclear magnetic resonance structure in the CTD of eRF1; Mantsoyov et al., 2010) anchors eRF1 to the beak of the SSU via the rRNA expansion segment ES8 and ribosomal protein (r-protein) S31. The central domain of eRF1 is tightly packed against all three domains of eRF3 and forms a large interaction surface of 1,088 Å². As such, both the switch I and switch II regions of the G domain of eRF3 are in contact with eRF1 (Figure S4; Table S1).

Notably, we also observe a few differences when comparing our structure to the RNC-Pelota-Hbs1 structure or the rabbit pretermination complex. In our structure, the inward movement of the stalk base compared to the factor-free state (rRNA helices H43 and H44 and r-protein L11, according to the nomenclature introduced by Jenner et al., 2012) is less pronounced (Figure S4). Concomitantly, the central domain and the CTD (including the minidomain) of eRF1 as well as eRF3 are bound in a more outward position such that the central domain of eRF1 is positioned closer to the small subunit and even contacts rRNA helix h14 with helix $\alpha 5$ that directly connects to the GGQ loop (Figure 2A; Table S1). As a result, the functionally critical GGQ loop is sandwiched between the G domain of eRF3 and the SSU in a tightly locked conformation that is incompatible with peptide-release activity

at this pretermination stage. In order to be active for release, a dramatic conformational change is needed to position the GGQ motif of the eRF1 central domain in the peptidyl-transferase center.

The Termination/Prerecycling Complex

The overall conformation of the ribosome in the CMV RNC-eRF1-ABCE1 complex is indeed similar to that observed in the RNC-Pelota-ABCE1 complex (Becker et al., 2012). In both cases, the stalk base is moved downward toward the sarcin-ricin loop (SRL; H95) (Figure S4B), and as in the pretermination complex, we observe P site-tRNA and a nascent peptide in the ribosomal exit tunnel, indicating that minimal if any peptide release has occurred in this particle population (Figure 3B).

The conformation of ABCE1 bound to the ribosome was also remarkably similar when compared to the Pelota-ABCE1-containing complex. ABCE1 binds in the translation factor-binding site and adopts an intermediate conformation of its nucleotide-binding domains (NBDs), somewhere between a fully open, ADP-bound structure, and the proposed closed ATP-bound form (Becker et al., 2012; Karcher et al., 2008). ABCE1 contacts the small subunit (h5-h15, h8-h14) mainly via its unique helix-loop-helix (HLH) and hinge motifs. Additional contacts are observed between NBD2 and L10.

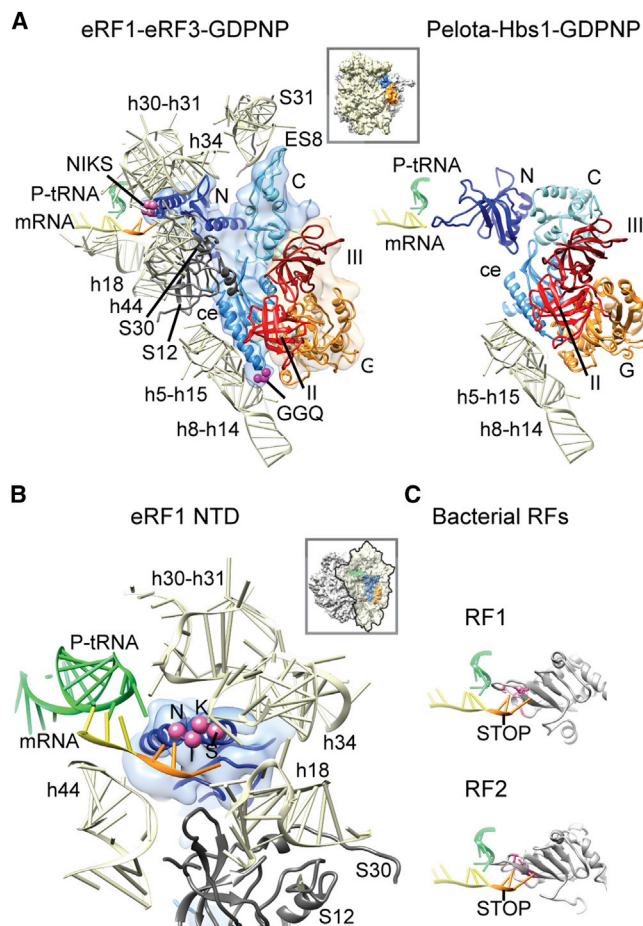


Figure 2. eRF1-Ribosome Interactions and Positioning of the NTD of eRF1 in the Pretermination Complex

(A) eRF1 forms multiple contacts with the ribosome (left) that are mostly identical to those of Pelota in complex with Hbs1 (right) (Becker et al., 2011), apart from a contact at h8-h14 of the 18S rRNA. The minidomain of the CTD of eRF1 contacts ES8 and S31 near the beak of the SSU.

(B) The NTD reaches deep into the decoding center and establishes multiple contacts with 18S rRNA and S12 (left). The NIKS motif is close to the stop codon in the A site (orange).

(C) For decoding of the stop codon, bacterial RF1 and RF2 (Korostelev et al., 2008; Laurberg et al., 2008) rely on domain II that is unrelated to eRF1 NTD. Interacting amino acids are marked in pink.

Notably, eRF1 adopts a dramatically changed elongated conformation similar to ribosome-bound Pelota in the presence of ABCE1 (Figure 3). This elongated conformation is broadly similar to that of bacterial ribosome-bound RFs (Korostelev et al., 2008; Laurberg et al., 2008; Weixlbaumer et al., 2008), though in contrast to the bacterial structures, the NTD (the codon-interaction domain) of eRF1 appears to be delocalized.

The CTD of eRF1 contacts the FeS domain of ABCE1, the stalk base (H43-H44 and L11), and the SRL (H95) in the LSU. The central domain of eRF1 undergoes the most drastic conformational rearrangements in this structure, establishing multiple contacts to the rRNA (H71, H89, H91, H92, and H93) and stretching out toward the P site-tRNA. The conserved loop containing the

GGQ motif is now located at the PTC of the LSU in close proximity to the CCA end of the peptidyl tRNA (Table S2). Modeling the GGQ region on the basis of previous crystal structures of bacterial RF1 and RF2 bound to the ribosome allowed for easily fitting of the density without further adjustments (Figure 3B). Although eRF1 is otherwise unrelated in sequence and structure (the class 1 RFs evolved independently in these two lineages), this structural finding suggests that the strictly conserved GGQ motif functions in the same way in these two systems.

Finally, we see stabilization of eRF1 in this active conformation by ABCE1 through contacting the CTD of eRF1. These structural observations rationalize how this ATPase can stimulate eRF1-dependent peptide-release activity (Shoemaker and Green, 2011). In order to fully appreciate the contribution that ABCE1 makes to positioning of eRF1 for catalysis, however, it will be useful to determine the structure of a ribosome complex loaded with eRF1 alone.

Conclusions

Our cryo-EM structures show that eukaryotic termination and ribosome recycling by eRF1, eRF3, and ABCE1 follow the same order of events and conformational transitions as observed previously for stalled ribosome rescue by Pelota, Hbs1, and ABCE1. In both pathways, the A site factor, eRF1 for termination and Pelota for ribosome rescue, is delivered by the EF-Tu-like GTPase eRF3 or Hbs1, respectively, which then dissociates from the ribosome after GTP hydrolysis (Figure 4). In their pre-GTP hydrolysis state, eRF1-eRF3 and Pelota-Hbs1 adopt similar conformations on the ribosome, though in the pre-termination (eRF1) complex, an additional prominent contact between the central domain of eRF1 and the SSU is established; as a consequence, this domain is more tightly locked between the SSU and eRF3. Notably, the central domain of eRF1 contacts both the switch I and switch II regions of eRF3 that control its GTP hydrolysis. Higher-resolution structures will be required to decipher how decoding of the stop codon coordinates these events on a molecular level.

Next, we see that after eRF3 dissociation, eRF1 changes its conformation such that the central domain of eRF1 moves toward the PTC for catalysis of peptide release. The ribosome-eRF1 complex allows for binding of ABCE1 that appears to stabilize the fully extended active conformation of eRF1, thereby stimulating peptide release (Movie S1). Interestingly, the NTD of eRF1 appears to disengage the A site codon in this complex, indicating that codon engagement may not be required at this stage for peptide release. Yet, in contrast to the bacterial RFs that dissociate after termination (Freistoffer et al., 1997), eRF1 is still required for ABCE1-dependent ribosomal subunit splitting (Pisarev et al., 2010; Shoemaker and Green, 2011).

In a final stage, we know that ABCE1 functions in concert with bound eRF1 (on the posttermination complex) to promote subunit dissociation (Pisarev et al., 2010; Shoemaker and Green, 2011). Here, we see that ABCE1 adopts a remarkably similar conformation as observed in the prerecycling complex with Pelota (Becker et al., 2012). These data indicate that the mechanism of 80S splitting follows the same principle, independent of the nature of the ribosome to be recycled. Like Pelota in the context of ribosome rescue, eRF1 may act as a structural

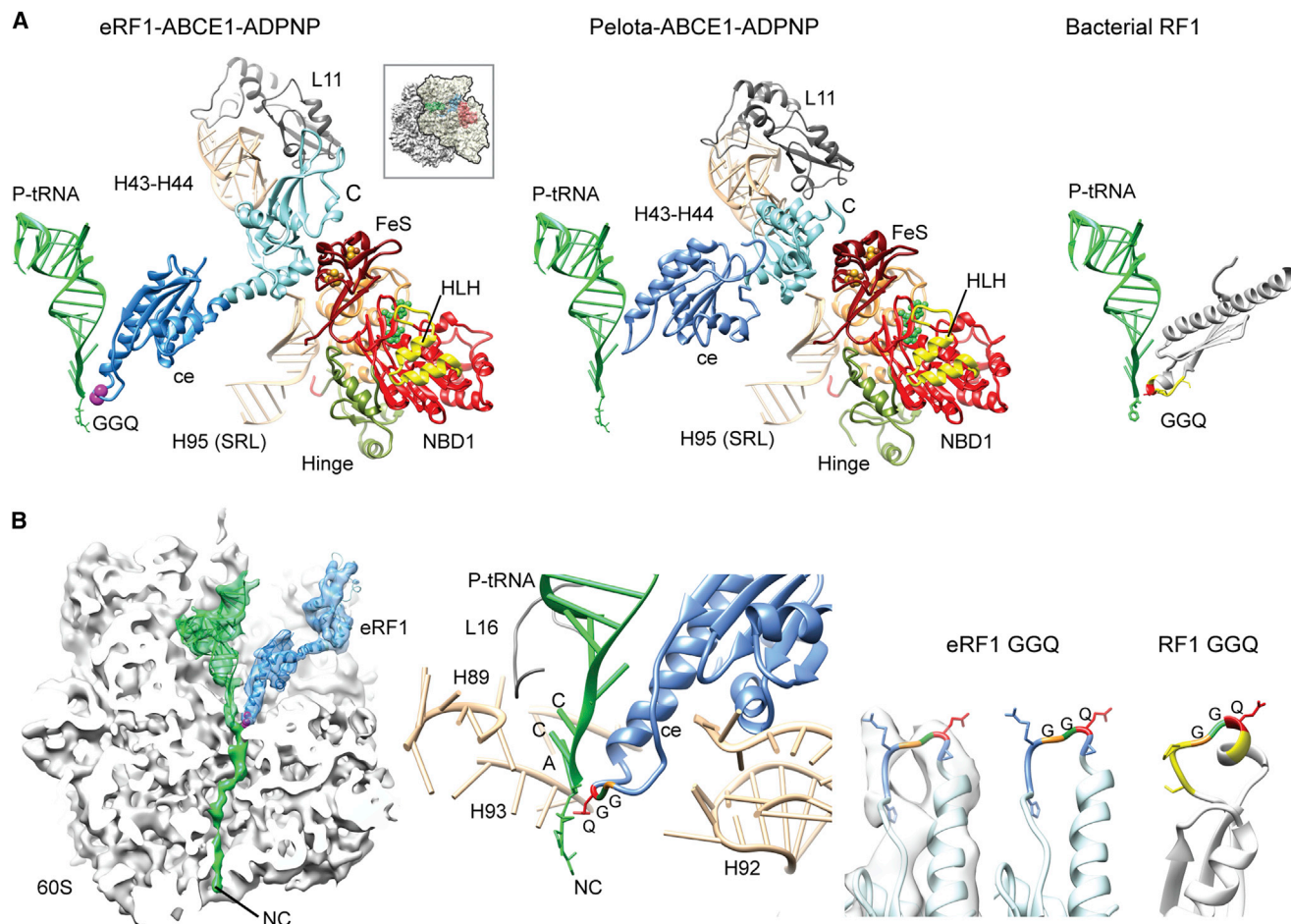


Figure 3. eRF1 Interactions and Positioning of Its Central Domain in the Termination/Prerecycling Complex

(A) The central domain of eRF1 undergoes a conformational change that positions the GGQ loop near the CCA end of the P site-tRNA (left). The CTD moves away from the SSU and forms contacts with the stalk base of the LSU and the SRL. These conformational changes are very similar to those of Pelota in complex with ABCE1 (middle). Unrelated domain III of bacterial RF1 possesses a different architecture but coordinates the highly conserved GGQ loop in an identical position (right).

(B) Cross-section and close-up view of the central domain of eRF1 with the GGQ loop close to the peptidyl tRNA (left and middle). Position and conformation of the GGQ loop are highly similar to that of bacterial RF1 (Laurberg et al., 2008).

“bolt” that transmits conformational changes within ABCE1 upon ATP hydrolysis to the ribosome and induces splitting of the subunits. More structural and biochemical data will be needed to understand how this reaction is triggered and how ordered ATP binding and ATP hydrolysis in the two NBDs of ABCE1 contribute to this process.

EXPERIMENTAL PROCEDURES

Programmed CMV-stalled RNCs were prepared from a wheat germ in-vitro translation extract as described by Bhushan et al. (2010). Recombinant yeast eRF1, eRF3, and ABCE1 were overexpressed in *E. coli* or *S. cerevisiae* and affinity purified. For release assays, RNCs were incubated together with the ligands, and tagged nascent peptidyl tRNA or free peptide was analyzed by western blotting.

Termination complexes were formed by in vitro reconstitution with recombinant-purified factors. The complexes were vitrified, and data were collected on a Titan Krios electron microscope (FEI). Single-particle analysis followed by 3D reconstruction was performed using the SPIDER software package (Frank

et al., 1996). For molecular interpretation of the *Triticum aestivum* 80S ribosome, we used an updated model (Gogala et al., 2014). Models of eRF1, eRF3, and ABCE1 were based on existing crystal structures. See Supplemental Experimental Procedures for a detailed description of the Experimental Procedures.

ACCESSION NUMBERS

Cryo-EM maps for the pretermination complex (RNC-eRF1-eRF3) and the termination/prerecycling complex (RNC-eRF1-ABCE1) have been deposited in the EMDataBank under accession codes EMD-2597 and EMD-2598. The respective coordinates for EM-based models are deposited in the Protein Data Bank under ID codes 4rcn and 4rcm.

SUPPLEMENTAL INFORMATION

Supplemental Information includes Supplemental Experimental Procedures, four figures, two tables, and one movie and can be found with this article online at <http://dx.doi.org/10.1016/j.celrep.2014.04.058>.

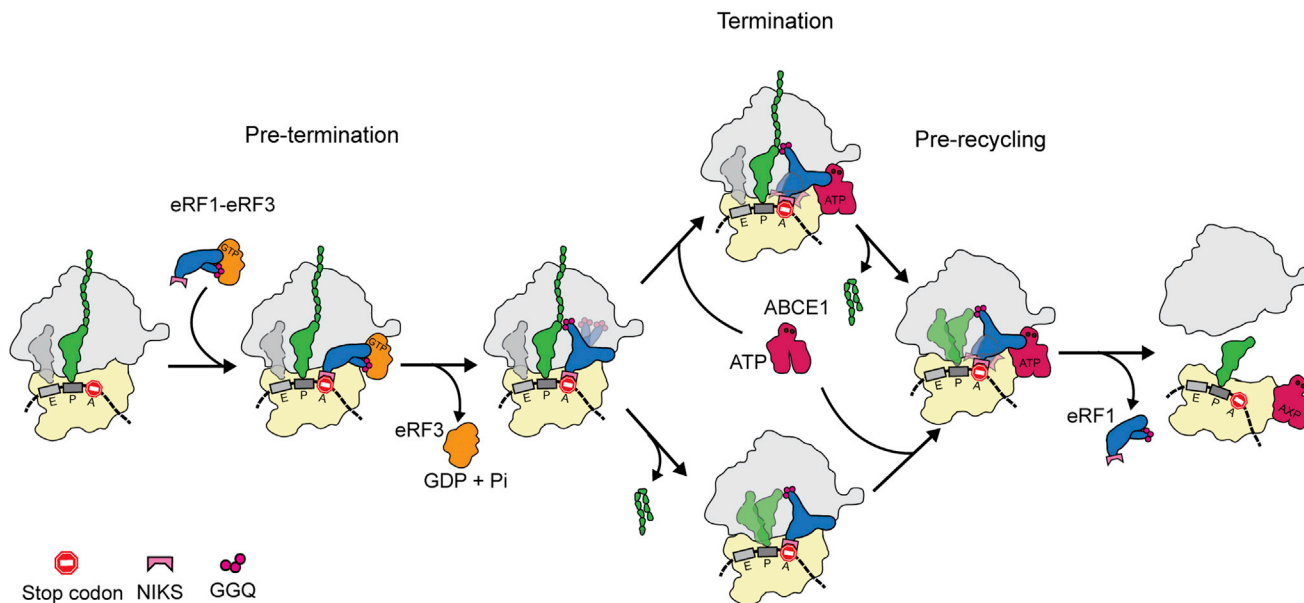


Figure 4. Scheme of Eukaryotic Translation Termination and Ribosome Recycling

For termination, the stop codon in the A site is recognized by the eRF1-eRF3-GTP ternary complex. eRF3 dissociates after GTP hydrolysis and allows the central domain of eRF1 to swing to the PTC. Proper positioning of the GGQ motif in the central domain of eRF1 may already allow peptide release, resulting in a termination complex with the deacyl-tRNA in the P state or P/E hybrid state. Alternatively, the active conformation of eRF1 in the pretermination complex is stabilized after binding of ABCE1. This stimulates peptide release while the NTD of eRF1 is delocalized, thus decoupling decoding from peptide release. Independent of the termination mechanism, ABCE1 together with eRF1 functions in concert to dissociate the ribosome into small and large subunits.

AUTHOR CONTRIBUTIONS

A.P., T.B., and R.B. designed the study. D.E.E. generated expression plasmids. A.P. carried out RNC and release factor purifications, generation of termination factor complexes, and biochemical assays. A. Heuer purified ABCE1. O.B. collected cryo-EM data. A. Hauser developed the Starfish software. A.P. and A. Heuer processed and interpreted the cryo-EM structures. T.B. built molecular models for eRF1 and eRF3. A.P. and T.B. prepared all figures. C.B.-G. built a refined model of the wheat germ ribosome. A. Heuer created [Movie S1](#). A.P., T.B., R.B., and R.G. interpreted results and wrote the paper.

ACKNOWLEDGMENTS

We thank Charlotte Ungewickell for assistance with cryo-EM and Heidemarie Sieber for assistance with biochemical experiments. This work was supported by grants from the German Research Council (GRK 1721, FOR 1805, and SFB646 to R.B., and SFB646 to T.B.). R.B. acknowledges support by the Center for Integrated Protein Science and the European Research Council (Advanced Grant CRYOTRANSLATION).

Received: January 25, 2014

Revised: March 1, 2014

Accepted: April 3, 2014

Published: July 3, 2014

REFERENCES

Alkalaeva, E.Z., Pisarev, A.V., Frolova, L.Y., Kisselev, L.L., and Pestova, T.V. (2006). In vitro reconstitution of eukaryotic translation reveals cooperativity between release factors eRF1 and eRF3. *Cell* 125, 1125–1136.

Barthelme, D., Dinkelaker, S., Albers, S.V., Londei, P., Ermler, U., and Tampé, R. (2011). Ribosome recycling depends on a mechanistic link between the FeS

cluster domain and a conformational switch of the twin-ATPase ABCE1. *Proc. Natl. Acad. Sci. USA* 108, 3228–3233.

Becker, T., Armache, J.P., Jarasch, A., Anger, A.M., Villa, E., Sieber, H., Mottaal, B.A., Mielke, T., Berninghausen, O., and Beckmann, R. (2011). Structure of the no-go mRNA decay complex Dom34-Hbs1 bound to a stalled 80S ribosome. *Nat. Struct. Mol. Biol.* 18, 715–720.

Becker, T., Franckenberg, S., Wickles, S., Shoemaker, C.J., Anger, A.M., Armache, J.P., Sieber, H., Ungewickell, C., Berninghausen, O., Daberkow, I., et al. (2012). Structural basis of highly conserved ribosome recycling in eukaryotes and archaea. *Nature* 482, 501–506.

Bhushan, S., Meyer, H., Starosta, A.L., Becker, T., Mielke, T., Berninghausen, O., Sattler, M., Wilson, D.N., and Beckmann, R. (2010). Structural basis for translational stalling by human cytomegalovirus and fungal arginine attenuator peptide. *Mol. Cell* 40, 138–146.

Cheng, Z., Saito, K., Pisarev, A.V., Wada, M., Pisareva, V.P., Pestova, T.V., Gajda, M., Round, A., Kong, C., Lim, M., et al. (2009). Structural insights into eRF3 and stop codon recognition by eRF1. *Genes Dev.* 23, 1106–1118.

des Georges, A., Hashem, Y., Unbehaun, A., Grassucci, R.A., Taylor, D., Hellen, C.U., Pestova, T.V., and Frank, J. (2014). Structure of the mammalian ribosomal pre-termination complex associated with eRF1.eRF3.GDPNP. *Nucleic Acids Res.* 42, 3409–3418.

Doma, M.K., and Parker, R. (2006). Endonucleolytic cleavage of eukaryotic mRNAs with stalls in translation elongation. *Nature* 440, 561–564.

Franckenberg, S., Becker, T., and Beckmann, R. (2012). Structural view on recycling of archaeal and eukaryotic ribosomes after canonical termination and ribosome rescue. *Curr. Opin. Struct. Biol.* 22, 786–796.

Frank, J., Radermacher, M., Penczek, P., Zhu, J., Li, Y., Ladjadj, M., and Leith, A. (1996). SPIDER and WEB: processing and visualization of images in 3D electron microscopy and related fields. *J. Struct. Biol.* 116, 190–199.

Freistroffer, D.V., Pavlov, M.Y., MacDougall, J., Buckingham, R.H., and Ehrenberg, M. (1997). Release factor RF3 in *E. coli* accelerates the dissociation of

- release factors RF1 and RF2 from the ribosome in a GTP-dependent manner. *EMBO J.* **16**, 4126–4133.
- Frolova, L., Le Goff, X., Zhouravleva, G., Davydova, E., Philippe, M., and Kisselev, L. (1996). Eukaryotic polypeptide chain release factor eRF3 is an eRF1- and ribosome-dependent guanosine triphosphatase. *RNA* **2**, 334–341.
- Gogala, M., Becker, T., Beatrix, B., Armache, J.P., Barrio-Garcia, C., Berninghausen, O., and Beckmann, R. (2014). Structures of the Sec61 complex engaged in nascent peptide translocation or membrane insertion. *Nature* **506**, 107–110.
- Janzen, D.M., Frolova, L., and Geballe, A.P. (2002). Inhibition of translation termination mediated by an interaction of eukaryotic release factor 1 with a nascent peptidyl-tRNA. *Mol. Cell. Biol.* **22**, 8562–8570.
- Jenner, L., Melnikov, S., Garreau de Loubresse, N., Ben-Shem, A., Iskakova, M., Urzhumtsev, A., Meskauskas, A., Dinman, J., Yusupova, G., and Yusupov, M. (2012). Crystal structure of the 80S yeast ribosome. *Curr. Opin. Struct. Biol.* **22**, 759–767.
- Karcher, A., Schele, A., and Hopfner, K.P. (2008). X-ray structure of the complete ABC enzyme ABCE1 from *Pyrococcus abyssi*. *J. Biol. Chem.* **283**, 7962–7971.
- Kong, C., Ito, K., Walsh, M.A., Wada, M., Liu, Y., Kumar, S., Barford, D., Nakamura, Y., and Song, H. (2004). Crystal structure and functional analysis of the eukaryotic class II release factor eRF3 from *S. pombe*. *Mol. Cell* **14**, 233–245.
- Korostelev, A., Asahara, H., Lancaster, L., Laurberg, M., Hirschi, A., Zhu, J., Trakhanov, S., Scott, W.G., and Noller, H.F. (2008). Crystal structure of a translation termination complex formed with release factor RF2. *Proc. Natl. Acad. Sci. USA* **105**, 19684–19689.
- Kryuchkova, P., Grishin, A., Eliseev, B., Karyagina, A., Frolova, L., and Alkalaeva, E. (2013). Two-step model of stop codon recognition by eukaryotic release factor eRF1. *Nucleic Acids Res.* **41**, 4573–4586.
- Laurberg, M., Asahara, H., Korostelev, A., Zhu, J., Trakhanov, S., and Noller, H.F. (2008). Structural basis for translation termination on the 70S ribosome. *Nature* **454**, 852–857.
- Mantsyzov, A.B., Ivanova, E.V., Birdsall, B., Alkalaeva, E.Z., Kryuchkova, P.N., Kelly, G., Frolova, L.Y., and Polshakov, V.I. (2010). NMR solution structure and function of the C-terminal domain of eukaryotic class 1 polypeptide chain release factor. *FEBS J.* **277**, 2611–2627.
- Pisarev, A.V., Skabkin, M.A., Pisareva, V.P., Skabkina, O.V., Rakotondrafara, A.M., Hentze, M.W., Hellen, C.U., and Pestova, T.V. (2010). The role of ABCE1 in eukaryotic posttermination ribosomal recycling. *Mol. Cell* **37**, 196–210.
- Pisareva, V.P., Skabkin, M.A., Hellen, C.U., Pestova, T.V., and Pisarev, A.V. (2011). Dissociation by Pelota, Hbs1 and ABCE1 of mammalian vacant 80S ribosomes and stalled elongation complexes. *EMBO J.* **30**, 1804–1817.
- Shoemaker, C.J., and Green, R. (2011). Kinetic analysis reveals the ordered coupling of translation termination and ribosome recycling in yeast. *Proc. Natl. Acad. Sci. USA* **108**, E1392–E1398.
- Shoemaker, C.J., Eyster, D.E., and Green, R. (2010). Dom34:Hbs1 promotes subunit dissociation and peptidyl-tRNA drop-off to initiate no-go decay. *Science* **330**, 369–372.
- Song, H., Mugnier, P., Das, A.K., Webb, H.M., Evans, D.R., Tuite, M.F., Hemmings, B.A., and Barford, D. (2000). The crystal structure of human eukaryotic release factor eRF1—mechanism of stop codon recognition and peptidyl-tRNA hydrolysis. *Cell* **100**, 311–321.
- Taylor, D., Unbehauen, A., Li, W., Das, S., Lei, J., Liao, H.Y., Grassucci, R.A., Pestova, T.V., and Frank, J. (2012). Cryo-EM structure of the mammalian eukaryotic release factor eRF1-eRF3-associated termination complex. *Proc. Natl. Acad. Sci. USA* **109**, 18413–18418.
- Weixlbaumer, A., Jin, H., Neubauer, C., Voorhees, R.M., Petry, S., Kelley, A.C., and Ramakrishnan, V. (2008). Insights into translational termination from the structure of RF2 bound to the ribosome. *Science* **322**, 953–956.

Cell Reports, Volume 8

Supplemental Information

**Cryoelectron Microscopic Structures
of Eukaryotic Translation Termination Complexes
Containing eRF1-eRF3 or eRF1-ABCE1**

Anne Preis, Andre Heuer, Clara Barrio-Garcia, Andreas Hauser, Daniel E. Eyler, Otto Berninghausen, Rachel Green, Thomas Becker, and Roland Beckmann

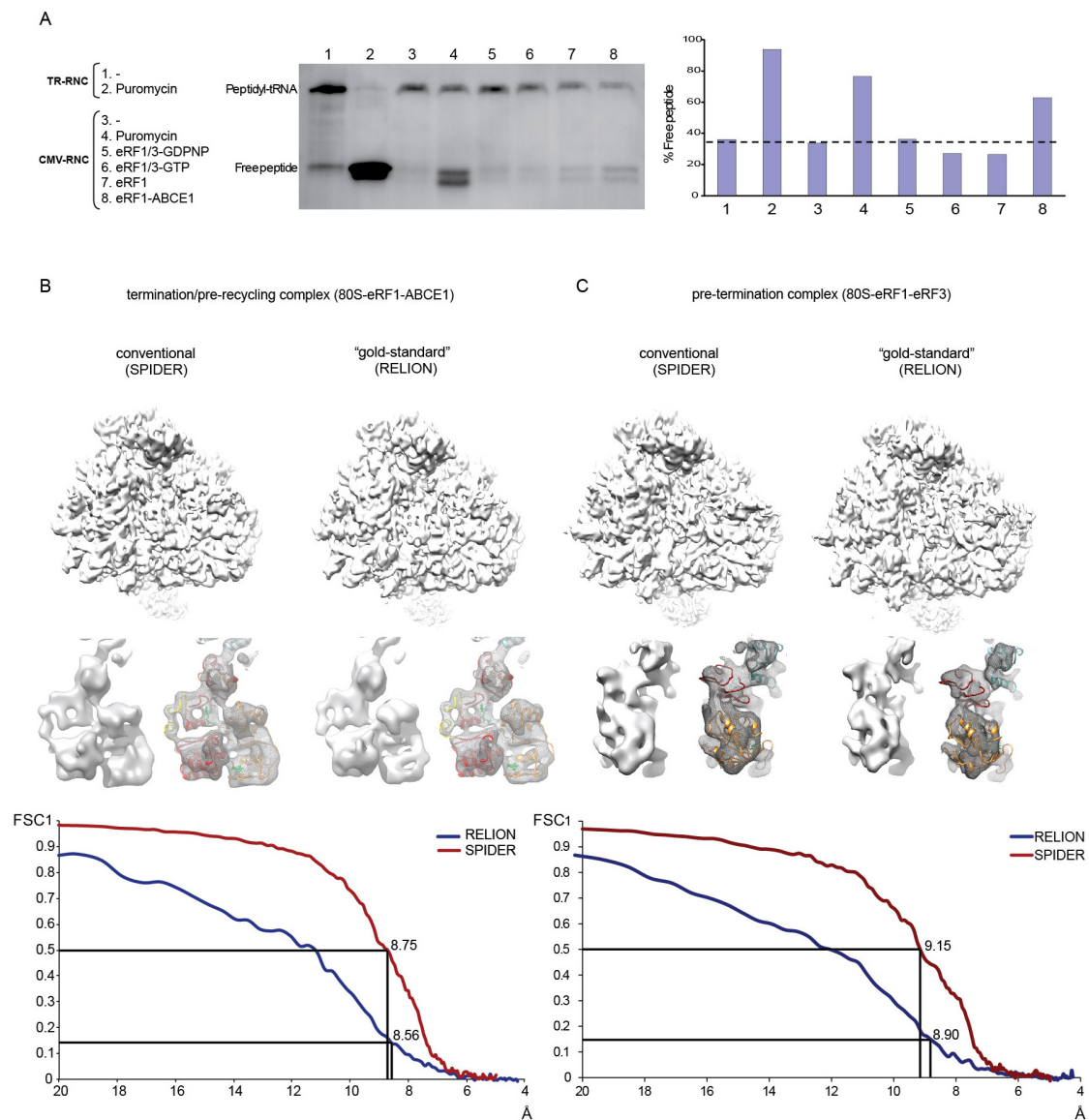


Figure S1 (related to Results and Discussion, Experimental Procedures and Figure 1) : Release Assays and Comparison between conventional refinement and “gold-standard” refinement (B,C)

“CMV-stalled” RNCs with a stop-codon in the A-site were either treated with puromycin or incubated with a 5-fold molar excess of release/recycling factor complexes and subjected to Western Blot analysis using an anti-HA antibody (A). Bands for peptidyl-tRNA and free peptide are indicated. As a measure for release activity the relative amount of free peptide was quantified using ImageJ. As a control, RNCs stalled by truncated mRNA (TR-RNC) were used.

Cryo-EM maps and resolution curves resulting from conventional SPIDER and “gold-standard” RELION refinement are shown for (B) the termination/pre-recycling dataset and (C) the pre-termination dataset. Snapshots were taken from the entire ribosome, the ribosomal exit site and isolated densities for the ligands (ABCE1 in (B), eRF3 in (C)).

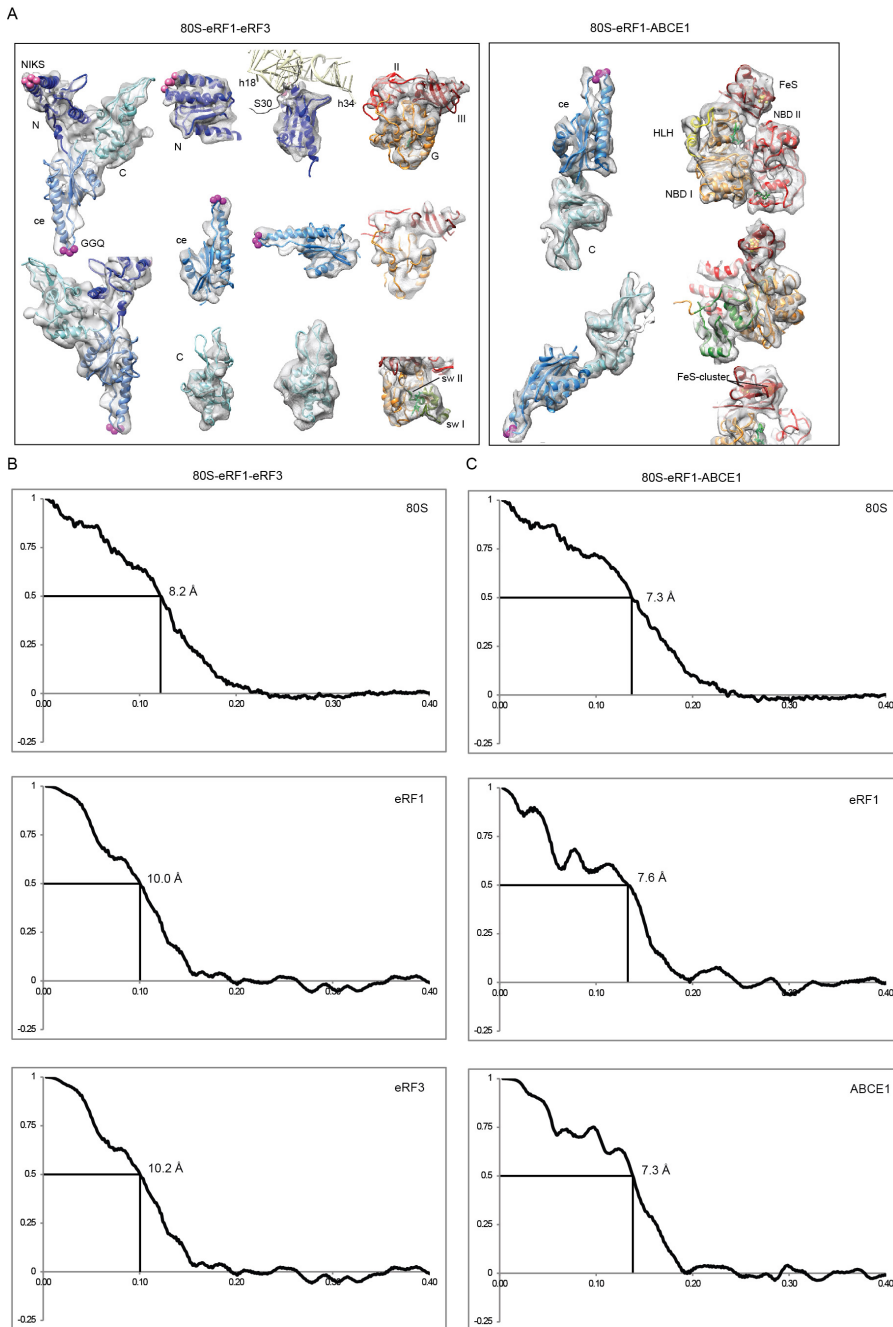


Figure S2 (related to Figures 1-3): Fitting of eRF1, eRF3 and ABCE1 and FSC curves between experimental maps and molecular models.

Isolated densities for eRF1, eRF3 and ABCE1 are shown in transparent mesh with homology models fitted based on resolved secondary structure. The color code for individual domains is as in **Figure 1B**. In addition, for the eRF1-NTD the ribosomal interaction site is shown. The mini-domain insert of the eRF1-CTD can only be seen with low contour levels. Density for the two FeS-clusters of ABCE1 is shown in red mesh. Nucleotides (GDPNP for eRF3, ATP for ABCE1) are shown in green.

FSC curves between models and maps for the 80S-eRF1-eRF3 dataset (**B**) and the 80S-eRF1-ABCE1 dataset (**C**) were calculated for the entire 80S ribosome using the model for the wheat germ ribosome (3J5Z, 3J60, 3J61 and 3J62) and for individual ligands. For ligands, respective densities were cut out using a soft mask and the resolution was read at a cutoff at a FSC 0.5.

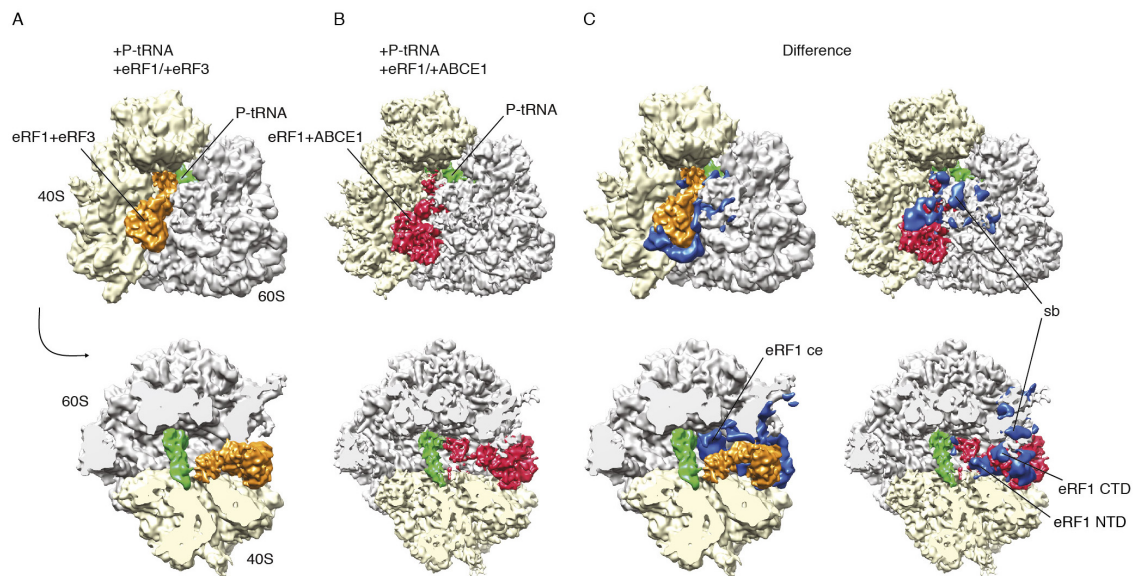


Figure S3 (related to Figure 1): Difference maps.

Front and top views of pre-termination (**A**) and termination/pre-recycling (**B**) complexes. In (**C**) the difference map of (**B**) minus (**A**) is shown in blue. Differences can be seen for the ribosomal stalk base (rRNA helices H43-H44 and r-protein L11), the eRF1 central domain and ABCE1. (**D**) represents the difference map (**A**) minus (**B**). Differences can be seen for the ribosomal stalk base (sb), eRF3 and the CTD and the NTD of eRF1.

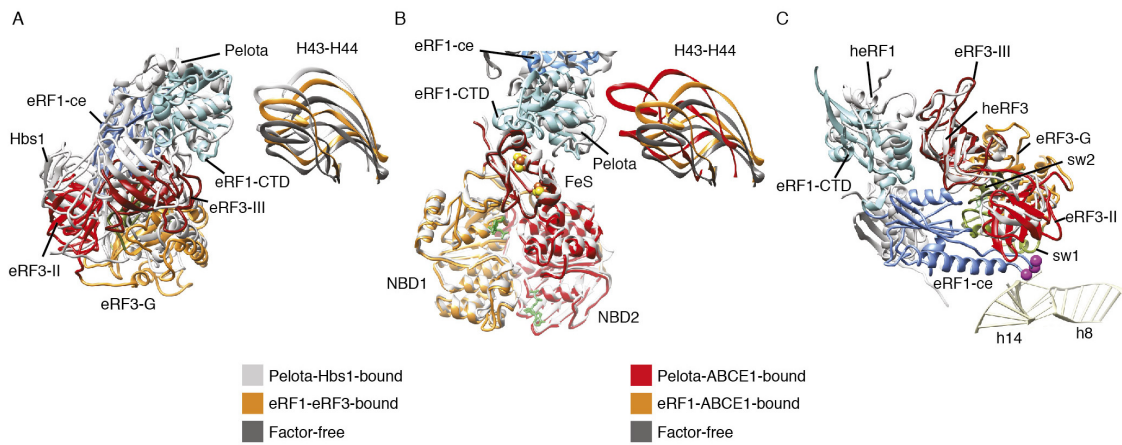


Figure S4 (related to Figures 2 and 3): Comparative analysis of ribosome-bound eRF1-eRF3 and eRF1-ABCE1 complexes.

(A) Overlay of the model for eRF1-eRF3 (color code as in **Figure 1B**) with Pelota-Hbs1 (PDB accession 3IZQ) (17) (grey). (B) Overlay of eRF1-ABCE1 (color code as in **Figure 1B**) with Pelota-ABCE1 (PDB accession 3J16) (18) (grey). The position of stalk-base helices H43-H44 in given in dark grey (factor-free), orange (bound to eRF1-eRF3), grey (bound to Pelota-Hbs1) and red (bound to eRF1-ABCE1 or Pelota-ABCE1). (C) Overlay of model for eRF1-eRF3 with the crystal structure of the human eRF1-eRF3 complex (PDB accession 3E1Y) (12) lacking the eRF3-G domain (grey).

Movie S1 (related to Figure 4): Eukaryotic translation termination.

Table S1: Contacts in the RNC-eRF1-eRF3:GDPNP pre-termination complex (related to Figure 2).

Table S2: Contacts in the RNC-eRF1-ABCE1:ADPNP termination/pre-recycling complex (related to Figure 3).

Supplemental Experimental Procedures

Purification of CMV-stalled ribosome nascent chain complexes

Wheat germ ribosomes were programmed with mRNA containing the first 98 amino acids of dipeptidyl-peptidase (DPAP-B98) carrying a type II signal anchor sequence followed by the 22-codon long human CMV *gp48* uORF stalling sequence. The template also encoded for N-terminal hexahistidine (His₆) and hemeagglutinin (HA) tags. The PCR-amplified DNA template was used for synthesis of uncapped mRNA using T7 RNA polymerase. RNCs were purified from the wheat germ cell-free translation extract as described before (Bhushan et al., 2010).

RNCs stalled by truncated mRNA coding for the first 120 amino acids of DPAP-B (DP120) were generated as described before (Becker et al., 2009).

Purification of eRF1, eRF3 and ABCE1

eRF1 and eRF3 Δ N97 were cloned into pTYB2 (part of the IMPACT system by NEB) between the NdeI and SmaI sites and individually overexpressed in *E coli* BL21(DE3). Expression was carried out in Terrific Broth and induced with IPTG at 16 °C for 15 h. Cells expressing release factors were washed with cold 1 % KCl, resuspended in lysis buffer eRF1 (20 mM HEPES pH 7.5, 500 mM NaCl, 1 mM EDTA) or lysis buffer eRF3 (20 mM HEPES pH 7.5, 500 mM NaCl, 0.1 mM GTP) and lysed using a French press.

The lysate was clarified at 20,000 g for 30 min (Beckmann Type 45 Ti) and loaded on Chitin Beads (NEB), 2 ml bed volume per 1 l of expression culture. The column was washed with 20 column volumes (CV) of corresponding lysis buffer and 20 CV of wash buffer (20 mM HEPES pH 7.5, 1 M NaCl, 1 mM EDTA). The column was flushed with 3 CV of elution buffer (20 mM HEPES pH 7.5, 500 mM KCl, 1 mM EDTA, 50 mM DTT) and incubated for 16 h at 4 °C. The factors were eluted with 6 CV of elution buffer, concentrated and exchanged into gel filtration buffer (20mM HEPES pH 7.5, 200 mM KCl, 2 mM DTT, 1.5 mM MgCl₂, 10% Glycerol) in Microspin centrifugal filter units (threshold 10,000, Invitrogen) in 10-minute steps at 2500 g (5417/R, Eppendorf). Prior to gel filtration, the factors were incubated together in gel filtration buffer in the presence of 500 μM GDPNP or GTP on ice for 15 min. The complexes were purified on a Superdex 200 10/300 GL column and stored in gel filtration buffer. ABCE1 was purified from *S. cerevisiae* as described before (Shoemaker and Green, 2011).

Release assays

2 pmol RNCs were incubated with a ten-fold molar excess of eRF1-eRF3-GDPNP, eRF1 alone or eRF1 and ABCE1 in binding buffer (20 mM HEPES pH 7.5, 200 mM KCl, 1.5 MgCl₂, 2 mM DTT, 10 μg/ml cycloheximide, supplied with 500 μM GDPNP, GTP or ADPNP). Puromycin was added to a final concentration of 0.1 mM. The assays were incubated for 1 h at 27 °C and analyzed by Western blot for HA-tag.

Reconstitution of RNC-eRF1-eRF3 and RNC-eRF1-ABCE1 complexes and cryo-EM sample preparation

RNCs were incubated with a ten-fold molar excess of preformed eRF1-eRF3 complex or eRF1 and ABCE1 in grid buffer (20 mM HEPES pH 7.5, 200 mM KCl, 1.5 MgCl₂, 2

mM DTT, 10 $\mu\text{g/ml}$ cycloheximide, 0.05 % Nikkol, 0.03 % DBC, 500 μM GDPNP/ADPNP). Sec61 was added at a five-fold molar excess to saturate the hydrophobic signal-anchor sequence and avoid orientational bias on the cryo-grids.

Electron microscopy and image processing

For sample preparation, 2nm-carbon coated Quantifoil grids were used. The grids were prepared as described before (Wagenknecht et al., 1988). Both datasets were collected at 200 keV at a magnification of $147,136\times$ at the plane of the CCD using a TemCam-F416 CMOS camera (TVIPS GmbH, 4096×4096 pixel, $15.6\ \mu\text{m}$ pixel, 1 s/full frame) resulting in an image pixel size of $1.06\ \text{\AA}$ (object scale). The particles were picked with starfish_boxing version 0.2.0, which is part of the new StarFish single particle analysis program suite. Starfish_boxing detects electron dense features by binarizing the raw micrographs into pixels with a value above an expected threshold and below. The binarization of the micrograph uses two arithmetic mean filtered images representing foreground and local background and are computed with either a very fast real space SSE2 implementation of with an FFT library. Only two parameters are required for a given dataset: the expected radius of the particle and a threshold for the binarization. After the binarization one usually gets many connected components ("white areas") in the shape of the densities present, e.g. particles, ice or similarly sized contamination. The connected components are then detected with a very simple algorithm. Based on the assumption that most connected components are particles a filter based on the median box size is used to filter out non-particles. The final coordinates were used for boxing out the particle images followed by import into SPIDER (Frank et al., 1996).

The RNC-eRF1-eRF3 dataset (224,689 particles) was sorted for presence of P-site tRNA first followed by sorting for the presence of factors. For the final reconstruction 39,309 particles were used. Sorting the RNC-eRF1-ABCE1 dataset (149,673 particles) was carried out analogously with 51,049 particles used for the final reconstruction.

The final datasets were also subjected to refinement using the “gold-standard” approach applied by the RELION software (Scheres, 2012). Here, the dataset is split into two data-subsets that are refined independently. The resolution was read at a FSC of 0.143 and, in good agreement with the results from conventional SPIDER processing, final resolutions after “gold-standard” processing were determined to 8.9 Å for the RNC-eRF1-eRF3 dataset and 8.6 Å for the RNC-eRF1-ABCE1 dataset.

Model building

For molecular interpretation of the *Triticum aestivum* 80S ribosome we used the updated model (pdb codes 3J5Z, 3J60, 3J61 and 3J62) (Gogala, 2014). Homology models of the central and NTD of eRF1 were built using HHPRED (Soding et al., 2005) on the basis of *Homo sapiens* and *Schizosaccharomyces pombe* crystal structures (Cheng et al., 2009; Song et al., 2000) (PDB accession 3E20 and 1DT9) The CTD (including the mini-domain insert that is not present in the crystal structures) was built on the basis of a NMR structure of the CTD of human eRF1 (PDB accession 2KTU) (Mantsyzov et al., 2010). The GGQ-loop (residues 177-183 of eRF1) was modeled based the GGQ-loop of RF2 (PDB accession 2XRT) (Jin et al., 2010) and RF1 (PDB accession 3MR8) (Korostelev et al., 2010). The eRF3 homology model was built on the basis of crystal structures of *S. pombe* Hbs1 (PDB accession 3MCA) (Chen et al., 2010) and eRF3 (PDB accession 1R5O) (Kong et al., 2004). Models for ABCE1 in the open ADP-bound, intermediate and closed ATP-bound state were described previously (Becker et al., 2012). Individual

domains of eRF1 and eRF3 were fitted as rigid bodies first and then manually adjusted using UCSF Chimera (Pettersen et al., 2004) and Coot (Emsley and Cowtan, 2004). Final models were minimized in UCSF Chimera and clashes were removed using VMD (Phillips et al., 2005) and MDFF (Trabuco et al., 2008).

To validate the quality of the models the cross-resolution between the maps and the model was calculated. Using Chimera, we generated a map from the model-pdbs and calculated the resolution between these maps and our experimental maps. This was done for the entire ribosome as well as for individual factors eRF1, eRF3 and ABCE1. Isolated densities for the factors were extracted using soft masks in SPIDER.

SUPPLEMENTAL REFERENCES

Becker, T., Bhushan, S., Jarasch, A., Armache, J.P., Funes, S., Jossinet, F., Gumbart, J., Mielke, T., Berninghausen, O., Schulten, K., *et al.* (2009). Structure of monomeric yeast and mammalian Sec61 complexes interacting with the translating ribosome. *Science* *326*, 1369-1373.

Chen, L., Muhrad, D., Haurlyiuk, V., Cheng, Z., Lim, M.K., Shyp, V., Parker, R., and Song, H. (2010). Structure of the Dom34-Hbs1 complex and implications for no-go decay. *Nat. Struct. Mol. Biol.* *17*, 1233-1240.

Emsley, P., and Cowtan, K. (2004). Coot: model-building tools for molecular graphics. *Acta. Crystallogr. D. Biol. Crystallogr.* *60*, 2126-2132.

Gogala, M., Becker, T., Beatrix, B., Armache, J.-P., Barrio-Garcia, C., Berninghausen, O., Beckmann, R. (2014). Cryo-EM structures of the Sec61-complex engaged in nascent peptide translocation or membrane insertion. *Nature* *506* 107-110.

Jin, H., Kelley, A.C., Loakes, D., and Ramakrishnan, V. (2010). Structure of the 70S ribosome bound to release factor 2 and a substrate analog provides insights into catalysis of peptide release. *Proc. Natl. Acad. Sci. USA* *107*, 8593-8598.

Korostelev, A., Zhu, J., Asahara, H., and Noller, H.F. (2010). Recognition of the amber UAG stop codon by release factor RF1. *EMBO J.* *29*, 2577-2585.

Pettersen, E.F., Goddard, T.D., Huang, C.C., Couch, G.S., Greenblatt, D.M., Meng, E.C., and Ferrin, T.E. (2004). UCSF Chimera--a visualization system for exploratory research and analysis. *J. Comput. Chem.* *25*, 1605-1612.

Phillips, J.C., Braun, R., Wang, W., Gumbart, J., Tajkhorshid, E., Villa, E., Chipot, C., Skeel, R.D., Kale, L., and Schulten, K. (2005). Scalable molecular dynamics with NAMD. *J. Comput. Chem.* *26*, 1781-1802.

Scheres, S.H. (2012). RELION: implementation of a Bayesian approach to cryo-EM structure determination. *J. Struct. Biol.* *180*, 519-530.

Trabuco, L.G., Villa, E., Mitra, K., Frank, J., and Schulten, K. (2008). Flexible fitting of atomic structures into electron microscopy maps using molecular dynamics. *Structure* *16*, 673-683.

Wagenknecht, T., Grassucci, R., and Frank, J. (1988). Electron microscopy and computer image averaging of ice-embedded large ribosomal subunits from *Escherichia coli*. *J. Mol. Biol.* *199*, 137-147.

ARTICLE

Received 24 Dec 2015 | Accepted 15 Sep 2016 | Published 8 Nov 2016

DOI: 10.1038/ncomms13248

OPEN

Structure of the ribosome post-recycling complex probed by chemical cross-linking and mass spectrometry

Kristin Kiosze-Becker¹, Alessandro Ori^{2,†}, Milan Gerovac¹, André Heuer³, Elina Nürenberg-Goloub¹, Umar Jan Rashid¹, Thomas Becker³, Roland Beckmann³, Martin Beck² & Robert Tampé¹

Ribosome recycling orchestrated by the ATP binding cassette (ABC) protein ABCE1 can be considered as the final—or the first—step within the cyclic process of protein synthesis, connecting translation termination and mRNA surveillance with re-initiation. An ATP-dependent tweezer-like motion of the nucleotide-binding domains in ABCE1 transfers mechanical energy to the ribosome and tears the ribosome subunits apart. The post-recycling complex (PRC) then re-initiates mRNA translation. Here, we probed the so far unknown architecture of the 1-MDa PRC (40S/30S•ABCE1) by chemical cross-linking and mass spectrometry (XL-MS). Our study reveals ABCE1 bound to the translational factor-binding (GTPase) site with multiple cross-link contacts of the helix-loop-helix motif to the S24e ribosomal protein. Cross-linking of the FeS cluster domain to the ribosomal protein S12 substantiates an extreme lever-arm movement of the FeS cluster domain during ribosome recycling. We were thus able to reconstitute and structurally analyse a key complex in the translational cycle, resembling the link between translation initiation and ribosome recycling.

¹Institute of Biochemistry, Biocenter, Goethe University Frankfurt, Max-von-Laue-Str. 9, 60438 Frankfurt a.M., Germany. ²Structural and Computational Biology Unit, EMBL Heidelberg, Meyerhofstr. 1, 69117 Heidelberg, Germany. ³Gene Center and Center for Integrated Protein Science Munich (CiPSM), Department of Biochemistry, University of Munich, Feodor-Lynen-Str. 25, 81377 Munich, Germany. † Present address: Leibniz Institute on Aging—Fritz Lipmann Institute (FLI) Beutenbergstrasse 11 07745 Jena, Germany. Correspondence and requests for materials should be addressed to R.T. (email: tampe@em.uni-frankfurt.de).

Ribosome-driven protein biosynthesis is a cyclic process, which comprises four steps: initiation, elongation, termination and recycling^{1–3}. In Eukarya and Archaea, the ATP binding cassette (ABC) protein ABCE1 catalyses the essential step of ribosome recycling by splitting the ribosome into its small 40/30S and large 60/50S subunits^{4–6}. Hence, ABCE1 emerges as the missing link between termination and initiation by potentially coordinating the re-initiation via the released 40/30S•ABCE1 complex, named post-recycling complex (PRC), where ABCE1 remains bound after ribosome splitting until ATP hydrolysis has occurred^{2,4,7}. Structural insights of ABCE1 have recently become available, for example, by X-ray structures of ABCE1 as well as cryo-electron microscopy (cryo-EM) analyses of termination/pre-recycling complexes^{4,8–10}. However, the structure of the PRC and conformational changes during ribosome recycling remain elusive up to the present day.

ABCE1 is one of the most conserved proteins and it is essential for life in all Eukarya and Archaea examined so far^{11–13}. It is the sole member of the subfamily E within the superfamily of ABC proteins¹⁴. ABCE1 is equipped with two nucleotide-binding domains (NBDs) oriented in a head-to-tail fashion and connected via hinge 1 and 2 region^{4,9}. Furthermore, it contains a unique N-terminal FeS cluster domain, aligned by two diamagnetic [4Fe–4S]²⁺ clusters¹⁵. ABCE1 was originally classified as RNase L inhibitor 1 (RLI1) in antiviral ribonucleic acid (RNA) immunity and as host protein 68 (HP68) required for HIV capsid assembly in human cells^{16,17}. Nevertheless, in accordance to its strong sequence conservation, ABCE1 proved to be indispensable for the fundamental process of ribosome recycling^{2,5}. ABCE1 is able to recycle post-termination complexes after canonical translation as well as vacant ribosomes and stalled ribosomal complexes, which are further processed by messenger RNA (mRNA) surveillance mechanisms^{2,18–21}. During canonical translation, ABCE1 is recruited to the post-termination complex after dissociation of the GTPase eRF3/aEF1 α (ref. 8). It is anticipated that ABCE1 goes through a tweezer-like motion typical of ABC proteins, cycling between stages of closing and opening of the NBD interface triggered by ATP binding and hydrolysis, respectively^{22,23}. On ATP binding, the closing of the NBDs presumably forces the FeS cluster domain to swing out of the NBD cleft into the inter-subunit space of the ribosome, which tears the ribosomal subunits apart either directly or via the bound eRF1/aRF1 or e/aPelota⁸. Hence, the released subunits are now available for a new translation round²⁴. Notably, ABCE1 itself remains bound within the PRC (40S/30S•ABCE1•ATP) until ATP is hydrolysed, and might assist here in the re-initiation via the reported interactions with initiation factors^{4,12,25}.

Up to now, only pre-recycling complexes have structurally been resolved by cryo-EM, demonstrating that ABCE1 binds to the translational GTPase binding site and adopts a semi-closed conformation^{8,10,26}. The overall conformation of ABCE1 within the canonical termination/pre-recycling complex (80S•eRF1•ABCE1) as well as in the pre-recycling state within mRNA surveillance (80S•ePelota•ABCE1) is very similar^{8,10,26}. In both cases, ABCE1 establishes various contacts to the small ribosomal subunit and minor contacts to the large ribosomal subunit^{8,10}. Still, the location of ABCE1 and conformational changes in all sequent steps along the recycling process, especially the post-splitting state as platform for re-initiation, remains elusive so far. Termination and ribosome recycling are multi-step processes consisting of several sub-steps including the 80S/70S termination complex, with the pre- and post-peptidyl-hydrolysis state accompanied by peptide release, the post-termination/pre-recycling step followed by the PRC (addressed here), which further includes steps such as ribosome splitting, e/aRF1 release and recycling of mRNA and transfer RNA (tRNA). Furthermore,

the exact role and movement of the FeS cluster domain during ribosome recycling are not understood yet. Attempts to determine the structure of 40S/30S•ABCE1•ATP complexes have failed, likely due to the complexity and variability of the 40S/30S subunit as well as to the short-lived nature of this intermediate state.

XL-MS studies provide an advanced technique to discover the site of protein interactions as well as transient binding partners and to construct protein interaction networks. This approach has been recently applied to reveal the architecture of the nuclear pore complex, the 26S proteasome, the protein phosphatase 2A network, polymerase II complexes and various others^{27–30}. Moreover, it contributed in a hybrid approach of low-resolution structural methods to the dissection of the molecular architecture of the 40S•eIF1•eIF3 translation initiation complex, characterized by a number of transient RNA–protein interactions³¹. Stable and rigid core complexes are often resolved by crystallography, whereas the positions of additional, peripheral factors, such as ABCE1 on the ribosome, are mapped by cross-linking approaches or cryo-EM²⁸.

Here, we combined chemical cross-linking with mass spectrometry (XL-MS)³² to address the architecture of the PRC (30S•ABCE1). In addition, we reconstructed the PRC at low resolution by cryo-EM. Using a homogeneously purified population of the 1-MDa PRC composed of 16S ribosomal RNA (rRNA), 28 ribosomal (r-)proteins and ABCE1 stably arrested by non-hydrolysable AMP-PNP, we mapped the position of ABCE1 within this multisubunit ribonucleoprotein particle by means of XL-MS. AMP-PNP is crucial for the preparation of a post-splitting complex as (i) ATP hydrolysis triggers the release of ABCE1 from the small subunit and (ii) ADP is unable to induce conformational changes of ABCE1 required for ribosome binding^{4,5}. Notwithstanding, taking a two-step mechanism with two distinct nucleotide-binding events into account, AMP-PNP prevents the second step, the splitting process, because ABCE1 is trapped in the first termination step and cannot proceed to the splitting step⁶. Hence, the PRC can be experimentally addressed only by the reverse reaction by AMP-PNP dependent occupation of small ribosomal subunit by ABCE1. Further, ABCE1 is able to split translationally inactive ribosomes, for example, vacant or starved (Stm1 occupied) ribosomes^{20,21}. Hence, mRNA or tRNA, which is released during ribosome splitting, are not essential for the PRC studied in the present context⁵.

Following the two independent structural approaches, namely XL-MS and cryo-EM, we demonstrate that ABCE1 remains bound at the translational GTPase binding site after ribosome splitting, contacting the S24e protein of the small subunit. Notably, the FeS cluster domain of ABCE1 undergoes a large rotational and translational rearrangement towards the ribosomal protein S12 on nucleotide-dependent closure of the NBDs. Thus, we were able to dissect a key complex in the mRNA translation process, which turns into a cyclic process by connecting translation initiation to termination/recycling events.

Results

Preparation of the post-recycling complex. The structure of the post-recycling/post-splitting complex is of crucial importance in understanding the recycling process and the subsequent re-initiation of mRNA translation. As the cryo-EM and X-ray analyses of the post-splitting complex remained notoriously difficult, we probed the architecture of the PRC by chemical cross-linking in combination with mass spectrometry (XL-MS). An essential prerequisite in the structural analysis of the PRC is a stably arrested, homogeneous population of ABCE1 trapped at the small ribosomal subunit. We established this using the non-

hydrolysable ATP analogue AMP-PNP in combination with sucrose density gradient (SDG) centrifugation to arrest ABCE1 in the closed state on the small ribosomal subunit and to separate the 30S•ABCE1•AMP-PNP complex from non-assembled components, respectively (Fig. 1a,b, Supplementary Fig. 1a). Alternatively, we assembled the post-splitting complex under identical conditions without SDG centrifugation. This approach allowed us to directly compare the assembly of the PRC in the presence of AMP-PNP or ADP, the latter of which does not promote ribosome recycling and prevents a stable arrest of ABCE1 on the small ribosomal subunit⁴. Assembled complexes were subsequently cross-linked under identical conditions using either a 30- or 80-fold molar excess of the isotope-coded amine-specific cross-linker disuccinimidyl suberate (2 mM or 5 mM DSS, d0/d12). The monodispersity and homogeneity of each sample were checked by immunoblotting and negative-stain EM, respectively (Supplementary Fig. 1). Subsequent proteolysis resulted in a complex mixture of tryptic peptides, which were analysed by tandem mass spectrometry and identified using the xQuest/xProphet tool searching against a database containing the protein sequences of ABCE1 and all 28 proteins of the small ribosomal subunit from *Sulfolobus solfataricus* (Supplementary Data; Supplementary Table 1)^{30,33}.

XL-MS analysis of the post-recycling complex. Using the XL-MS approach, we analysed the arrested PRC and successfully identified 56 inter-protein cross-links across all samples analysed. Thereof, 22 are cross-links between ABCE1 and ribosomal proteins, and all the remaining cross-links are found between r-proteins (Table 1; Supplementary Table 2, Supplementary Fig. 2). The number of identified cross-links is in line with recent analyses of ribonucleoprotein complexes³⁴. A detailed analysis of the SDG-purified PRC (30S•ABCE1•AMP-PNP) cross-linked with 2 mM or 5 mM DSS (30- or 80-fold molar excess of cross-linker) revealed 63 intra-ABCE1 cross-links (Fig. 1c), and more important 33 inter-protein cross-links, resulting in eight unique C α -C α restraints between r-proteins and eight distinct restraints between ABCE1 and r-proteins (Fig. 2). Additionally, we were

able to identify in all samples 138 intra-ABCE1 cross-links as well as a quantity of 28 mono-links to lysine residues of ABCE1 (Supplementary Table 3, Supplementary Fig. 3). These results derived from the combination of two independent preparations of the PRC with multiple samples per preparation. Independently of their purification approach, all three SDG-purified samples as well as the two samples prepared in presence of AMP-PNP resulted in the same major cross-links between ABCE1 and S24e. The statistics of identification of intra cross-links within ABCE1 (Supplementary Table 3) and all the inter-protein cross-links are provided (Supplementary Table 2).

Inter and intra cross-links were further validated by analysing the distances between the two cross-linked lysine residues on a homology model of the 30S subunit from *S. solfataricus*. Thus, homology models of each known ribosomal protein from *S. solfataricus* (Supplementary Table 1) were constructed using Phyre² (Protein Homology/Analogy Recognition Engine V 2.0)³⁵. To construct the 30S of *S. solfataricus* *in silico*, the homology models of the archaeal ribosomal proteins were aligned to the known small ribosomal subunit from *Saccharomyces cerevisiae* (pdb: 3U5G, 3U5F)³⁶. Obtained cross-links were then analysed

Table 1 | Identified inter cross-links between ABCE1 and ribosomal proteins.

ABCE1		Ribosomal proteins		Identified inter cross-links		
Domain	Residue	Name	Residue	SDG-purified PRC	PRC with AMP-PNP	PRC with ADP
NBD1	136	S24e	119	+	+	-
NBD1	136	S24e	113	+	+	-
NBD1	133	S24e	119	+	-	-
NBD1	192	S24e	119	+	-	-
NBD1	141	S24e	119	+	-	-
NBD1	153	S24e	113	+	+	-
NBD1	141	S24e	113	+	-	-
FeS	60	S12	40	+	-	-

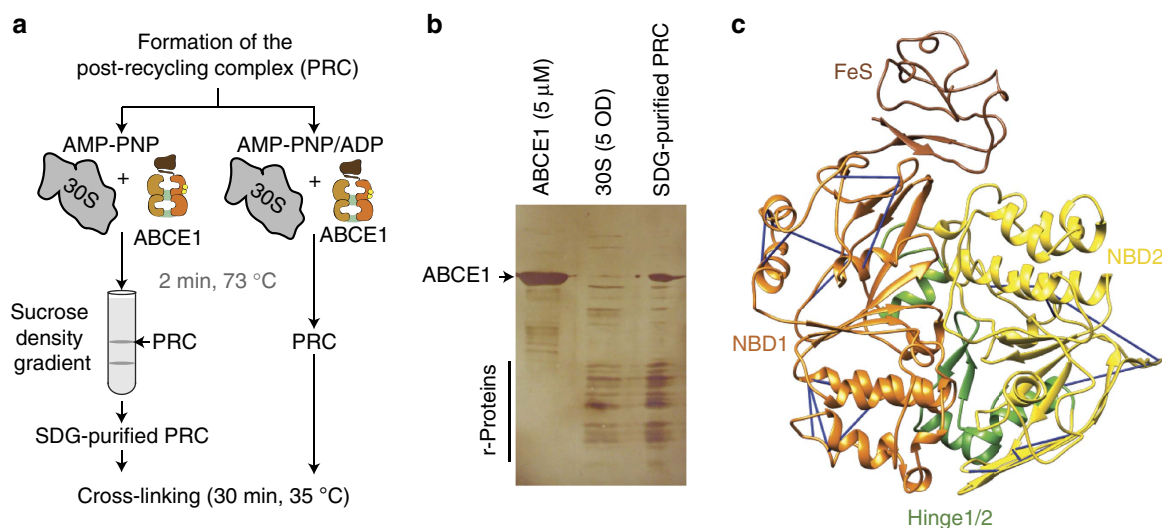


Figure 1 | Lysine-specific cross-linking of ABCE1 bound in the post-recycling complex (PRC). (a) A stably arrested and homogeneous population of PRC was isolated from sucrose density gradients (SDG) after reconstitution from purified components at physiological temperatures and in the presence of non-hydrolysable AMP-PNP. (b) Sample quality was analysed via SDS-polyacrylamide gel electrophoresis (silver-stain). Alternatively, PRCs were reconstituted under identical conditions from isolated components without any additional purification via SDG. As control, the sample was prepared in the presence of ADP, which does not promote a stable arrest of ABCE1 on the small ribosomal subunit. (c) Lysine specific cross-linking with DSS resulted in a distinct set of intra cross-links within ABCE1. Cross-links shown here are those of the SDG-purified samples (closed model).

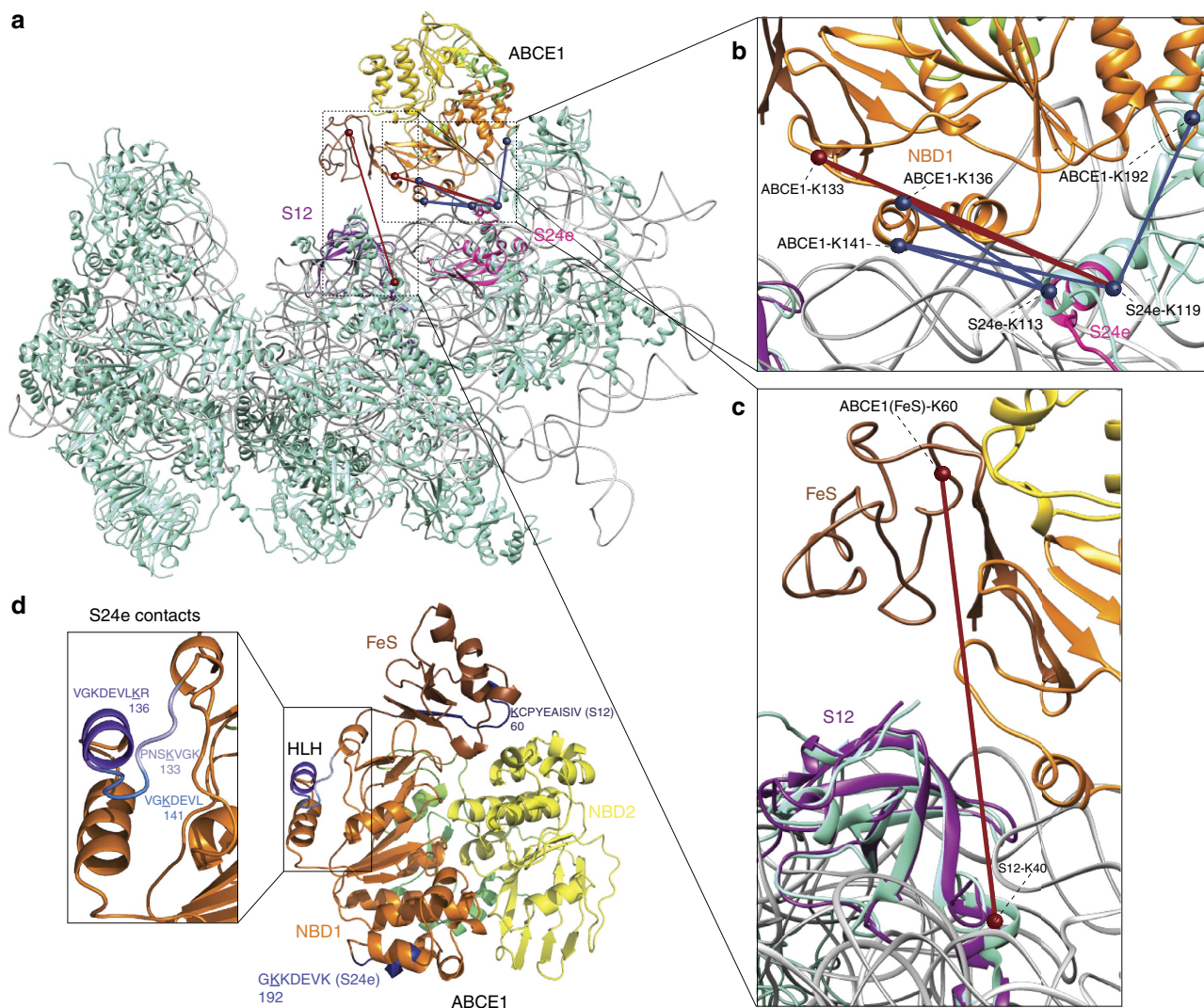


Figure 2 | Architecture of the PRC (30S•ABCE1•AMP-PNP) mapped by XL-MS. (a) The orientation of ABCE1 in the PRC based on the identified inter cross-links with the archaeal ribosomal proteins S24e (pink, **b**) and S12 (dark magenta, **c**), depicted in blue and red lines. Blue lines indicate cross-links with a length $< 30 \text{ \AA}$ and red lines cross-links $> 30 \text{ \AA}$. Identified inter cross-links were certified using an *in silico* model of the *S. solfataricus* 30S constructed by aligning the homology models of the archaeal ribosomal proteins to the small ribosomal subunit from *S. cerevisiae* (pdb: 3U5G/F, r-proteins: cyan, rRNA: grey) and positioning ABCE1 according to the cryo-EM map of the rescue/pre-recycling complex (pdb: 3J16). (d) The major contact area of ABCE1 towards the 30S primarily locates in the helix-loop-helix region (HLH).

and certified using the XlinkAnalyzer tool for Chimera³⁷. Yeast ribosomal proteins are thereby named according to the new nomenclature of ribosomal proteins, while the archaeal r-proteins hold their UniProt entry name going along with the MS analysis³⁸. ABCE1 itself is positioned according to the cryo-EM map of the pre-recycling complex (pdb: 3J16)⁸. The median C α -C α distance for all obtained cross-links is 17 Å, with 83.9% of the distances below 30 Å, respectively (Supplementary Fig. 2a). When only cross-links between ribosomal proteins are considered, 32 out of the 34 identified inter-protein cross-links (94.1%) displayed a C α -C α distance between cross-linked lysines $< 30 \text{ \AA}$. The estimated average for the DSS cross-linker lies at 17 Å with a maximum threshold at 30 Å, accounting for cross-linked side-chains, protein flexibilities and model inaccuracies^{29,32,39}. Thus, we are able to demonstrate reliable and reproducible inter-protein cross-links between ABCE1 and especially the S24e r-protein. Further, the identified inter-protein ribosomal cross-links connect structurally adjacent ribosomal

proteins, confirming the reliability of the acquired results (Supplementary Fig. 2b). Inter cross-links exceeding the expected distance mainly occur in samples that were not separated via SDG and that likely contained a conformationally heterogeneous population of PRCs (Supplementary Table 2). The two cross-links exceeding the 30 Å maximum thresholds, as for example the 63.9 Å cross-link between the N-terminal region of the ribosomal protein S30e (position 9) and the central region of the S5 protein, can be explained by poor homology models (performed by Phyre²). The structure of the archaeal S30e is not well defined. In particular, the N- and C-terminal regions of the ribosomal proteins, which are cross-linked, are often less conserved between species and, thus, affect accuracy of the homology models. This explains the uncertainty in the length of the cross-link. The same argument holds true for the 33.8 Å crosslink between S3A and the carboxy terminus of S28.

The obtained intra cross-links of ABCE1 were analysed using an available crystal structure and a model of the closed state,

revealing an even distribution, surface accessibility and valid distance constraints (Fig. 1c, Supplementary Fig. 3)^{4,9}. Noteworthy, we do not see any intra cross-links between both NBDs, spanning the NBD cleft. Notably, a majority of the seemingly violated intra-ABCE1 cross-links (red, ≥ 25 Å) originated from cross-links to the FeS cluster domain (Supplementary Fig. 3a), supporting the notion that this domain is highly dynamic^{8,9}. The set of obtained mono-links confirms the solvent accessibility of the ABCE1 surface and the reactivity of the lysines with respect to the cross-linker. All mono-links are thereby evenly distributed over the protein surface, limiting solid conclusions about the interaction sites with the post-splitting complex via a protected region (Supplementary Fig. 3b). To conclude, using the XL-MS approach, we obtained a significant set of inter-protein cross-links between ABCE1 and r-proteins, which allows us to dissect the ABCE1-binding site in the PRC.

Structural organization of the post-recycling complex. We mapped the position of ABCE1 on the PRC by XL-MS and identified eight prominent cross-links of ABCE1 to the archaeal S24e and S12 ribosomal proteins (Fig. 2a–c, Supplementary Table 2). Lysines 133, 136, 141, 153 and 192 of ABCE1, most of them residing in the helix–loop–helix (HLH) region (aa 132–161; Fig. 2d), form cross-links with lysine 113 or 119 of the ribosomal subunit S24e (Table 1). In addition, lysine 60 of the FeS cluster domain (ABCE1) cross-links with lysine 40 of the ribosomal protein S12 (Fig. 2c). Thus, the identified ABCE1-binding site at the small ribosomal subunit is confined to two proteins (S24e and S12), which are highly conserved in Archaea, yeast and humans (eS24 and uS12 according to the new nomenclature)³⁸. The S24 cross-links were confirmed by two independent preparations of the PRC with a number of different samples per preparation, with two unique restraints consistent across independent replicates. Importantly, two of these most prominent restraints to the S24e r-protein were consistently identified using different cross-linker amounts and complexes prepared in the presence of AMP-PNP without separation by SDG (Supplementary Fig. 4). Moreover, reliable cross-links were not detected when ABCE1 and 30S were analysed in the presence of ADP (Supplementary Table 2).

Valid distances of all cross-links to S24e (11–40 Å) were confirmed using our model of *S. solfataricus* 30S. In particular, the unique HLH region of ABCE1 plays here a major role within the formation of the PRC (Fig. 2b, d). Furthermore, the cross-link between S12 and ABCE1 was identified in two independent samples (30- or 80-fold molar excess of DSS) of one preparation and within four technical replicates (two per condition; Supplementary Fig. 5). Considering that the predicted cross-link distance in the pre-splitting complex should be 59.5 Å (Fig. 2c), this post-splitting contact could be established by a large conformational movement of the FeS cluster domain, resulting in a repositioning of the FeS cluster domain closer to the A site where ribosomal subunit S12 is located (Fig. 3). It is worth mentioning that the FeS cluster domain is very small (75 aa) and harbours only seven lysines. Since five of them locate on the opposite site of the FeS cluster domain compared with lysine 60 and cross-linking of the neighbouring lysine 59 prevents trypsin cleavage, the cross-link from ABCE1 (lysine 60, fragment KCPYEAIISIVNLPDELEGEVIHR) to the S12 ribosomal subunit (lysine 40, fragment EKYPDPLGGAPMAR) reproducibly found in four technical replications is of high significance (Supplementary Table 2, Supplementary Fig. 5).

To provide a second, independent line of evidence for the position of ABCE1 and the extreme structural reorganization of the FeS cluster domain in the PRC, we analysed the archaeal 30S•ABCE1•AMP-PNP complex by cryo-EM. In spite of the

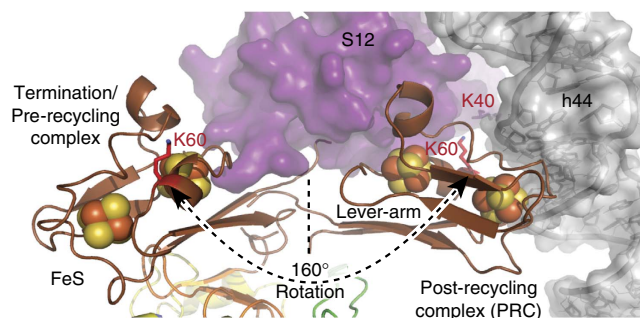


Figure 3 | Extensive movement of the FeS cluster domain. The FeS cluster domain, anchored to NBD1 via a two β -strand lever arm, swings out of the NBD cleft and converges towards the 30S subunit to occupy a cleft between the S12 r-protein and rRNA (h44) of the small ribosomal subunit. Due to this conformational change, the $C\alpha$ – $C\alpha$ distance between these highly conserved lysines in Archaea, yeast and human is reduced from 59.5 Å in the pre-splitting state to 17.5 Å in the post-recycling state.

facts that archaeal 30S ribosomal particles were up to now not accessible to cryo-EM analyses and occupancy was low, we resolved the structural architecture of the PRC by a low-resolution cryo-EM reconstruction, in which, indeed, an extra density near rRNA helix 44 (h44) and S12 was observed (Fig. 4). The small subunit is well-known for orientation bias and inhomogeneity by dimerization and aggregation in negative stain. While the two NBDs fit into the body part of the ABCE1 density as shown in the pre-splitting state, confirming the cross-links between the HLH region and the ribosomal subunit S24e, there was no visible density for the FeS cluster domain in the pre-splitting position. Notably, with a 160-degree rotation of the FeS cluster domain from the pivot point (proline 76), the extra density near S12 and h44 could be easily positioned in a way that explains the cross-link data described above (Fig. 4). The orientation of the FeS cluster domain is based on positioning lysine 60 of ABCE1 and lysine 40 of S12 at a $C\alpha$ – $C\alpha$ distance of 17.5 Å, using cross-linker and lever length as restraints. Because of this conformational change, the $C\alpha$ – $C\alpha$ distance between these highly conserved lysines in Archaea, yeast and human is reduced from 59.5 Å in the pre-splitting state to 17.5 Å in the post-recycling state. Thus, the low-resolution cryo-EM structure of the archaeal PRC undoubtedly corroborates the conformational reorganization of ABCE1 in the PRC complex as revealed by XL-MS.

A closer inspection of all identified cross-links from ABCE1 reveals that almost all contacts to the small ribosomal subunit are established via NBD1 and the FeS cluster domain. Based on this ribosome splitting-persistent contact between the HLH motif of NBD1 in ABCE1 and the ribosomal subunit S24e (eS24 in yeast), the cross-link between the FeS cluster domain and the ribosomal subunit S12 (uS12 in yeast) becomes highly relevant in explaining the large conformational rearrangement of the FeS cluster domain during ribosome recycling.

Discussion

In this study, we reconstituted and structurally dissected the PRC (30S•ABCE1•AMP-PNP) using a combined cross-linking and mass spectrometry approach. We provide direct evidence that ABCE1 establishes major contacts with the S24e ribosomal protein in the PRC, demonstrating that the recycling factor remains bound at the so-called translational GTPase binding site after ribosome splitting. Thus, the connectivity map (Fig. 2) largely recapitulates recent cryo-EM structures of the yeast and

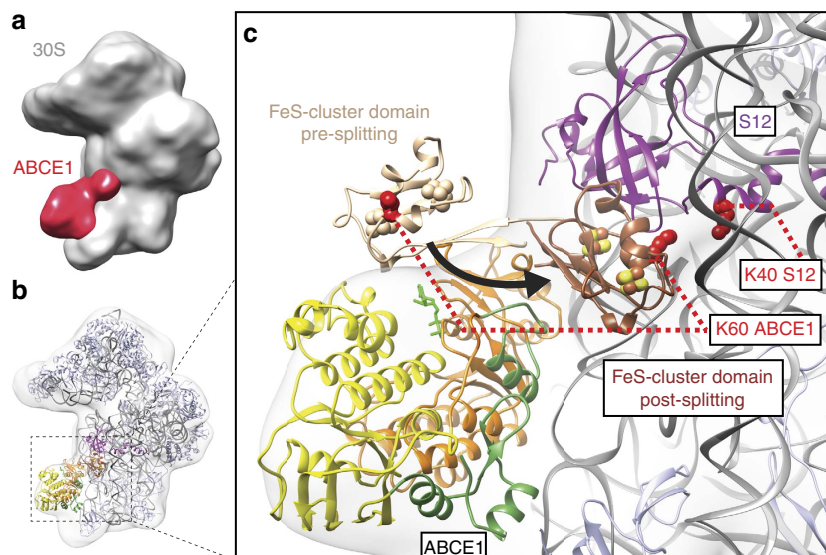


Figure 4 | Low-resolution cryo-EM structure of the 30S•ABCE1 post-splitting complex. (a) Overview of the 30S•ABCE1 post-splitting complex electron density map low-pass filtered at ~ 25 Å. The final 30S•ABCE1 data set contained 19,500 particles and the final resolution was 17 Å (Fourier shell correlation 0.5). The ABCE1 extra density is shown in red. (b) Model of the 30S•ABCE1 complex in post-splitting state showing the models of the *P. furiosus* small 30S subunit (grey; 4V6U)⁵² and ribosome-bound ABCE1 (FeS cluster domain brown; NBD1 orange and NBD2 yellow; hinges 1 and 2 green, ADP-bound green; 3J15)⁹. The FeS cluster domain was fitted into the extra density located near ribosomal proteins S12 (purple). (c) Zoom-in showing the pre-splitting (wheat) and post-splitting (brown) state of the FeS cluster domain. The post-splitting state was modelled based on a specific inter-crosslink in XL-MS between lysine 60 of ABCE1 (lysine 64 in *P. furiosus*) and lysine 40 of S12 (shown in red). Because of this conformational change, the C α -C α distance between these highly conserved lysines in Archaea, yeast and human is reduced from 59.5 Å in the pre-splitting state to 17.5 Å in the post-splitting state.

mammalian pre-recycling complex, which pointed out a related binding site of ABCE1 at the GTPase center contacting ribosomal proteins S24e and S6e as well as rRNA (h5, h8, h14 and h15) on the small ribosomal subunit^{8,10,26}. These findings imply that ABCE1, despite unaltered ribosomal contact sites of NBD1 before and after splitting, undergoes large conformational changes during ribosome splitting. Based on the unexpected finding of the statistically significant cross-link between the FeS cluster domain of ABCE1 (lysine 60) and the S12 (lysine 40) ribosomal protein, we infer a 160-degree rotation. This extensive rearrangement of the FeS cluster domain brings lysine 60 of ABCE1 in cross-linking distance to lysine 40 of the S12 subunit (Fig. 3). The cross-link of the FeS cluster domain to the S12 r-protein is in perfect agreement with our low-resolution cryo-EM data (Fig. 4). We therefore anticipate that ABCE1 undergoes a tweezer-like movement as other ABC proteins. On NBD closure, the FeS cluster domain, anchored to NBD1 via a two β -strand lever-arm, swings out of the NBD cleft and converges towards the 30S subunit to occupy a cleft between the S12 r-protein and rRNA (h44) of the small ribosomal subunit (Fig. 4). The FeS cluster domain remains anchored in the groove between S12 and rRNA (h44) until ATP is hydrolysed by one or both NBDs, which releases the tensed lever-arm and allows the FeS cluster domain to swing back into its resting position, illustrated by the X-ray structure of the open state of ABCE1 (ref. 9). So, ABCE1 can dissociate from the small ribosomal subunit primed for a subsequent round of translation (Fig. 5).

The fact that NBD1 remains bound to the small subunit after ribosome splitting enables ABCE1 to act as a platform for subsequent re-initiation via its known interactions with initiation factors¹². By occupying the ribosomal subunit interface, ABCE1 may prevent ribosomal subunit association before the initiation process is correctly triggered. Interactions of ABCE1 with eIF2, eIF3 and eIF5 have been observed in yeast¹². According to recent

structures of initiation complexes, ABCE1 most likely blocks the binding of eIF3B, eIF3G and eIF3I to the small ribosomal subunit by steric hindrance, thus preventing premature assembly of initiation complexes^{31,40–43}. Further, a potential interaction of ABCE1 with eIF3B is feasible, based on their positions on the small ribosomal subunit, going along with the known interactions of ABCE1 with the eIF3B, eIF3G and eIF3J subunits of the eIF3 multi-component complex^{12,31,40,43}. However, in Archaea, the initiation system is less complex than in Eukarya. Currently, only five archaeal initiation factors are known (aIF1, aIF1A, aIF2/5B, aIF2 and aIF6), showing a different functional spectrum compared with their eukaryotic homologues⁴⁴.

Based on the XL-MS confinement map and supported by the low-resolution cryo-EM reconstruction of the archaeal 30S•ABCE1•ATP PRC, we demonstrated that ABCE1 binds to the GTPase binding center on the small ribosomal subunit, establishing major contacts with S24e and S12. Notably, on ribosomal splitting, the FeS cluster domain undergoes major conformational rearrangements, which position the FeS cluster domain in a cleft between S12 and rRNA (h44) on the small subunit. We thus delineated for the first time the interaction sites and large conformational rearrangements of ABCE1 in the post-splitting/PRC, which forms a potential platform for subsequent translation re-initiation.

Methods

Cloning and expression of ABCE1. Full-length ABCE1^{wt} from *S. solfataricus* were cloned with a C-terminal His₆-tag in pSA4 vector, which is based on a pET15b expression vector^{4,15,45}. For heterologous expression in *Escherichia coli*, the plasmid coding for ABCE1 was co-transformed with the pRARE plasmid (Novagen) coding for rare tRNAs into the BL21(DE3) *E. coli* strain (Novagen). Growth was conducted in lysogeny broth (LB) medium supplemented with 100 $\mu\text{g ml}^{-1}$ ampicillin and 25 $\mu\text{g ml}^{-1}$ chloramphenicol at 37 °C until an OD₆₀₀ (optical density) of 0.6–0.8 was reached and expression was induced by adding 0.35 mM isopropyl- β -D-thiogalactopyranoside. Cells were harvested after 3 h of expression at 30 °C.

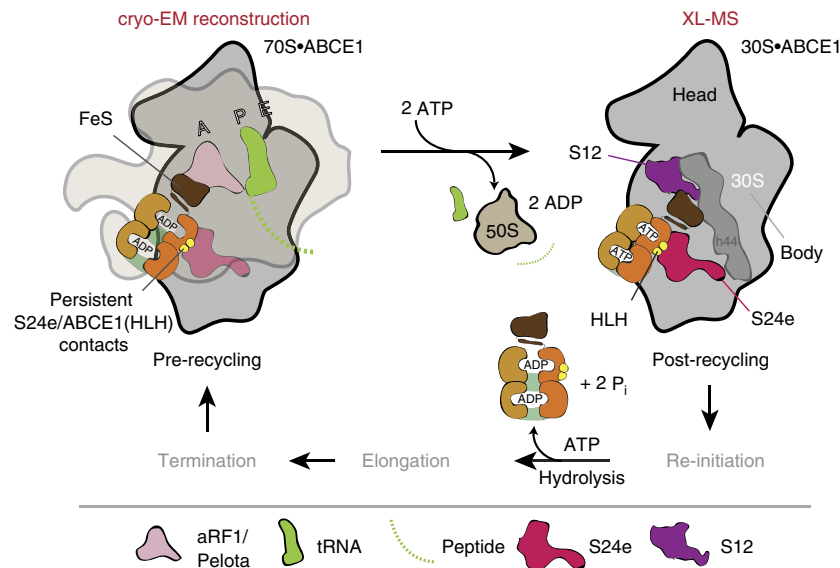


Figure 5 | Conformational changes of ABCE1 during ribosome recycling. During the cyclic process of translation, post-termination/pre-recycling complexes occur, which need to be recycled into their components to be available for the subsequent re-initiation. After *e*/aRF3 dissociation, ABCE1 binds to the GTPase binding site of these complexes, establishing contacts to the *r*-proteins of the large and small subunit (PO, L9, S24, S6)⁸. ATP occlusion of ABCE1 leads to major conformational changes, especially a large rotational and translational repositioning of the FeS cluster domain, which splits the ribosomal subunits apart—either directly or via the bound *e*/aRF1. ABCE1 itself remains bound to the small subunit until ATP is hydrolysed (PRC). Consequently, the contacts to proteins of the large subunit are released and major contacts to the proteins of the small subunit like S24e are preserved. Additionally, a new contact to the S12 protein is established, caused by the large rotational and translational movement of the FeS cluster domain, anchoring ABCE1 on the 30S.

Purification of ABCE1. For protein purification of ABCE1^{wt}, all buffers were supplemented with 1 mM of β -mercaptoethanol. Frozen cell pellet was thawed in lysis buffer (20 mM Tris-HCl pH 8.0, 1 mM EDTA, 500 mM NaCl) and disrupted with 4–5 pulses of 3 min on ice using a Branson Sonifier 250 at 70% output. The lysate was centrifuged at 130,000g for 30 min. The supernatant was heated for 10 min at 72 °C followed by a second centrifugation at 130,000g for 30 min. ABCE1 was purified by immobilized metal affinity chromatography (IMAC, HiTrap Chelating HP, 5 ml, GE Healthcare) using IMAC A buffer (20 mM Tris-HCl pH 8.0, 100 mM NaCl, 20 mM imidazole). After a washing step with 70 mM imidazole (25% IMAC B: 20 mM Tris-HCl pH 8.0, 100 mM NaCl, 200 mM imidazole), ABCE1 was eluted with 200 mM imidazole (100% IMAC B). Fractions containing ABCE1 were pooled and dialyzed against AIEX A buffer (20 mM Tris-HCl pH 8.5) using an Amicon Ultra centrifuge device (30 kDa cut-off, Merck Millipore). The protein was further purified by anion exchange chromatography (AIEX, HiTrap Q column, 1 ml, GE Healthcare) applying a linear gradient from 0 mM to 250 mM NaCl (0–25% of AIEX B buffer: 20 mM Tris-HCl pH 8.5, 1 M NaCl) followed by a final washing step with 1 M NaCl. Protein containing fractions eluted around 15% AIEX B buffer were pooled, dialyzed against HEPES buffer (20 mM HEPES-KOH pH 7.5, 100 mM KCl, 5 mM MgCl₂), and stored at –20 °C. Protein concentration was determined by ultraviolet absorbance (ϵ_{280} 58,720 M⁻¹ cm⁻¹).

Purification of ribosomal subunits. To isolate 30S and 50S ribosomal subunits from *S. solfataricus*, a sulfolink resin chromatography was performed as described⁴⁶. Briefly, 5 ml of SulfoLink Coupling Resin (Thermo Scientific) was washed three times with 5 ml coupling buffer (50 mM Tris-HCl pH 8.5, 5 mM EDTA), incubated for 1 h at 20 °C in coupling buffer supplemented with 50 mM L-cysteine and washed again as before. The resin was poured into a spin column device (BioRad, 1,000g for 1 min) and equilibrated four times with 5 ml binding buffer (20 mM HEPES-KOH pH 7.5, 5 mM Mg(OAc)₂, 60 mM NH₄Cl, 1 mM DTT). *S. solfataricus* cells were resuspended in buffer M (20 mM HEPES-KOH pH 7.5, 5 mM KCl, 10 mM MgCl₂, 0.5 mM EDTA, 2 mM DTT, 1 mM PMSF, 1 mM Na-heparin, 1 μ g RNase-free DNase, 133 U ml⁻¹ Ribolock (Fermentas), 1 \times protease inhibitor (Serva)), sonicated with two pulses of 1 min on ice using a Branson Sonifier 250 at 70% output, and centrifuged for 30 min at 30,000g. The cleared lysate was added onto the SulfoLink column and incubated twice for 15 min on ice. Afterwards, the column was washed three times with binding buffer and elution was performed twice with 1.25 ml of elution buffer (20 mM HEPES-KOH pH 7.5, 10 mM Mg(OAc)₂, 500 mM NH₄Cl, 2 mM DTT, 0.5 mg ml⁻¹ Na-heparin). The eluate (2.5 ml) was layered onto a 2 ml glycerol cushion (20 mM HEPES-KOH pH 7.5, 10 mM Mg(OAc)₂, 500 mM KCl, 2 mM DTT, 50% (v/v) glycerol) and centrifuged at 100,000g for 15 h at 4 °C to pellet the ribosomes. Pellets were resuspended in 100 μ l of cushion buffer without glycerol and incubated for 1 h at

4 °C while shaking. To separate 30S and 50S subunits, 10–30% SDGs (10%/30% (w/v) sucrose, 20 mM HEPES-KOH pH 7.5, 10 mM KCl, 1 mM MgCl₂) were performed. The resuspended ribosomes were loaded onto the gradients and centrifuged without brake in an SW41 rotor (Beckman Coulter) either for 4 h at 36,000 r.p.m. or for 14 h at 20,000 r.p.m. at 4 °C, respectively. Gradients were fractionated from top to bottom (Piston Gradient Fractionator, Biocomp), recording the absorbance at 254 nm. Fractions containing either 30S or 50S were pooled and concentrated in HEPES buffer using an Amicon Ultra centrifuge device (30 kDa cut-off, Merck Millipore). Concentration of the ribosomes was determined using the absorbance at 254 nm. One OD equals 120 and 60 pmol of 30S or 50S subunit, respectively⁴⁷.

Purification of 30S•ABCE1•AMP-PNP complex. The 30S•ABCE1•AMP-PNP complex was isolated from SDGs. For this purpose, ABCE1 (10 μ M) in HEPES buffer was incubated with 30S (20 OD) and AMP-PNP (2 mM) for 4 min at 73 °C. After cooling on ice (2 min), the samples were loaded on a 10–30% SDG. Fractions containing 30S were pooled and concentrated in HEPES buffer using an Amicon Ultra centrifuge device (30 kDa cut-off, Merck Millipore). Concentration of 30S subunits was determined using the absorbance at 254 nm. One OD equals 120 pmol of 30S. The quality of assembled particles was routinely analysed using negative-stain EM.

Lysine cross-linking. For lysine-specific cross-linking, 30S•ABCE1•AMP-PNP complexes were formed *in vitro*. Complexes were cross-linked with a heavy-light mixture of disuccinimidyl suberate (DSS-d0/d12, Creative Molecules Inc.), and all measurements done for this study were thereby performed in triplicates. For complex formation, ABCE1 (1 mg ml⁻¹) was incubated with a two-fold molar excess of 30S subunit and ADP or AMP-PNP (2 mM each) for 2 min at 73 °C. Either 30- or 80-fold molar excess of DSS cross-linker (2 or 5 mM of DSS) was directly added to this reaction or a further purification step of the PRC via SDG (see above) was performed before adding the cross-linker to obtain a uniform population. The cross-link reaction was incubated for 30 min at 35 °C. To quench the reaction, 0.1 M ammonium bicarbonate was added and incubated for 5 min at 35 °C. Afterwards, the reaction was transferred into acidic conditions by adding 8 M urea and 0.2% (v/v) RapiGest (Waters). Then, 10 mM DTT and 15 mM iodoacetamide were added successively and incubated for 30 min at 37 °C and 600 r.p.m. and for 30 min at 18 °C in the dark, respectively. To digest the cross-linked protein complex, the endoproteinase LysC (1:100, 0.1 μ g μ l⁻¹, Wako) was added and incubated for 4 h at 37 °C and 600 r.p.m. Afterwards, the urea concentration was adjusted to 1.5 M. Trypsin (1:50, 1 μ g μ l⁻¹, Promega) was added and incubated over night at 37 °C. To stop the reaction and allow cleavage of

RapiGest 0.5% (v/v), trifluoroacetic acid was added and incubated for 30 min at 37 °C. Subsequently, the peptides were purified and concentrated using C18 micro-spin columns (Harvard apparatus). The columns were equilibrated using 100 µl methanol, 100 µl buffer B (50% acetonitrile, 0.1% formic acid) and two times 100 µl buffer A (5% acetonitrile, 0.1% formic acid) always centrifuged for 1 min at 1,000g. The samples were loaded twice with an additional centrifugation step at the end to clean the column. Next, the column was washed four times with 100 µl buffer A and again cleaned with an additional centrifuge step. The elution was performed twice with 75 µl of buffer B. The samples were dried using a Speed-Vac and resuspended in 50 µl of gel filtration buffer (30% acetonitrile, 0.1% trifluoroacetic acid). To analyse the cross-links as well as to separate the cross-linked peptides from others, the samples were examined via gel filtration using a Superdex Peptide PC 3.2/30 column (GE) on a Ettan LC system (GE) at a flow rate of 50 µl min⁻¹. Fractions eluting between 0.9 and 1.3 ml were generally pooled, evaporated to dryness and reconstituted in 20–50 µl 5% (v/v) acetonitrile (ACN) in 0.1% formic acid (FA) according to 215 nm absorbance.

Mass spectrometry. Between 2 and 10% of the collected fractions were analysed by LC–MS/MS using a nanoAcquity UPLC system (Waters Corporation, Manchester, UK) connected online to an LTQ-Orbitrap Velos Pro instrument (Thermo). Peptides were separated on a BEH300 C18 (75 µm × 250 mm, 1.7 µm) nanoAcquity UPLC column (Waters) using a stepwise 60 min gradient between 3 and 85% (v/v) ACN in 0.1% (v/v) FA. Data acquisition was performed using a TOP-20 strategy where survey MS scans (*m/z* range 375–1,600) were acquired in the Orbitrap (*R* = 30,000) and up to 20 of the most abundant ions per full scan were fragmented by collision-induced dissociation (normalized collision energy = 40, activation *Q* = 0.250) and analysed in the LTQ Orbitrap. To focus the acquisition on larger cross-linked peptides, charge states 1, 2 and unknown were rejected. Dynamic exclusion was enabled with repeat count = 1, exclusion duration = 60 s, list size = 500 and mass window ± 15 p.p.m. Ion target values were 1,000,000 (or 500 ms maximum fill time) for full scans and 10,000 (or 50 ms maximum fill time) for MS/MS scans. All the samples were analysed in at least technical duplicates.

Identification and analysis of cross-links. Raw files converted to centroid *mzXML* were searched with xQuest⁴⁸ against sequences of ABCE1 and all the 28 proteins of the small ribosomal subunit from *S. solfataricus* (Supplementary Table 1). Posterior probabilities were calculated with xProphet³⁰, and results were filtered with the following parameters: for intra- and mono-links FDR = 0.05, min delta score = 0.95, MS1 tolerance window ± 3 p.p.m. and for inter-protein cross-links FDR = 0.2, min delta score = 0.95, MS1 tolerance window ± 3 p.p.m. The reliability of the identified inter-protein cross-links was ultimately assessed in the context of available X-ray structures or homology models using Xlink Analyzer (Supplementary Fig. 2a)³⁷. For these analyses, an additional conservative cut-off of LD score ≥ 30 was applied within Xlink Analyzer.

Model building. An *in silico* homology model of the 30S subunit from *S. solfataricus* was constructed to analyse obtained cross-links. To this end, homology models of each known ribosomal protein from *S. solfataricus* (Supplementary Table 1) were constructed using Phyre² (ref. 35). To construct the small 30S subunit of the *S. solfataricus* ribosome, the homology models of the archaeal ribosomal proteins were aligned to the known small ribosomal subunit from *S. cerevisiae* (pdb: 3U5G, 3U5F)³⁶. Yeast ribosomal proteins are thereby named according to the new nomenclature of ribosomal proteins, while the archaeal r-proteins hold their UniProt entry name going along with the MS analysis¹⁹. A model of ABCE1 in the closed state is positioned according to the cryo-EM map of the pre-recycling complex (pdb: 3J16)⁸. Finally, the XlinkAnalyzer tool for Chimera was used to analyse and certify the obtained cross-links³⁷.

Sample preparation for Cryo-EM. A concentration of 50 nM *S. solfataricus* 30S was incubated with 100 nM *S. solfataricus* ABCE1^{E238A/E485A} and 2 mM of AMP-PNP in binding buffer (20 mM Tris pH 7.5, 100 mM KCl, 5 mM MgCl₂, 2 mM DTT) for 5 min at 25 °C. Samples were vitrified on carbon supported grids by standard procedure for cryo-EM imaging.

Electron microscopy and image processing. Freshly prepared sample was applied to 2 nm pre-coated Quantifoil R3/3 holey carbon supported grids and vitrified using a Vitrobot Mark IV (FEI Company) and visualized on a Spirit TEM (FEI Company) with about 20e⁻ Å⁻² at a nominal magnification of × 105,000 with a nominal defocus between -1 µm and -3.5 µm. Automatic particle detection was performed by the programme SIGNATURE⁴⁹. Initial *in silico* sorting of the data set consisting of 54,800 particles in total was performed using the SPIDER software package⁴⁹. Classes were obtained by competitive projection matching in SPIDER^{50,51}. The final 30S•ABCE1 data set contained 19,500 particles and the final resolution was 17 Å (Fourier shell correlation 0.5).

For interpretation of the 30S•ABCE1 electron density at a molecular level, the models for the *Pyrococcus furiosus* 30S subunit (4V6U)⁵² and ribosome-bound ABCE1 in (3J15)⁸ were fitted as rigid bodies using UCSF Chimera. The FeS cluster

domain was repositioned by a rotation of ~160° around a hinge (residues 76–78) into an unaccounted electron density near ribosomal protein S12. This repositioning results in a close contact between lysine 60 of ABCE1 (Lys64 in *P. furiosus*) and lysine 40 of S12 and is consistent with above described XL-MS data.

Data availability. The structural coordinates of ABCE1 and the electron density map of the archaeal PRC 30S•ABCE1•ATP-PNP have been deposited in the Protein Database under ID code 5LW7 and the electron microscopy databank under code EMD-4113. The data that support the findings of this study are available from the corresponding author on reasonable request.

References

- Jackson, R. J., Hellen, C. U. & Pestova, T. V. Termination and post-termination events in eukaryotic translation. *Adv. Protein Chem. Struct. Biol.* **86**, 45–93 (2012).
- Nürenberg, E. & Tampé, R. Tying up loose ends: ribosome recycling in eukaryotes and archaea. *Trends Biochem. Sci.* **38**, 64–74 (2013).
- Shoemaker, C. J. & Green, R. Translation drives mRNA quality control. *Nat. Struct. Mol. Biol.* **19**, 594–601 (2012).
- Barthelme, D. *et al.* Ribosome recycling depends on a mechanistic link between the FeS cluster domain and a conformational switch of the twin-ATPase ABCE1. *Proc. Natl Acad. Sci. USA* **108**, 3228–3233 (2011).
- Pisarev, A. V. *et al.* The role of ABCE1 in eukaryotic posttermination ribosomal recycling. *Mol. Cell* **37**, 196–210 (2010).
- Shoemaker, C. J. & Green, R. Kinetic analysis reveals the ordered coupling of translation termination and ribosome recycling in yeast. *Proc. Natl Acad. Sci. USA* **108**, E1392–E1398 (2011).
- Schutz, S. & Panse, V. G. Getting ready to commit: ribosomes rehearse translation. *Nat. Struct. Mol. Biol.* **19**, 861–862 (2012).
- Becker, T. *et al.* Structural basis of highly conserved ribosome recycling in eukaryotes and archaea. *Nature* **482**, 501–506 (2012).
- Karcher, A., Schele, A. & Hopfner, K. P. X-ray structure of the complete ABC enzyme ABCE1 from *Pyrococcus abyssi*. *J. Biol. Chem.* **283**, 7962–7971 (2008).
- Preis, A. *et al.* Cryoelectron microscopic structures of eukaryotic translation termination complexes containing eRF1-eRF3 or eRF1-ABCE1. *Cell Rep.* **8**, 59–65 (2014).
- Chen, Z. Q. *et al.* The essential vertebrate ABCE1 protein interacts with eukaryotic initiation factors. *J. Biol. Chem.* **281**, 7452–7457 (2006).
- Dong, J. *et al.* The essential ATP-binding cassette protein RLI1 functions in translation by promoting preinitiation complex assembly. *J. Biol. Chem.* **279**, 42157–42168 (2004).
- Zhao, Z., Fang, L. L., Johnsen, R. & Baillie, D. L. ATP-binding cassette protein E1 is involved in gene transcription and translation in *Caenorhabditis elegans*. *Biochem. Biophys. Res. Commun.* **323**, 104–111 (2004).
- Kerr, I. D. Sequence analysis of twin ATP binding cassette proteins involved in translational control, antibiotic resistance, and ribonuclease L inhibition. *Biochem. Biophys. Res. Commun.* **315**, 166–173 (2004).
- Barthelme, D. *et al.* Structural organization of essential iron-sulfur clusters in the evolutionarily highly conserved ATP-binding cassette protein ABCE1. *J. Biol. Chem.* **282**, 14598–14607 (2007).
- Bisbal, C., Martinand, C., Silhol, M., Lebleu, B. & Salehzada, T. Cloning and characterization of a RNase L inhibitor. A new component of the interferon-regulated 2-5A pathway. *J. Biol. Chem.* **270**, 13308–13317 (1995).
- Zimmerman, C. *et al.* Identification of a host protein essential for assembly of immature HIV-1 capsids. *Nature* **415**, 88–92 (2002).
- Franckenberg, S., Becker, T. & Beckmann, R. Structural view on recycling of archaeal and eukaryotic ribosomes after canonical termination and ribosome rescue. *Curr. Opin. Struct. Biol.* **22**, 786–796 (2012).
- Kashima, I. *et al.* A functional involvement of ABCE1, eukaryotic ribosome recycling factor, in nonstop mRNA decay in *Drosophila melanogaster* cells. *Biochimie* **106**, 10–16 (2014).
- Pisareva, V. P., Skabkin, M. A., Hellen, C. U., Pestova, T. V. & Pisarev, A. V. Dissociation by Pelota, Hbs1 and ABCE1 of mammalian vacant 80S ribosomes and stalled elongation complexes. *EMBO J.* **30**, 1804–1817 (2011).
- van den Elzen, A. M., Schuller, A., Green, R. & Seraphin, B. Dom34-Hbs1 mediated dissociation of inactive 80S ribosomes promotes restart of translation after stress. *EMBO J.* **33**, 265–276 (2014).
- Chen, J., Lu, G., Lin, J., Davidson, A. L. & Quijcho, F. A. A tweezers-like motion of the ATP-binding cassette dimer in an ABC transport cycle. *Mol. Cell* **12**, 651–661 (2003).
- George, A. M. & Jones, P. M. Perspectives on the structure–function of ABC transporters: the switch and constant contact models. *Prog. Biophys. Mol. Biol.* **109**, 95–107 (2012).
- Skabkin, M. A. *et al.* Activities of ligatin and MCT-1/DENR in eukaryotic translation initiation and ribosomal recycling. *Genes Dev.* **24**, 1787–1801 (2010).
- Andersen, D. S. & Leivers, S. J. The essential *Drosophila* ATP-binding cassette domain protein, Pixie, binds the 40S ribosome in an ATP-dependent manner

- and is required for translation initiation. *J. Biol. Chem.* **282**, 14752–14760 (2007).
26. Brown, A., Shao, S., Murray, J., Hegde, R. S. & Ramakrishnan, V. Structural basis for stop codon recognition in eukaryotes. *Nature* **524**, 493–496 (2015).
 27. Bui, K. H. *et al.* Integrated structural analysis of the human nuclear pore complex scaffold. *Cell* **155**, 1233–1243 (2013).
 28. Chen, Z. A. *et al.* Architecture of the RNA polymerase II-TFIIF complex revealed by cross-linking and mass spectrometry. *EMBO J.* **29**, 717–726 (2010).
 29. Herzog, F. *et al.* Structural probing of a protein phosphatase 2A network by chemical cross-linking and mass spectrometry. *Science* **337**, 1348–1352 (2012).
 30. Walzthoeni, T. *et al.* False discovery rate estimation for cross-linked peptides identified by mass spectrometry. *Nat. Methods* **9**, 901–903 (2012).
 31. Erzberger, J. P. *et al.* Molecular architecture of the 40S eIF1eIF3 translation initiation complex. *Cell* **158**, 1123–1135 (2014).
 32. Leitner, A. *et al.* Probing native protein structures by chemical cross-linking, mass spectrometry, and bioinformatics. *Mol. Cell. Proteom.* **9**, 1634–1649 (2010).
 33. She, Q. *et al.* The complete genome of the crenarchaeon *Sulfolobus solfataricus* P2. *Proc. Natl Acad. Sci. USA* **98**, 7835–7840 (2001).
 34. Greber, B. J. *et al.* Insertion of the biogenesis factor Re1 probes the ribosomal tunnel during 60S maturation. *Cell* **164**, 91–102 (2016).
 35. Kelley, L. A., Mezulis, S., Yates, C. M., Wass, M. N. & Sternberg, M. J. E. The Phyre2 web portal for protein modeling, prediction and analysis. *Nat. Protoc.* **10**, 845–858 (2015).
 36. Ben-Shem, A. *et al.* The structure of the eukaryotic ribosome at 3.0 Å resolution. *Science* **334**, 1524–1529 (2011).
 37. Kosinski, J. *et al.* Xlink Analyzer: software for analysis and visualization of cross-linking data in the context of three-dimensional structures. *J. Struct. Biol.* **189**, 177–183 (2015).
 38. Ban, N. *et al.* A new system for naming ribosomal proteins. *Curr. Opin. Struct. Biol.* **24**, 165–169 (2014).
 39. Merkley, E. D. *et al.* Distance restraints from crosslinking mass spectrometry: mining a molecular dynamics simulation database to evaluate lysine-lysine distances. *Protein Sci.* **23**, 747–759 (2014).
 40. Aylett, C. H. S., Boehringer, D., Erzberger, J. P., Schaefer, T. & Ban, N. Structure of a Yeast 40S-eIF1-eIF1A-eIF3-eIF3j initiation complex. *Nat. Struct. Mol. Biol.* **22**, 269–271 (2015).
 41. des Georges, A. *et al.* Structure of mammalian eIF3 in the context of the 43S preinitiation complex. *Nature* **525**, 491–495 (2015).
 42. Hashem, Y. *et al.* Structure of the mammalian ribosomal 43S preinitiation complex bound to the scanning factor DHX29. *Cell* **153**, 1108–1119 (2013).
 43. Llácer, J. L. *et al.* Conformational differences between open and closed states of the eukaryotic translation initiation complex. *Mol. Cell* **59**, 399–412 (2015).
 44. Benelli, D. & Londei, P. Translation initiation in Archaea: conserved and domain-specific features. *Biochem. Soc. Trans.* **39**, 89–93 (2011).
 45. Albers, S. V., Szabo, Z. & Driessen, A. J. Archaeal homolog of bacterial type IV prepilin signal peptidases with broad substrate specificity. *J. Bacteriol.* **185**, 3918–3925 (2003).
 46. Leshin, J. A., Rakauskaitė, R., Dinman, J. D. & Meskauskas, A. Enhanced purity, activity and structural integrity of yeast ribosomes purified using a general chromatographic method. *RNA Biol.* **7**, 354–360 (2010).
 47. Benelli, D. & Londei, P. *In vitro* studies of archaeal translational initiation. in *Methods in Enzymology* Vol. 430 (ed. Jon, L.) 79–109 (Academic Press, 2007).
 48. Rinner, O. *et al.* Identification of cross-linked peptides from large sequence databases. *Nat. Methods* **5**, 315–318 (2008).
 49. Chen, J. Z. & Grigorieff, N. SIGNATURE: a single-particle selection system for molecular electron microscopy. *J. Struct. Biol.* **157**, 168–173 (2007).
 50. Leidig, C. *et al.* 60S ribosome biogenesis requires rotation of the 5S ribonucleoprotein particle. *Nat. Commun.* **5**, 3491 (2014).
 51. Penczek, P. A., Frank, J. & Spahn, C. M. A method of focused classification, based on the bootstrap 3D variance analysis, and its application to EF-G-dependent translocation. *J. Struct. Biol.* **154**, 184–194 (2006).
 52. Armache, J. P. *et al.* Promiscuous behaviour of archaeal ribosomal proteins: implications for eukaryotic ribosome evolution. *Nucleic Acids Res.* **41**, 1284–1293 (2013).

Acknowledgements

We thank Dr Jan Kosinski for his help in analysing the data and modeling potential movements of the FeS cluster domain as well as Dr Christoph Thomas and Christine Le Gal for helpful comments on the manuscript. We gratefully acknowledge support from EMBL's proteomic core facility. We thank Drs Hadas Leonov, Bert de Groot and Helmut Grubmüller (MPI for Biophysical Chemistry, Göttingen) for their MD simulations of ABCE1 in the closed state. The Boehringer Ingelheim Fonds (BIF to M.G.) and the German Research Foundation (DFG) supported this work (FOR 1805—Ribosome Dynamics in Regulation of Speed and Accuracy of Translation to R.B.; GRK1721 to R.B.; CRC 902—Molecular Principles of RNA-based Regulation to R.T.).

Author contributions

K.K.-B. conducted the biochemical and cross-linking experiments. A.O. and M.B. performed the MS analysis and interpreted the MS data. U.J.R. supported the project in its initial phase. M.G., A.H., E.N.-G., T.B. and R.B. carried out the cryo-EM analysis. K.K.-B., A.O., M.B. and R.T. wrote the manuscript, and R.T. conceived the experiments. All authors reviewed the manuscript.

Additional information

Supplementary Information accompanies this paper at <http://www.nature.com/naturecommunications>

Competing financial interests: The authors declare no competing financial interests.

Reprints and permission information is available online at <http://npg.nature.com/reprintsandpermissions/>

How to cite this article: Kiosze-Becker, K. *et al.* Structure of the ribosome post-recycling complex probed by chemical cross-linking and mass spectrometry. *Nat. Commun.* **7**, 13248 doi: 10.1038/ncomms13248 (2016).

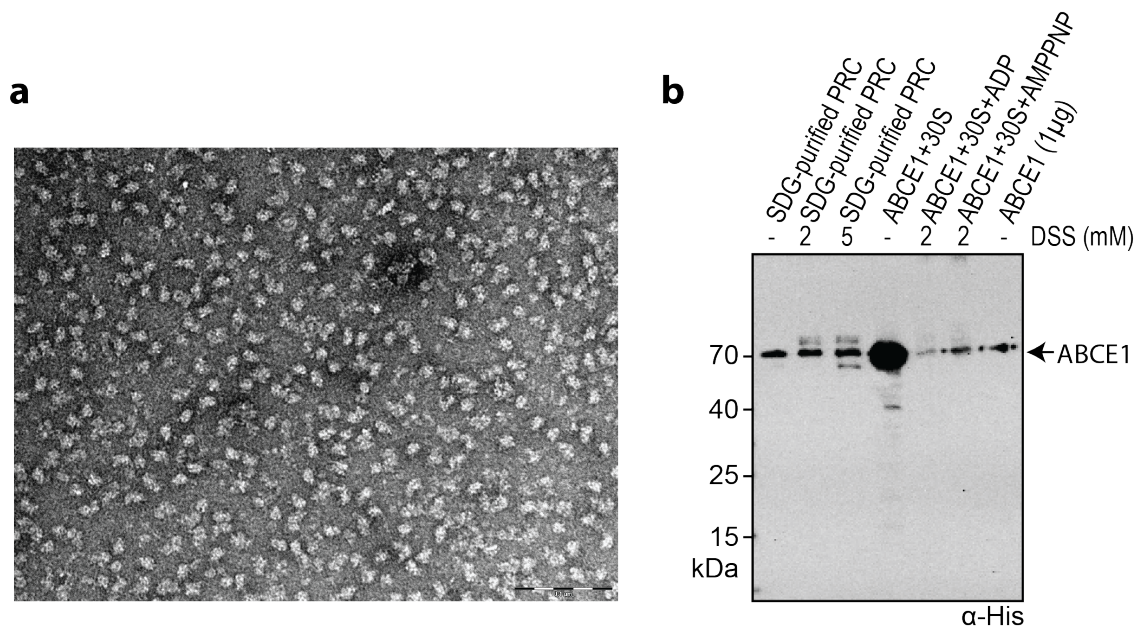
Publisher's note: Springer Nature remains neutral with regard to jurisdictional claims in published maps and institutional affiliations.



This work is licensed under a Creative Commons Attribution 4.0 International License. The images or other third party material in this article are included in the article's Creative Commons license, unless indicated otherwise in the credit line; if the material is not included under the Creative Commons license, users will need to obtain permission from the license holder to reproduce the material. To view a copy of this license, visit <http://creativecommons.org/licenses/by/4.0/>

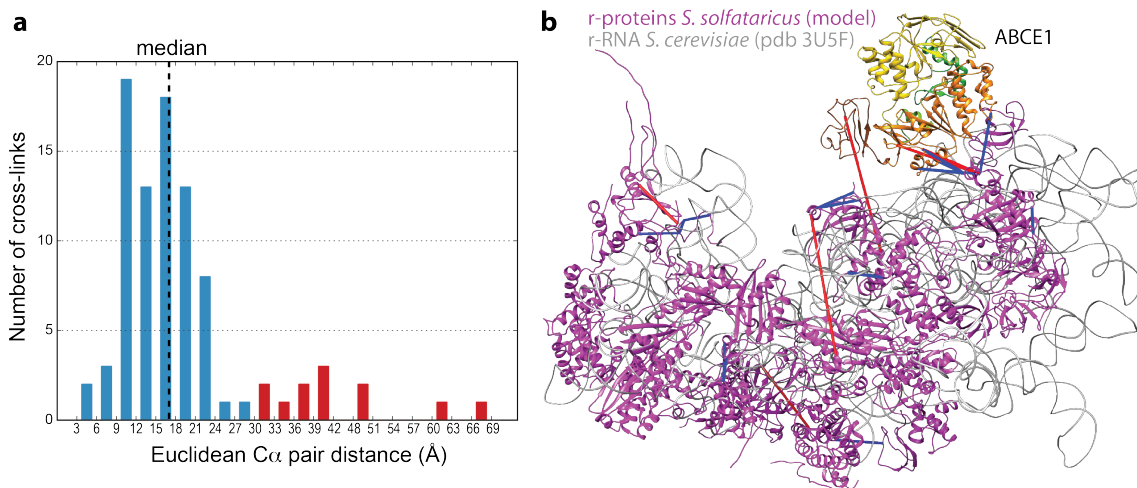
© The Author(s) 2016

Supplementary Figures



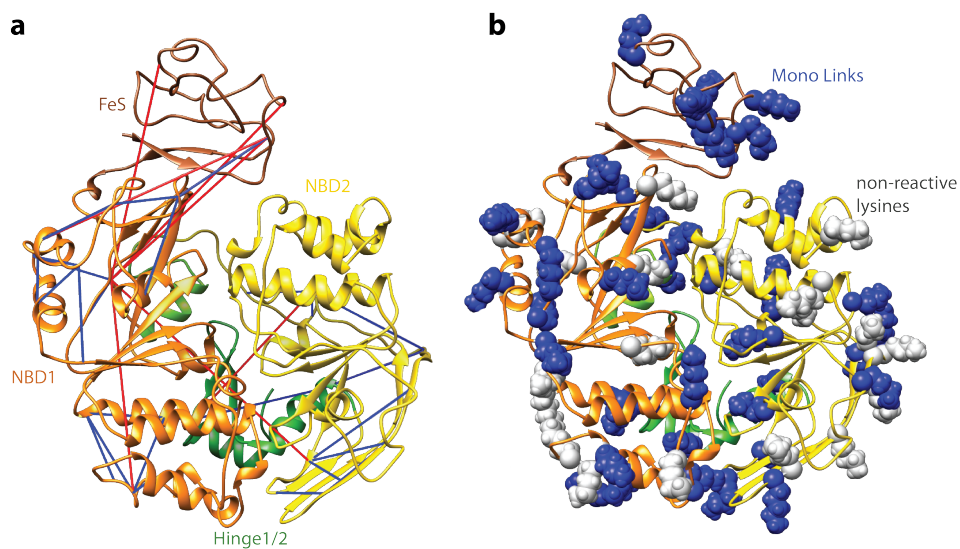
Supplementary Figure 1: Quality control of the purified post-recycling complex.

a, The quality of purified PRCs was analyzed via negative stain EM, depicting an even distribution in particle size and a clear homogeneity of the sample (bar 100 nm). **b**, Immunoblotting of the PRC samples before and after cross-linking (with 30- or 80-fold molar excess of DSS) displays a distinct band for ABCE1 and no undesired aggregation upon cross-linking.



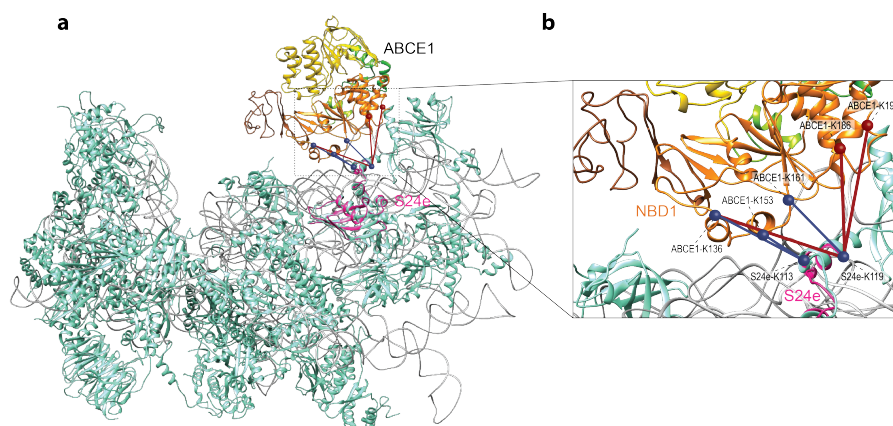
Supplementary Figure 2: Inter cross-links.

a, A histogram of all identified distance restraints of the post-recycling complexes with the median distance at 17 Å and with 86.7% of all cross-links below 30 Å. **b**, All identified inter cross-links are depicted using an *in silico* constructed model of the *S. solfataricus* 30S, which was built by aligning the homology models of the archaeal ribosomal proteins (magenta) to the small ribosomal subunit from *S. cerevisiae* (pdb: 3U5G/F, rRNA: gray) and positioning ABCE1 according to the cryo-EM map of the rescue/pre-recycling complex (pdb: 3J16). Inter cross-links between different r-proteins as well as between ABCE1 and r-proteins are depicted as blue and red lines (cross-links ≤ 30 Å blue and > 30 Å red).



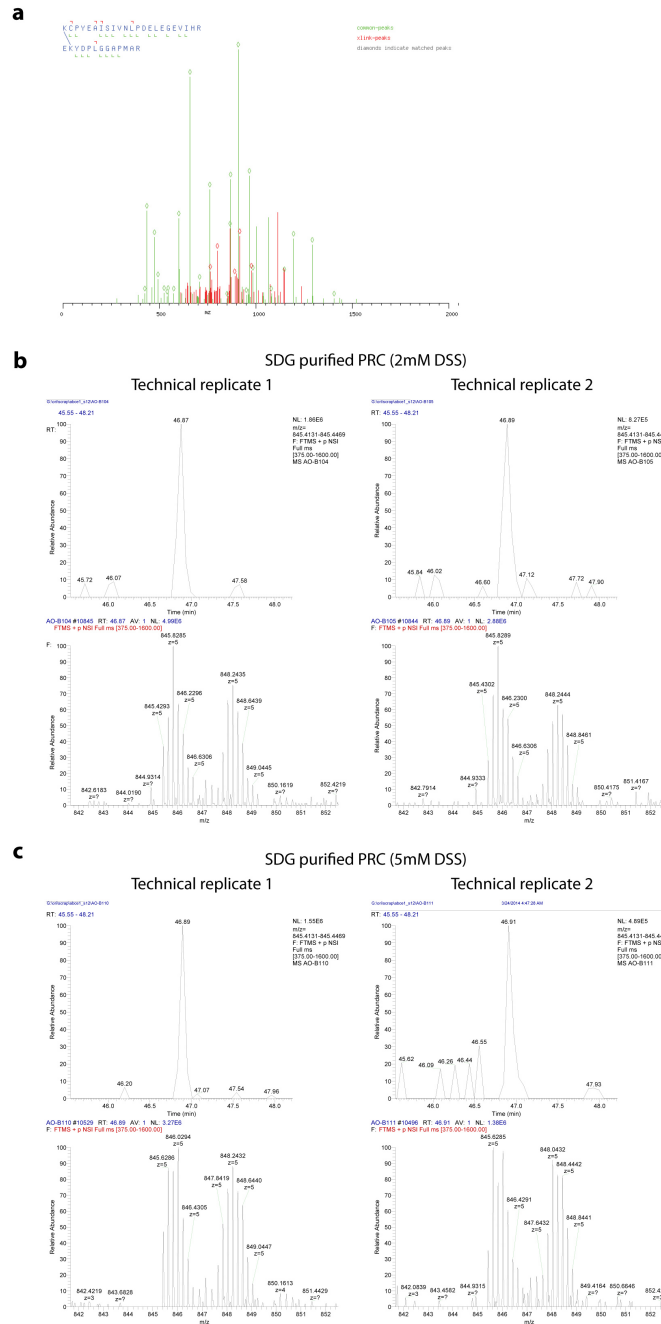
Supplementary Figure 3: Intra-cross links and mono links of ABCE1.

a, Intra ABCE1 cross-links combined from all independent experiments are certified using a model of the closed state of ABCE1 and are depicted as blue and red lines (cross-links ≤ 30 Å, blue and > 30 Å red). **b**, Lysine residues, which formed a mono-link by reacting with the DSS molecule, are depicted as blue spheres, while non-reactive lysines are shown in grey.



Supplementary Figure 4: Inter cross-links of the PRC AMP-PNP sample.

a, Orientation of ABCE1 in the PRC, based on the identified inter cross-links with the archaeal ribosomal protein S24e (purple, **b**), depicted as blue and red lines. Blue lines indicate cross-links with a length below 30 Å and red lines cross-links longer than 30 Å. Identified inter cross-links were certified with a constructed *in silico* model of the *S. solfataricus* 30S by aligning the homology models of the archaeal ribosomal proteins to the small ribosomal subunit from *S. cerevisiae* (pdb: 3U5G/F, r-proteins: cyan, rRNA: gray) and positioning ABCE1 according to the cryo-EM map of the rescue/pre-recycling complex (pdb: 3J16).



Supplementary Figure 5: Spectra of the S12-ABCE1 cross-link.

a, Fragment ion spectrum of two cross-linked peptides from ABCE1 (KCPYEAIIVNLPDELEGEVIHR) and RS12 (EKYDPLGGAPMAR). Ion series for both peptides are indicated, red peaks in the spectrum correspond to fragment ions containing the cross-linked lysine pair (cross-link peaks), green peaks correspond to fragment ions that do not include the linked site (common peaks). All fragment ions that match a peak in the spectrum are marked with diamonds. The ABCE1-RS12 cross-link was consistently present in two independent cross-linking reactions: one was carried out using 30-fold molar excess of DSS (2 mM DSS) (**b**) and the second using 80-fold molar excess of DSS (5 mM DSS) (**c**). In both cases, the characteristic precursor ion pattern corresponding to the peptides cross-linked with the light and heavy version of DSS is apparent in the MS1 spectra of both technical replicates (repeated injection of the same sample). For each technical replicate, the upper panel shows the extracted ion chromatogram for the light version of the cross-linked peptide ion that is consistently eluting at a retention time of ~46.9 min in all samples. The bottom panel shows the corresponding MS1 spectrum derived from the maximum intensity point of the extracted ion chromatogram.

Supplementary Tables

Supplementary Table 1 Protein database used for peptide identification

UniProt entry	UniProt name	Gene name	Sequence	Length (aa)
Q980K5	Q980K5	SSO028 7/ABCE 1/RLI1	MRVAVINYDFCKPDKCNLECFVDRSGGKAI ELSEIVKGPVIYEETCIGCGICVKKCPYEAI VNLPDELEGEVIHRYKVNGFKLFGGLPTPKNNTIL GVLGKNGVGKTTVLKILAGEIIPNFGDPNSKV DEVLKRFRGKEIYNYFKELYSNELKIVHKIQYVE YASKFLKGTVNEILTKIDERGKKDEVKELLNMTN LWNKDANILSGGGLQRLVAASLLREADVYIFDE PSSYLDVRRERMNMAKAIRELLKNKYVIVVDHDLI VLDYLTDLIHIYGESSVYGRVSKSYAARVGINN FLKGYLPAENMKIRPDEIKFMLKEVSDLDLSDKL KTKMKWTKIIKKLGDFQLVVDNGEAKEGEIIGIL GPNIGIKTTFARILVGEITADEGSVTPEKQILSY KPQRIFPNYDGTVQQYLENASKDALSTSSWFFEE VTKRLNLHRLLESNVNDLSGGELQKLYIAATLAK EADLYVLDEPSSYLDVEERYIVAKAIKRVTRERK AVTFIIDHDLSDIHDYIADRIIVFKGEPEKAGLAT SPVTLKTMNEFLRELEVTFRRDAETGRPRVNI GSYLDREVQKERGDYYSMVLSTQ	600
P95993	RS2	rps2	MKVNTLSEKEERGELTEAEKEELRKSEKGAIE LLVPVDTYLSAGVHIGTHSCTKYMESFVYRVRAE GLYVLDVRKIDERLRIAAKFLSRYDPQDIIVVAS RPYAYRPVQKFAEVVGSRALVGRIPGTFITNPYL STYIEPKVLLVSDPRTDTQAIKEAAKVGPIVAF ADTDAKIDYIDLIIANNKGRKSLALLYWALARQ ILRERRVIPPDGLAVPVSEFEMRLVQ	231
Q9UXA0	RS3	rps3	MPNIKRYFLEKSIVKVKIDEYLAKQYYNAEYAGV EVLKTPIGTRVIIYAGRPSMIIGRGGRNKQLAQ IFEKVFLENPQITITNVENPELNARVMAFRLAI ALEKGYHFRAAFISMRRIMNAGALGAEIISGK LTTERARYEKLKEGIVYKSGQOLEKMIDRAIAIA MLKPGIFGVEVVITKPLKIEDKINLKESPSVPQE VSVTNVTFIEESSQKSEEKSEGEKE	229
P95987	RS4	rps4	MGDPKKSRRKWPETPGHPWIKERIGYEQELLGKYG LRNKREIWIQAQSIIRKFRHQARSLALPPAERAV REKQLVGKLLKMGLLKKETATVDDILSLTEQDLL ERRLQTIYKGLSNTIYQARQLITHGHIAVNGK RVTSPGYIVNVDEENLIDYYVTSSFKSRPPVMSQ QEGGEIGVKQA	181
Q9UX87	RS5	rps5	MAEEVPSLNIEEWKPRTSIGSLVKEGKISSIKEL FDRNLPITEPEIVDVLLPKLYEVVDIKVVQKQT DAGEISRYKVLVIMGNMDGYVSI GTGKAKQLRVA IQKAIRDAKMNIIPVRRGCGSWQCTCGEPHSLPF KVVGKAGSVEVDLLPAPKGTGLVVGSVLKTLLTY AGIKDAWSTTKGETRTTENFVRAGYSALYNTYKF VTLQDWVRKR	214
P35026	RS7	rps7	MSLENLQLDIKVF GKWDTKVEIRDPSLKKYISLM PVYLPHTGGRHEHRRFGKAKVPIVERLINQIMRP	193

			GRNKGKKHLAYNIVKLAFDIIYLKTGQNPIQVLV RAIENSAPREEVTRIMYGGIVYYVAVDVSPQRR DLALRHIATGAKDASFNNPKPIEEVLAEEIIAAA NNDKSKFAIKRKEEIERIALSSR	
Q9UX92	RS8	rps8	MVFNPLANALTSIYNNEMRRNKQAIIMPASKLV INVLVVMQKEGYVGEFEYIDDGRWGKITVQLLGR VNKCGPITPRYPLSYRQMIALPDYVRRYLPSKEI GIIIVSTSKGVMESHKEAARLRIGGVALGYVY	133
P95992	RS9	rps9	MSEEQKLVISSARRKTARATCYIYAGKGRVFN VPIELIPIEMVRLKIMEPLLLAGNDIRSKIDAKI ITYGGIMGQADAARMALARALVKFTGSKELEKI YRAYDRTMLAGDPRQTESEKWMRYSARRWRQKSY R	137
P35027	RS10	rps10	MPTKARIRLWSTNVENLNYVITQIRGIVEKTGIE MRGPIPLPTSKLEVPIMRLPHGEGRKKWEKWE VHKRLIDIAADERVMRQLMRVVRVPEDVYIEIQLI	102
P95988	RS11	rps11	MSSRREIRWGIAHIYASQNNTLLTISDLTGAEII SRASGGMVVKADREKSSPYAAMLAANKAASDALE KGIMALHIKVRAPGGYGSKTPGPGAQPAIRALAR AGFIIGRIEDVTPIPHDTIRRPGGRRGRRV	132
P39573	RS12	rps12	MVKSCKSPKGIYAARKLRLKRLKFRRSQRKYKTKI LKLKEYDPLGGAPMARGIVLEKVGIESRQPN VRKCVRVQLVRNGRVVTAFFVPGDGGVNFIDEHDE VIITGIGGTLGRSMGDLPGVRYKVMVNGVSLDA LYKGGKQKQKPV	147
P95986	RS13	rps13	MSQQFKYVVRIFGQDVGTMKLPYALAMVKGIGY NTAKAIIRKLGMDPNARLGELSDAEVKKVESVIS DHTIKGLPSWLYNRRKDYESGLDLHLVTSDLIFY VRNDIEREKKSRSWRGVRHSLGLKVRGQRTRTTG RTGMTIGVARKKAAQPOSQSSSQQKSS	136
Q97ZQ5	RS14Z	rps14	MGKYKPPAERKYGKGVQSCQRCGSKDSVIQKYGI YLCRQCFREVAYELGFRKYW	54
Q980A8	RS15	rps15	MNKRRAKGKSHSIRPARAGAPKWVRLTREEVEM VEELAKRGYTPSMIGIILRDQYGIPLVKQIVGKK VTQILEERGLAPQIPEDLFNLIRKAVNVRRHINE YPRDKTAKKGLEEIESKIRRLTRYKYGIGKLPQE WVYDPAKAELLVAGAS	152
Q9UX98	RS17	rps17p	MVSKGKTVKDPGIPNITPEKVCEDDCPYHGSL RVRGITLEGVIVKYRGTAAVIERQYLYYDSKYK RYERRRSRIHAHVPPCINVREGDKVIGECRPLS KSISFVVLGKVS	114
D0KTC1	D0KTC1	rps19p	MSLEIPPEWKNFKYRGKSIDELLNMPMDEFIKLL PSRQRRSLKRGFTDAQRHLLKVRKYRREGKFNK TIKTHVRNLVILPELIGLKMAVYNGKEFVEFTVT PEMIGHYLGEYSITTKKVEHGEPGLKATRSSLFL AMKG	119
Q9UXD4	RS3A	rps3ae	MSAKGGAIKDKWKMKKWYSVITPKAFGEVSLGST PAYDITQITIGRRVETTLYDLTGDFSQVYVHLYFK IIGNEGDRLITRFVGHLSRDYLRSLIRRKSSKI NSIFDVTTKDGYYVRVKGLVLTYYKCHQSOKTAI RKIINETVSKKASELSFDDFTQEVVFGRLANEIF EAAKKIYPLRKAIEKTKVLKVPENLGKQVESS VSSG	208

Q9UX94	RS4E	rps4e	MAHITRFEAPWFLMISKKQYKWTVRPNAGPHSIE KSIPLAVVIRDYKLAGTIREAKHIIIFDGKVLVD GKVRKDYKYPVGLMDIVSIPSADLYFRVLPDNR FMRFSKISADEARYKYVRIINKTTIKEGRIQLNL EDGRNILVDKETAKNFKTLMTLKIELPSQQILDS FTISERSYAI FVGGRNVIHGIVKNINLSKFKSR KYSVITLESRDGNTYQTNIMNVMSIGREKSDLRV D	239
Q980A6	RS6E	rps6e	MPDFKIVISDPQSVPEPKRIKVKVKASDQVKSITG EKDGKAVPQAKVNEKTKQLLNVDTLTLEITKQE GDKKVKVKGHFVVDVNSVPDNEVWISKMAEF GAEDFEAFAYRTKTLQISVDQNKATNLVGLKIGD VFEANQLIGLPVKLKITGGSDNSGFPMRFDVIGA AKRKILLSGPPGFYPNENGERRRKTIRGNTISQE IVQINTIIVR	214
Q980W3	RS8E	rps8e	MGFYQGPDNRKITGGLKGGKHRDKRKYEIGNPPTF TTLSAEDIRIKDRTLGGNFVKVRLKYTTTANVLDP ATNTAKKVKILEILETPANKELARRGIIIRGAKI RTEAGLAVVTSRPGQDGVINAVLLKNESQRS	133
Q980K7	RS17E	rps17e	MGNIIYTKDIKRIVKEIYDRYKDEIKDDYNTNKQI VIRYVDVKSCKVRNRIAGYLTRYKIMKEKETSP AEEKEEISEEI	79
Q980F7	Q980F7	rps19e	MSLIMITAEMVPPDLLIKRLAIYKENVKTVDPP EWALLAKTASFKEVPDNAEDWWYIRAASLLRKL YVNSIIGIEKTRTIYGGRRRGRTRPEKFKAPGH VNRLIFQQLEKAGLVQKIKNKGRSLSPKGRSLD KLALEIFKELAENNTSLKVYLE	158
Q97ZY6	RS24	rps24e	MESQAKVKISDKAEGIIERDMQNSVIGRREISLK VYHMGSGTPSRKDIKAI IQALGSQENLVVVRKI STSYGAGISNVKLHIYKSREILEKVEPKYLLDRD AGTKQKKGGSKGGQAKG	120
Q97ZZ6	RS25	rps25e	MGGASKKPISTMEKRLKKEAEKQQAEEKKGKPS KTGKEIISRVAVTIDEETKKKVLDEIKKESIITPY ALATKSGISISVARKILKELENQNVVKLYSKNRR LEIYIAAS	110
Q97ZR1	Q97ZR1	rps26e	MPKKRENRRRKGDKGHVGYISCDQCGARVPEDK AVCVTKMYSPVDASLASELEKKGAI IARYPVTKC YCVNCAVFLGIIKIRAENERKQKARLR	95
Q97Z80	RS27	rps27e	MMRKLRLVLIPEPKSRFLRVKCPNCGNEQTIFSHA TFPVRCLSCGTELVSMMGGKAKIVGEVVRIMG	66
Q97ZY7	RS27A	rps27ae	MLELNKRKEEAKVAKEQKVKAIVRTYYVIEGNKV KLKNKKCPRCGSIMAHLKPNERNWSCGKCGYTEF IGASKKR	75
Q980Q5	RS28	rps28e	MSEKTQOSQSSIIIEFGFPAEVIQILDRTGVTG EVTQVRVRVLEGRDKGRILTRNVKGPVVRVGDILI LRETEREARKITTKR	83
Q97ZH4	Q97ZH4	rps30E	MPSHGSLTKAGKRSQTPKIQPKKHEVPRVRN RKEYEKRVVKARQQAPAR	52

Supplementary Table 2 Inter cross-links between ABCE1 and ribosomal proteins (ld-score cutoff ≥ 30)

ABCE1		r-proteins		modeled to 40S yeast (pdb:3U5G/F)	distance [Å]	Independent cross-linked peptides							
peptide	residue	peptide	residue			PRC preparation 2				PRC preparation 1			
						SDG purified (5mM DSS)	SDG purified (2mM DSS)	ADP	AMP-PNP	SDG purified (2mM DSS)	ADP	AMP-PNP	
VGKDEVLR	136	S24e	GGQGAKG	119	eS24	31.3	1	1	-	-	2	-	2
VGKDEVLR	136	S24e	GGSKGGQGAK	113	eS24	22.4	1	3	-	2	3	-	-
ILAGEIIPNFGDPNSKVGKDEVLR	133	S24e	GGQGAKG	119	eS24	40.6	-	1	-	-	-	-	-
GKKDEVK	192	S24e	GGQGAKG	119	eS24	26.9	-	1	-	-	-	-	-
VGKDEVLR	141	S24e	GGQGAKG	119	eS24	28.4	-	1	-	-	-	-	-
EIYNYFKELYSNELK	153	S24e	KGGSKGGQGAK	113	eS24	11.6	1	-	-	1	-	-	-
VGKDEVLR	141	S24e	KGGSKGGQGAK	113	eS24	20.0	1	-	-	-	-	-	-
KCPYEAISIVNLPDELEGEVIHR	60	RS12	EKYDPLGGAPMAR	40	uS12	59.5*	1 [#]	1	-	-	-	-	-
r-protein 1			r-protein 2										
peptide	residue	r-protein	peptide	residue	r-protein								
SGQQLKQKIDR	161	RS3	YVDVKSK	42	RS17E	15.2	1	1	1	1	1	1	1
KAAQPQSQSSSQQQK	148	RS13	KVEHGEPGLK	119	RS19	15.8	2	1	-	-	1	-	-
KAAQPQSQSSSQQQK	148	RS13	KVEHGEPGLKATR	128	RS19	16.3	1	1	-	1	-	-	-
HIIFDGKVLVDGK	64	RS4E	LHIYKSR	85	RS24	17.6	-	1	1	1	-	-	-
NDIEREKK	111	RS13	KVEHGEPGLK	119	RS19	16.5	-	1	-	1	-	1	1
SQTPKIQPK	19	RS30E	KQKPVR	142	RS12	16.2	-	1	-	-	-	1	1
IGYEQELLGKYGLR	32	RS4	RVVKAR	44	RS30E	13.9	-	1	-	-	-	-	-
AKIVGEVVR	56	RS27	KIYPLR	175	RS3A	20.8	1	-	-	-	1	1	1
AIRDAKMNIIPVR	111	RS5	MPSHGSLTKAGK	9	RS30E	63.9	-	-	-	-	-	-	1
SQTPKIQPK	19	RS30E	KQKPVR	144	RS12	18.0	-	-	-	-	-	-	1
KAEIEK	181	RS3A	KITTKR	82	RS28	33.8	-	-	-	-	-	-	1
IEDKINLK	192	RS3	YVDVKSK	42	RS17E	21.5	-	-	-	-	1	-	1

*Conformational reorganization of the FeS-cluster domain from 59.5 to 17.5 Å before and after ribosome splitting; [#]this cross-link was identified with high confidence in the SDG purified (2mM DSS) sample and the characteristic precursor ion pattern corresponding to the peptides cross-linked with the light and heavy version of DSS was apparent in the MS1 spectra of both technical replicates also for the SDG purified (5mM DSS) sample, see Supplementary Fig. 5 for details.

Supplementary Table 3 Intra cross-links within ABCE1

peptide	res.1	peptide	res.2	dist. [Å]	domain	Independent cross-linked peptides						
						PRC preparation 2				PRC preparation 1		
						SDG purified (5mM DSS)	SDG purified (2mM DSS)	ADP	AMP-PNP	SDG purified (2mM DSS)	ADP	AMP-PNP
IRPDEIKFMLK	325	YIVAKAIK	500	9.4	NBD2/NBD2	1	2	1	1	-	-	-
GEPEKAGLATSPV TLK	539	KLGDFQLVVDNGE AK	352	10.5	NBD2/NBD2	1	1	1	1	1	1	1
IIVFKGEPEK	534	WTKIIK	348	15.9	NBD2/NBD2	3	3	1	3	1	-	-
MNMAKAIR	253	ELLKNK	260	12.1	NBD1/NBD1	2	2	-	1	1	-	1
VNKIGSYLDR	577	ELLKNK	260	14.1	Hinge2/NBD1	1	1	1	1	-	1	1
GKEIYNYFK	146	VSKSYAAR	296	12.5	NBD1/NBD1	2	1	2	2	-	1	1
AGLATSPVTLKTG MNEFLR	550	EVSDLDLISKDLK	338	17	Hinge2/NBD2	1	1	-	1	-	-	-
EIYNYFKELYSNELK	153	VGKDEVLR	141	9.6	NBD1/NBD1	-	1	1	1	-	-	-
VNKIGSYLDR	577	MNMAKAIR	253	8.2	Hinge2/NBD1	1	1	-	1	1	-	-
KLGDFQLVVDNGE AK	352	WTKIIK	348	13.4	NBD2/NBD2	1	1	1	1	1	1	1
LFGLPTPKNNTILG VLGK	97	VSKSYAAR	296	13.6	NBD1/NBD1	1	1	1	1	-	1	1
IIVFKGEPEK	534	WTKIIK	351	16	NBD2/NBD2	1	1	-	-	-	-	-
TTVLKILAGEIIPNF GDPNSK	117	YKVNQFK	84	17.2	NBD1/NBD1	1	1	1	1	-	-	-
YIVAKAIK	500	EVSDLDLISKDLK	338	20.6	NBD2/NBD2	1	1	-	-	1	-	-
EIYNYFKELYSNELK	153	VGKDEVLR	136	8	NBD1/NBD1	1	1	-	2	-	-	1
ILAGEIIPNFGDPN SKVQK	133	YKVNQFK	84	16.4	NBD1/NBD1	2	2	-	1	1	2	1
ILAGEIIPNFGDPN SKVQK	133	DEVLR	141	10.8	NBD1/NBD1	1	1	1	1	-	-	1
FMLKEVSDLISK	329	YIVAKAIK	500	11.8	NBD2/NBD2	1	1	-	-	-	-	-
GTVNEILTKIDER	186	GKKDEVK	193	10.2	NBD1/NBD1	1	1	1	1	-	-	-
GKEIYNYFK	146	VGKDEVLR	141	9.9	NBD1/NBD1	1	1	2	2	-	1	-
ELYSNELKIVHK	161	VGKDEVLR	136	14.5	NBD1/NBD1	2	2	1	1	-	-	1
GKKDEVK	192	ELLKNK	260	15	NBD1/NBD1	1	-	1	1	-	-	1
MNMAKAIR	253	GKKDEVK	193	17.7	NBD1/NBD1	1	-	-	-	-	-	-
IIVFKGEPEK	534	MKWTKIIK	345	21.5	NBD2/NBD2	-	-	-	1	-	-	-
VNKIGSYLDR	577	YIVAKAIK	500	27.7	Hinge2/NBD2	-	-	1	1	-	-	-
VAVINYDFCKPDK	12	YKVNQFK	84	19.1	FeS/NBD1	-	-	-	-	-	1	1
VSKSYAAR	296	GKKDEVK	193	37.6	NBD1/NBD1	-	-	-	-	-	1	1

VN <u>K</u> IGSYLDR	577	AGLATSPVTL <u>K</u> TG MNEFLR	550	19.8	Hinge2/NBD2	-	-	1	1	-	-	1
VAVINYDF <u>C</u> K <u>P</u> DK CNLECI <u>N</u> FC <u>P</u> VDR	12	V <u>S</u> K <u>S</u> YAAR	296	39.2	FeS/NBD1	-	-	1	-	-	1	1
DEV <u>L</u> K <u>R</u>	141	ILAGEIIPNFGDPNS K <u>V</u> G <u>K</u>	136	8.4	NBD1/NBD1	-	-	-	-	1	-	-
VAVINYDF <u>C</u> K <u>P</u> DK CNLECI <u>N</u> FC <u>P</u> VDR	15	V <u>S</u> K <u>S</u> YAAR	296	43.9	FeS/NBD1	-	-	-	-	-	-	1
SGG <u>K</u> AIE <u>L</u> SEIVK	32	V <u>S</u> K <u>S</u> YAAR	296	37.0	FeS/NBD1	-	-	-	-	-	-	1
IIV <u>F</u> K <u>G</u> EPEK	534	V <u>S</u> K <u>S</u> YAAR	296	41.8	NBD2/NBD1	-	-	-	-	-	-	1

Structure of the 40S–ABCE1 post-splitting complex in ribosome recycling and translation initiation

André Heuer^{1,4}, Milan Gerovac^{2,4}, Christian Schmidt¹, Simon Trowitzsch², Anne Preis¹, Peter Kötter³, Otto Berninghausen¹, Thomas Becker¹, Roland Beckmann¹ & Robert Tampé²

The essential ATP-binding cassette protein ABCE1 splits 80S ribosomes into 60S and 40S subunits after canonical termination or quality-control-based mRNA surveillance processes. However, the underlying splitting mechanism remains enigmatic. Here, we present a cryo-EM structure of the yeast 40S–ABCE1 post-splitting complex at 3.9-Å resolution. Compared to the pre-splitting state, we observe repositioning of ABCE1's iron-sulfur cluster domain, which rotates 150° into a binding pocket on the 40S subunit. This repositioning explains a newly observed anti-association activity of ABCE1. Notably, the movement implies a collision with A-site factors, thus explaining the splitting mechanism. Disruption of key interactions in the post-splitting complex impairs cellular homeostasis. Additionally, the structure of a native post-splitting complex reveals ABCE1 to be part of the 43S initiation complex, suggesting a coordination of termination, recycling, and initiation.

ATP-binding cassette (ABC) proteins drive fundamental biological processes such as membrane transport, genome maintenance, and protein biosynthesis^{1–4}. All ABC systems feature two nucleotide-binding domains (NBDs), which form sandwich-like nucleotide-binding sites (NBSs) for two ATP molecules. Conformational dynamics of NBDs are believed to allosterically induce structural changes in adjacent domains or subunits. The ribosome-recycling factor ABCE1 is one of the most conserved proteins in evolution and is essential for life in *Archaea* and *Eukarya*^{4–8}. The twin-ATPase protein is equipped with a unique N-terminal iron–sulfur (FeS) cluster domain^{9,10}, which contains two [4Fe-4S]²⁺ clusters and is connected to the core protein by a characteristic antiparallel β -sheet called the cantilever arm along with a flexible linker, the cantilever hinge. Additionally, ABCE1 constitutes a helix–loop–helix (HLH) motif and a bipartite architecture of hinge 1 and hinge 2 domains that mediate interaction of the NBDs with the ribosome^{11–13}. ABCE1 has a crucial function in splitting 80S ribosomes into small 40S and large 60S subunits after translation termination^{14,15}. It also rescues stalled ribosomes on truncated or secondary-structure-containing no-go mRNAs during mRNA surveillance and reactivates hibernating ribosomes^{15–17}.

For splitting, ABCE1 acts in concert with the termination factor eRF1 or its homologous rescue factor Pelota (Dom34p in yeast)^{14–18}. Pre-splitting 80S–ABCE1 complexes obtained by translation stalling or termination inhibition have been observed by cryo-EM^{11–13}. These complexes carry either eRF1 or Pelota in the ribosomal A-site, which is already in close contact with the FeS cluster domain of the bound ABCE1. In the presence of ATP, these complexes proceed to splitting, and ABCE1 is released from the post-splitting complex, most likely after ATP hydrolysis,

because it is bound to 40S in the presence of non-hydrolyzable ATP-analog adenylyl-imidodiphosphate (AMP-PNP)^{14,18}. Nevertheless, the exact timing and role of ATP binding and hydrolysis in the two NBSs is still elusive, and the ATP-driven conformational transitions of ABCE1 between the pre- and post-splitting states are unknown.

Apart from these functions, ABCE1 controls reinitiation in 3' untranslated mRNA regions^{19,20} and is supposed to play a role in assembling initiation complexes^{21–23}. In *Drosophila melanogaster* and *Saccharomyces cerevisiae*, 40S–ABCE1 complexes were shown to associate with initiation factors eIF2, eIF5, and the multiprotein complex eIF3 (refs. 21–24). The latter has been proposed to act as a main interaction platform for initiation factors. Taken together, currently available data suggest that ABCE1 links not only termination and recycling, but also recycling and initiation⁷.

Here, we determined the structures of 40S–ABCE1 post-splitting complexes that were reconstituted *in vitro* from purified components or isolated as native 40S–ABCE1 initiation complexes. Cryo-EM structures of these complexes show ABCE1 in a conformation distinct from pre-splitting complexes with a rotated FeS cluster domain and the NBDs in a closed, nucleotide-occluded conformation. Together with biochemical and mutational analyses, these structures provide fresh insights into the splitting mechanism and involvement of ABCE1 in translation initiation.

RESULTS

Post-splitting complex reconstituted by facilitated splitting

The transient state after splitting was efficiently captured by a 'facilitated splitting' approach under conditions that allowed splitting of 80S ribosomes by ABCE1 at low magnesium and high potassium levels and

¹Gene Center and Center of Integrated Protein Science Munich, Department of Biochemistry, University of Munich, Munich, Germany. ²Institute of Biochemistry, Biocenter, Goethe University, Frankfurt/Main, Germany. ³Institute for Molecular Genetics and Cellular Microbiology, Biocenter, Goethe University, Frankfurt/Main, Germany. ⁴These authors contributed equally to this work. Correspondence should be addressed to R.B. (beckmann@genzentrum.lmu.de) or R.T. (tampe@em.uni-frankfurt.de).

Received 16 June 2016; accepted 7 March 2017; published online 3 April 2017; doi:10.1038/nsmb.3396

Table 1 EM data collection, refinement, and validation statistics

	40S _{BODY} -ABCE1 (EMD 4071, PDB 5LL6)	ABCE1 (EMD 4071, PDB 5LL6)
Data collection		
Number of particles	101,000	
Pixel size (Å)	1.084	
Defocus range (µm)	-0.8 to -2.5	
Voltage (kV)	300	
Electron dose (e ⁻ /Å ⁻²)	28	
Refinement		
Model resolution (Å)	4.0	4.0
Map-sharpening <i>B</i> factor (Å ²)	-96.9	-96.9
Average <i>B</i> factor (Å ²)	131.6	130.6
FSC _{average}	0.82	0.71
Model composition		
Non-hydrogen atoms	55,263	4,645
Protein residues	3,431	578
RNA bases	1,325	-
R.m.s. deviation		
Bond lengths (Å)	0.0114	0.0283
Bond angles (°)	1.41	2.49
Validation		
MolProbity score	2.16	2.98
Clashscore (all atoms)	4.87	15.41
Good rotamers (%)	97.78	94.15
Ramachandran plot		
Favored (%)	85.74	82.23
Outliers (%)	3.66	3.48
Validation (RNA)		
Correct sugar puckers (%)	95.1	-
Good backbone conformations (%)	62.0	-

trapping of the post-splitting state in the presence of the AMP-PNP (see Online Methods). This approach bypasses the AMP-PNP-dependent arrest of the pre-splitting state^{11,12,14,15} and thereby enables populations of 40S subunits with ABCE1, which are specifically stabilized in the post-splitting state. The 40S-ABCE1 post-splitting complex was harvested by sucrose density gradient centrifugation under conditions promoting the reassociation of ribosomal subunits to 80S complexes (**Supplementary Fig. 1**). We observed that ABCE1-AMP-PNP is stably bound to the 40S subunit and displays anti-association activity, which in turn allowed the preparation of a highly enriched 40S-ABCE1 fraction.

The reconstituted and purified post-splitting complex was subjected to single-particle cryo-EM analysis. After 2D and 3D classification (**Supplementary Fig. 2**) and masking of the flexible head region of the 40S subunit, we obtained a structure of the 40S-ABCE1 post-splitting complex at an average resolution of 3.9 Å according to the gold-standard criteria (**Table 1** and **Supplementary Fig. 3**). Local resolution was between 3.5 and 4.5 Å for the 40S body, the ABCE1 FeS cluster domain, and NBS I, but it was lower for NBS II and flexible regions such as the 40S head. We built, refined, and validated a molecular model based on known structures of ABCE1 and the 40S ribosomal subunit (**Fig. 1** and **Supplementary Fig. 3**).

The structure showed that ABCE1 binds the 40S subunit at a site used by other translation factors, for example, eRF3 or Hbs1, eEF1A, eEF2, or eIF5B^{12,25-29} (**Fig. 1a**). We found the NBDs of ABCE1 repositioned with NBD1, the HLH, and the hinge regions (H1 and H2) contacting the 18S rRNA and the ribosomal protein eS24. Compared to the pre-splitting state, the FeS cluster domain is dramatically

rearranged and binds to a pocket formed by uS12 and rRNA helices h5 and h44. This interaction site has recently been identified by chemical cross-linking and MS in the archaeal post-recycling complex³⁰. Notably, the NBDs are in a closed conformation, and both NBSs clearly occlude a bound nucleotide.

Nucleotide-binding domains are closed with two occluded nucleotides

So far, ABCE1 has been observed only in the free, ADP-bound open conformation^{10,18} or in an intermediate, semi-closed 80S-associated pre-splitting state. In the structures of the pre-splitting state, the nucleotide occupancy in either NBS is unclear¹¹⁻¹³. Compared to the pre-splitting state, the post-splitting state shows a rotation of NBD2 toward NBD1 (**Fig. 2a**). This rotation results in a full closure of the two NBSs and occlusion of two nucleotides (**Fig. 2a** and **Supplementary Video 1**). In the post-splitting state, the phosphates and the ribose of the bound nucleotides are coordinated by the Walker A and B motifs as well as the C-loops of the opposing NBDs (**Fig. 2b-d**). In NBS I, density is clearly present for an AMP-PNP-Mg moiety and we observe π - π stacking of the adenosine base with a tyrosine residue (Tyr87) in the A-loop (**Fig. 2b**). Moreover, critical residues in the C-loop of NBD2, the Walker A motif of NBD1, and the Q-loop of NBD1 are well defined by the density and adopt similar conformations to those observed in structures of other ABC proteins in the NBD-closed state^{31,32}. Clear density for a bound nucleotide was also present in NBS II, but the local resolution was lower (**Supplementary Fig. 2c**). Yet based on the structure of AMP-PNP-bound BtuCD³², we were able to build a model for NBS II that shows a similar arrangement of the Walker A motif and the C-loop to that in NBS I (**Fig. 2d**). In addition to the canonical motifs forming the NBSs in ABC proteins, we identified the conserved Phe366 of NBD2 as contributing to the coordination of the nucleotide ribose moiety. Taking these observations together, in the post-splitting state, we observe the NBDs of ABCE1 fully closed with two occluded nucleotides. The hallmark residues involved in ATP binding are in a conformation comparable to the one observed in canonical ABC-type ATPases (**Fig. 2d** and **Supplementary Video 1**).

Apparently, ABCE1 remains bound to the 40S subunit with both NBSs in a closed state only in the presence of non-hydrolyzable ATP analogs, but not in the presence of ATP as demonstrated previously^{14,18,21,22}. This indicates that ATP hydrolysis still has to occur and may be required for release of ABCE1 from the 40S subunit. In agreement with this idea, ATP- and GTPase assays with ABCE1 in the presence of 40S ribosomes revealed a weak stimulation (2-3-fold) of nucleotide hydrolysis (**Supplementary Fig. 4**; source data in **Supplementary Data Set 1**).

Ribosome binding of ABCE1 and FeS cluster domain repositioning

The most striking reorganization from the pre- to the post-splitting state is the repositioning of the FeS cluster domain on the ribosome by rotation of 150° around a flexible linker (cantilever hinge) into a binding cleft formed by the rRNA helices h5-h15 and h44 and the ribosomal protein uS12 (**Fig. 1b** and **Supplementary Video 1**). This interaction is established by salt bridges between basic residues of the FeS cluster domain and the rRNA (**Fig. 3a,b**) as well as by a hydrophobic contact between Pro30 of ABCE1 and Ile52 of uS12 (**Fig. 3c**). In addition, the HLH motif as well as the hinge 1 and 2 motifs of ABCE1 form contacts with the rRNA (**Figs. 1c** and **3d-f**). Notably, these ABCE1-rRNA interactions largely differ from those that occur in the pre-splitting state: while hinge 2 still contacts the junction between h8 and h14 by Arg573 (**Fig. 3e**), which plays a role in the activation of

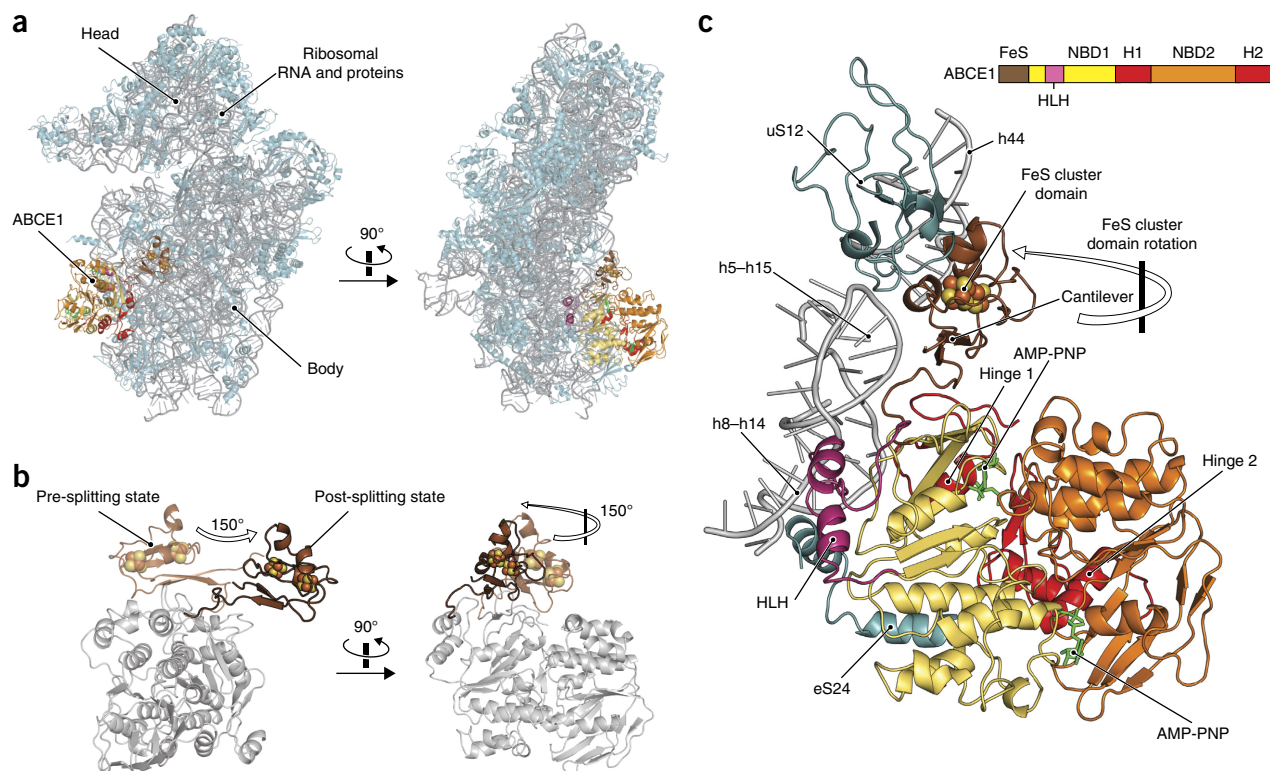


Figure 1 Overall structure of the 40S-ABCE1 post-splitting complex. **(a)** Structure of the 40S-ABCE1 post-splitting complex in front and side views with ribosomal proteins in teal, rRNA in gray, ABCE1 with domains colored as indicated in the schematic in **c**, and AMP-PNP in green. **(b)** Movement of the FeS cluster domain by 150° rotation from the pre-splitting state (PDB 4CRM; ref. 12; transparent) to the post-splitting state (brown). The body of ABCE1 (lacking the FeS cluster domain) in the pre-splitting state is shown in gray. **(c)** Interactions of ABCE1 with the small 40S ribosomal subunit. The FeS cluster domain interacts with h5, h44, and uS12, and the HLH and hinge domains form contacts to rRNA (h5-h15 and h8-h14) and to eS24. The two NBDs are closed with two AMP-PNP molecules occluded.

translational GTPases³³, hinge 1 moves closer to the 40S subunit toward the base pair A51-U440 forming the h5-h15 junction (Fig. 3f). In the pre-splitting state, this A-U base pair also interacts with the HLH motif, which rearranges to establish a new contact with h15 (U440) by Ser150 (Fig. 3d,f and Supplementary Video 1). The contact between the C-terminal helix of eS24 and NBD1 (Gln262) is maintained in pre- and post-splitting states in yeast, but differs significantly between yeast and human, in which it is found in 90° rotated conformation (Fig. 3g).

Notably, the cantilever hinge, which forms an α -helix in the pre-splitting complex, is unwound in the post-splitting state (Fig. 4a,b and Supplementary Fig. 5). This unwinding establishes a new intramolecular contact between the cantilever hinge and NBD1 by a side chain-backbone interaction between the conserved residues Tyr301 and Asn78. The new position of the FeS cluster domain is stabilized by a number of contacts to the rRNA (h5 and h44) and uS12 (Pro30), and particularly by the contact between the conserved Arg7 of the cantilever arm and helix h5 of the rRNA (Fig. 4b and Supplementary Video 1).

The post-splitting state is essential for cellular homeostasis

To address the physiological significance of the 40S-ABCE1 structure, we tested whether substitution of key interaction residues of the FeS cluster domain and NBD1 in the post-splitting state could impair the function of ABCE1 *in vitro* or *in vivo*. Importantly, our *in vitro* 'facilitated splitting' assay allows us to assess the anti-association activity (inhibition of 40S-60S rejoining) of wild-type (wt)

and mutant ABCE1. To this end, we analyzed the ribosomal subunit (40S and 60S) to monosome (80S) ratio in ribosome profiles. In the presence of AMP-PNP, wt ABCE1 shows anti-association activity, as in the case of anti-association factor eIF6 (Fig. 4c and Supplementary Fig. 1)³⁴. Strikingly, substitution of Arg7, Pro30, or Tyr301 with alanine impaired the anti-association activity of ABCE1, as indicated by high levels of 80S ribosomes and a low subunit-to-monomer ratio as compared to those occurring with 80S ribosomes alone or with wt ABCE1 but no addition of AMP-PNP. In contrast, ABCE1 mutants with alanine substitution of His95, which is not involved in stabilizing FeS cluster domain contacts, and Asn78, which is only interacting with Tyr301 via its backbone, still exerted full anti-association activity (Fig. 4c).

The ABCE1 mutants that showed anti-association activity were analyzed for growth defects *in vivo* by means of a plasmid shuffling assay, in which the endogenous *ABCE1* gene (*RLI1*) was chromosomally deleted and substituted by plasmid-encoded wt or mutant *ABCE1*. Surprisingly, cells expressing ABCE1 carrying single alanine substitutions for Arg7, Pro30, and Tyr301 were still viable, whereas a double substitution of Arg7 and Tyr301 was lethal (Fig. 4d). In order to examine if these alanine substitutions impact ribosome splitting, we overexpressed epitope-tagged wt and mutant ABCE1 and recorded ribosome profiles (Supplementary Fig. 6a). We observed a significant increase of the 80S ribosome population in cells expressing alanine mutants of Arg7, Pro30, and Tyr301 as compared to wt ABCE1. In addition, we observed a strongly increased enrichment of mutant ABCE1 protein in the 80S ribosome fraction (Supplementary Fig. 6b).

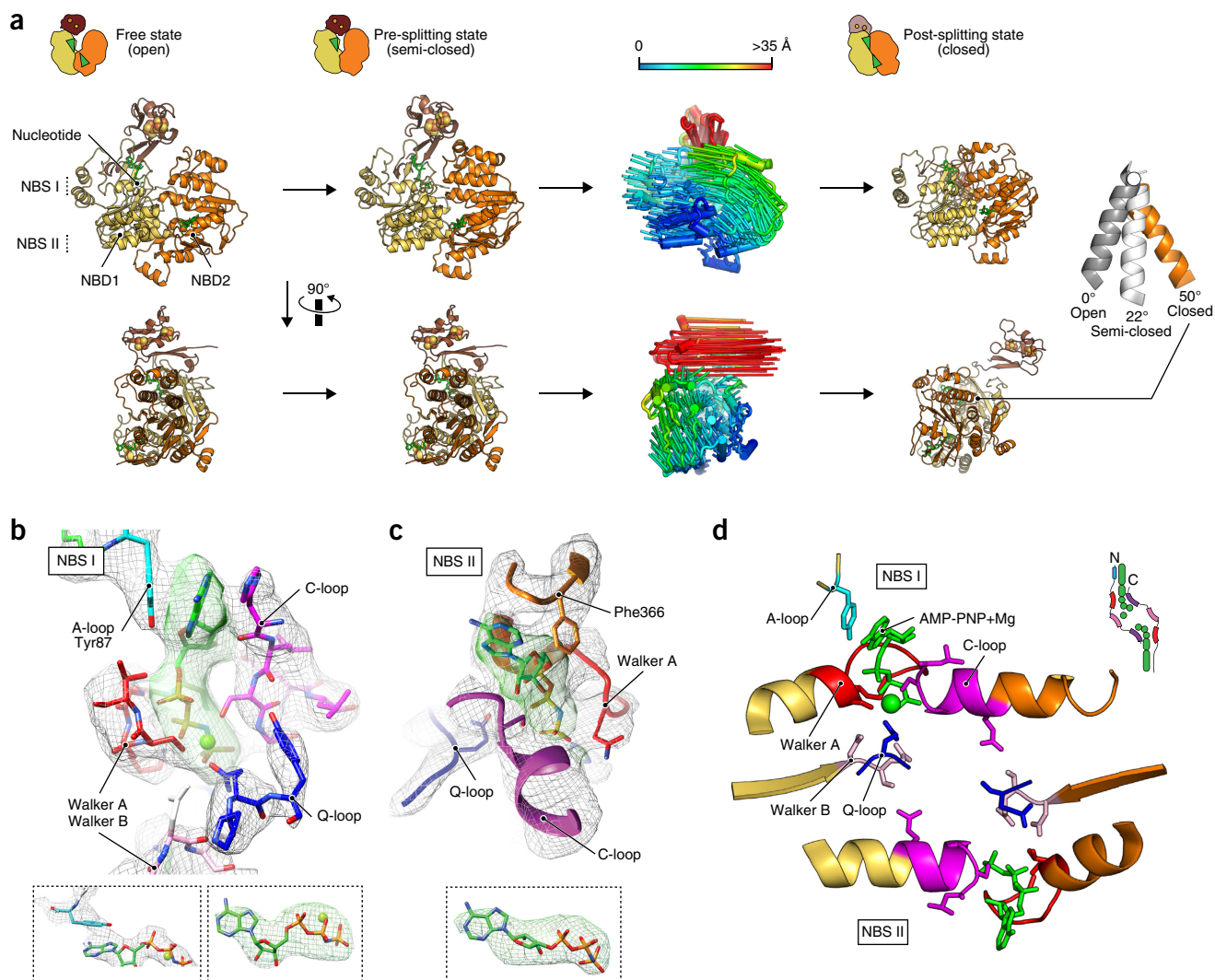


Figure 2 Conformational transition of NBSs of ABCE1 from pre-splitting to post-splitting state. **(a)** Free state of ABCE1 (PDB 3BK7; ref. 10); intermediate, semi-closed pre-splitting state bound to 80S ribosomes (PDB 4CRM; ref. 12); and 40S-bound fully closed post-splitting state, with nucleotides shown in green. Conformational transitions from 80S ribosome-bound pre-splitting state to 40S subunit-bound post-splitting state are represented by vectors displayed as rods. Length and color of the rods denote the r.m.s. deviation distance between the two C_α atoms as indicated in the scale bar above (superimposed on the 40S subunit). NBD closing is exemplified by a helix in NBD2 (residue 500–516 in yeast ABCE1), with rotation angles of 0°, 22°, and 50° for open, semi-closed, and closed states, respectively. Models were superimposed onto NBD1, and the pivot point is indicated by a white circle. **(b,c)** Isolated densities with models of NBS I **(b)** and NBS II **(c)** with AMP-PNP occluded by Walker A and Walker B motifs, C-, and Q-loops. Side chains not visible in the map are colored white for NBS I or omitted for NBS II. Isolated densities of the AMP-PNP and the π-π stacking of Tyr87 (A-loop of NBS I) with the adenosine base are shown in the boxes below. For NBS I, densities are low-pass filtered to 3.9 Å and displayed at 6 σ. For NBS II, maps are low-pass filtered at 4.5 Å and displayed at 4.5 σ. **(d)** Model and schematic representation (inlet) of both NBSs occluding two AMP-PNP (green) in the post-splitting state. In all panels, the conserved motifs of ABC-ATPases are colored as follows: Walker A, red; Walker B, light pink; C-loop, magenta; Q-loop, blue. Tyr87 in the A-loop of NBS I (cyan) forms a π-π stacking with the base of the nucleotide. Notably, no A-loop motif is present in NBS II.

The physiological relevance is underlined by the partial or complete loss of anti-association activity of ABCE1 *in vitro* that confirms a stabilizing role of the three proposed interaction residues. In addition, a lethal phenotype is observed for the double substitution of Arg7 and Tyr301 to alanine. Moreover, enrichment of interaction variants (Arg7, Pro30, and Tyr301) of ABCE1 on 80S ribosomes points toward an impaired splitting activity that may be explained by a lack of stabilization in the post-splitting state or by a compromised conformational freedom of the FeS cluster domain. Similarly, enriched 80S ribosomal fractions were observed upon impairment of ABCE1 activity or translational stalling *in vivo*^{20–22,35}, strongly indicating that these ABCE1 interaction variants are defective in ribosome splitting and accumulate as 80S–ABCE1 pre-splitting complexes.

The native 40S–ABCE1 post-splitting complex

To complement our observations, we decided to use affinity-tagged ABCE1 to purify native ABCE1-containing 40S complexes from yeast cells cultivated in logarithmic growth phase. In the presence of AMP-PNP we isolated complexes that, in addition to ABCE1, also contained initiation factors eIF1A and eIF2 and subunits of eIF3 as identified by MS (**Supplementary Fig. 7a,b**). Cryo-EM analysis showed that 63% of the particles contained ABCE1 in a conformation indistinguishable from that observed in the sample reconstituted *in vitro* (**Supplementary Fig. 7c,d**). Moreover, we identified several three-dimensional subclasses with characteristic density for the initiator tRNA (tRNA_i) in the P-site and one class with additional density for eIF1A in the A-site

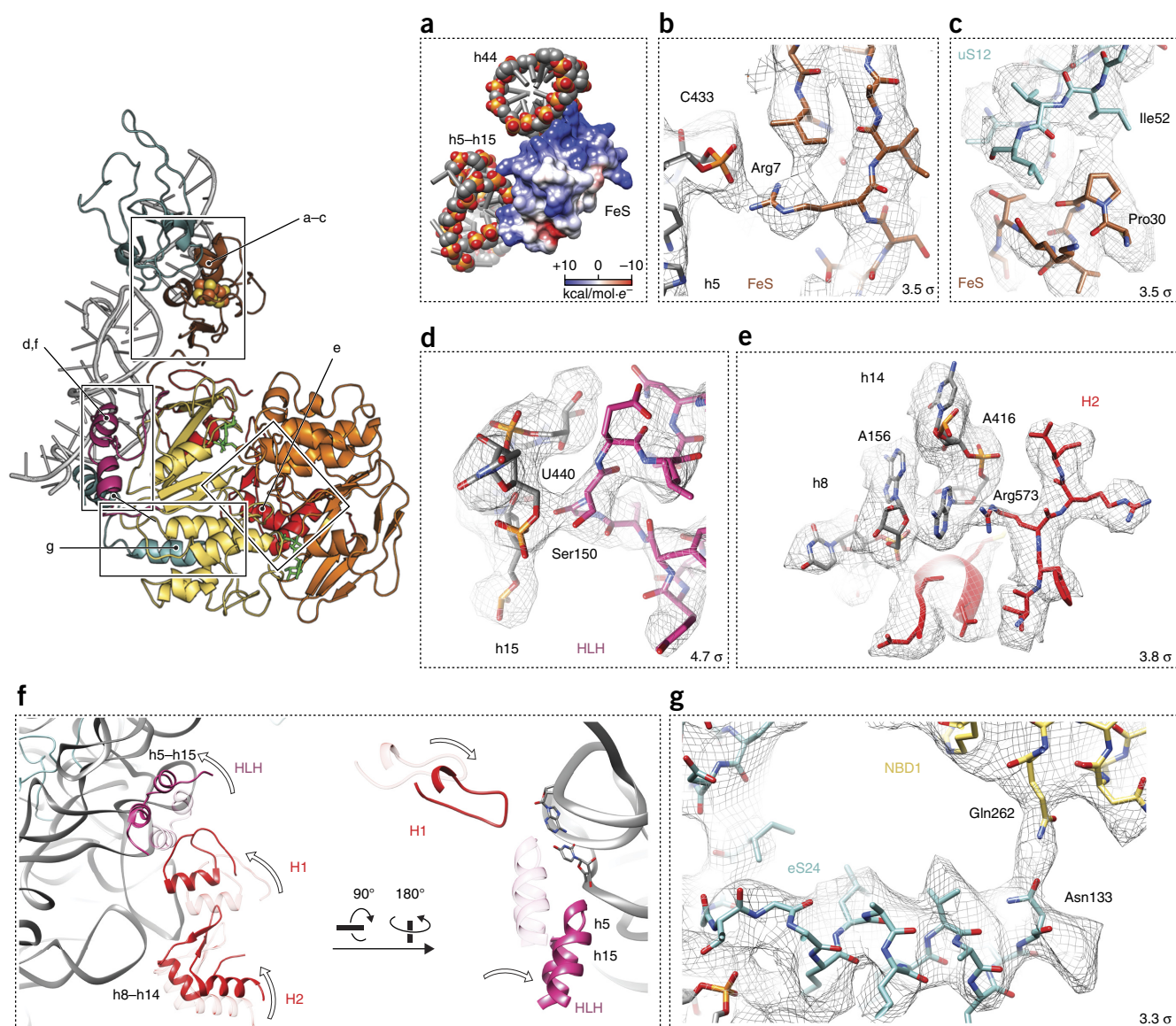


Figure 3 Interactions between the 40S subunit and ABCE1 in the post-splitting state. (a) Electrostatic surface potential of the FeS cluster domain (blue, positive; red, negative) bound to the 40S subunit, positive charges face toward the phosphate backbone of the rRNA (h44 and h5-h15). (b) Zoom on the cantilever β -sheet displaying the contact of Arg7 (brown) to the phosphate backbone of h5. The density map is shown as gray mesh at the 3.5 σ level. (c) Zoom on the interaction between the Pro30 (FeS cluster domain) and Ile52 of uS12. Density is shown as mesh at 3.5 σ . (d) Close-up view on the HLH motif contacting the backbone of U440 in h15 (mesh; 4.7 σ). (e) Zoom on hinge 2 interactions with the h8-h14 junction (formed by A156 and A416). Density is shown as mesh at 3.8 σ . Arg573 likely stacks to A416 via a cation- π interaction. A second interaction is observed between the loop (Asp587 and Ser588) preceding the terminal helix of hinge 2 (shown in ribbon) and the backbone of A156. (f) Rearrangements in the HLH, hinge 1, and hinge 2 motifs and their interactions with h5-h15 and h8-h14. ABCE1 in the pre-splitting state is superimposed in transparent on the post-splitting model. All other parts of ABCE1 are omitted for clarity. (g) Model for the C-terminal helix of eS24 in the post-splitting state (cyan) contacting NBD1 (density shown as mesh at 3.3 σ). The density was low-pass filtered at 3.9 Å for all snapshots.

(Supplementary Fig. 7d-f). We did not observe any clear density for eIF2 or eIF3, which apparently dissociate under the chosen freezing conditions. Difference maps between the *in vitro* reconstituted and the native 40S-ABCE1 complexes not only confirmed the presence of eIF1A and tRNA_i, but also demonstrated an identical conformation of ABCE1 in the native and the *in vitro* reconstituted complexes. Thus, the EM reconstructions of the native 40S-ABCE1 complexes corroborate the reconstructions of the reconstituted complex. Moreover, the presence of initiation factors in native 40S-ABCE1 complexes support the idea of a principal role of ABCE1 in the formation of initiation complexes.

DISCUSSION

The FeS cluster domain is an ancient prosthetic group involved in various cellular processes³⁶. In this work we describe the FeS cluster domain of ABCE1 as a mechanical device for dissociation of ribosomal subunits. Despite an extreme displacement from the pre- to the post-splitting state, the structure of the FeS cluster domain of ABCE1 remains essentially unchanged (r.m.s. deviation 0.87 Å). Hence, the FeS cluster domain serves as a compact and very rigid entity. To examine how the transition from the pre- to the post-splitting state may result in subunit dissociation, we examined the potential transition

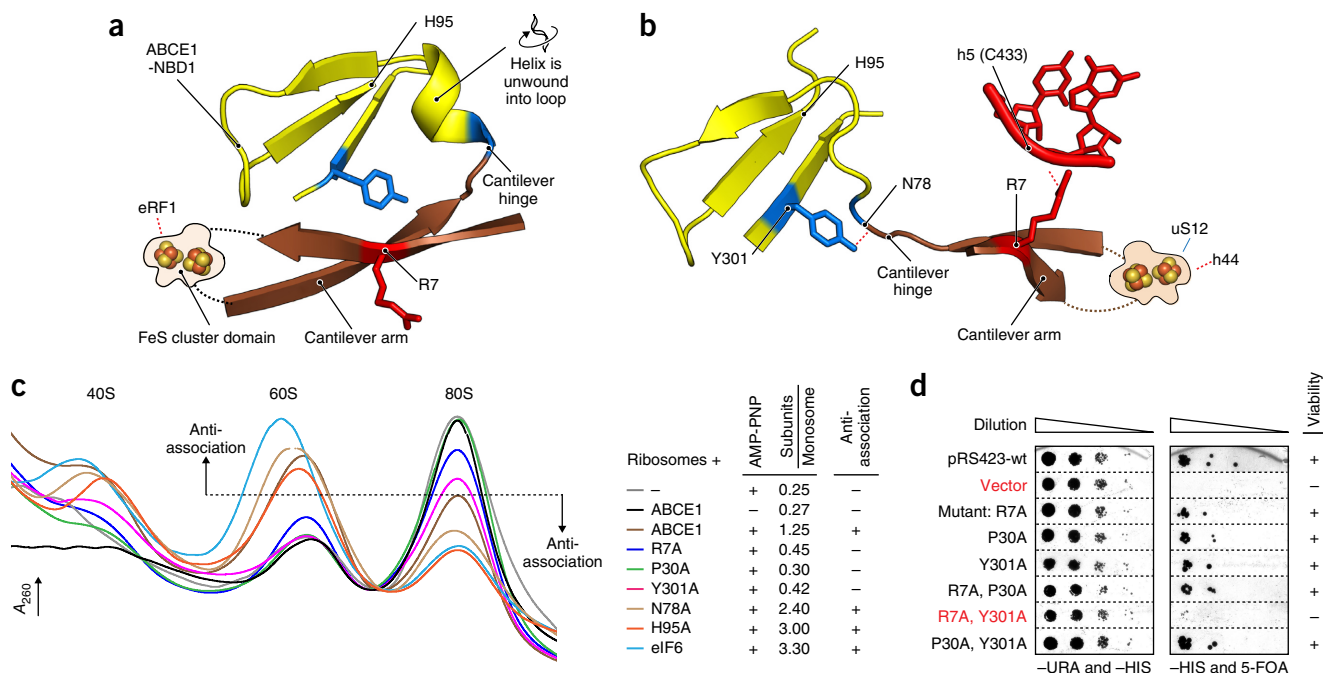


Figure 4 NBD1 stabilizes FeS cluster domain in post-splitting state by an essential cantilever arm interaction. (a) In the pre-splitting state, the cantilever hinge forms an α -helix, which is unwound in the post-splitting state in b. (b) Upon splitting, the FeS cluster domain rotates by 150° . In the post-splitting state, the FeS cluster domain is stabilized mainly by two interactions of the cantilever arm (brown): the backbone of Asn78 interacts with Tyr301 (blue) of NBD1 (yellow) and Arg7 with the rRNA backbone of C433 at h5 (red). (c) Ribosome profiles recorded after the facilitated splitting reaction. ABCE1 mutants of Arg7, Pro30, and Tyr301 are defective in anti-association of 80S ribosomes in the facilitated splitting assay. Wild-type ABCE1, alanine substitutions of His95 and Asn78, and eIF6 show a strong anti-association effect. An increase of 40S and 60S subunit populations indicates an anti-association effect. Representative profiles of two independent experiments are shown. (d) Combined alanine substitutions of Arg7 and Tyr301 are lethal after plasmid shuffling in yeast strains, whose survival relies only on mutated ABCE1. Colony growth data shown are representative of two independent experiments.

trajectory of the FeS cluster domain from pre- to post-splitting state. Based on our findings, ribosome splitting can be divided into two phases (corresponding to the two arrows in Fig. 5). In the first phase, the FeS cluster domain is in contact with the C-terminal domain of eRF1 or Pelota, located in the A-site^{11–13}, and pushes these factors into the intersubunit space upon closure of the two NBDs. The A-site factors, eRF1 or Pelota, likely act as a ‘molecular wedge’ and destabilize intersubunit bridges. In agreement with this idea, the presence of an A-site factor was shown to be essential for splitting activity of ABCE1 (refs. 14–18). In the second phase, once the A-site factor and the 60S subunit are unlocked, the FeS cluster domain can complete its transition by fully rotating into its new interaction site on the 40S subunit (Supplementary Video 2)³⁰. In this position, ABCE1 is stabilized by new contacts to the 40S subunit, preventing 60S reassociation through steric hindrance. The intersubunit bridge B5, which is formed in 80S ribosomes between the 60S protein uL14 and the 40S rRNA helix h44, would clash with the FeS cluster domain, thus explaining the observed anti-association property of ABCE1 (Fig. 5 and 6).

In conclusion, we propose a model for ribosome recycling based on our near-atomic structure of the post-splitting complex (Fig. 6). The recycling process is initiated by recognition of ribosomal pre-termination complexes or stalled ribosomes by eRF1–eRF3 or Pelota–Hbs1, respectively, followed by dissociation of the GTPase factor, eRF3 or Hbs1, and binding of ABCE1. ATP binding to the pre-splitting complex and closure of the NBDs push the FeS cluster domain toward the A-site factors eRF1 or Pelota, which are in turn forced into the intersubunit space. After splitting, reassociation of the 60S and 40S subunits is prevented by the translocated FeS cluster

domain now clashing with uL14 of the 60S subunit. ABCE1 remains transiently bound to the 40S subunit, a state that can be trapped *in vitro* and *in vivo* using AMP-PNP.

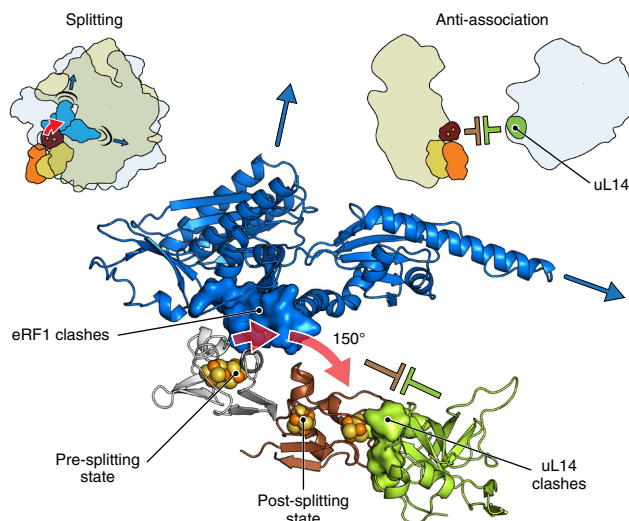


Figure 5 FeS cluster domain rotation and implications for ribosome splitting. The trajectory of the FeS cluster domain rotation leads to a clash into the C-terminal domain of the A-site factor eRF1 (blue; PDB 3JAH)¹³ or Pelota, which is pushed into the intersubunit space. In the post-splitting state, the FeS cluster domain occupies a position that prevents rejoining of the 60S subunit by steric hindrance with uL14 (green; PDB 3JAH)¹³. Clashing residues are shown as surface.

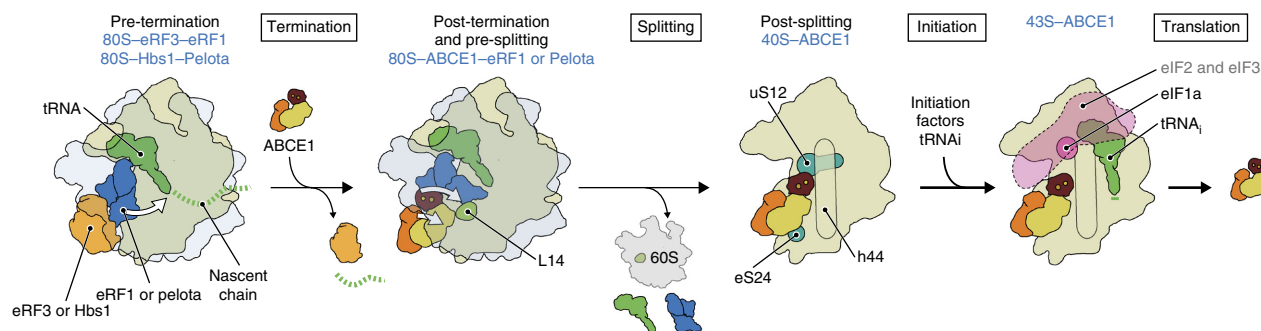


Figure 6 Model of ribosome recycling. After recognition of a terminating or stalled ribosome by eRF1 and eRF3, or Pelota and Hbs1, and dissociation of the GTPases eRF3 or Hbs1, ABCE1 binds to these A-site factor-containing complexes in an intermediate, semi-closed conformation. Splitting may be promoted in two steps. First, closure of the NBDs drives the FeS cluster domain toward the A-site factor. This leads to an immediate force exerted on eRF1 or Pelota, acting as a wedge to destabilize the intersubunit bridges. Second, once the 40S subunit is idle, reassociation of the 60S subunit is blocked, since the FeS cluster domain adopts a position that prevents formation of intersubunit bridge B5 between uL14 and h44 of the 18S rRNA. ABCE1 is also likely to be a transient component of the 43S pre-initiation complex (containing eIF1a, eIF2, eIF3, and initiator tRNA). However, the exact role of ABCE1 in these complexes is still elusive.

This mechanistic model is in agreement with our *in vitro* and *in vivo* analysis of ABCE1 mutants (Fig. 4c,d and Supplementary Fig. 6), in which substitutions of key interacting residues of the FeS cluster domain impair the formation of a post-splitting complex. Strikingly, in *Drosophila*, mutation of a conserved proline corresponding to Pro30 in our study is lethal at the larval stage. Our structure suggests that this substitution weakens the interaction of the FeS cluster domain to uS12. In addition, substitutions in hinge 1 and the HLH motif of *Drosophila* ABCE1 result in reduced wing size³⁷, an effect presumably resulting from impaired 40S subunit interaction. This underlines the importance of the post-splitting state in cellular homeostasis, embryogenesis, and morphogenesis.

The structure of the 40S-ABCE1 post-splitting complex provides the first example of an asymmetric twin-ABC-type ATPase system in a fully closed, nucleotide-occluded state. Nevertheless, the question remains how termination, recycling, and initiation are connected via the ATPase cycle of the two asymmetric NBDs of ABCE1 (ref. 18). On the basis of existing biochemical data and structures of ABCE1 in free, pre-splitting, and post-splitting states, we can derive the following working model on the nucleotide hydrolysis cycle. Free ABCE1 has low intrinsic ATPase and GTPase activity^{14,15,18}, which is strongly stimulated by ATP occlusion in NBS II¹⁸ and binds to pre-termination complexes containing eRF1, Dom34, or Pelota^{14,15}. In agreement with the working model for other ABC systems^{1,3,4}, closure of NBDs by ATP occlusion leads to a ‘power stroke’, which is required for ribosome splitting in the case of ABCE1. In fact, our structures show that this closed state must exist during the process of ribosome splitting (Fig. 5).

After binding to pre-termination complexes, ABCE1 must adopt the closed state occluding two NTP moieties to initiate ribosome splitting. We speculate that NTP hydrolysis in NBS I might drive ribosome splitting because it is in direct contact with the FeS cluster domain and its ATPase is hyperstimulated upon ATP occlusion in NBS II. Similar to other disassembly machines^{38,39}, ribosome splitting may be dependent on multiple rounds of NTP binding, occlusion, and hydrolysis. It is likely that, in the post-splitting structure, we trapped a late 40S-bound intermediate of the splitting process, in which both NBDs are occluded by nucleotides, suggesting that a final ATP hydrolysis event will release ABCE1 from 40S subunits. Indeed, we observe a slight ATPase stimulation of ABCE1 upon addition of 40S subunits, supporting our hypothesis. However, future experiments will need to elaborate the exact order and timing of

ATP binding, occlusion, and hydrolysis events during the ribosome splitting and further downstream processes.

We suggest that ABCE1 might also play a role in translation initiation due to its presence in 43S initiation complexes together with canonical initiation factors (Fig. 6). The structure of native post-splitting complexes obtained after co-purification of translation initiation factors using tagged ABCE1 suggests that a transient ABCE1-containing pre-initiation complex exists in cells. Notably, a comparison of our 40S-ABCE1 post-splitting complex to structures of 48S initiation complexes implies that ABCE1 is in proximity to the peripheral domains of eIF3 in the intersubunit space⁴⁰. Thus, our structure provides a plausible architectural scenario for a role of ABCE1 during 43S or 48S initiation-complex assembly, linking ribosome recycling and translation initiation. However, the exact role of ABCE1 in translation initiation will require further investigation.

METHODS

Methods, including statements of data availability and any associated accession codes and references, are available in the [online version of the paper](#).

Note: Any Supplementary Information and Source Data files are available in the online version of the paper.

ACKNOWLEDGMENTS

The authors thank K. Kiosze-Becker, E. Nürenberg-Goloub, B. Hetzert, C. Le Gal and C. Thomas for helpful suggestions on the manuscript and C. Ungewickell, S. Lange and S. Lamberth for technical assistance. This work was supported by the German Research Council (grants SFB 902 to R.T., SFB 646 to R.B. and T.B., FOR 1805 to R.B., GRK 1721 to R.B.). R.B. acknowledges support by the Center for Integrated Protein Science Munich (CIPS-M) and the European Research Council (Advanced Grants CRYOTRANSLATION). The Cluster of Excellence-Macromolecular Complexes (EXC 115 to R.T.) supported the work. M.G. and C.S. were supported by Boehringer Ingelheim Fonds PhD fellowships. We thank the Leibniz-Rechenzentrum Munich (LRZ) for providing computational services and support.

AUTHOR CONTRIBUTIONS

M.G., A.H., T.B., R.B. and R.T. designed the study. M.G. developed the preparation of the post-splitting complex and performed all functional assays. M.G. and P.K. conducted the plasmid shuffling experiment. M.G. and S.T. designed the NTPase assays. M.G. and A.H. prepared the EM samples. A.P. and A.H. prepared the initiation complex. A.H. and O.B. collected and A.H. processed the cryo-EM data. C.S., A.H. and T.B. built and refined the model. C.S., T.B., A.H. and M.G. analyzed and interpreted the structures. M.G., T.B., A.H., S.T., R.B. and R.T. wrote the manuscript. R.T. initiated and R.B. and R.T. conceived the project.

COMPETING FINANCIAL INTERESTS

The authors declare no competing financial interests.

Reprints and permissions information is available online at <http://www.nature.com/reprints/index.html>.

- Schmitt, L. & Tampé, R. Structure and mechanism of ABC transporters. *Curr. Opin. Struct. Biol.* **12**, 754–760 (2002).
- Dean, M. & Annilo, T. Evolution of the ATP-binding cassette (ABC) transporter superfamily in vertebrates. *Annu. Rev. Genomics Hum. Genet.* **6**, 123–142 (2005).
- Rees, D.C., Johnson, E. & Lewinson, O. ABC transporters: the power to change. *Nat. Rev. Mol. Cell Biol.* **10**, 218–227 (2009).
- Hopfner, K.P. Invited review: architectures and mechanisms of ATP binding cassette proteins. *Biopolymers* **105**, 492–504 (2016).
- Jackson, R.J., Hellen, C.U. & Pestova, T.V. Termination and post-termination events in eukaryotic translation. *Adv. Protein Chem. Struct. Biol.* **86**, 45–93 (2012).
- Franckenberg, S., Becker, T. & Beckmann, R. Structural view on recycling of archaeal and eukaryotic ribosomes after canonical termination and ribosome rescue. *Curr. Opin. Struct. Biol.* **22**, 786–796 (2012).
- Nürenberg, E. & Tampé, R. Tying up loose ends: ribosome recycling in eukaryotes and archaea. *Trends Biochem. Sci.* **38**, 64–74 (2013).
- Shoemaker, C.J. & Green, R. Translation drives mRNA quality control. *Nat. Struct. Mol. Biol.* **19**, 594–601 (2012).
- Barthelme, D. *et al.* Structural organization of essential iron-sulfur clusters in the evolutionarily highly conserved ATP-binding cassette protein ABCE1. *J. Biol. Chem.* **282**, 14598–14607 (2007).
- Karcher, A., Schele, A. & Hopfner, K.P. X-ray structure of the complete ABC enzyme ABCE1 from *Pyrococcus abyssi*. *J. Biol. Chem.* **283**, 7962–7971 (2008).
- Becker, T. *et al.* Structural basis of highly conserved ribosome recycling in eukaryotes and archaea. *Nature* **482**, 501–506 (2012).
- Preis, A. *et al.* Cryoelectron microscopic structures of eukaryotic translation termination complexes containing eRF1-eRF3 or eRF1-ABCE1. *Cell Rep.* **8**, 59–65 (2014).
- Brown, A., Shao, S., Murray, J., Hegde, R.S. & Ramakrishnan, V. Structural basis for stop codon recognition in eukaryotes. *Nature* **524**, 493–496 (2015).
- Pisarev, A.V. *et al.* The role of ABCE1 in eukaryotic posttermination ribosomal recycling. *Mol. Cell* **37**, 196–210 (2010).
- Shoemaker, C.J. & Green, R. Kinetic analysis reveals the ordered coupling of translation termination and ribosome recycling in yeast. *Proc. Natl. Acad. Sci. USA* **108**, E1392–E1398 (2011).
- Pisareva, V.P., Skabkin, M.A., Hellen, C.U., Pestova, T.V. & Pisarev, A.V. Dissociation by Pelota, Hbs1 and ABCE1 of mammalian vacant 80S ribosomes and stalled elongation complexes. *EMBO J.* **30**, 1804–1817 (2011).
- van den Elzen, A.M., Schuller, A., Green, R. & Séraphin, B. Dom34-Hbs1 mediated dissociation of inactive 80S ribosomes promotes restart of translation after stress. *EMBO J.* **33**, 265–276 (2014).
- Barthelme, D. *et al.* Ribosome recycling depends on a mechanistic link between the FeS cluster domain and a conformational switch of the twin-ATPase ABCE1. *Proc. Natl. Acad. Sci. USA* **108**, 3228–3233 (2011).
- Guydosh, N.R. & Green, R. Dom34 rescues ribosomes in 3' untranslated regions. *Cell* **156**, 950–962 (2014).
- Young, D.J., Guydosh, N.R., Zhang, F., Hinnebusch, A.G. & Green, R. Rli1/ABCE1 recycles terminating ribosomes and controls translation reinitiation in 3'UTRs *in vivo*. *Cell* **162**, 872–884 (2015).
- Dong, J. *et al.* The essential ATP-binding cassette protein RLI1 functions in translation by promoting preinitiation complex assembly. *J. Biol. Chem.* **279**, 42157–42168 (2004).
- Andersen, D.S. & Leevers, S.J. The essential *Drosophila* ATP-binding cassette domain protein, pixie, binds the 40 S ribosome in an ATP-dependent manner and is required for translation initiation. *J. Biol. Chem.* **282**, 14752–14760 (2007).
- Skabkin, M.A., Skabkina, O.V., Hellen, C.U. & Pestova, T.V. Reinitiation and other unconventional posttermination events during eukaryotic translation. *Mol. Cell* **51**, 249–264 (2013).
- Hinnebusch, A.G. eIF3: a versatile scaffold for translation initiation complexes. *Trends Biochem. Sci.* **31**, 553–562 (2006).
- Fernández, I.S. *et al.* Molecular architecture of a eukaryotic translational initiation complex. *Science* **342**, 1240585 (2013).
- Behrmann, E. *et al.* Structural snapshots of actively translating human ribosomes. *Cell* **161**, 845–857 (2015).
- Taylor, D.J. *et al.* Structures of modified eEF2 80S ribosome complexes reveal the role of GTP hydrolysis in translocation. *EMBO J.* **26**, 2421–2431 (2007).
- Spahn, C.M. *et al.* Domain movements of elongation factor eEF2 and the eukaryotic 80S ribosome facilitate tRNA translocation. *EMBO J.* **23**, 1008–1019 (2004).
- Becker, T. *et al.* Structure of the no-go mRNA decay complex Dom34-Hbs1 bound to a stalled 80S ribosome. *Nat. Struct. Mol. Biol.* **18**, 715–720 (2011).
- Kiosze-Becker, K. *et al.* Structure of the ribosome post-recycling complex probed by chemical cross-linking and mass spectrometry. *Nat. Commun.* **7**, 13248 (2016).
- Oldham, M.L. & Chen, J. Snapshots of the maltose transporter during ATP hydrolysis. *Proc. Natl. Acad. Sci. USA* **108**, 15152–15156 (2011).
- Korkhov, V.M., Mireku, S.A., Veprintsev, D.B. & Locher, K.P. Structure of AMP-PNP-bound BtuCD and mechanism of ATP-powered vitamin B12 transport by BtuCD-F. *Nat. Struct. Mol. Biol.* **21**, 1097–1099 (2014).
- Villa, E. *et al.* Ribosome-induced changes in elongation factor Tu conformation control GTP hydrolysis. *Proc. Natl. Acad. Sci. USA* **106**, 1063–1068 (2009).
- Groft, C.M., Beckmann, R., Sali, A. & Burley, S.K. Crystal structures of ribosome anti-association factor IF6. *Nat. Struct. Mol. Biol.* **7**, 1156–1164 (2000).
- Tsuboi, T. *et al.* Dom34-hbs1 plays a general role in quality-control systems by dissociation of a stalled ribosome at the 3' end of aberrant mRNA. *Mol. Cell* **46**, 518–529 (2012).
- Lill, R. Function and biogenesis of iron-sulphur proteins. *Nature* **460**, 831–838 (2009).
- Coelho, C.M. *et al.* Growth and cell survival are unevenly impaired in pixie mutant wing discs. *Development* **132**, 5411–5424 (2005).
- Sauer, R.T. *et al.* Sculpting the proteome with AAA(+) proteases and disassembly machines. *Cell* **119**, 9–18 (2004).
- Monroe, N. & Hill, C.P. Meiotic clade AAA ATPases: protein polymer disassembly machines. *J. Mol. Biol.* **428**, 1897–1911 (2016).
- Llácer, J.L. *et al.* Conformational differences between open and closed states of the eukaryotic translation initiation complex. *Mol. Cell* **59**, 399–412 (2015).

ONLINE METHODS

Strains and plasmids. We used the *S. cerevisiae* BY4741 strain (*MATa his3Δ1 leu2Δ0 met15Δ0 ura3Δ0*) for 80S ribosome preparation. C-terminally His₆-tagged ABCE1 (ABCE1_{-H6}) was expressed in the INVSc1 strain (*MATa/MATα his3Δ1/his3Δ1 leu2/leu2 trp1-289/trp-289 ura3-52/ura3-52*, Invitrogen), which was transformed with the pYes2-ABCE1_{-H6} plasmid (kindly provided by R. Green, Department of Molecular Biology and Genetics, Johns Hopkins University School of Medicine)¹⁵. For plasmid shuffling the diploid strain CEN.PK744 (*MATa/MATα his3Δ1/his3Δ1 leu2-3,112/leu2-3,112 trp1-289/trp1-289 MAL2-8^C/MAL2-8^CSUC2/SUC2 ura3-52/ura3-52 RLI1/rli1::KanMX4*) was transformed with pRS426-ABCE1 [*URA3*] and selected on SCD –*URA*. After tetrad dissection, the haploid yeast strain CEN.MG1-9B (*MATa his3Δ1 leu2-3,112 trp1-289 MAL2-8^CSUC2 ura3-52 rli1::KanMX4 + pRS426-ABCE1*) was isolated where the essential *ABCE1* gene (*RLI1*) was deleted by *KanMX4* and substituted by pRS426-ABCE1 expressing wild-type (wt) *ABCE1* under the control of the endogenous promoter. Plasmids pRS423-ABCE1 [*HIS3*] and pRS426-ABCE1 [*URA*] were cloned by amplification of *ABCE1* gene with primers in the promoter and terminator region and integrated into the vector via restriction sites *Sall* and *SmaI* (5'-GGGCGA ATTGGGTACCGGGCCCCCTCGAGGTGCGACGGTATCGATAAGCTTG CCGCGGCTCCCGCAGAATCTAATCATTAAGCTTGACTAG-3', 5'-GCT CCACCGCG GTGGCGCGCTCTAGAACTAGTGGATCCCCGGGC TGCTAAACTGGAGTACGGATCACCGAAGAGGAGG-3'). For tandem affinity purification of 40S–ABCE1 complexes, the TAP-tagged ABCE1 yeast strain was used (SC1900, *MATa leu2-3, 112 trp1-289 ade2 arg4 ura3-52 rli1::TAP-KIURA3, EUROSCARF*).

Ribosome preparation. The *S. cerevisiae* BY4741 strain was grown in YPD media to an OD₆₀₀ of 1.2, harvested, and resuspended in lysis buffer (20 mM HEPES-KOH, pH 7.5, 500 mM KCl, 25 mM MgCl₂, 4 mM β-mercaptoethanol (2-ME)). Cells were lysed by disruption (Cell Disrupter, Constant Systems Ltd) at 1.5-MPa pressure, cleared at 20,000 × g for 10 min, and loaded on a 10–50% sucrose density gradient in lysis buffer and centrifuged using a SW41 rotor (Beckman Coulter) at 200,000 × g for 4 h. 80S fractions were collected and pelleted using the TLA110 rotor (Beckman Coulter) at 417,000 × g for 2 h. Ribosome pellets were resuspended in storage buffer (50 mM Tris-OAc, pH 7.0, 50 mM NH₄Cl, 5 mM Mg(OAc)₂, 2 mM spermidine, 25% (v/v) glycerol, 5 mM 2-ME) and frozen in liquid nitrogen. 40S subunits were prepared by standard techniques using puromycin treatment⁴¹.

Facilitated splitting assay and reconstitution of the post-splitting complex. The assay was developed based on the anti/reassociation assay to test binding of the anti-association factor eIF6 to large ribosomal 60S subunits³⁴. ABCE1 and mutants R7A, P30A, N78A, H95A, and Y301A were expressed in INVSc1 yeast cells and purified as described with minor modifications¹⁵. 80S ribosomes were mixed with ten molar excess of ABCE1 and 0.5 mM AMP-PNP in splitting facilitating buffer (20 mM HEPES-KOH, pH 7.4, 515 mM KCl, 2 mM MgCl₂, 1 mM dithiothreitol (DTT)), and incubated for 20 min at 25 °C. The sample was diluted 1:0.7 with reassociation buffer (20 mM HEPES-KOH, pH 7.4, 100 mM KCl, 25 mM MgCl₂, 1 mM DTT) and incubated for 20 min at 25 °C, cooled down to 4 °C, loaded onto 10–30% sucrose density gradient in grid buffer (20 mM HEPES-KOH, pH 7.4, 100 mM KOAc, 5 mM MgCl₂, 2 mM DTT) and centrifuged at 200,000 × g for 4 h in a SW41 rotor (Beckman Coulter). In the case of sample preparation for cryo-EM, 1 mM MgCl₂ and 500 mM KCl were used in splitting facilitating buffer, sample was loaded onto 10–50% sucrose density gradient and 40S fractions were collected and re-buffered in grid buffer by using PD-10 column (GE Healthcare). The sample was diluted in grid buffer and used for cryo-EM.

Preparation of native post-splitting complexes. Cells were grown in YPD media to an OD₆₀₀ of 1.5. The cells were spun down and washed with 1% KCl at 4 °C then incubated for 15 min at 25 °C in 10 mM DTT, 100 mM Tris pH 8.0, and finally resuspended in lysis buffer (50 mM Tris-OAc, pH 7.5, 15 mM Mg(OAc)₂, 50 mM KOAc, 1 mM DTT, 300 nM AMP-PNP, 300 nM GMP-PNP, 500 nM PMSE, 1 pill cComplete EDTA-free Protease Inhibitor Cocktail per 50 ml buffer). The cell suspension was processed in a cell disruptor at 1.5 MPa and the lysate was spun in a SS-34 rotor (ThermoFisher) at 27,000 × g for 15 min to remove cell debris. The lysate was clarified in a Type 45 Ti rotor (Beckman Coulter) for 20 min at 119,000 × g. The cleared lysate was incubated with IgG Sepharose 6 FastFlow

beads (GE Healthcare) for 1 h at 4 °C. The beads were washed with TAP buffer (50 mM Tris-OAc, pH 7.5, 15 mM Mg(OAc)₂, 50 mM KOAc, 1 mM DTT, 500 nM PMSE, 1 pill cComplete EDTA-free Protease Inhibitor Cocktail per 50 ml buffer). For elution, the beads were incubated with AcTEV protease (Invitrogen) in TAP buffer for 90 min at 4 °C. The eluate was loaded onto 5–30% sucrose density gradient in TAP buffer and centrifuged in a SW41 rotor (Beckman Coulter) for 15 h at 56,000 × g. 40S fractions were collected and sucrose was removed using a PD-10 column (GE Healthcare). The sample was then used for cryo-EM.

Plasmid shuffling assay. CEN.MG1-9B strain was transformed with pRS423-ABCE1 [*HIS3*] plasmid (cloned as described for pRS426-ABCE1 and mutated by single-site directed mutagenesis) coding for wt and mutated *ABCE1* and selected on –*URA* and –*HIS* medium. In order to force the strain to survive only in the presence of pRS423-ABCE1, cells were selected on –*HIS* and 5-*FOA*, resulting in a strain in which *ABCE1* (*RLI1*) is deleted, wt plasmid is toxic, and growth of the strain is only dependent on the plasmid expressing mutated *ABCE1*. Growth and survival were checked by growth studies in a serial dilution assay.

Ribosome profile analysis. The CEN.MG1-9B strain was transformed with pRS423-TDH3-ABCE1-HA [*HIS3*] (pUJ2) coding for HA-tagged wt and mutant *ABCE1* under the control of the strong *TDH3* promoter and selected on –*HIS* and –*URA*. Cells were grown to an OD₆₀₀ of 1.5, resuspended in RiboA buffer (20 mM HEPES-KOH, pH 7.4, 100 mM KOAc, 2.5 mM Mg(OAc)₂, 2 mM DTT) and disrupted by glass beads. The lysate was cleared at 20,000 × g for 10 min and adjusted by addition of RiboA buffer to an A₂₆₀ of 10. 300 μl were loaded on a 10–50% sucrose density gradient in RiboA buffer and centrifuged for 14 h at 50,000 × g at 4 °C. The ribosome UV profile was recorded and the gradient was collected in fractions of 600 μl. Fractions were precipitated by addition of 7% (w/v) trichloroacetic acid and 0.02% (w/v) sodium deoxycholate and centrifuged at 15,000 × g for 5 min. Pellets were resuspended in SDS-PAGE loading buffer with additional 750 mM Tris-OAc, pH 8.0 and analyzed by SDS-PAGE and immunoblot against the HA-tag (primary antibody: anti-HA (Abcam, [HA.C5], cat. no. ab18181); secondary antibody: anti-mouse IgG, HRP conjugate (Promega, cat. no. W4021)) of *ABCE1*.

NTPase assay. NTPase activity of *ABCE1* was analyzed by formation of ³²P_i upon hydrolysis of γ-³²P-labeled GTP as previously described^{14,15}. Stimulation was assayed by incubating 0.066 μM *ABCE1*, 0.25 μM Dom34, 0.12 μM 40S or vacant 80S ribosomes, 0.1 mM ATP, 0.1 mM GTP and 0.8 μM [γ-³²P]GTP in 10 μl at 30 °C for 0, 5, 10, 20, and 30 min in NTPase buffer (20 mM Tris-HCl, pH 7.5, 100 mM KCl, 2.5 mM MgCl₂, 0.25 mM spermidine, 2 mM DTT). 1 μl aliquots were spotted on polyethylene imine cellulose thin layer chromatography plates and resolved by 0.8 M LiCl and 0.8 M acetic acid. Release of ³²P_i was monitored by autoradiography.

Electron microscopy and image processing. The reconstituted 40S–*ABCE1* complex was obtained after facilitated splitting as described above with minor modifications. Freshly prepared samples were adjusted to 1.5 A₂₆₀ (50 nM 40S ribosomes) and applied to 2-nm pre-coated Quantifoil R3/3 holey carbon supported grids. Data were collected on a Titan Krios TEM (FEI Company) equipped with a Falcon II direct electron detector at 300 keV under low dose conditions of about 2.4 e⁻/Å² per frame for 10 frames (plus 4 e⁻/Å² pre-exposure) resulting in a dose of 28 e⁻/Å² in total. We used the software EM-TOOLS (TVIPS) and a defocus range of –0.8 to –2.5 μm (underfocus) (Table 1). Magnification settings resulted in a pixel size of 1.084 Å/pixel. Original image stacks were summed and corrected for drift and beam-induced motion at micrograph level using MotionCor2 (ref. 42). The contrast transfer function parameters and resolution range of each micrograph were estimated by GCTF (<http://www.mrc-lmb.cam.ac.uk/kzhang/>).

In the case of the reconstituted 40S–*ABCE1* complex, only micrographs showing a clear signal below 4 Å resolution were used. All 2D and 3D classifications and refinements were performed with RELION-2 (ref. 43) after automated particle picking by Gautomatch (<http://www.mrc-lmb.cam.ac.uk/kzhang/>). 2D reference-free classification was performed to screen for particle quality (Supplementary Fig. 2b); non-ribosomal particles as well as poorly resolved 2D classes were discarded. 518,000 particles from good classes were selected for 3D refinement. Notably, the first 3D reconstructions displayed a distortion in

one direction resulting from preferred orientation of 40S particles on the carbon-coated grid and also misalignment. We performed two subsequent rounds of 3D classification in order to omit poorly aligned and distorted particles and to enrich 40S subunits with ABCE1 bound. First, the whole data set was classified into 4 classes: classes 1 and 2 contained poorly resolved and distorted 40S ribosomes, whereas classes 3 and 4 showed well-resolved 40S ribosomes with a strong ABCE1 density. Classes 3 and 4 were joined (401,000 particles) for a second round of 3D classification. Here, we used a mask for the well-resolved 40S body including ABCE1 and excluded the highly flexible 40S head, which impaired the alignment. Four out of five classes (299,000 particles in total) showed a strong distortion and were discarded. The best resolved class (102,000 particles) showed a well resolved 40S body with stoichiometric occupancy of ABCE1. This final volume was refined to 3.9 Å according to the “gold standard” criterion (FCS = 0.143), corrected for the modulation transfer function of the Falcon 2 detector and sharpened by applying a negative B-factor automatically estimated by RELION-2. Local resolution was calculated from 3.5 to 8.5 Å in steps of 0.5 Å using ResMap⁴⁴.

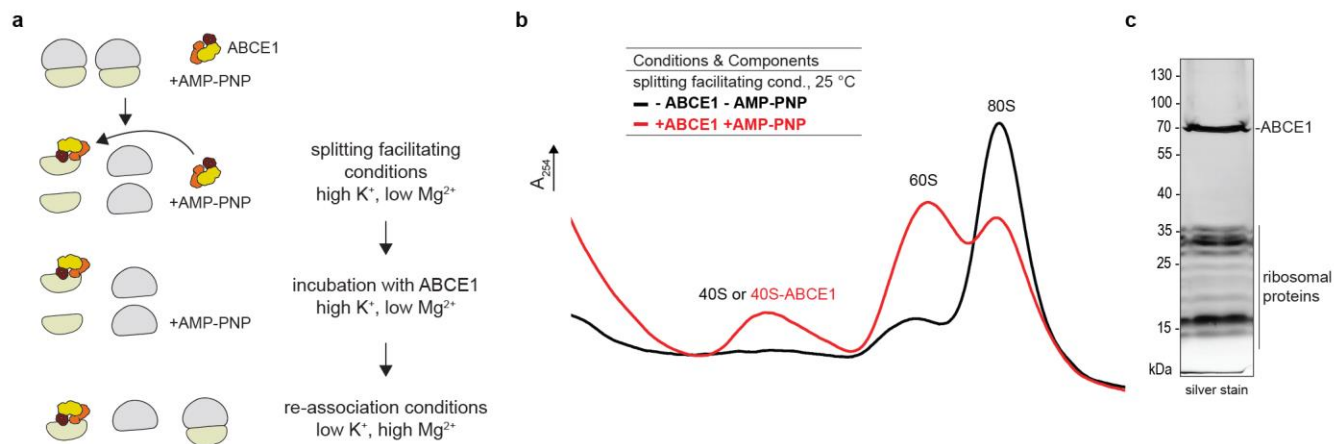
The native 40S–ABCE1 data set was chiefly processed in the same way as the reconstituted sample using MotionCor2, GCTF, Gautomatch and RELION-2. 2D classes displaying non-ribosomal particles as well as the fatty acid synthetase (FAS) were discarded. After 3D refinement of 131,000 particles, 3D classification was performed. In the first round three classes (63.0%, 82,000 particles) showed a clear density for ABCE1 and two of them presented additional extra density emerging from the P-site. These two classes were combined (43.5%, 57,000 particles) and subjected to an additional round of classification. Here, four out of five classes only differ in the appearance of density in the P-site. One class displayed additional density in the position where eIF1A is located. This class (17.6%, 9,500 particles) was refined to a final resolution of 14 Å according to the gold standard criterion (FSC = 0.143).

Model building. For molecular interpretation, we used the crystal structure of the yeast 40S ribosomal subunit (PDB 4V88)⁴⁵ and generated homology models of ABCE1 based on the crystal structures of archaeal ABCE1 and known structures of the closed state of other ABC transporters (MalK³¹, BtuCD³², MJ0796 (ref. 46)). Models were initially fitted into the electron density using UCSF Chimera⁴⁷ and jiggle-fitted using Coot^{48,49}. Because of flexibility (Supplementary Fig. 2b), the local resolution (Supplementary Fig. 3a) of the 40S head was significantly lower compared to the 40S body. Thus, only the model of the 40S body with ABCE1 (40S_{BODY}–ABCE1, see Table 1) was used for subsequent model refinement. First, the 40S_{BODY}–ABCE1 model was subjected to real-space refinement in PHENIX⁵⁰. Afterwards, the model was further subjected to reciprocal space refinement using REFMAC (v5.8)⁵¹ and restraints generated by ProSMART and LIBG as previously shown^{48,52}. To avoid overfitting, refinement weights were carefully estimated as

described⁵³. FSC_{average} was monitored throughout the refinement and the final model was validated using MolProbity⁵⁴. Cross-validation against overfitting was performed as described^{52,53}. Figures were created with the PyMOL Molecular Graphics System (Version 1.7.4, Schrödinger, LLC) and with UCSF Chimera. The ABCE1 model of the post-splitting state could be fit as rigid body into the native 40S–ABCE1 complex without further adjustments. eIF1A (blue) as well as tRNA_i (green) could be identified by rigid body fitting of 43S and 48S initiation complex structures (eIF1A from 4UER, ref. 55; tRNA_i from 3JAP, ref. 40).

Data availability. EM density maps are deposited in the EMDB (reconstituted 40S–ABCE1 complex, EMD-4071; native reconstituted 40S–ABCE1 complex, EMD-3452), and the coordinates or EM-based models are deposited in the Protein Data Bank (post-splitting complex: 5LL6). Primary data are available upon request from the corresponding authors.

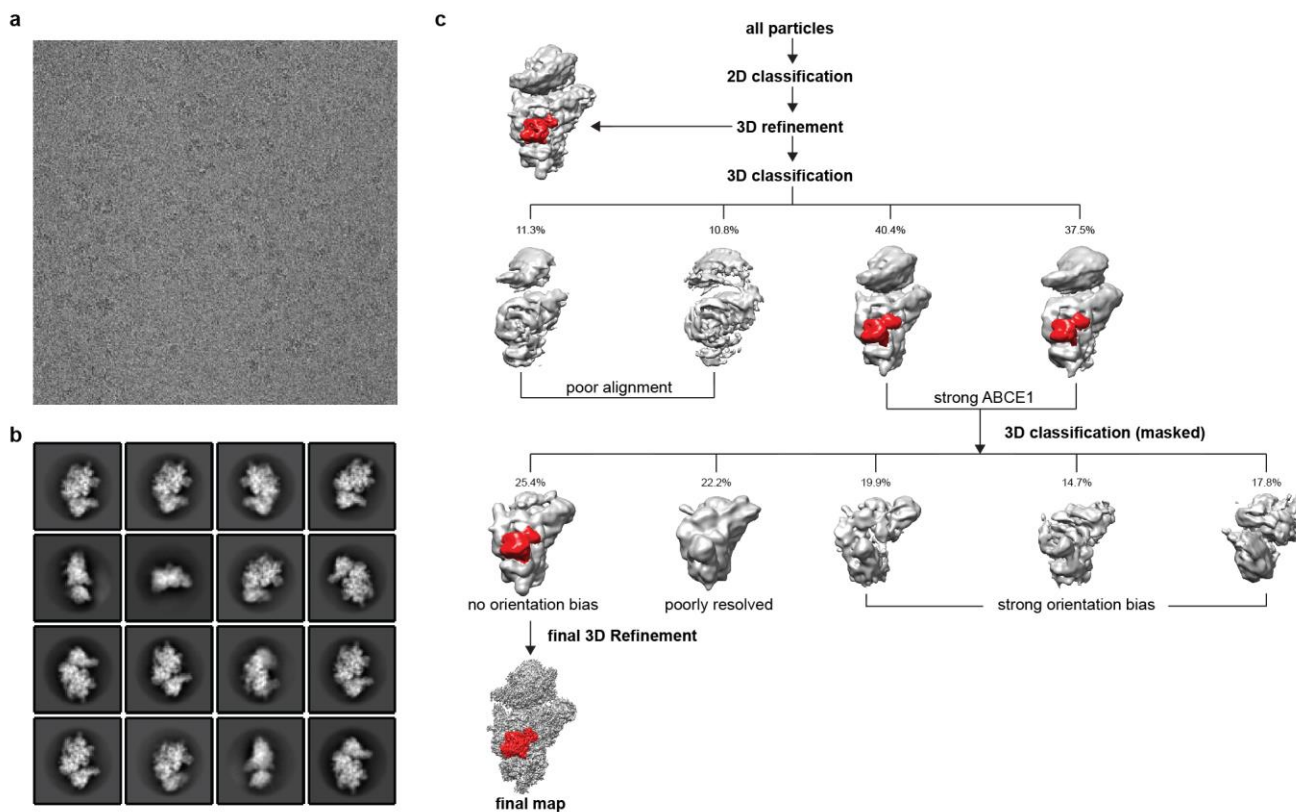
41. Merrick, W.C. & Hensold, J.O. Analysis of eukaryotic translation in purified and semipurified systems. *Curr. Protoc. Cell. Biol.* **8**, 11.19.1–11.19.26 (2001).
42. Zheng, S.Q. *et al.* MotionCor2: anisotropic correction of beam-induced motion for improved cryo-electron microscopy. *Nat. Methods* **14**, 331–332 (2017).
43. Kimanius, D., Forsberg, B.O., Scheres, S.H. & Lindahl, E. Accelerated cryo-EM structure determination with parallelisation using GPUs in RELION-2. *eLife* **5**, e18722 (2016).
44. Kucukelbir, A., Sigworth, F.J. & Tagare, H.D. Quantifying the local resolution of cryo-EM density maps. *Nat. Methods* **11**, 63–65 (2014).
45. Ben-Shem, A. *et al.* The structure of the eukaryotic ribosome at 3.0 Å resolution. *Science* **334**, 1524–1529 (2011).
46. Smith, P.C. *et al.* ATP binding to the motor domain from an ABC transporter drives formation of a nucleotide sandwich dimer. *Mol. Cell* **10**, 139–149 (2002).
47. Pettersen, E.F. *et al.* UCSF Chimera—a visualization system for exploratory research and analysis. *J. Comput. Chem.* **25**, 1605–1612 (2004).
48. Brown, A. *et al.* Tools for macromolecular model building and refinement into electron cryo-microscopy reconstructions. *Acta Crystallogr. D Biol. Crystallogr.* **71**, 136–153 (2015).
49. Emsley, P. & Cowtan, K. Coot: model-building tools for molecular graphics. *Acta Crystallogr. D Biol. Crystallogr.* **60**, 2126–2132 (2004).
50. Adams, P.D. *et al.* PHENIX: a comprehensive Python-based system for macromolecular structure solution. *Acta Crystallogr. D Biol. Crystallogr.* **66**, 213–221 (2010).
51. Murshudov, G.N., Vagin, A.A. & Dodson, E.J. Refinement of macromolecular structures by the maximum-likelihood method. *Acta Crystallogr. D Biol. Crystallogr.* **53**, 240–255 (1997).
52. Amunts, A. *et al.* Structure of the yeast mitochondrial large ribosomal subunit. *Science* **343**, 1485–1489 (2014).
53. Fernández, I.S., Bai, X.C., Murshudov, G., Scheres, S.H. & Ramakrishnan, V. Initiation of translation by cricket paralysis virus IRES requires its translocation in the ribosome. *Cell* **157**, 823–831 (2014).
54. Chen, V.B. *et al.* MolProbity: all-atom structure validation for macromolecular crystallography. *Acta Crystallogr. D Biol. Crystallogr.* **66**, 12–21 (2010).
55. Aylett, C.H.S. *et al.* Structure of a yeast 40S–Eif1–Eif1A–Eif3–Eif3j initiation complex. *Nat. Struct. Mol. Biol.* **22**, 269–271 (2015).



Supplementary Figure 1

Preparation of 40S-ABCE1 post-splitting complex.

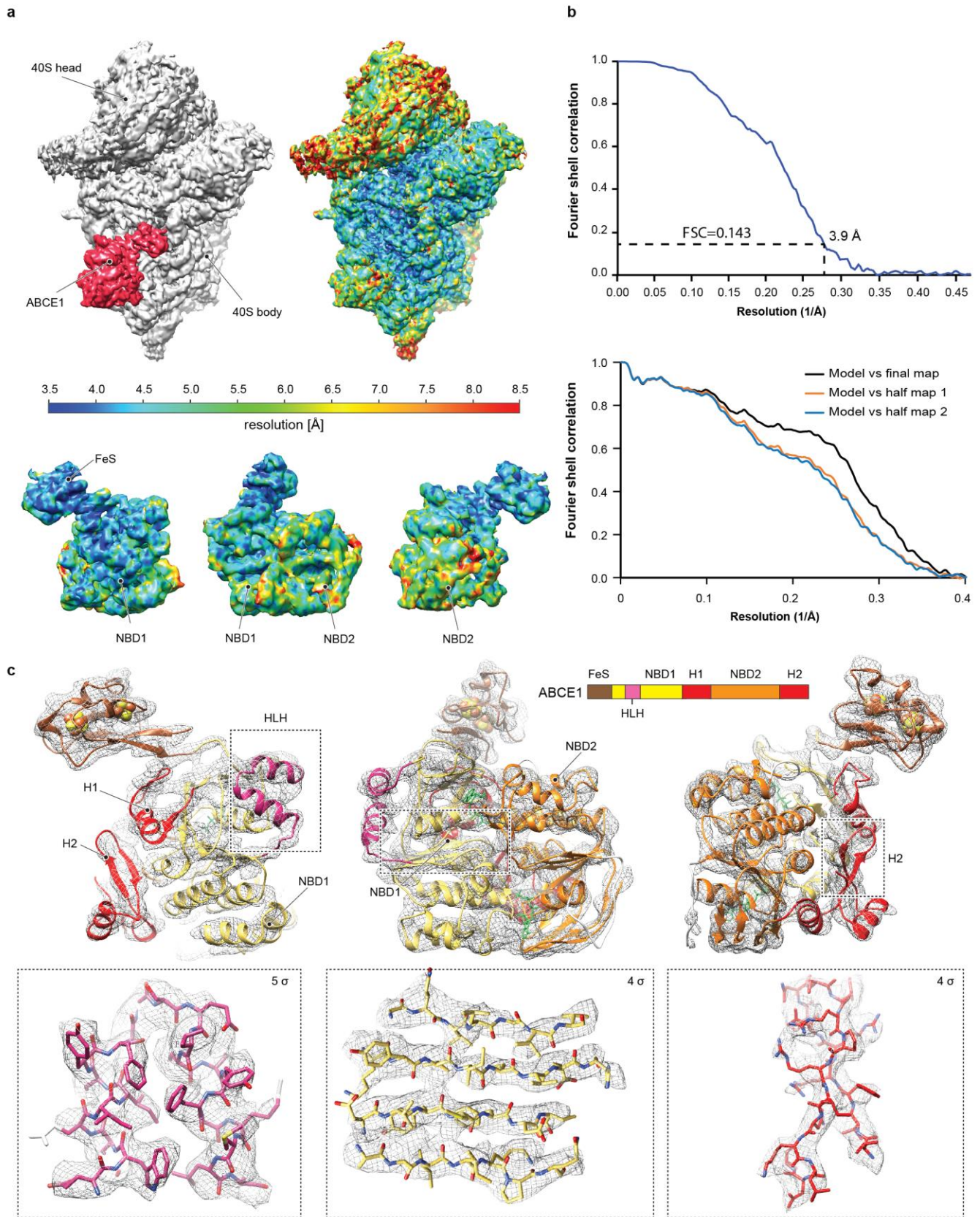
a, Outline of the facilitated splitting approach: 80S ribosomes were dissociated under high potassium (500 mM) and low magnesium (1 mM) conditions, followed by AMP-PNP-dependent ABCE1 binding to the 40S subunit. Under re-association conditions (low potassium and high magnesium concentration (100 mM and 20 mM), free 40S subunits were allowed to rejoin with free 60S subunit. A representative profile of four individual preparations is shown. **b**, In ribosome profiles, the 40S-ABCE1 complex only appears in the 40S fraction if AMP-PNP is present and ABCE1 is added under splitting-facilitating conditions. **c**, Pooled 40S ribosomal fractions show stoichiometric binding of ABCE1 to 40S subunits as analyzed by SDS-PAGE.



Supplementary Figure 2

Raw cryo-EM data and classification of the reconstituted 40S–ABCE1 complex.

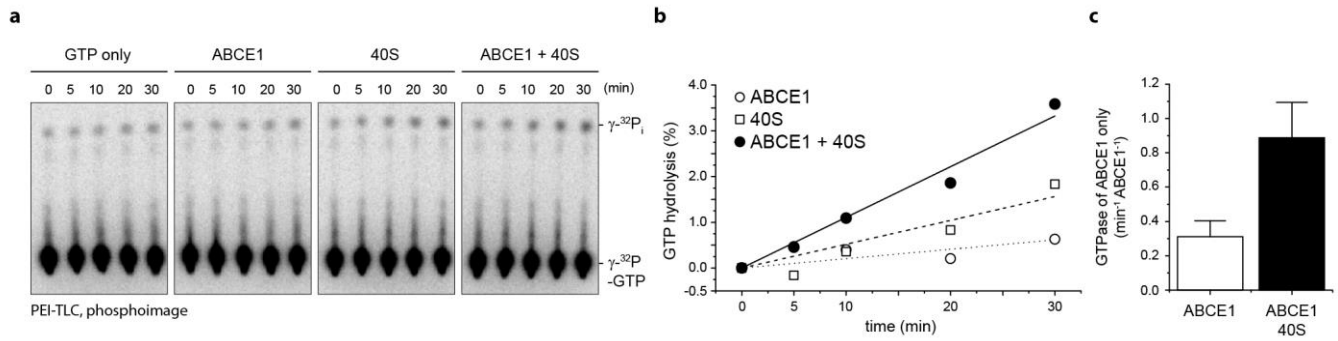
a, Representative micrograph showing 40S–ABCE1 particles. **b**, Representative 2D classes predominantly showing various side views of the 40S subunits. **c**, 3D classification scheme. After 2D classification and removal of non-ribosomal particles, the dataset was refined and subjected to 3D classification in RELION-2. The dataset was initially classified into four classes: class 1 and 2 contained poorly resolved and distorted 40S ribosomes whereas Class 3 and 4 showed well-resolved 40S ribosomes with a strong ABCE1 density. These classes were joined for a second round of 3D classification (five classes) using a mask excluding the highly flexible 40S head. Four out of five classes showed either a strong distortion which is likely a result of orientation bias or poor alignment and were discarded. The best resolved class 1 showed a strong ABCE1 density and a well resolved 40S body and was used for the refinement yielding a map at 3.9 Å resolution.



Supplementary Figure 3

Cryo-EM structure of the reconstituted 40S–ABCE1 complex and assessment of resolution.

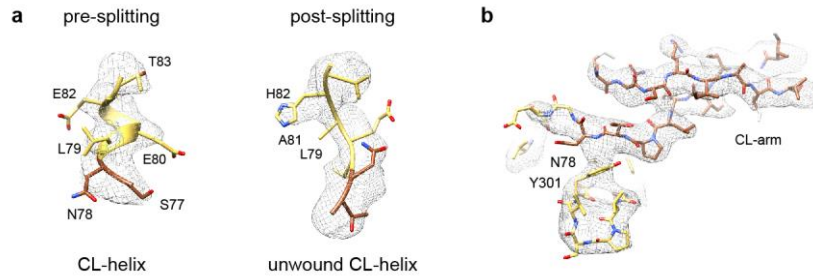
a, Cryo-EM density of the 40S–ABCE1 complex and isolated ABCE1 low-pass filtered at 3.9 Å showing the 40S subunit (grey), and ABCE1 (red), as well as local resolution as calculated by ResMap. The ResMap plots show a range from maximum 3.5 Å to 8.5 Å in the periphery. It is to note, in ABCE1, the FeS cluster domain and NBD1 are well resolved whereas resolution in NBD2 and peripheral regions of ABCE1 is slightly decreased. Maps are contoured at 3.5 σ . **b**, FSC plot shows the 3.9 Å average resolution of the map according to the “gold standard” criterion (FSC = 0.143; top) and FSC curves calculated between the cryo-EM map and the final models (bottom) as calculated by REFMAC. Values are plotted for the model versus the final map (FSC_{average}, black), for the model that was refined into the first half-map and FSC calculated either for the same map (model vs first half-map, orange) or for the second half-map (model vs second half map, blue). **c**, Density snapshots of isolated ABCE1 (contoured as indicated in the panels) with the fitted model shown in three orientations. Below, selected areas are shown illustrating the quality of the map (side chain densities in the α -helices forming the HLH motif; a separated β -sheet in NBD1 and a β -sheet with resolved bulky side chains in hinge 2). Domains are colored as indicated in the schematic panel.



Supplementary Figure 4

NTPase stimulation of ABCE1 by 40S subunit.

a, Hydrolyzed γ - ^{32}P -GTP resulted in released $^{32}\text{P}_i$ that was separated by thin layer chromatography and quantified by autoradiography. **b**, Time traces of $^{32}\text{P}_i$ formation were normalized to GTP only and time point 0 min and analyzed by a linear fit. NTP hydrolysis by ABCE1 was stimulated by addition of 40S subunits. **c**, Corrected GTPase activity of ABCE1 only shows stimulation by 3-fold upon addition of 40S subunit. Data derived from the slope in panel b are given as mean \pm s.e.m. ($n = 5$).

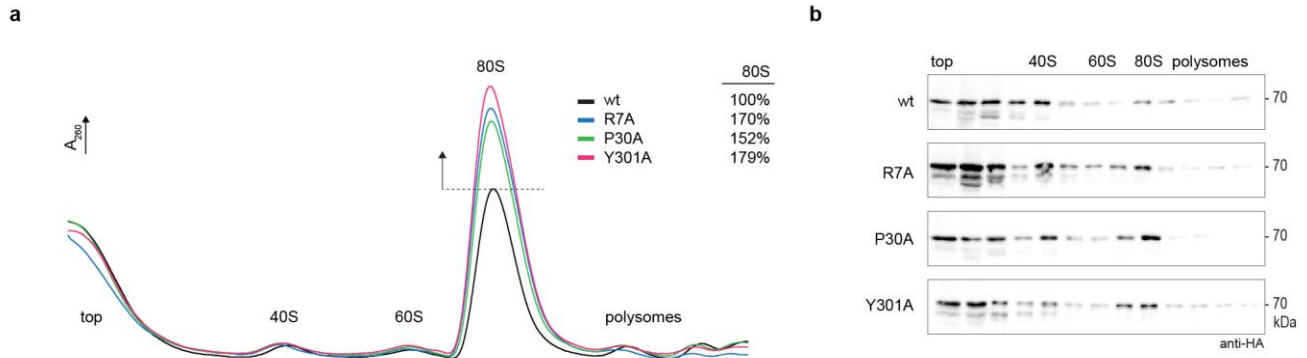


Supplementary Figure 5

Dynamic conformation of the cantilever hinge.

In the pre-splitting state (left, 3JAH)¹³, the cantilever hinge (CL) forms an α -helix, which is unwound in the ABCE1 post-splitting state (right). Isolated densities are low-pass filtered at 3.9 Å (contoured at 5 σ) and shown with the respective models. **b**, In the post-splitting state, the FeS cluster domain is mainly stabilized by two interactions of the cantilever arm: the backbone of Asn78 interacts with Tyr301 of NBD1. Density of the ABCE1 post-splitting complex was low-pass filtered at 3.9 Å (contoured at 5 σ).

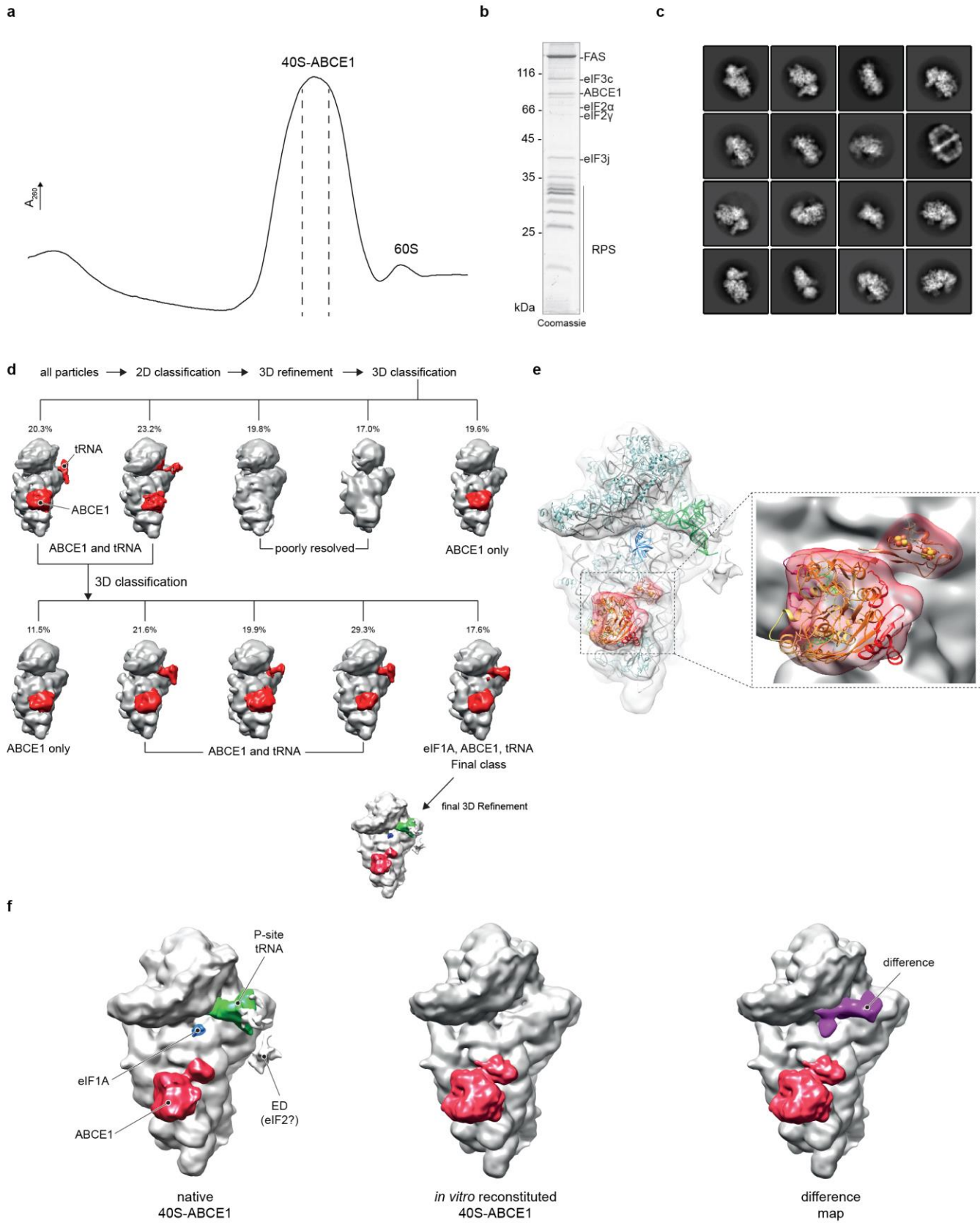
- 13 Brown, A., Shao, S., Murray, J., Hegde, R.S. & Ramakrishnan, V. Structural basis for stop codon recognition in eukaryotes. *Nature* **524**, 493-496 (2015).



Supplementary Figure 6

Ribosome profiles from cells expressing wild-type and mutant ABCE1.

a, Lysates from cells expressing wild-type and mutant ABCE1 were subjected to 10-50% sucrose density gradient centrifugation and A_{260} profiles were recorded. Compared to wild-type (wt, black), the relative amount of 80S ribosome was strongly increased in the alanine mutants R7A, P30A and Y301A. **b**, SDS-PAGE and immunoblotting of the gradient fractions using an anti-HA antibody to probe for tagged ABCE1. Wild-type ABCE1 was mainly found in the top fractions or bound to 40S subunits, while the mutants R7A, P30A, and Y301A were enriched on 80S ribosomes.



Supplementary Figure 7

Preparation and cryo-EM of the native 40S–ABCE1 complex.

a, The TEV-eluate of affinity purified tandem-affinity tagged ribosome–ABCE1 complexes was applied to a 5-30% sucrose density gradient and the A_{260} profile was recorded. **b**, Fractions containing 40S subunits and ABCE1 were pooled and analyzed by SDS-PAGE. Proteins were identified by mass spectrometry. Notably, in addition to ABCE1 and 40S proteins (RPS), the complex also contains components of the 43S pre-initiation complex (eIF2 α and eIF2 γ , eIF3c and eIF3j) together with the fatty acid synthase as a common contaminant of 40S preparations. **c**, Samples were subjected to cryo-EM and single-particle analysis. The fatty acid synthase could be easily sorted out during 2D classification. **d**, After refinement, 3D classification was performed in RELION-2. In the first round three classes (63%) show a clear density for ABCE1 and two of them showed additional extra density emerging from the P-site. These classes (43.5%) were joined for a second round of classification. Here, four of five classes only differ in the appearance of the density in the P-site, which most likely represents initiator tRNA (tRNA_i) in various positions. One class, however showed additional density in the position where eIF1A is located. This class (17.6%; 9,500 particles) was refined to a final resolution of 14 Å (**e**) according to the “gold standard” criterion (FSC = 0.143). The model of ABCE1 in the post-splitting state was fitted as rigid body without further adjustments into the ABCE1 density. eIF1A (blue) as well as tRNA_i (green) could be identified by rigid body fitting of 43 and 48S-initiation complex structures (eIF1A from 4UER, ref. 55, tRNA_i taken from 3JAP, ref. 40). **f**, A difference map was calculated between the native (left) and the *in vitro* reconstituted 40S–ABCE1 maps (middle). The difference map was superimposed to the *in vitro* reconstituted 40S–ABCE1 map (contoured at 3.5 σ). Notably, significant difference between the two maps (left and middle) occurred in the region of initiator tRNA (tRNA_i) and eIF1A. No conformational differences were observed for ABCE1.

40 Llacer, J.L. *et al.* Conformational differences between open and closed states of the eukaryotic translation initiation complex. *Mol. Cell* **59**, 399-412 (2015).

55 Aylett, C.H. *et al.* Structure of a yeast 40S–eIF1–eIF1A–eIF3–eIF3j initiation complex. *Nat. Struct. Mol. Biol.* **22**, 269-271 (2015).

Cryo-EM structure of a late pre-40S ribosomal subunit from *Saccharomyces cerevisiae*

André Heuer^{1†*}, Emma Thomson^{2†‡}, Christian Schmidt¹, Otto Berninghausen¹, Thomas Becker¹, Ed Hurt^{1,2*}, Roland Beckmann^{1*}

¹Gene Center Munich, Department of Biochemistry, University of Munich, Munich, Germany; ²Heidelberg University Biochemistry Center, Heidelberg University, Heidelberg, Germany

Abstract Mechanistic understanding of eukaryotic ribosome formation requires a detailed structural knowledge of the numerous assembly intermediates, generated along a complex pathway. Here, we present the structure of a late pre-40S particle at 3.6 Å resolution, revealing in molecular detail how assembly factors regulate the timely folding of pre-18S rRNA. The structure shows that, rather than sterically blocking 40S translational active sites, the associated assembly factors Tsr1, Enp1, Rio2 and Pno1 collectively preclude their final maturation, thereby preventing untimely tRNA and mRNA binding and error prone translation. Moreover, the structure explains how Pno1 coordinates the 3' end cleavage of the 18S rRNA by Nob1 and how the late factor's removal in the cytoplasm ensures the structural integrity of the maturing 40S subunit.

DOI: <https://doi.org/10.7554/eLife.30189.001>

*For correspondence: heuer@genzentrum.lmu.de (AH); ed.hurt@bzh.uni-heidelberg.de (EH); beckmann@genzentrum.lmu.de (RB)

†These authors contributed equally to this work

Present address: ‡University of Sheffield, Sheffield, United Kingdom

Competing interests: The authors declare that no competing interests exist.

Funding: See page 12

Received: 05 July 2017

Accepted: 03 November 2017

Published: 20 November 2017

Reviewing editor: Rachel Green, Johns Hopkins School of Medicine, United States

© Copyright Heuer et al. This article is distributed under the terms of the [Creative Commons Attribution License](https://creativecommons.org/licenses/by/4.0/), which permits unrestricted use and redistribution provided that the original author and source are credited.

Introduction

Ribosomes are the cellular machines that translate mRNAs into proteins. In eukaryotes, they consist of a small 40S and large 60S subunit, which carry the decoding and peptidyl transferase activity, respectively, and together comprise four ribosomal (r)RNAs (18S, 5.8S, 25S and 5S rRNA) and 78 ribosomal proteins in yeast. The synthesis of eukaryotic ribosomal subunits requires the concerted activity of ~200 assembly factors that drive ribosome biogenesis through a series of pre-rRNA cleavage, folding and modification reactions, which are coupled to the incorporation of ribosomal proteins (Henras et al., 2015; Woolford and Baserga, 2013; Zemp and Kutay, 2007). Initial steps of 40S biogenesis occur in the nucleolus, which leads to the formation of the first stable assembly intermediate, called the 90S pre-ribosome (Dragon et al., 2002; Grandi et al., 2002; Kornprobst et al., 2016), within which many of the early assembly steps for the 40S take place. This process requires between 50–70 different ribosome biogenesis factors (RBFs) (Woolford and Baserga, 2013; Grandi et al., 2002), which were shown by recent cryo-electron microscopy (cryo-EM) analysis to engulf the nascent pre-18S rRNA (Kornprobst et al., 2016; Sun et al., 2017; Chaker-Margot et al., 2017). Following early maturation steps, the pre-40S moiety detaches and is subsequently exported to the cytoplasm, containing only a handful of biogenesis factors including Pno1, Tsr1, Enp1, Ltv1, Nob1, Dim1 and Rio2 (Schäfer et al., 2006; Schäfer et al., 2003). Once in the cytoplasm, it has been proposed that assembly factors physically block the association of the translation machinery by occupying functional sites on the 40S subunit (Strunk et al., 2011). Structural insights into the architecture of pre-40S particles have previously been obtained through cryo-EM analysis, using preparations from both yeast and human cells (Strunk et al., 2011; Johnson et al., 2017; Larburu et al., 2016). In combination with RNA-protein crosslinking data, these structures have allowed the approximate positioning of most of the biogenesis factors on the late pre-40S particles (Strunk et al.,

2011; Granneman et al., 2010). However, in contrast to recent higher resolution structures obtained for the early 60S intermediates (Greber, 2016), no late pre-40S structures with atomic resolution are available. Accordingly, detailed insight into the molecular interactions of the RBFs and the conformation of the pre-rRNA in late 40S pre-ribosomes was lacking.

Results and discussion

To gain a better understanding of the small ribosomal subunit biogenesis on a molecular level we purified late pre-40S particles via the well-defined biogenesis factor Ltv1 (Schäfer et al., 2006; Johnson et al., 2017), using Ltv1-Flag-TEV-ProteinA (FTpA) as bait (Figure 1—figure supplement 1A). With this strategy, we obtained a high yield of homogeneous pre-40S particles, which were used for single particle cryo-EM (Figure 1—figure supplement 1B–C). After classification we obtained a major class containing the stably bound RBFs Enp1, Tsr1, Rio2 and Pno1 (Figure 1—figure supplement 1D) but lacking a number of late binding ribosomal proteins (RACK1, uS10, uS14, eS10, eS26 and uS3) (Ferreira-Cerca et al., 2007). This main class could be refined to an average resolution of 3.6 Å, with the local resolution ranging from 3.5 Å in the core to approximately 8 Å for flexible regions (Figure 1—figure supplement 2). We built atomic models for Tsr1 and Pno1, and were able to model Enp1 and Rio2 on a secondary structure level (Figure 1A and Figure 1—figure supplements 2–3). In addition, the structure of the pre-18S rRNA revealed very distinct conformational differences, as compared to the mature state (Heuer et al., 2017), of functionally important regions including all three tRNA binding sites (A,P and E) and the entire mRNA path. We found that two major rRNA condensation steps still have to happen for these sites to mature: one in the head/beak region and the other in the central region of the 18S rRNA (Figure 1B).

The characteristic tertiary structure of the head rRNA (h28 to h43) is mainly determined by three-way junctions (Mohan et al., 2014). We observe that in the pre-18S rRNA only one such junction is not yet formed, namely that which connects h34, h35 and h38 (Figure 1C and Figure 1—figure supplement 4A). It joins three blocks of rRNA, which all contain parts of functionally important regions: one block contains h33 of the beak and h34, a central element in the formation of the A-site decoding center, while the block comprising h29-h32 and h38-h42 contains key residues for mRNA binding and accommodation of anticodon-arms for all three tRNAs. The third block (h35-h37) contains h36, which forms important tertiary interactions between head and body and is part of the central region of the 18S rRNA (Wimberly et al., 2000) (see below). Due to the absence of this junction, these blocks are shifted relative to each other and relative to the body, preventing the formation of the active sites. Notably, formation of this junction requires the incorporation and stabilisation of the late associating ribosomal proteins uS3, uS10 and uS14 (Lescoute and Westhof, 2006), which are absent from the pre-40S particle (Figure 2—figure supplement 1).

The central region of the 18S rRNA comprises the central pseudoknot (CPK), a universally conserved structure that connects the head with the body via h28, h1 and h2. It provides a core structure around which major parts of the active A- and P-sites form, with the most central being h44 and h28. The tip of h44 contains two universally conserved adenosine bases (A1755/A1755, A1492/A1493 in *E. coli*) critical for mRNA decoding (Ogle et al., 2003) and the 'neck helix' h28 provides a hinge for head rotation, which is crucial for tRNA movement during elongation (Mohan et al., 2014; Korostelev et al., 2008). Formation of the CPK is a major structural landmark and we observe that, unlike in the 90S, the CPK is fully folded and the contact with the head (h36) has been established (Figure 1—figure supplement 4B–C). In contrast, we observe that the top of h44 is not yet base-paired, and the linker of h44 with h28 and h45 remains highly flexible. Notably, this linker forms major parts of the A and P sites in the mature state (Figure 1D and Figure 1—figure supplement 4B). Moreover, h44 is repositioned outwards relative to its mature position and h28 is tilted by 12 degrees in the direction of the beak (Figure 1—figure supplement 4B–C). Collectively, we observe that the pre-18S rRNA is still in a non-functional immature state since all elements forming the active decoding and mRNA interaction sites are prevented from adopting their mature fold (Figure 2).

We next investigated the role that the RBFs play regarding the immature pre-18S rRNA conformation. The first RBF, Tsr1, shares a similar domain architecture (I-IV) to several translational GTPases with an additional N-terminal extension, which was unresolved in previous studies (Johnson et al., 2017; McCaughan et al., 2016). Tsr1 mainly binds to the region which forms the universal translation factor binding site on the small subunit. Tsr1 contacts the junction of h5 - h15 and uS12 via its

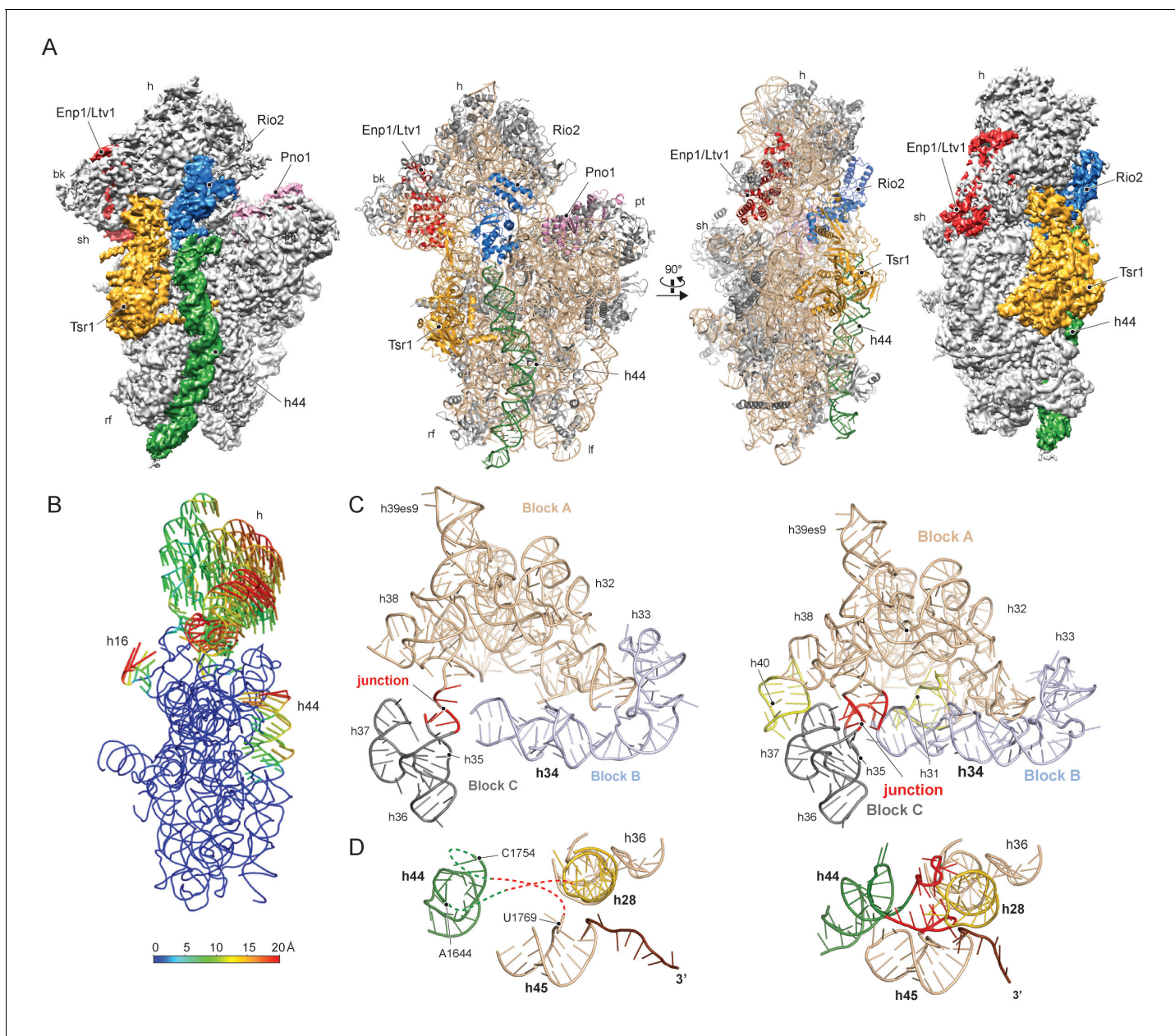


Figure 1. Structure of the pre-40S particle and conformation of the 18S rRNA. (A) 3.6 Å cryo-EM reconstruction and molecular model of the pre-40S complex containing Enp1/Ltv1, Tsr1, Rio2 and Pno1 (B) Conformational transition of the 18S rRNA from the pre-mature to the mature state represented by vectors (superimposed on the 40S body). (C) Condensation of the head-forming rRNA on the h34/35/38 three-way junction from pre- (left) to mature state (right). Block A (h29–h32, h38–h42) mostly resembles the mature state and served as the moiety for superposition. Relative to block A, blocks B (h34 and h33) and C (h35–h37) are still shifted, since the three-way junction linking the blocks is not yet established. The connection of h40 to h37 and the loop of h31 are not established in the pre-state. (D) View focusing on the linker between h44 with h28 and h45 from the central region of 18S rRNA. In the pre-state (left), the linker region as well as parts of h44 are unfolded and h28 (yellow) is tilted compared to the mature state (right).

DOI: <https://doi.org/10.7554/eLife.30189.002>

The following figure supplements are available for figure 1:

Figure supplement 1. Purification and cryo-EM of the pre-40S complex.

DOI: <https://doi.org/10.7554/eLife.30189.003>

Figure supplement 2. Assessment of resolution and model quality of the cryo-EM structure.

DOI: <https://doi.org/10.7554/eLife.30189.004>

Figure supplement 3. Fitting of the RBFs.

DOI: <https://doi.org/10.7554/eLife.30189.005>

Figure 1 continued on next page

Figure 1 continued

Figure supplement 4. Conformation and flexibility of the pre-18S rRNA

DOI: <https://doi.org/10.7554/eLife.30189.006>

domains I and III (**Figure 3A**). Specific interactions are established with h17 and to the N-terminal tail of eS30, which is yet to adopt its mature position (**Figure 4—figure supplement 1**). Further, domain IV of Tsr1 links the body with the immature head contacting h30 to h32, as well as the shifted h34. Notably, these rRNA structures are contacted from the opposite side by Enp1/Ltv1 (see below), resulting in the coordinated stabilization of the ribosomal beak in its immature conformation.

Due to high local resolution, we were able to build the N-terminal part of Tsr1. It forms a 35 Å long α -helix, which pierces through the ribosome between h5 and h44. By reaching further it touches h11-h12 (**Figure 3A–B**), thus serving as a distance enforcing wedge for h44. Thereby, via a long distance effect, Tsr1 keeps the linker connecting h44 with h28 and h45 unfolded and immaturely positioned. To assess the functional significance of the interaction of the N-terminal helix of Tsr1 and h44 we generated reverse charge mutants (R54D, K55D, K57D and K59D) where combinations of 3 or more substitutions indeed resulted in a slow growth phenotype (**Figure 3C**). All mutants showed the same nuclear localization, but a decrease in association with pre-ribosomes as compared to wild-type Tsr1 (wt) (**Figure 4—figure supplement 1A–B**). These data suggest that the N-terminus of Tsr1 is important for both, the stabilization of h44 in its immature conformation and the association of Tsr1 with pre-ribosomes. We also assessed the consequences of abolishing the interaction between domain IV of Tsr1 and the head of the pre-40S by removing domain IV. This mutant no longer supported yeast cell growth but continued to interact with pre-ribosomal particles (**Figure 4—figure supplement 1C–D**). We therefore propose that domain IV is not necessary for the association of Tsr1 with the pre-ribosome, but rather plays an important role to stabilize the pre-40S head in its immature conformation.

Enp1 is one of the few assembly factors that is already present in the 90S particle and remains associated until the integration of uS3 during late pre-40S biogenesis in the cytoplasm (**Kornprobst et al., 2016; Schäfer et al., 2003**). We observe Enp1 binding to the tip of the bent h16 near the mRNA entry site (**Figure 3D, 4A**). From there it reaches over to bind h32 - h34, thus keeping the head in its immature conformation together with Tsr1. Notably, we observe that Enp1 binds the same rRNA elements as in the 90S (**Kornprobst et al., 2016; Sun et al., 2017; Chaker-Margot et al., 2017**), further suggesting an early stabilization of the ribosomal beak. Ltv1, Enp1 and Rps3 are known to form a stable protein complex (**Schäfer et al., 2006**). Most likely due to the absence of Rps3 in our structure, only the extra density on top of Enp1 likely corresponds to its interaction partner Ltv1, which is in agreement with previous structural studies (**Strunk et al., 2011; Larburu et al., 2016**). The binding site of Enp1/Ltv1 occupies the position of the as yet unincorporated protein eS10 (**Figure 4A**) and explains Enp1/Ltv1's described role in facilitating uS3 integration at an adjacent site (**Schäfer et al., 2006**). It further suggests a role for Enp1 in the maturation of h34 and the h34-h35-h38 three-way junction.

Rio2 a RBF conserved in all archaea and eukaryotes (**Geerlings et al., 2003; Vanrobays et al., 2003; Schäfer et al., 2003**), is an essential serine kinase required for 40S maturation. It binds the pre-40S at the A and P site region with all three domains (**Figure 3E**). The N-terminal winged-helix-turn-helix motif (wHTH) contacts the tip of h18, which forms the 'latch' for the mRNA in the mature 40S together with uS3, h34 and uS12 (**Schluenzen et al., 2000**). The two-lobed kinase domains of Rio2, K1 and K2, are positioned close to h28 whereby K1 contacts the region, which serves as a hinge during the 40S head rotation (**Mohan et al., 2014**). Rio2's K1 also contacts the 40S head via h30 at a position close to domain IV of Tsr1. Finally, K2 contacts h29 and h42, which forms the P-site for binding the (initiation) tRNA in the mature ribosome.

We further identified Pno1, a factor that together with the endonuclease Nob1 controls one of the final events of 40S biogenesis, the maturation of the 18S rRNA through cleavage of the 3'-end at cleavage site D (**Lamanna and Karbstein, 2009; Lamanna and Karbstein, 2011**). This cleavage event is believed to be regulated by Pno1 (**Vanrobays et al., 2004**), which belongs to the family of single-stranded RNA binding proteins with KH-domains. It is located on the platform of the pre-40S (**Figure 5A**) where it interacts with uS11/uS1, the tilted rRNA h28, h45 and the 3'-end of the

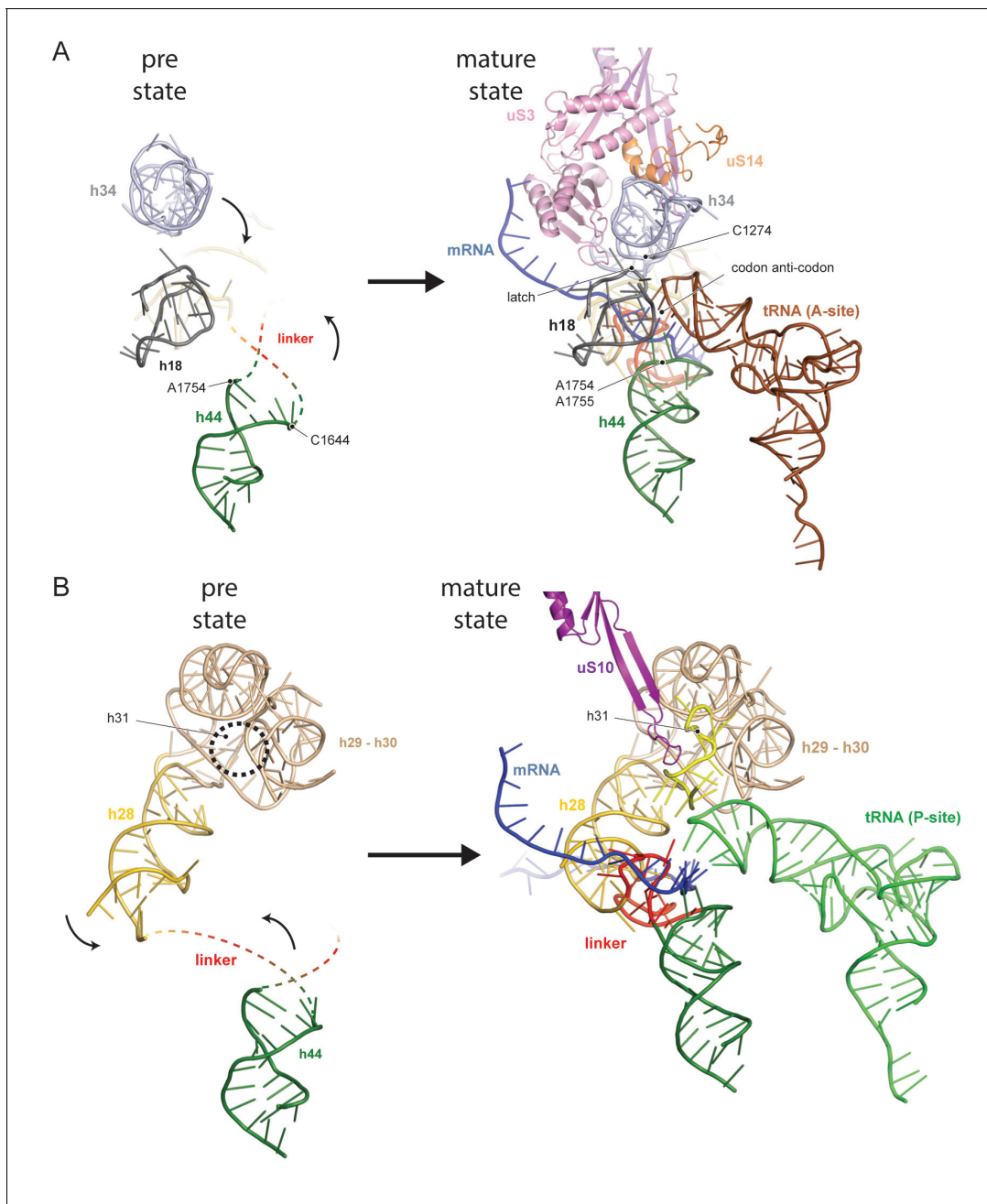


Figure 2. Comparison between pre- and native 40S focusing on the active sites. (A) View focusing on the mRNA entry and A-site. The A-site is composed of h18, h34 and h44, where in a translating ribosome the anticodon-loop of a A-tRNA is bound and the mRNA enters the 40S via the latch structure formed between h18, h34 and uS3. In the pre-40S, uS3 is absent and h34 is displaced. Moreover, h44 is shifted and its tip including the decoding adenines A1754 and A1755 is unfolded. (B) View focusing on the mRNA exit and the P-site. The P-site is composed of h24 (not shown), h28, h29 and h31 as well as the linker between h44 and h45. In the pre-40S this linker is delocalized and h28 is shifted. Moreover, the tip of h31 which is stabilized by uS10 in the mature state and binds the P-site tRNA in a translating ribosome is not folded in the pre-state.

DOI: <https://doi.org/10.7554/eLife.30189.007>

The following figure supplement is available for figure 2:

Figure supplement 1. Structure and environment of the native h34-h35-h38 three-way junction.

DOI: <https://doi.org/10.7554/eLife.30189.008>

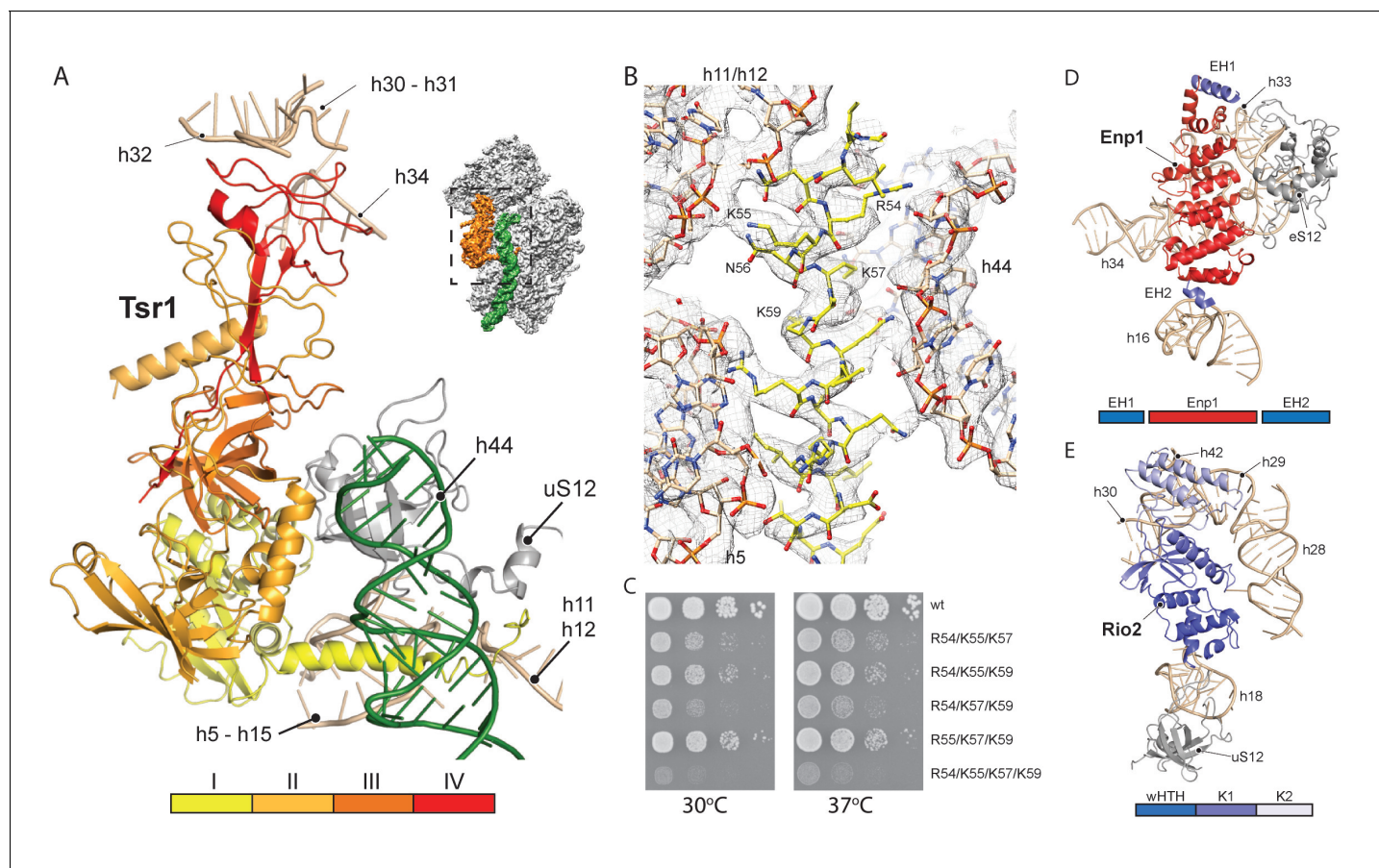


Figure 3. Interactions of Tsr1, Enp1/Ltv1 and Rio2 with the pre-40S. **(A)** Tsr1 binds the 40S body (h5–h15, h17 and uS12) via domains I and III, the 40S head (h30–h31, h32 and h34) via domain IV. The N-terminal α -helix of Tsr1 intercalates between h44, h5 and h11–h12. **(B)** Model of the Tsr1 N-terminal α -helix fitted into density low-pass filtered at 3.6 Å. **(C)** Growth analysis of wt Tsr1 and reverse-charge point mutations in residues interacting with h44 (R54D, K55D, K57D and K59D). Constructs were transformed into a Tsr1 shuffle strain and selected on SDC + FOA plates. Strains were spotted in 10-fold serial dilution on YPD plates and incubated for 2 days at the indicated temperatures. Different temperatures were used to assess if the growth defect observed at 30 degrees was enhanced at higher temperatures. **(D)** Enp1 binds to h33, h34 and eS12 and to the kinked h16; EH = extra helix for Enp1 or Ltv1. **(E)** Rio2 binds the 40S body via its N-terminal winged-helix-turn-helix-domain (wHTH) (h18, uS12), and the 40S head via the two-lobed kinase domain (K1/K2) (h28, h30). Moreover, K2 reaches into the P-site contacting h29, h42 and the region in between.

DOI: <https://doi.org/10.7554/eLife.30189.009>

The following figure supplement is available for figure 3:

Figure supplement 1. Functional analyses of mutant forms of Tsr1.

DOI: <https://doi.org/10.7554/eLife.30189.010>

pre-18S rRNA. Importantly, in this position, Pno1 sterically hinders h28 from adopting its mature conformation and the binding of eS26 (**Figure 4B**). We were able to follow the 3' rRNA end, bound by Pno1, up to the pre-terminal base (U1799, D cleavage occurs after A1800) in molecular detail: A multitude of interactions is formed by three α -helices of the KH2 domain of Pno1, which recognize the first two single-stranded bases (G1793 and A1794) as well as the stem of h45 (**Figure 5B**) including the last base of the h44–h45 linker (U1769), which later will form a part of the active P- and mRNA binding sites. Thus Pno1, like Tsr1 and Rio2, prevents compaction of the central region of 18S rRNA.

Like other members of the KH family (**Nicastro et al., 2015**), Pno1-KH2 uses its hallmark GXXG-RNA binding motif to position four nucleobases (residues 1795–1798) in a hydrophobic pocket (**Figure 5C–D**). Interestingly, KH1, which lacks the signature GXXG sequence in yeast (**Woolls et al., 2011**), also contributes to 3'-binding and contacts the terminal 18S rRNA bases 1797–1799 via its α -helix h1. Sequence alignments for the 3'-end revealed not only that the UCAU sequence -

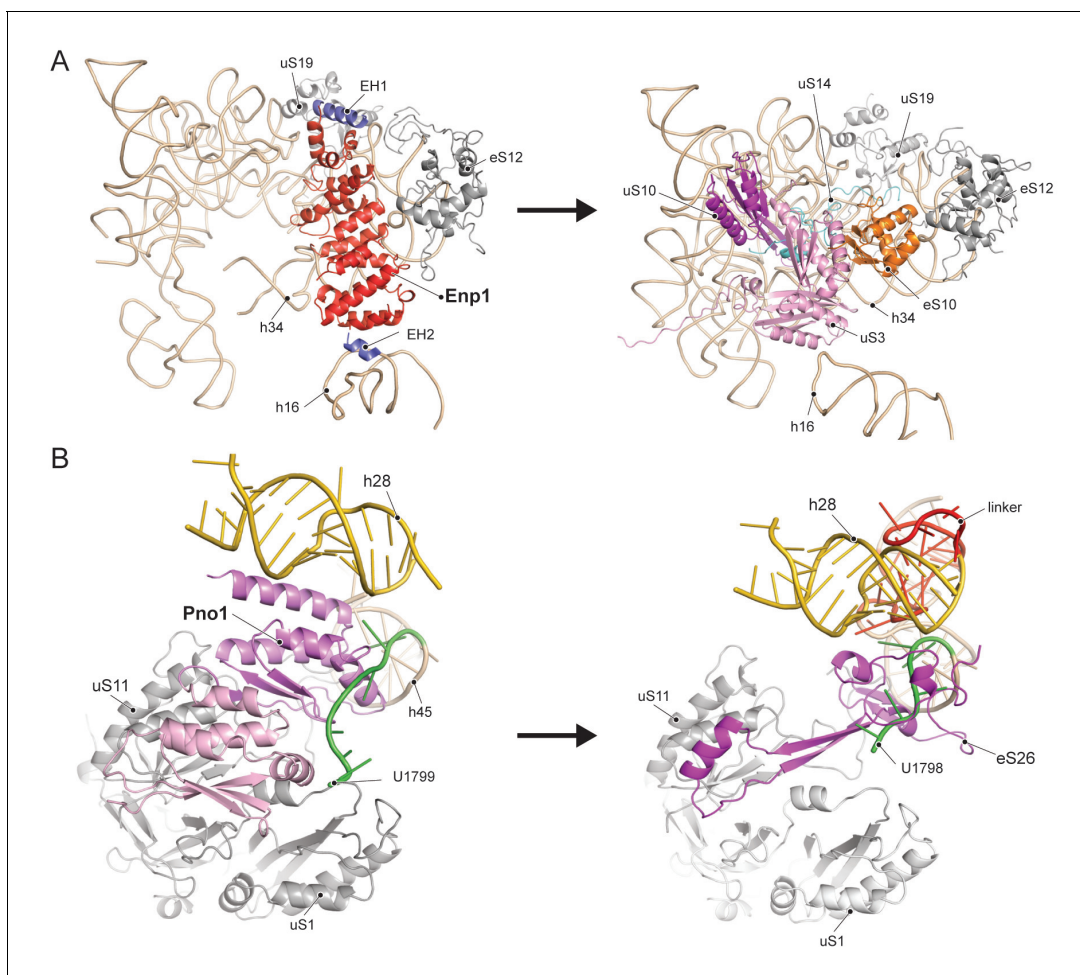


Figure 4. Comparison of RBF binding sites in the premature and the mature 40S. (A) Enp1/Ltv1 binds near the mRNA entry channel and connects the shoulder (h16) with the beak (h33, h34 and eS12). It occupies the position of the eS10. Moreover, uS3, uS10 and uS14 are not incorporated into the pre-40S particle. Note that h16 is in a bent conformation compared to the mature state. (B) Pno1 binds at the platform of the pre-40S contacting uS1, uS11, the kinked h28 as well as h45 and the 3'-end of 18S rRNA. It thereby occupies the position of eS26, which binds the rearranged 3' end in the mature state.

DOI: <https://doi.org/10.7554/eLife.30189.011>

The following figure supplement is available for figure 4:

Figure supplement 1. Binding of Tsr1 to h17 and eS30.

DOI: <https://doi.org/10.7554/eLife.30189.012>

that contacts KH2 - is conserved from yeast to humans, but also the surrounding bases up to the D-cleavage site. This suggests that specific binding of Pno1 and positioning of the 3'-end in a distinct conformation may be a universal feature of eukaryotic ribosome maturation. Notably, Pno1 is in an ideal location to sense any further maturation of 18S rRNA, in particular conformational changes of the close-by h28, which may allow Pno1 to productively present the D-site for cleavage by the neighbouring endonuclease Nob1. In addition, Pno1 may protect the 3' end against further cleavage until the small ribosomal subunit is fully matured.

In conclusion, we have discovered that the collective association of a few ribosome biogenesis factors on the late pre-40S ribosome regulates final rRNA folding steps at functionally important sites, in particular at the decoding centre. It appears that the role of these factors is to temporarily maintain the 40S subunit in a translationally incompetent state during ribosome biogenesis, preventing premature substrate interaction or entry into cycles of translation, which would be error-prone and potentially harmful to the cell. We envision that removal of biogenesis factors and the maturation of these regions are inter-dependent and coordinated processes. Conditional stepwise removal

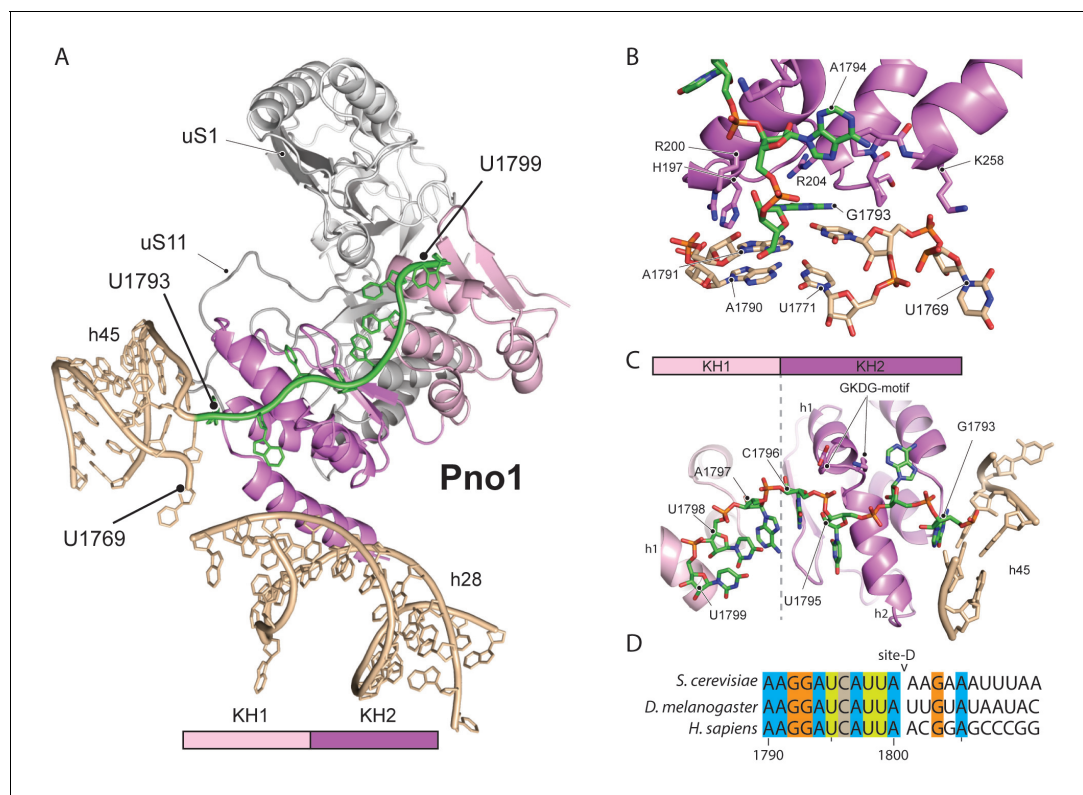


Figure 5. Molecular interactions of Pno1. (A) Pno1 binds uS11/uS1, h45, the tilted h28 and the 3' end (green) at the platform. (B) View focusing on the molecular interactions of KH2 with h45. Three C-terminal α -helices recognize the stem of h45 (A1791:U1770 and A1790:U1769), upon which G1793 is stacked. Specifically, Arg204 contacts G1793 and Arg200 together with His197 the backbone of the 3' strand (A1791 and A1790). The loop between two of the C-terminal helices of Pno1 (Gly253-Lys258) contacts U1770 and U1769 of the 5'-strand of h45. This loop also participates in binding of the first single-stranded base A1794 which is sandwiched between Pro256 and the GKDG-loop of KH2 (C) View focusing on the molecular interactions between Pno1 and the 3' rRNA end. Both KH domains interact with the 3'-end rRNA residues (G1793-U1799) which lead up to the D-cleavage site. The GKDG-loop of KH2 positions four nucleobases (U1795-U1798) close to its hydrophobic pocket and KH1 contacts the terminal bases (A1797-U1799) via h1 (D) Sequence alignment for eukaryotic 3' rRNA ends showing conservation up to the D-cleavage site.

DOI: <https://doi.org/10.7554/eLife.30189.013>

of these biogenesis factors may therefore serve as checkpoints that ensure the structural integrity of the ribosomal subunit, and thereby fitness for translation.

Materials and methods

Key resource table

Reagent type (species) or resource	Designation	Source or reference	Identifiers	Additional information
strain, strain background (Saccharomyces cerevisiae)	Ltv1-FTpA;Tsr1shuffle	This paper	NA	Ltv1-FTpA- Genomic copy of Ltv1 tagged at the c-terminus with FLAG-TEV-proteinA tag; Tsr1 shuffle- genomic copy of Tsr1 deleted and rescued with a plasmid with a wild-type copy

Continued on next page

Continued

Reagent type (species) or resource	Designation	Source or reference	Identifiers	Additional information
genetic reagent (plasmids used for expression in <i>Saccharomyces cerevisiae</i>)	YCplac111-Tsr1-FTpA; YCplac111-Tsr1 R54D, K55D,K57D-FTpA; YCplac111-Tsr1 R54D, K55D,K59D-FTpA; YCplac111-Tsr1 R54D, K57D,K59D-FTpA; YCplac111-Tsr1 K55D, K57D,K59D-FTpA; YCplac111-Tsr1 R54D, K55D,K57D,K59D-FTpA; YCplac111-Tsr1-GFP; YCplac111-Tsr1 R54D, K55D,K57D,K59D-GFP; YCplac111- Tsr1DC86-FTpA	This paper	NA	Plasmids containing wild-type Tsr1 or the described point mutants. Expression is under the control of the Tsr1 promoter, and are tagged at the c-terminus with either FLAG-TEV-proteinA or GFP.
software, algorithm	EM-TOOLS	TVIPS GmbH	NA	http://www.tvips.com/imagingsoftware/em-tools/
software, algorithm	MotionCorr2.1	https://doi.org/10.1038/nmeth.4193	NA	http://cryoem.ucsf.edu/software/driftcorr.html
software, algorithm	GCTF	https://doi.org/10.1016/j.jsb.2015.11.003	NA	http://www.mrcmb.cam.ac.uk/kzhang
software, algorithm	Gautomatch	public	NA	http://www.mrcmb.cam.ac.uk/kzhang
software, algorithm	Relion-2	https://doi.org/10.7554/eLife.18722	NA	http://www2.mrcmb.cam.ac.uk/relion/index.php
software, algorithm	Phenix suite (phenix.real_space_refine, molprobity)	Python-based Hierarchical ENvironment for Integrated Xtallography	RRID:SCR_014224	https://www.phenix-online.org/
software, algorithm	CCP4 (LIBG, ProSMART, Refmac5, COOT)	Collaborative Computational Project No. 4 Software for Macromolecular X-Ray Crystallography	RRID:SCR_007255	http://www.ccp4.ac.uk/
software, algorithm	UCSF Chimera	UCSF Resource for Biocomputing, Visualization, and Bioinformatics	RRID:SCR_004097	http://www.cgl.ucsf.edu/chimera/
software, algorithm	Pymol	PyMOL Molecular Graphics System, Schrödinger, LLC	RRID:SCR_000305	https://pymol.org/

Yeast strains and plasmids

For affinity purification of pre-40S particles for EM analysis, endogenous Ltv1 was tagged in a DS1-2b background (Nissan *et al.*, 2002) at its C-terminus with a FLAG-Tev-protA (FTpA), as previously described (Longtine *et al.*, 1998). All wt and mutant Tsr1-FLAG-Tev-protA or Tsr1-GFP constructs were expressed from plasmids under the control of the endogenous promoter. For Tsr1 affinity purification and localization studies, constructs were expressed in a BY4741 background. For growth analysis, constructs were transformed into a Tsr1 shuffle strain (in a BY4741 background), followed by selection on SDC + FOA. All constructs used in this study can be found in the key resource table.

Affinity purification from yeast lysates

Purifications of all FTpA-tagged bait proteins were performed in buffer containing 50 mM Tris-HCl (pH 7.5), 100 mM NaCl, 1.5 mM MgCl₂, 5% glycerol, 0.1% NP-40, and 1 mM DTT. Cell lysates were prepared using a beadbeater (Fritsch), followed by centrifugation. Pre-equilibrated IgG Sepharose (GE) was added to the supernatant and incubated for 90 min at 4°C. Extensive washing was followed by TEV cleavage and a second step of purification on anti-FLAG MS2-agarose beads. Beads were washed, and proteins were eluted using a buffer containing 50 mM Tris-HCl (pH 7.5), 100 mM NaCl, 1.5 mM MgCl₂, 1 mM DTT, 3xFLAG peptide. For cryo-EM analysis the FLAG eluate was directly used. For Tsr1 purifications FLAG eluates were precipitated with TCA (10% final) and resuspended in

Table 1. EM data collection and refinement statistics.

Data collection	
Particles	84100
Pixel size (Å)	1.084
Defocus range (µm)	0.8-2.4
Voltage (kV)	300
Electron dose (e ⁻ Å ⁻²)	28
MODEL REFINEMENT	Pre40S particle
Model composition	
Non-hydrogen atoms	71923
Protein residues	4718
RNA bases	1635
Refinement	
Resolution for refinement (Å)	3.7
Map sharpening B-factor (Å ²)	-92.8
Average B-factor (Å ²)	164.6
FSC _{average}	0.85
R.m.s. deviations	
Bond lengths (Å)	0.0177
Bond angles (°)	1.61
VALIDATION and STATISTICS	Pre40S particle
Validation	
Molprobrity score	2.20
Clashscore, all atoms	9.60
Good rotamers (%)	94.04
Ramachandran Plot	
Favored (%)	85.79
Outliers (%)	1.21
Validation (RNA)	
Correct sugar puckers (%)	97.8
Good backbone conformations (%)	65.6

DOI: <https://doi.org/10.7554/eLife.30189.014>

SDS sample buffer. Proteins were separated on 4–12% NuPAGE polyacrylamide gel and stained with colloidal Coomassie.

Electron microscopy and image processing

Freshly prepared samples were adjusted to 1.5 A₂₆₀ (50 nM 40S ribosomes) and applied to Quantifoil R3/3 holey grids pre-coated with 2 nm carbon. Data was collected on a Titan Krios TEM (FEI Company) equipped with a Falcon II direct electron detector at 300 keV under low dose conditions of about 2.4 e-/Å² per frame for 10 frames in total using the software EM-TOOLS (TVIPS) and a defocus range of -0.8 to -2.4 µm at a pixel size of 1.08 Å. Original image stacks were summed up and corrected for drift and beam-induced motion at micrograph level using MotionCor2 (Zheng et al., 2017). The contrast transfer function parameters and resolution range of each micrograph were estimated by GCTF (Zhang, 2016). All 2D and 3D classifications and refinements were performed with RELION-2 (Kimanius et al., 2016) after automated particle picking by Gautomatch (<http://www.mrc-lmb.cam.ac.uk/kzhang/>). Two-dimensional reference-free classification was performed to screen for particle quality (Figure 1—figure supplement 1C), non-ribosomal particles as well as poorly resolved 2D classes were discarded. 266,800 particles from good classes were

selected for 3D refinement using a mature 40S ribosome as reference. We performed two subsequent rounds of 3D classification in order to enrich pre-40S complexes (**Figure 1—figure supplement 1D**). First, the whole dataset was classified into 7 classes: class 1 and 2 contained orientation biased 40S ribosomes whereas classes 3 to 5 showed well-resolved 40S ribosomes with strong extra densities for the RBFs. In addition, class 6 showed poorly resolved pre-40S ribosomes and class 7 displayed a pre-40S ribosome with a very flexible head domain. The classes 3 to 5 were joined for movie refinement and a second round of 3D classification (six classes). Here, class 1 displayed distorted density due to orientation bias, while class 2 and 3 showed a very strong density for the majority of RBFs. Class 4 displayed a less distorted volume than class 1 but showed an extra density emanating from the platform to the head, which is likely Nob1 (**Strunk et al., 2011**). In addition Class 5 showed weak densities for RACK1, uS3 and the Dim1 (**Johnson et al., 2017**). The most promising classes 2 and 3 were joined for final refinement and used for further interpretation. This final volume contained 84,100 particles was refined to 3.6 Å (FCS = 0.143) according to the 'gold standard' criterion, corrected for the modulation transfer function of the Falcon two detector and sharpened by applying a negative B-factor automatically estimated by RELION-2. Local resolution was calculated from 3.5 to 8.0 Å in steps of 0.5 Å using ResMap (**Kucukelbir et al., 2014**).

Model building

For model building of the pre-40S subunit the structure of the mature *S. cerevisiae* 40S post splitting complex was used as a template (PDB 5LL6 [**Heuer et al., 2017**]). Available structures of the biogenesis factors Rio2 (PDB 4GYG [**Ferreira-Cerca et al., 2012**]), Tsr1 (PDB 5IW7 [**McCaughan et al., 2016**]), Pno1 (PDB 5WYJ [**Sun et al., 2017**]) and Enp1 (PDB 5WYJ [**Sun et al., 2017**]) were first fitted as rigid bodies into the isolated and appropriately low-pass filtered electron densities using UCSF Chimera (**Pettersen et al., 2004**). After rough docking, and manual adjustments where needed, flexible fitting and jiggle fitting was applied in Coot (**Brown et al., 2015; Emsley and Cowtan, 2004**). Regions not present in the available structures were modelled de novo, where the local resolution of the map allowed it (for example Tsr1, Pno1). rRNA which could, due to flexibility not be modelled with sufficient reliability, was removed from the model. In order to identify the extra density that may correspond to Ltv1, we fitted the structure of Enp1 found in the 90S pre-ribosome into the density. This fit left two rod-like densities unexplained, which we designated as extra helices 1 and 2 (EH1 and EH2). We speculated that these extra densities are either Ltv1 or an as yet unidentified part of Enp1. All models were subsequently combined and subjected to real-space refinement using PHENIX (**Adams et al., 2010**). After PHENIX refinement, the model was further subjected to reciprocal space refinement in REFMAC v5.8 (**Murshudov et al., 1997**) using restraints generated by ProS-MART and LIBG as previously shown (**Brown et al., 2015; Amunts et al., 2014**). Because of the difference in local resolution and to avoid overfitting, h34, Enp1/Ltv1 and Rio2 were not subjected to REFMAC refinement. The final model was validated using MolProbity (**Chen et al., 2010**), summarized statistics are displayed in **Table 1**. Cross-validation against overfitting was performed as previously described (**Amunts et al., 2014; Fernández et al., 2014**) for both model refinements separately. Figures were created with the PyMOL Molecular Graphics System (Version 1.7.4, Schrödinger, LLC) and with UCSF Chimera.

Accession codes

The EM density map is deposited in the 3D-EM database (EMD-3886) and the coordinates of the EM-based model is deposited in the Protein Data Bank (PDB-6EML).

Acknowledgements

The authors thank S Lange, H Sieber, M Gnädig and S Griesel for technical assistance; M Thoms for the Ltv1-FTpA strain; L Kater for valuable assistance with high-performance computing; J Cheng for fruitful discussions. We thank the Leibniz-Rechenzentrum Munich (LRZ) for providing computational services and support.

Additional information

Funding

Funder	Grant reference number	Author
Deutsche Forschungsgemeinschaft	FOR1805	Roland Beckmann
Deutsche Forschungsgemeinschaft	GRK1721	Roland Beckmann
Deutsche Forschungsgemeinschaft	SFB 646	Thomas Becker Roland Beckmann
Center for Integrated Protein Science Munich	CiPSM	Roland Beckmann
European Research Council	Advanced Grants CRYOTRANSLATION	Roland Beckmann
Deutsche Forschungsgemeinschaft	HU363/12-1	Ed Hurt
Boehringer Ingelheim Stiftung	Boehringer Ingelheim Fonds PhD fellowships	Christian Schmidt

The funders had no role in study design, data collection and interpretation, or the decision to submit the work for publication.

Author contributions

André Heuer, Data curation, Formal analysis, Validation, Investigation, Visualization, Methodology, Writing—original draft, Writing—review and editing; Emma Thomson, Resources, Data curation, Validation, Writing—review and editing; Christian Schmidt, Validation, Writing—review and editing; Otto Berninghausen, Data curation; Thomas Becker, Conceptualization, Supervision, Writing—original draft, Writing—review and editing; Ed Hurt, Conceptualization, Funding acquisition, Writing—review and editing; Roland Beckmann, Conceptualization, Supervision, Funding acquisition, Validation, Writing—original draft, Project administration, Writing—review and editing

Author ORCIDs

André Heuer,  <https://orcid.org/0000-0001-6144-4316>

Thomas Becker,  <http://orcid.org/0000-0001-8458-2738>

Roland Beckmann,  <https://orcid.org/0000-0003-4291-3898>

Decision letter and Author response

Decision letter <https://doi.org/10.7554/eLife.30189.016>

Author response <https://doi.org/10.7554/eLife.30189.017>

Additional files

Supplementary files

- Transparent reporting form

DOI: <https://doi.org/10.7554/eLife.30189.015>

References

- Adams PD, Afonine PV, Bunkóczi G, Chen VB, Davis IW, Echols N, Headd JJ, Hung LW, Kapral GJ, Grosse-Kunstleve RW, McCoy AJ, Moriarty NW, Oeffner R, Read RJ, Richardson DC, Richardson JS, Terwilliger TC, Zwart PH. 2010. PHENIX: a comprehensive Python-based system for macromolecular structure solution. *Acta Crystallographica Section D Biological Crystallography* **66**:213–221. DOI: <https://doi.org/10.1107/S0907444909052925>, PMID: 20124702
- Amunts A, Brown A, Bai XC, Llácer JL, Hussain T, Emsley P, Long F, Murshudov G, Scheres SHW, Ramakrishnan V. 2014. Structure of the yeast mitochondrial large ribosomal subunit. *Science* **343**:1485–1489. DOI: <https://doi.org/10.1126/science.1249410>, PMID: 24675956

- Brown A**, Long F, Nicholls RA, Toots J, Emsley P, Murshudov G. 2015. Tools for macromolecular model building and refinement into electron cryo-microscopy reconstructions. *Acta Crystallographica Section D Biological Crystallography* **71**:136–153. DOI: <https://doi.org/10.1107/S1399004714021683>, PMID: 25615868
- Chaker-Margot M**, Barandun J, Hunziker M, Klinge S. 2017. Architecture of the yeast small subunit processome. *Science* **355**:eaal1880–1889. DOI: <https://doi.org/10.1126/science.aal1880>, PMID: 27980088
- Chen VB**, Arendall WB, Headd JJ, Keedy DA, Immormino RM, Kapral GJ, Murray LW, Richardson JS, Richardson DC. 2010. MolProbity: all-atom structure validation for macromolecular crystallography. *Acta Crystallographica Section D Biological Crystallography* **66**:12–21. DOI: <https://doi.org/10.1107/S0907444909042073>, PMID: 20057044
- Dragon F**, Gallagher JE, Compagnone-Post PA, Mitchell BM, Porwancher KA, Wehner KA, Wormsley S, Settlage RE, Shabanowitz J, Osheim Y, Beyer AL, Hunt DF, Baserga SJ. 2002. A large nucleolar U3 ribonucleoprotein required for 18S ribosomal RNA biogenesis. *Nature* **417**:967–970. DOI: <https://doi.org/10.1038/nature00769>, PMID: 12068309
- Emsley P**, Cowtan K. 2004. Coot: model-building tools for molecular graphics. *Acta Crystallographica. Section D, Biological Crystallography* **60**:2126–2132. DOI: <https://doi.org/10.1107/S0907444904019158>, PMID: 15572765
- Fernández IS**, Bai XC, Murshudov G, Scheres SH, Ramakrishnan V. 2014. Initiation of translation by cricket paralysis virus IRES requires its translocation in the ribosome. *Cell* **157**:823–831. DOI: <https://doi.org/10.1016/j.cell.2014.04.015>, PMID: 24792965
- Ferreira-Cerca S**, Pöll G, Kühn H, Neueder A, Jakob S, Tschochner H, Milkereit P. 2007. Analysis of the in vivo assembly pathway of eukaryotic 40S ribosomal proteins. *Molecular Cell* **28**:446–457. DOI: <https://doi.org/10.1016/j.molcel.2007.09.029>, PMID: 17996708
- Ferreira-Cerca S**, Sagar V, Schäfer T, Diop M, Wesseling AM, Lu H, Chai E, Hurt E, LaRonde-LeBlanc N. 2012. ATPase-dependent role of the atypical kinase Rio2 on the evolving pre-40S ribosomal subunit. *Nature Structural & Molecular Biology* **19**:1316–1323. DOI: <https://doi.org/10.1038/nsmb.2403>, PMID: 23104056
- Geerlings TH**, Faber AW, Bister MD, Vos JC, Raué HA. 2003. Rio2p, an evolutionarily conserved, low abundant protein kinase essential for processing of 20 S Pre-rRNA in *Saccharomyces cerevisiae*. *Journal of Biological Chemistry* **278**:22537–22545. DOI: <https://doi.org/10.1074/jbc.M300759200>, PMID: 12690111
- Grandi P**, Rybin V, Bassler J, Petfalski E, Strauss D, Marzioch M, Schäfer T, Kuster B, Tschochner H, Tollervey D, Gavin AC, Hurt E. 2002. 90S pre-ribosomes include the 35S pre-rRNA, the U3 snoRNP, and 40S subunit processing factors but predominantly lack 60S synthesis factors. *Molecular Cell* **10**:105–115. DOI: [https://doi.org/10.1016/S1097-2765\(02\)00579-8](https://doi.org/10.1016/S1097-2765(02)00579-8), PMID: 12150911
- Granneman S**, Petfalski E, Swiatkowska A, Tollervey D. 2010. Cracking pre-40S ribosomal subunit structure by systematic analyses of RNA-protein cross-linking. *The EMBO Journal* **29**:2026–2036. DOI: <https://doi.org/10.1038/emboj.2010.86>, PMID: 20453830
- Greber BJ**. 2016. Mechanistic insight into eukaryotic 60S ribosomal subunit biogenesis by cryo-electron microscopy. *RNA* **22**:1643–1662. DOI: <https://doi.org/10.1261/rna.057927.116>, PMID: 27875256
- Henras AK**, Plisson-Chastang C, O'Donohue MF, Chakraborty A, Gleizes PE. 2015. An overview of pre-ribosomal RNA processing in eukaryotes. *Wiley Interdisciplinary Reviews: RNA* **6**:225–242. DOI: <https://doi.org/10.1002/wrna.1269>, PMID: 25346433
- Heuer A**, Gerovac M, Schmidt C, Trowitzsch S, Preis A, Kötter P, Berninghausen O, Becker T, Beckmann R, Tampé R. 2017. Structure of the 40S-ABCE1 post-splitting complex in ribosome recycling and translation initiation. *Nature Structural & Molecular Biology* **24**:453–460. DOI: <https://doi.org/10.1038/nsmb.3396>, PMID: 28368393
- Johnson MC**, Ghalei H, Doxtader KA, Karbstein K, Stroupe ME. 2017. Structural Heterogeneity in Pre-40S Ribosomes. *Structure* **25**:329–340. DOI: <https://doi.org/10.1016/j.str.2016.12.011>, PMID: 28111018
- Kimanius D**, Forsberg BO, Scheres SH, Lindahl E. 2016. Accelerated cryo-EM structure determination with parallelisation using GPUs in RELION-2. *eLife* **5**:e18722. DOI: <https://doi.org/10.7554/eLife.18722>, PMID: 27845625
- Kornprobst M**, Turk M, Kellner N, Cheng J, Flemming D, Koš-Braun I, Koš M, Thoms M, Berninghausen O, Beckmann R, Hurt E. 2016. Architecture of the 90S Pre-ribosome: A Structural View on the Birth of the Eukaryotic Ribosome. *Cell* **166**:380–393. DOI: <https://doi.org/10.1016/j.cell.2016.06.014>, PMID: 27419870
- Korostelev A**, Ermolenko DN, Noller HF. 2008. Structural dynamics of the ribosome. *Current Opinion in Chemical Biology* **12**:674–683. DOI: <https://doi.org/10.1016/j.cbpa.2008.08.037>, PMID: 18848900
- Kucukelbir A**, Sigworth FJ, Tagare HD. 2014. Quantifying the local resolution of cryo-EM density maps. *Nature Methods* **11**:63–65. DOI: <https://doi.org/10.1038/nmeth.2727>, PMID: 24213166
- Lamanna AC**, Karbstein K. 2009. Nob1 binds the single-stranded cleavage site D at the 3'-end of 18S rRNA with its PIN domain. *PNAS* **106**:14259–14264. DOI: <https://doi.org/10.1073/pnas.0905403106>, PMID: 19706509
- Lamanna AC**, Karbstein K. 2011. An RNA conformational switch regulates pre-18S rRNA cleavage. *Journal of Molecular Biology* **405**:3–17. DOI: <https://doi.org/10.1016/j.jmb.2010.09.064>, PMID: 20934433
- Larburu N**, Montellèse C, O'Donohue MF, Kutay U, Gleizes PE, Plisson-Chastang C. 2016. Structure of a human pre-40S particle points to a role for RACK1 in the final steps of 18S rRNA processing. *Nucleic Acids Research* **44**:8465–8478. DOI: <https://doi.org/10.1093/nar/gkw714>, PMID: 27530427
- Lescoute A**, Westhof E. 2006. Topology of three-way junctions in folded RNAs. *RNA* **12**:83–93. DOI: <https://doi.org/10.1261/rna.2208106>, PMID: 16373494
- Longtine MS**, McKenzie A, Demarini DJ, Shah NG, Wach A, Brachat A, Philippsen P, Pringle JR. 1998. Additional modules for versatile and economical PCR-based gene deletion and modification in *Saccharomyces cerevisiae*.

- Yeast **14**:953–961. DOI: [https://doi.org/10.1002/\(SICI\)1097-0061\(199807\)14:10<953::AID-YEA293>3.0.CO;2-U](https://doi.org/10.1002/(SICI)1097-0061(199807)14:10<953::AID-YEA293>3.0.CO;2-U), PMID: 9717241
- McCaughan UM**, Jayachandran U, Shchepachev V, Chen ZA, Rappsilber J, Tollervey D, Cook AG. 2016. Pre-40S ribosome biogenesis factor Tsr1 is an inactive structural mimic of translational GTPases. *Nature Communications* **7**:11789. DOI: <https://doi.org/10.1038/ncomms11789>, PMID: 27250689
- Mohan S**, Donohue JP, Noller HF. 2014. Molecular mechanics of 30S subunit head rotation. *PNAS* **111**:13325–13330. DOI: <https://doi.org/10.1073/pnas.1413731111>, PMID: 25187561
- Murshudov GN**, Vagin AA, Dodson EJ. 1997. Refinement of macromolecular structures by the maximum-likelihood method. *Acta Crystallographica Section D Biological Crystallography* **53**:240–255. DOI: <https://doi.org/10.1107/S0907444996012255>, PMID: 15299926
- Nicastro G**, Taylor IA, Ramos A. 2015. KH-RNA interactions: back in the groove. *Current Opinion in Structural Biology* **30**:63–70. DOI: <https://doi.org/10.1016/j.sbi.2015.01.002>, PMID: 25625331
- Nissan TA**, Bassler J, Petfalski E, Tollervey D, Hurt E. 2002. 60S pre-ribosome formation viewed from assembly in the nucleolus until export to the cytoplasm. *The EMBO Journal* **21**:5539–5547. DOI: <https://doi.org/10.1093/emboj/cdf547>, PMID: 12374754
- Ogle JM**, Carter AP, Ramakrishnan V. 2003. Insights into the decoding mechanism from recent ribosome structures. *Trends in Biochemical Sciences* **28**:259–266. DOI: [https://doi.org/10.1016/S0968-0004\(03\)00066-5](https://doi.org/10.1016/S0968-0004(03)00066-5), PMID: 12765838
- Pettersen EF**, Goddard TD, Huang CC, Couch GS, Greenblatt DM, Meng EC, Ferrin TE. 2004. UCSF Chimera—a visualization system for exploratory research and analysis. *Journal of Computational Chemistry* **25**:1605–1612. DOI: <https://doi.org/10.1002/jcc.20084>, PMID: 15264254
- Schluenzen F**, Tocilj A, Zarivach R, Harms J, Gluehmann M, Janell D, Bashan A, Bartels H, Agmon I, Franceschi F, Yonath A. 2000. Structure of functionally activated small ribosomal subunit at 3.3 angstroms resolution. *Cell* **102**:615–623. DOI: [https://doi.org/10.1016/S0092-8674\(00\)00084-2](https://doi.org/10.1016/S0092-8674(00)00084-2), PMID: 11007480
- Schäfer T**, Strauss D, Petfalski E, Tollervey D, Hurt E. 2003. The path from nucleolar 90S to cytoplasmic 40S pre-ribosomes. *The EMBO Journal* **22**:1370–1380. DOI: <https://doi.org/10.1093/emboj/cdg121>, PMID: 12628929
- Schäfer T**, Maco B, Petfalski E, Tollervey D, Böttcher B, Aebi U, Hurt E. 2006. Hrr25-dependent phosphorylation state regulates organization of the pre-40S subunit. *Nature* **441**:651–655. DOI: <https://doi.org/10.1038/nature04840>, PMID: 16738661
- Strunk BS**, Loucks CR, Su M, Vashisth H, Cheng S, Schilling J, Brooks CL, Karbstein K, Skiniotis G. 2011. Ribosome assembly factors prevent premature translation initiation by 40S assembly intermediates. *Science* **333**:1449–1453. DOI: <https://doi.org/10.1126/science.1208245>, PMID: 21835981
- Sun Q**, Zhu X, Qi J, An W, Lan P, Tan D, Chen R, Wang B, Zheng S, Zhang C, Chen X, Zhang W, Chen J, Dong MQ, Ye K. 2017. Molecular architecture of the 90S small subunit pre-ribosome. *eLife* **6**:e22086. DOI: <https://doi.org/10.7554/eLife.22086>, PMID: 28244370
- Vanrobays E**, Gelugne JP, Gleizes PE, Caizergues-Ferrer M. 2003. Late cytoplasmic maturation of the small ribosomal subunit requires RIO proteins in *Saccharomyces cerevisiae*. *Molecular and Cellular Biology* **23**:2083–2095. DOI: <https://doi.org/10.1128/MCB.23.6.2083-2095.2003>, PMID: 12612080
- Vanrobays E**, Gélugne JP, Caizergues-Ferrer M, Lafontaine DL. 2004. Dim2p, a KH-domain protein required for small ribosomal subunit synthesis. *RNA* **10**:645–656. DOI: <https://doi.org/10.1261/ma.5162204>, PMID: 15037774
- Wimberly BT**, Brodersen DE, Clemons WM, Morgan-Warren RJ, Carter AP, Vonrhein C, Hartsch T, Ramakrishnan V. 2000. Structure of the 30S ribosomal subunit. *Nature* **407**:327–339. DOI: <https://doi.org/10.1038/35030006>, PMID: 11014182
- Woolford JL**, Baserga SJ. 2013. Ribosome biogenesis in the yeast *Saccharomyces cerevisiae*. *Genetics* **195**:643–681. DOI: <https://doi.org/10.1534/genetics.113.153197>, PMID: 24190922
- Woolfs HA**, Lamanna AC, Karbstein K. 2011. Roles of Dim2 in ribosome assembly. *Journal of Biological Chemistry* **286**:2578–2586. DOI: <https://doi.org/10.1074/jbc.M110.191494>, PMID: 21075849
- Zemp I**, Kutay U. 2007. Nuclear export and cytoplasmic maturation of ribosomal subunits. *FEBS Letters* **581**:2783–2793. DOI: <https://doi.org/10.1016/j.febslet.2007.05.013>, PMID: 17509569
- Zhang K**. 2016. Gctf: Real-time CTF determination and correction. *Journal of Structural Biology* **193**:1–12. DOI: <https://doi.org/10.1016/j.jsb.2015.11.003>, PMID: 26592709
- Zheng SQ**, Palovcak E, Armache JP, Verba KA, Cheng Y, Agard DA. 2017. MotionCor2: anisotropic correction of beam-induced motion for improved cryo-electron microscopy. *Nature Methods* **14**:331–332. DOI: <https://doi.org/10.1038/nmeth.4193>, PMID: 28250466

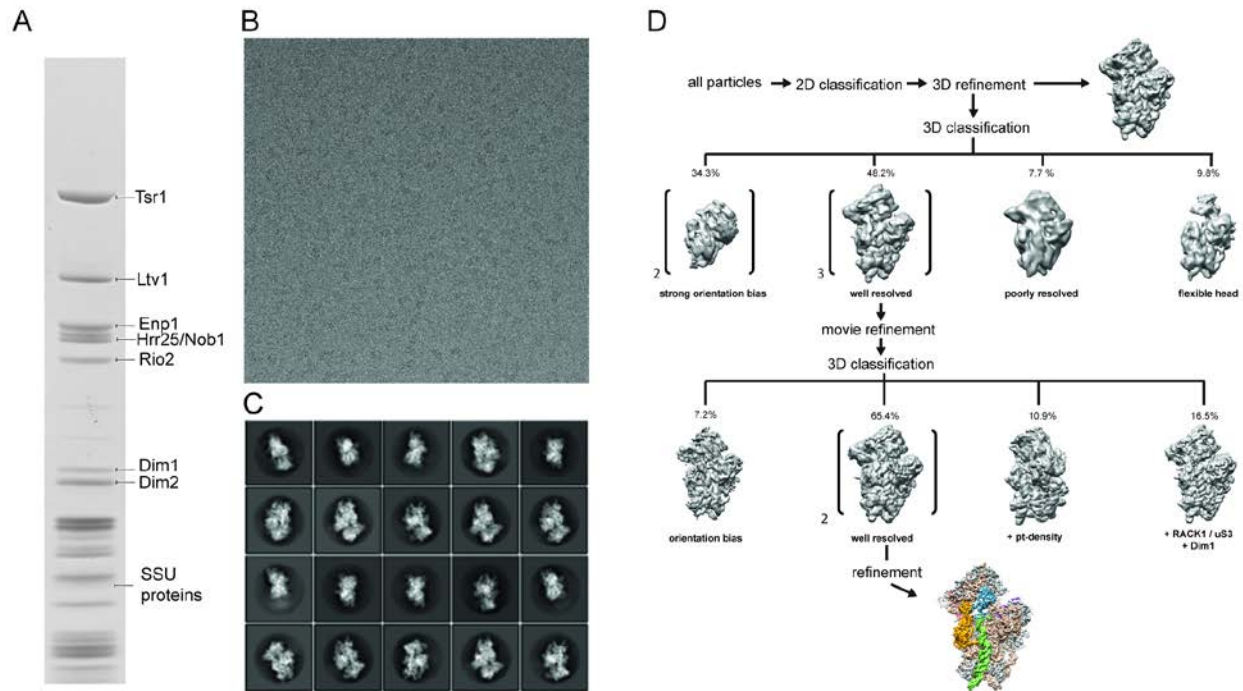


Figure 1 - figure supplement 1 | Purification and cryo-EM of the pre-40S complex

(A) Tandem affinity purification of pre-40S from yeast using Ltv1-FLAG-Tev-ProtA as bait.

Final eluates were analysed by SDS-PAGE and Coomassie staining. (B) Representative

micrograph showing pre-40S particles. (C) Representative 2D classes showing various

projections of pre-40S subunits. (D) Classification scheme. 2D classification was used to remove non-ribosomal particles. After refinement and 3D classification in RELION-2 (see Methods) three major classes were obtained. The main class showed density for the RBFs Tsr1, Enp1/Ltv1, Rio2 and Pno1 and was refined to 3.6 Å. Two other classes showed extra densities not seen in the main class. One class displayed distorted density at the platform in a position previously attributed to Nob1 [11]. The other class showed density for RACK1 and parts of uS3 in addition to density at a position previously attributed to Dim1[38]. However, due to the small number of particles and orientation bias, these classes were not further refined.

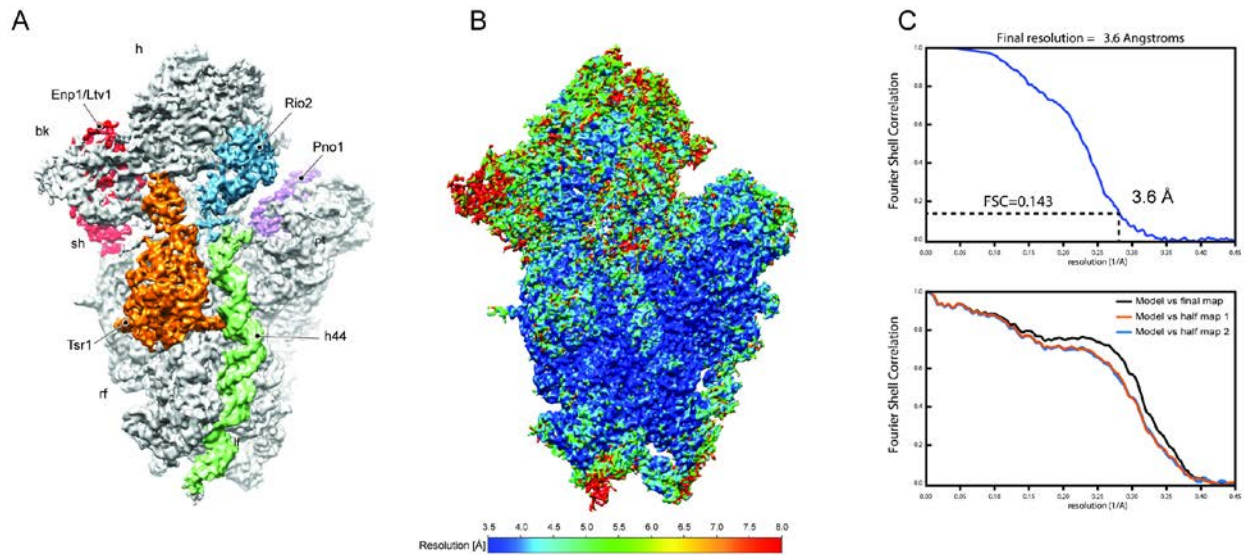


Figure 1 - figure supplement 2 | Assessment of resolution and model quality of the cryo-EM structure

(A) Cryo-EM density of the pre-40S complex low-pass filtered at 3.6 Å showing the 40S subunit (grey), Tsr1 (orange), Enp1 (red), Rio2 (blue) and Pno1 (pink). The rRNA helix h44 is highlighted in green. **(B)** Local resolution of the pre-40S complex as calculated by ResMap [39]. The ResMap plots show a range from a maximum of 3.5 Å to 8.0 Å in the periphery. **(C)** Fourier Shell Correlation (FSC) plot showing the 3.6 Å average resolution of the map according to the “gold standard” criterion (FSC=0.143; top) and FSC curves calculated between the cryo-EM map and the final models (bottom) as calculated by REFMAC. Values are plotted for the model versus the final map (FSC average, black), for the model that was refined into the first half-map and FSC calculated either for the same map (model vs first half-map, orange) or for the second half-map (model vs second half map, blue).

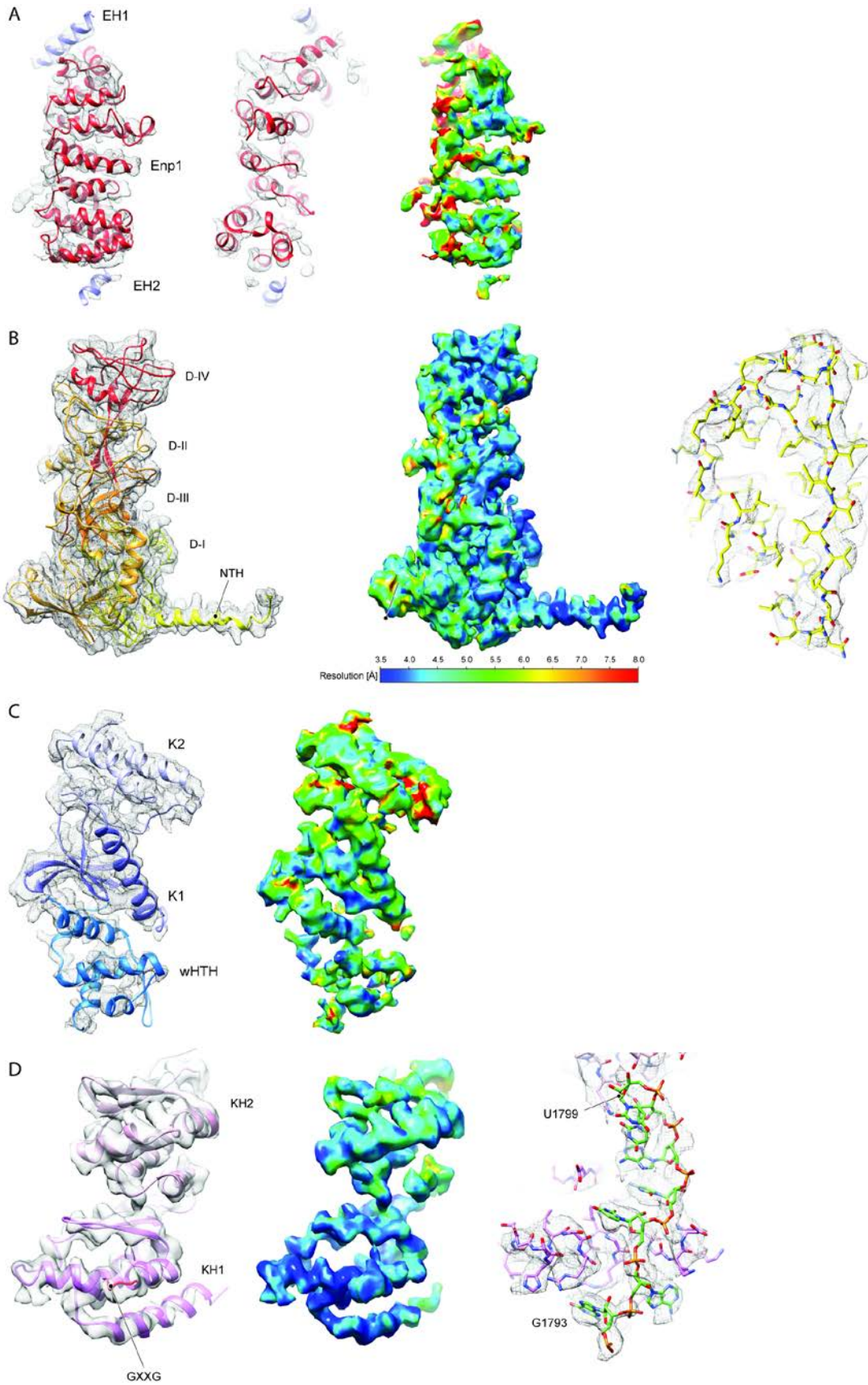


Figure 1 - figure supplement 3| Fitting of the RBFs

(A) Model for Enp1 fitted into isolated density low-pass filtered at approximately 5 Å. The model for Enp1 is shown in red, α -helical extra density was observed at the N- and C-terminal regions of Enp1 and model built as poly-Ala (EH1 and EH2; blue). These extra densities could be attributed to of Enp1 or to the bait protein Ltv1. At the given local resolution (between 4.5 and 8.5 Å) no molecular details are present to allow unambiguous assignment of the helices to either factor. **(B)** Model for Tsr1 fit into isolated density low-pass filtered at 3.6 Å. A high local resolution allowed unambiguous identification of most sidechains as exemplified on the right (zoom into domain I) and de novo determination of the α -helical structure in the Tsr1 N-terminus (see Fig. 3a). **(C)** Model for Rio2 fit into isolated density low-pass filtered at 5 Å. At a local resolution ranging mostly from 4 to 7.5 Å, all domains could be unambiguously docked. However, most of the loop regions displayed flexibility and could not be modelled at a molecular level. **(D)** Model for Pno1 fit into isolated density low-pass filtered at 3.6 Å. High local resolution, below 3.5 Å, especially for KH2, allowed the modelling of most side chains and contacts to the 3' end of 18S rRNA as depicted on the right.

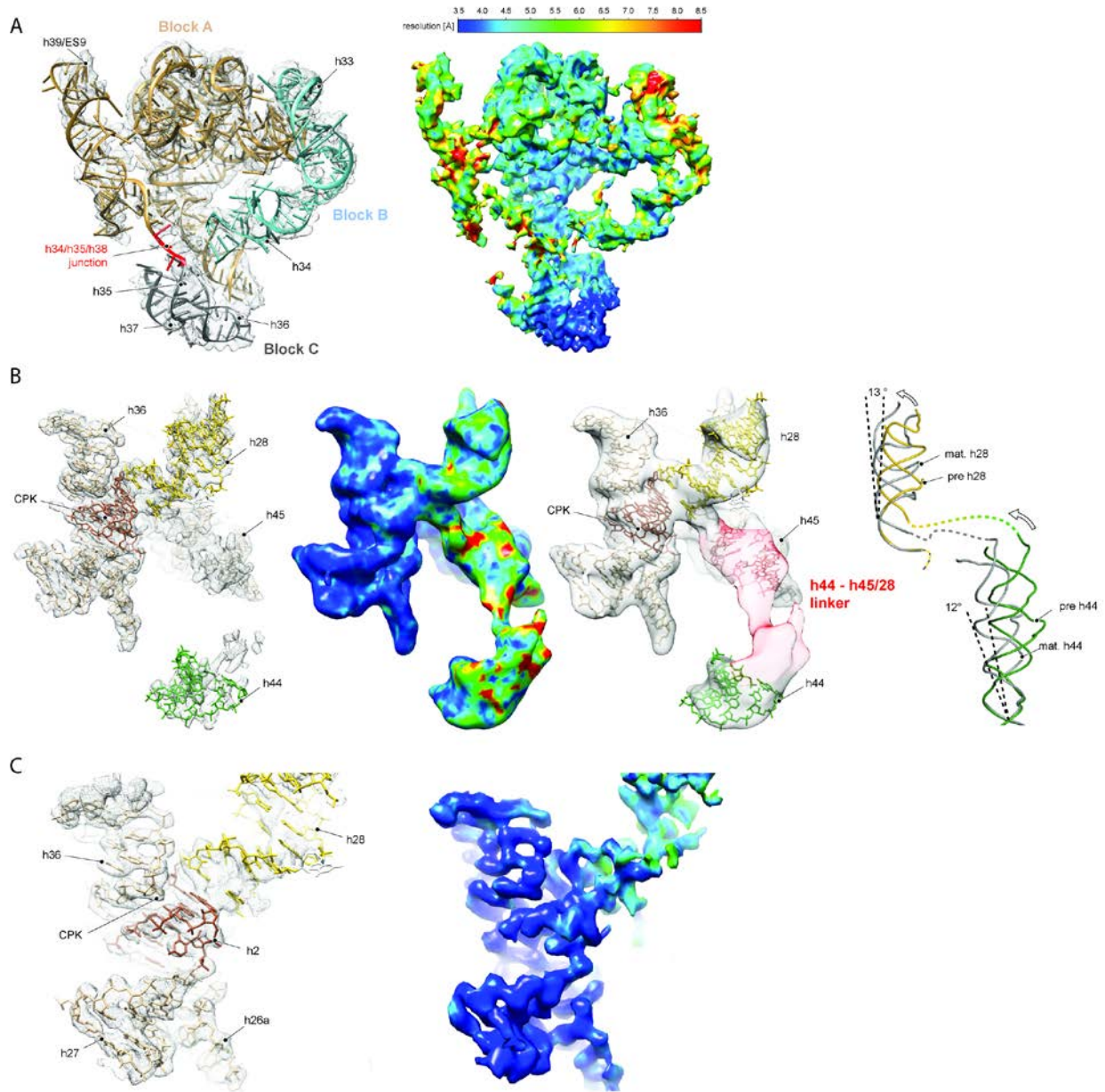


Figure 1 - figure supplement 4 | Conformation and flexibility of the pre-18S rRNA.

(A) Model for the head-forming 3' major domain (3'M; h28-h43) fitted into the cryo-EM density (left). The 3'M is divided into three blocks (block A, h29-h32; h38-h44, wheat; block B, h33-h34, light blue; block C, h35-h37, grey). The local resolution for block C and the major parts of the block A (h29-h32/h41-h43) is between 3.5 and 5.5 Å consistent with a stable and mature fold of these domains, whereas h39 and h40 and block B (h33-h34) are rather flexible, as indicated by a lower local resolution (right). Maps are low-pass filtered at 3.6 Å. (B) Model, density and local resolution of the central region of 18S rRNA connecting the 5' - (h1 and h2), central (h2 and

h27), 3'M (h36) and the 3'm (h44) domains (left). h1 and h2 form the central pseudoknot (CPK; brown). While the 5'- and central domains as well as h36 form a rigid structure as indicated by high local resolution (middle left), h28 and the 3'm are more flexible and the entire linker region linking h44 with h28 and h45 is not visible when low-pass filtered at 3.6 Å (left). Density for these flexible nucleotides (1633-1644 and 1754-1769; red) is only visible when low-pass filtering the map to below 15 Å (middle right). When compared to the mature state, h28 and h44 need to undergo a conformational transition. H28 is kinked by 13 degrees relative to its mature position and h44 is rotated outward towards the solvent side by 12 degrees (right). (C) view focusing on the rigid region around the CPK fitted into electron density (left). The connection between the 5' and central domains to h36 of 3'M is already stably formed in the pre-40S particle as indicated by high local resolution below 3.5 Å, whereas h28 is more flexible (right).

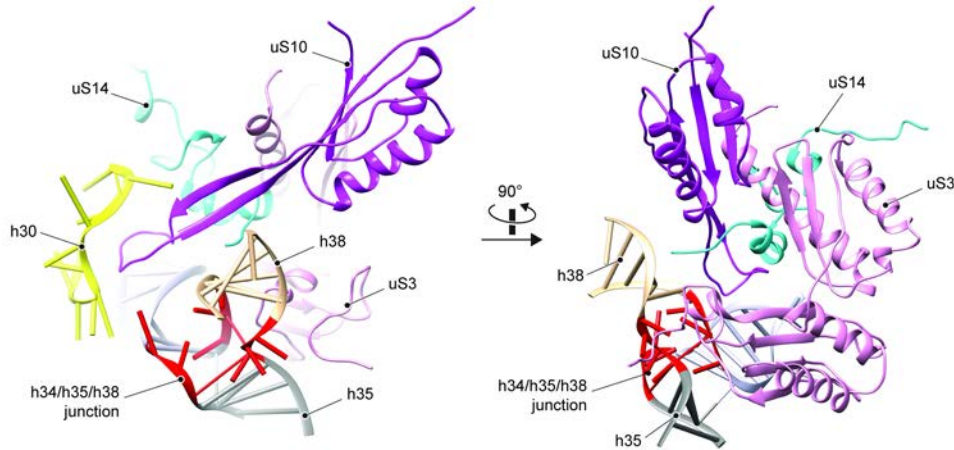


Figure 2 - figure supplement 1 | Structure and environment of the native h34-h35-h38 three-way junction

In the mature 40S subunit, h34-h35-h38 forms a family-A three-way junction that is stabilized by r-proteins uS3, uS10 and uS14, where uS10 also stabilizes the tip of h30 (nucleotides 1189-1200). All three proteins are absent in the pre-40S particle and neither the three-way junction nor the h30 tip is formed.

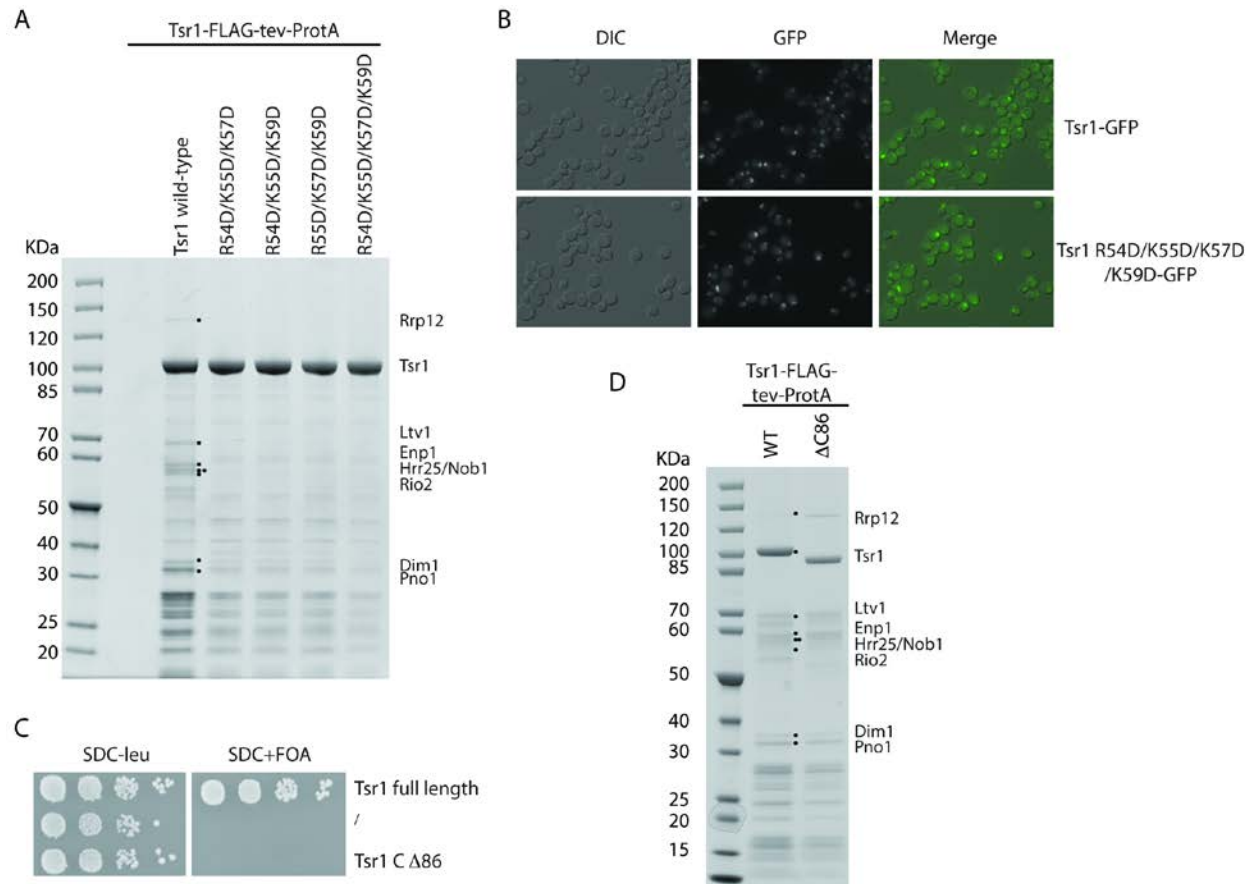


Figure 3 - figure supplement 1 | Functional analyses of mutant forms of Tsr1

(A) Tandem affinity purification of WT Tsr1 (Tsr1-FTpA) or the indicated mutants harbouring reverse-charge point mutations in residues interacting with h44 (R54D, K55D, K57D and K59D). Final eluates were analysed by SDS-PAGE and Coomassie staining. (B) Localization of wt Tsr1 (Tsr1-GFP) and Tsr1 harbouring reverse-charge point mutations in residues interacting with h44 (R54D, K55D, K57D and K59D). (C) Growth analysis of wt and truncated Tsr1, lacking domain IV (CΔ86). Constructs were transformed into a Tsr1 shuffle strain, spotted in 10-fold serial dilution and grown on SDC-leu (2 days) and SDC+FOA (4 days) plates at 30°C. (D) Tandem affinity purification of wt Tsr1 (Tsr1-FTpA) and Tsr1 lacking domain IV (CΔ86) as bait. Purifications were performed using FTpA constructs expressed from a plasmid, in a WT background. Final eluates were analysed by SDS-PAGE and Coomassie staining.

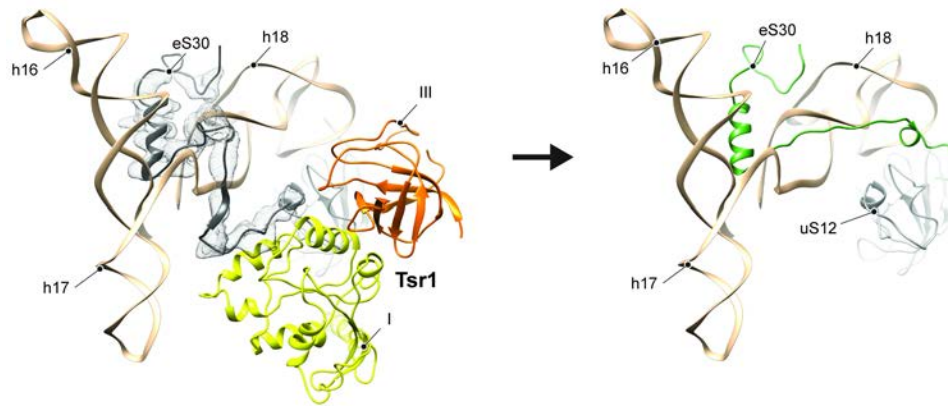


Figure 4 - figure supplement 1 | Comparison of RBP binding sites in the premature and the mature 40S

Distinct contacts are formed between domain I of Tsr1 and h17 as well as eS30 (model shown in density low-pass filtered according to local resolution using RELION-2). Notably the eS30 N-terminus is kept in an immature position by Tsr1. In the mature 40S, the eS30 N-terminus flips towards uS12, but in the pre-state this contact is hampered by Tsr1 domain III.